# The biology of the blackening phenomenon in cut carrots

Katie Elizabeth Schulz

Submitted in accordance with the requirements for the degree of Doctor of Philosophy

The University of Leeds

Faculty of Biological Sciences

Centre for Plant Sciences

September 2021

# Acknowledgements

I would like to thank my supervisors Christine Foyer and Paul Knox for all the support and guidance they have given me over the last four years, and for giving me the opportunity to do this PhD. Particular thanks to Paul Knox for his support and understanding throughout the good and bad times of the project.

I would like to express enormous gratitude to Barbara Karpinska for her knowledge, advice, and constant presence of chaotic good throughout my project. Her invaluable support helped me through many difficult moments.

I would also like to thank all my fellow lab mates, especially Richa, Rachel, Yat, Sarah, and Yousef for being great people to work with, and Sue Marcus for her help and guidance.

Many thanks to Rob Hancock and Susan Verrall at the James Hutton Institute, Dundee, Scotland, for their help with the metabolomics analysis. Thanks also to Gabriela Machaj at the University of Agriculture, Krakow, Poland, and Ian Carr and other members of the Leeds Institute of Medical Research at St James' Hospital, Leeds, for their help with the transcriptomics analysis. I am also most grateful to the lovely people at the Luke Institute, Finland, most notably Risto Korpinen, Pekka Saranpää, and Anna Kärkönen for their help and kindness during my visit.

Special thanks to my family and close friends, especially my sister Jenny, my mum Caroline, my dad Andy, and my closest friend John-Paul, without whom I would never have made it this far. Special mention to my grandparents John and Margaret Worle, who first sparked my interest in plant biology.
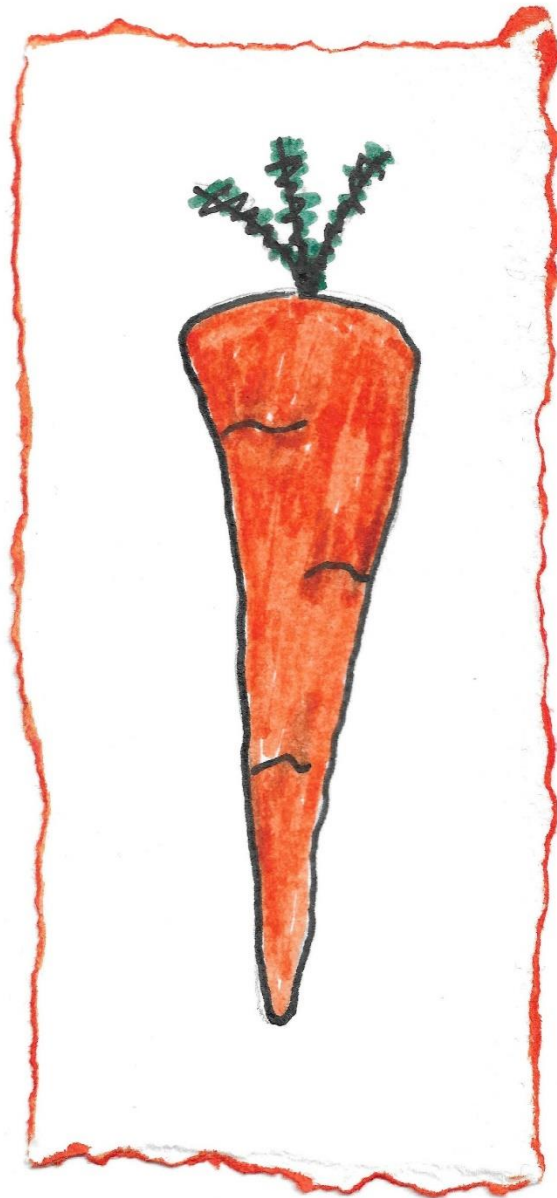
In memory of Helen Underhill, an amazing person, and her close friend Hege Ugradar, artist of this image.

# Abstract

A financially crippling blackening phenomenon of unknown cause has appeared in Scottish cut carrots in recent years. Full grown carrots are stored underground by the producers. They are covered in black plastic tarpaulin and straw throughout the harvesting year to prevent sprouting. The harvested carrots are then cut into batons and distributed to supermarkets and other outlets. Thereafter, blackening can occur within hours to days. Blackening is observed only in mature carrots that are over 1 year old and that have been stored underground until the end of the annual harvest period. This observation suggests that organ aging and/or length of storage underground are important factors contributing to the blackening. However, the environmental, metabolic and molecular triggers for blackening remain poorly characterised. An analysis of environmental conditions of carrot fields revealed that some fields yield carrots that show a higher level of blackening than others. The geographical locations of the fields or the local environmental conditions may enhance susceptibility to blackening. Metabolite profiling analysis revealed that the levels of amino acids and sugars were decreased in the blackened regions of the carrot batons, while fatty acids and phenolic compounds were increased. Immunofluorescence microscopy and a carbohydrate analysis revealed that pectin was less abundant in the cell walls in the blackened regions, which show high autofluorescence suggesting increased polyphenol accumulation. Moreover, lignin levels were higher in blackened regions. Transcript profiling analysis revealed that transcripts encoding proteins involved in phytohormone signalling were more abundant in the blacked regions. In particular, transcripts associated with auxin signalling and ethylene-responsive transcription factors were higher in the blackened regions. In contrast, the levels of transcripts encoding proteins associated with secondary metabolism were decreased in the blackened regions. Taken together, these findings suggest that hormonal and metabolic changes that occur during long periods of storage underground prior to harvest and that are associated with a loss of bud dormancy may predispose the carrots to wound-induced blackening discolouration. These studies provide new insights into the molecular and metabolic mechanisms that underpin the blackening process and will facilitate more rapid progress to solutions to address the problem.

# Table of Contents

# Lists of Tables

# Lists of Figures

# Lists of Abbreviations

| | |
|---|---|
| ABA | Abscisic acid |
| AcBr | Acetyl bromide |
| AIR | Alcohol-insoluble residue |
| AsA | Ascorbate |
| B or B/B | Blackened region on a blackened carrot baton |
| BF | Bright field |
| cm | Centimetre |
| CT | Orange region on an orange carrot baton |
| CWI | Cell wall integrity |
| DAMPS | Damage-associated molecular patterns |
| DEGs | Differentially expressed genes |
| FAO | Food and Agriculture Organization of the United Nations |
| FITC | Fluorescein isothiocyanate |
| G | Guaiacyl |
| GABA | γ-aminobutyric acid |
| GC | Gas chromatography |
| H | Hydroxyphenyl |
| h | Hour |
| HG | Homogalacturonan |
| HPLC | High performance liquid chromatography |
| JA | Jasmonic acid |
| L | Litres |
| LSD | Lesion simulating disease |
| m | Meter |
| M | Border region of orange tissue adjacent to blackened tissue on a blackened carrot baton |
| mAbs | Monoclonal antibodies |
| MEP | Methylerythritol 4-phosphate |
| mg | Milligram |
| min | Minute |
| ml | Millilitre |
| mM | Millimolar |
| MS | Mass spectrometer |
| NaCl | Sodium chloride |
| NCED | 9-cis-epoxycarotenoid dioxygenase |
| nm | Nanometre |
| O | Orange region on an orange carrot baton |
| O/B | Orange region on a blackened carrot baton |

| | |
|---|---|
| OB/B | Border region of orange tissue adjacent to blackened tissue on a blackened carrot baton |
| O/O | Orange region on an orange carrot baton |
| PAL | Phenylalanine ammonia-lyase |
| PCD | Programmed cell death |
| PI | Propidium iodide |
| POD | Peroxidases |
| PPO | Polyphenol oxidase |
| QC | Quality control |
| RG-I | Rhamnogalacturonan-I |
| RNA-seq | RNA sequencing |
| ROS | Reactive oxygen species |
| s | Seconds |
| S | Syringyl |
| SA | Salicylic acid |
| SD | Standard deviation |
| TBO | Toluidine blue O |
| µg | Microgram |
| µl | Microlitre |
| µM | Micromole |

# Chapter I

# Chapter 1: Introduction

## 1.1 Agricultural Crops

Crops have always been an essential food source worldwide for the human population, as well as a major aspect of global economy. In 2016, according to the Food and Agriculture Organization of the United Nations (FAO), 5,373,000 tonnes of potatoes, 811,117 tonnes of carrots and turnips (calculated together by the FAO) and 481,100 tonnes of apples were grown in the UK alone. However, despite this, large percentages of these crops are lost each year as a result of pests, plant diseases, post-harvest damages, and inadequate environmental conditions including lack of nutrients and poor soil quality (Zimmermann and Zentgraf 2005). This is a startling waste of food in a world where food security is becoming an ongoing and increasing concern.

## 1.2 Carrot as a crop

The domesticated carrot (*Daucus carota* subsp. *sativus*) is a member of the Apiaceae family. It is well known for its orange colour but can naturally be a wide variety of colours, including purple, yellow, red, white, and black. The domestic carrot was cultivated from the wild carrot species (*Daucus carota*) native to Central Asia, although this species of carrot is theorised to have originated in Persia (the region now known as Iran and Afghanistan) (Banga, 1957; Que et al., 2019).

The carrot is a biennial plant, meaning that the life cycle is completed over two years (Que et al., 2019). Carrot seeds are generally planted in moist soil in the spring before the last frost, although a second crop can often be planted in late summer or early autumn. Carrot seeds are slow to germinate taking up to 3 weeks and they frequently germinate unevenly over this period, so the soil must be kept moist. Once germinated the seedlings must be thinned because each plant requires space to grow. The shoots produce long thin leaves that provide carbohydrates via photosynthesis to drive production of a large taproot, which is the commonly eaten part of the plant (i.e. the carrot vegetable) (Figure 1.1).
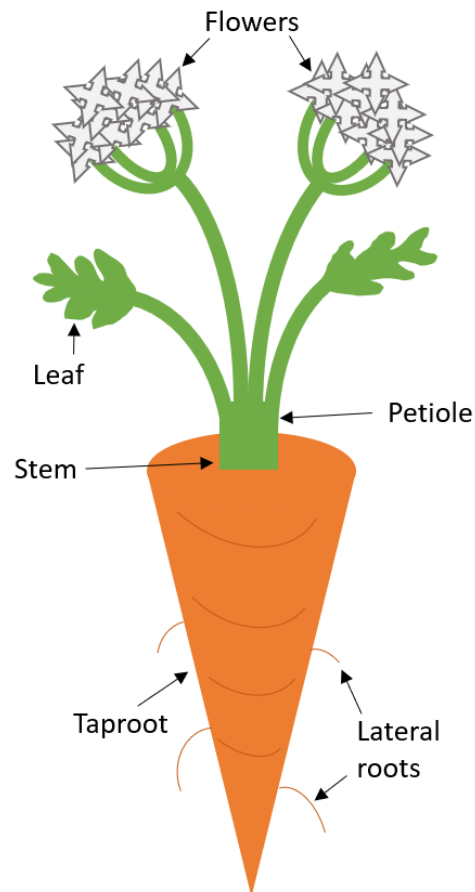
**Figure 1.1: Labelled schematic of a flowering carrot plant.**

Carrot development has been divided into three phases (Steingröver, 1983): (1) stage 1 where the seedling does not store sugars, (2) stage 2 in which only reducing sugars are stored in the tap root and (3) stage 3 in which sucrose is stored in the tap root. At the end of the vegetative growth cycle, the leaves undergo senescence with remobilisation of resources to the taproot, which overwinters underground. The plant requires vernalisation to flower and set seed in the second year of growth. After winter has passed, new leaves and stems grow, leading to flower development and ultimately seed production.

The taproot acts as a storage unit of carbohydrates (largely sucrose) and nutrients for the second year's growth and seed production. However, the maturity of the carrot tap root in terms of its suitability for harvest remains poorly defined in terms of molecular physiology and metabolic state. A much better understanding of carrot maturity and the factors that govern carrot development and senescence during storage are required to improve shelf life, eating quality and food value.

The carrot crop is classified as a root vegetable as the most commonly eaten section of the carrot plant is the storage organ that grows underground, also referred to as the 'tap root'. Carrot leaves are also edible but not generally utilised. Carrot crops take 80-120 days to mature depending on the growing rate of the individual cultivars and the mature taproots are largely secondary growth tissues that can be adequately stored in a refrigerator for several months before becoming unusable. Many carrot varieties are grown and are usually sold with the storage organ intact.

There are 4 main varieties of commercial carrot: Chantenay, Danvers, Imperator

**Figure 1.2: The 4 main varieties of the carrot root crop.** These categories are subject to the size and shape of the carrot storage organ, and each category is known for certain characteristics concerning growth and post-harvest issues.

and Nantes (Figure 1.2). Chantenay carrots are short compared to other varieties, have a wide girth with a rounded tip and are known for storing well. Danvers carrots also have a relatively wide girth but are considerably longer than Chantenay carrots. They are known for storing well and tolerating heavy soils. Nantes carrots have a consistent girth and blunt tip. They will produce greater yields in a variety of conditions, however do not store well and are damaged easily. Imperator carrots are long and thin and, due to having a high content of sugar, are the most commonly grown varieties of carrot. In recent years, other carrot products have been developed and sold in bulk to the public, including shredded carrot pieces, diced carrots and carrots sticks.

## 1.3   Nutritional value of carrot roots

Carrot taproots are especially well known for being rich in carotene (pro-vitamin A) and ascorbic acid (vitamin C). An ascorbic acid content of 0.11 mg per gram of fresh weight carrot root has been recorded in 82 day old carrots (Wang et al., 2015). However,

4

carotene content can vary drastically between common carrot varieties with a range of 0-40 mg carotene per 100 g root tissue being recorded. However, through selective breeding, carotene-rich carrot cultivars such as HCM (high carotene mass selection) have been recorded to contain up to 50 mg carotene per 100 g of root tissue (Fernandes Santos and Simon, 2006; Baranski et al., 2012; Wani and Prasad, 2015).

| Table 1.1: Nutritional content of carrot root. Data collected by (Wani and Prasad, 2015). | |
|---|---|
| Compound | Content in carrot root (%) |
| Moisture | 95-84% |
| Carbohydrates | 10.6-9.58% |
| Sugars | 7.5-5.4% |
| Fiber | 2.9-0.6% |
| Protein | 2.0-0.6 % |
| Fat | 0.2-0.7% |

## 1.4   Carrot tissue and cell types

Carrot plants are eudicots with a single thick taproot. For continued plant growth, continuous cell division and growth occurs in specialist tissue regions called meristems or cambia. The meristem contains mostly undifferentiated cells that divide quickly to produce further undifferentiated cells, eventually specialising into permanent tissue types depending on the location within the plant (Perilli et al., 2012). There are two types of meristem tissues in eudicots; apical meristems and lateral meristems. In roots and shoots, lateral meristems, also known as the vascular cambium and cork cambium, are responsible for secondary growth where the plant grows in thickness. Apical meristems are located at root and shoot tips and are the source of primary growth allowing the plant to grow in length (Matte Risopatron et al., 2010). Young carrot roots are formed mostly of primary xylem and phloem, whereas mature carrot taproots consist primarily of secondary xylem and secondary phloem (Figure 1.3). The periderm acts as a protective outer skin made of three layers: the outer cork, the cork cambium,

and the inner phelloderm. The xylem transports water and solutes throughout the plant, and the phloem transports sugars. In carrot taproots, xylem and phloem tissue are largely build of parenchyma cells, with xylem vessels also found throughout the xylem (McGarry, 1995). The pith also contains parenchyma cells and is closely associated with xylem tissue (Korolev et al., 2000). The vascular and cork cambium are meristems and the main sources of secondary tissue growth. Secondary growth from the vascular cambium leads to the development of secondary xylem towards the centre of the root and secondary phloem towards the outer half, allowing for the root to grow in width becoming thicker (Korolev et al., 2000). Xylem rays intrude into both secondary xylem and phloem tissue to transport solutes and provide mechanical support (Barlow, 2005). Small hair-like roots are located around the outer surface of the carrot root and are used to absorb nutrients from the surrounding soil. Each of these root structures have individual functions and adapted cell walls to aid with these functions. The phloem mainly transports sugars and consists of four cell types: sclerenchyma, parenchyma, fibres, and sieve elements. Sieve elements have thickened primary cell walls for resisting high turgidity. Parenchyma cells have thin cell walls, and store lipids and carbohydrates. Fibre cells provide strength and support and, although not always present, sclerenchyma cells have thick lignified secondary cell walls for increased strength (Pace, 2019). The xylem contains four cell types: vessels elements, tracheids, parenchyma and fibers. All xylem cell types, expect for parenchyma cells, have thicken, lignified secondary cell walls to withstand compression and to aid with water transportation.
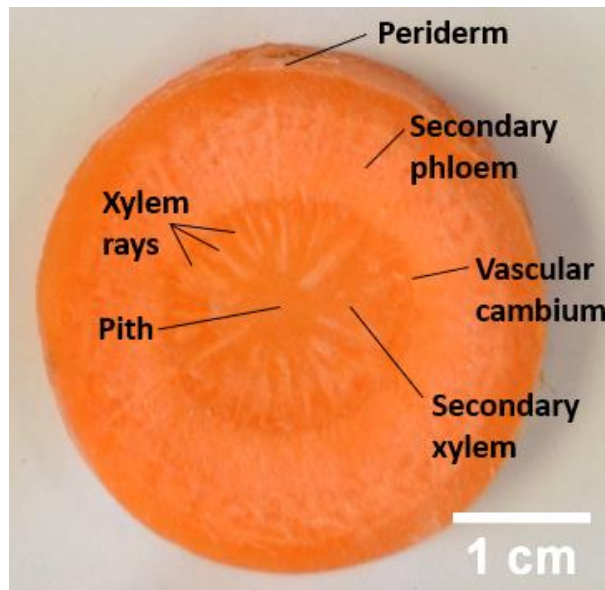
**Figure 1.3: Transverse slice of an orange carrot tap root.** Carrot was obtained from Kettle Produce Ltd. Labels are periderm, secondary phloem, secondary xylem, xylem rays, pith, and vascular cambium.

## 1.5    Carrot blackening phenomenon

The shelf life of fruits and vegetables is greatly reduced because of senescence occurring in the fruit and other organs, and leaf senescence will likely reduce the growth of the crops. As a result, senescence is a major issue for the agricultural industry as it may also influence traits such as grain quality and crop yield during the production of food and feed stock (Schippers *et al.* 2015; Smith 1962).

Recently, a 'blackening phenomenon' has been reported by the carrot growing industry of Scotland in their cut carrot product. Carrot blackening is known to appear on cut carrot products, including carrot batons and transverse slices taken from whole taproots. Carrot blackening can appear as clear patches of strong discolouration (Figure 1.4, B) or as faint discoloration throughout the carrot sample (Figure 1.4, A). For the purposes of this study, samples taken from regions of strong discolouration were prioritised.



**Figure 1.4: Carrot blackening**. Images of transverse slices of carrot taproot with clear patches of strong discolouration (B) or as faint discoloration throughout the carrot slice (A). Scale bar = 1 cm.

Blackened region samples were taken from visibly blackened carrots (B/B) (Figure 1.5, A and C). Border region samples were taken from the areas immediately bordering the blackened regions (OB/B) (Figure 1.5, A). Orange region samples were taken from orange carrots with no visible blackening (O/O) (Figure 1.5, B and D). RNA extracted from blackened (B), border (M) and orange (CT) regions were used for transcriptome analysis. Orange region samples were also taken from blackened batons (O/B) (Figure 1.5, A) and used for microscopy analysis. Samples taken from carrot transverse slices were used for metabolomics analysis. Samples taken from carrot batons were used for all other analyses.
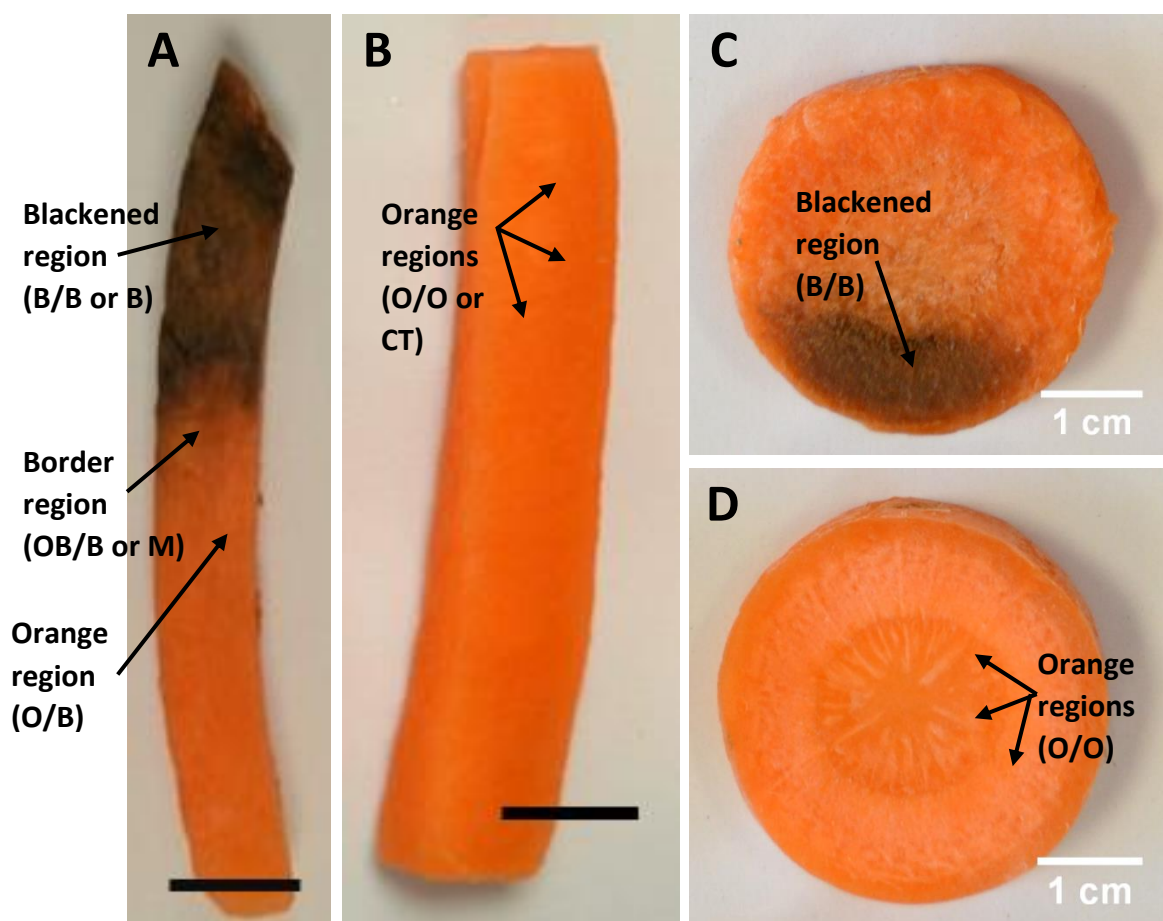


**Figure 1.5: Orange and blackened carrots**. Carrot batons (A and B) and transverse slices (C and D). Labelled carrot regions showing orange regions from non-blackened carrots (O/O) (B and D), orange regions from blackened samples (O/B), blackened regions (B/B) and border regions (OB/B) (A and C). Scale bar = 1 cm.

This phenomenon could possibly be linked to the senescence process occurring both before and after harvest, however very little is currently known about the exact cause. Much research has and still is being conducted to reduce post-harvest losses, though storing harvested fruits and vegetables in cold conditions (usually when being processed and transported) is an effective method of delaying ripening or general deterioration of crops. The cold temperatures also delay the onset of bacterial and microbial infections, ensuring more crops are of a marketable standard once reaching their destinations (Smith 1962). However, more recently transgenic technology has been developed, providing further methods of increasing the shelf life of fruits and vegetables. For example, a line of transgenic carrots expressing a chitinase (*chit42*) gene from the fungus *Trichoderma harzianum* was produced. The transgenic line had increased chitinases that induce fungal cell wall degradation and therefore increase resistance to storage rot (Ojaghian *et al.* 2018). If the problems of societal acceptance can be overcome, such technologies have much potential for improving shelf life and quality of crops.

## 1.6   Wound stress response

When experiencing biotic and abiotic stresses, plants exhibit a defensive response that involves many signalling mechanisms and changes in gene expression. Pathogen infection often occurs because of wounding. Mechanical stresses and tissue wounding damage the cell walls, allowing entry for microbes that cause infection. Damage to the cell wall produces signalling molecules, leading to damage-associated molecular patterns (DAMPS) that trigger immunological responses, such as increasing defence gene expression and reactive oxygen species (ROS) production, as well as callose formation over the wounded area (Bacete et al., 2017; Ferrari et al., 2013; Mélida et al., 2020). Lignin biosynthesis increases in wounded areas to strengthen the secondary cell walls to help prevent infection.

The cause of carrot blackening is unknown but it is likely to be related to several factors triggered when the carrots are cut into batons, wounding the taproot tissue. The phytohormones ethylene (Dong, 1998; Choi and Klessig, 2016), abscisic acid (ABA) (Leide et al., 2012), jasmonic acid (JA) (Lee et al., 2004; Halim et al., 2006; Koo and Howe, 2009), and salicylic acid (SA) (Pieterse and van Loon, 1999; Lee et al., 2004; Halim et al., 2006) are all closely associated with wound stress responses (Dong, 1998). JA is well known for its essential role in plant defence responses against biotic and abiotic stresses and has been reported to crosstalk between many other plant hormones during stress response. Upon wounding, JA promotes the biosynthesis of auxin necessary for regeneration of damaged areas of the plant (Zhang et al., 2016; Zhang et al., 2019; Hoermayer et al., 2020). JA and ethylene signalling pathways crosstalk to regulate other stress responses, generally to activate the expression of defence genes, such as *PLANT DEFENSIN 1.2* (*PDF1.2*), to aid in necrotrophic pathogen resistance (Yang et al., 2019). Crosstalk between the SA and JA pathways initiates early- and late- stage defence-related gene expression against pathogen attack, respectively. Meanwhile, crosstalk between the JA and ABA pathways and the JA and gibberellin pathways both coordinate a balance between defence resistance and plant growth (Yang et al., 2019). In potato tubers, cytokinins were found to increase upon wounding and so these phytohormones have been proposed to play a role in cell division and tissue repair (Dervinis et al., 2010). Ethylene, SA, ABA, and JA are also heavily associated with the senescence programme.

Given that blackening is only observed in some situations, wounding is not the only factor that triggers this phenomenon. The age of the carrots may be an important factor, particularly as older, possibly senescent, carrots as well as young carrots are used in processing.

## 1.7   Senescence

Senescence is a developmental programme that involves the mobilisation of nutrients from senescing cells to growing organs and storage organs, such as developing leaves and developing seeds respectively. The leaf senescence program is well defined however senescence in taproots/storage organs has not been well researched. During the senescence program leaves gradually loose both chlorophyll and protein, until the senescent leaves retain only the carotenoid pigments that give the characteristic yellow, brown, and red colours of the advanced stages of senescence in the autumn leaves on trees.
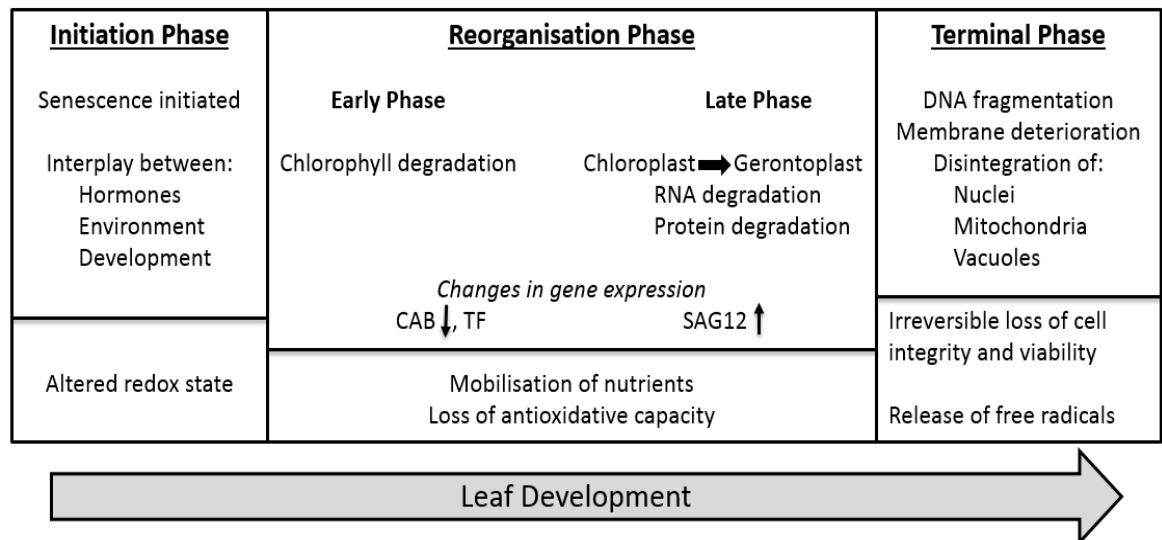


**Figure 1.6: The 3 phases of leaf senescence (initiation, reorganisation, and terminal) and the processes that occur during each phase.** Adapted from Zimmermann and Zentgraf, 2005.

For simplicity, senescence may be divided into 3 phases: initiation, reorganisation and the terminal phase (Figure 1.6) (Zimmermann and Zentgraf 2005). The senescence program begins with the initiation phase, which can be activated by metabolic and

developmental (age-related) cues, particularly phytohormones such as ethylene (Iqbal et al., 2017), JA (Hu et al., 2017), and SA (Morris et al., 2000). It is often triggered by external environmental factors such as temperature extremes or drought, which activate precocious or premature senescence. The sophisticated interplay between the senescence signalling pathways and abiotic and biotic stress responses enables modulation and fine-tuning of the developmental senescence programme in response to environmental conditions (Ay, Janack and Humbeck 2014). In the later stages of the reorganisation phase, senescence-associated genes are upregulated, assisting the relocation of all essential molecules. The terminal stage ends with programmed cell death (PCD) which is abscission of the dead leaves, as the tree prepares for winter. The first two phases of the senescence program are essentially reversible, because the dismantling of organelles and proteins is progressive. However, the accumulation of secondary metabolites together with the production of SA triggers the irreversible genetically programmed cell suicide pathways that underpin PCD (Roberts *et al.* 2012).

The terminal phase is characterised by PCD and the oxidation of secondary compounds (Zimmermann and Zentgraf 2005). SA, mitochondrial ROS production and autophagy play important roles in later stages of leaf senescence and cell death. While much remains to be understood regarding the molecular mechanisms underlying these processes, the mitochondrial AAA-protease gene FtSH4 was shown to be important in regulating autophagy and senescence in Arabidopsis. Loss of FtSH4 functions resulted in increased SA levels with much greater leaf senescence, PCD and autophagy, together with increased expression of WRKY genes, including WRKY40, WRKY46, WRKY51, WRKY60, WRKY63, and WRKY75; all of these WRKY proteins can bind to the promoter of the SA Induction Deficient2 gene, which is a SA synthesis and signalling gene (Zhang *et al.* 2017). The PCD program involves DNA degradation and a final translocation of nutrients to the seeds in order to promote post-germinative growth (Schippers *et al.* 2015). The mitochondria, nuclei, and vacuoles are the final structures to be degraded (Avila-Ospina *et al.* 2014; Lim, Woo and Nam 2003; Barth, De Tullio and Conklin 2006; Zimmermann and Zentgraf 2005).

Antioxidants such as ascorbate (AsA) play a role in the regulation of the developmental senescence program and cell death (Barth, De Tullio and Conklin 2006). AsA, also known as ascorbic acid or vitamin C, is a naturally occurring antioxidant and has been associated with developmental senescence, PCD, flowering time and pathogen response through a complex signal transduction network (Barth, De Tullio and Conklin 2006). Recent studies have suggested that AsA has a major role as a co-factor of other plant hormones and enzymes, particularly those concerned with cellular growth, immune defence and fruit ripening (Hou *et al.* 2015). AsA reacts with the excess ROS that accumulate in plants when undergoing a wide range of physiological activities, including senescence, environmental stressors, oxidative metabolism and photosynthesis (Hou *et al.* 2015). Consequently, increased levels of AsA have been observed during stress conditions (Noctor and Foyer 1998), where AsA proceeds to degrade the excess ROS, protecting the plant from oxidative stress (Hou *et al.* 2015; Noctor and Foyer 1998) and, therefore, delaying senescence.

The composition and structure of the cell wall also undergoes significant changes during senescence. This includes cell wall weakness and a loss of adhesion between cells (King and O'Donoghue 1995). During fruit ripening, pectic polymers and hemicelluloses become fragmented, long-chain pectin becomes soluble and certain sugars, such as arabinose and galactose, are lost from the cell wall (Fischer and Bennett 1991). Senescence induced by the harvesting of vegetables causes change in cell wall structure. For example, wall-bound galactose is lost from the tips of asparagus when harvested (Waldron and Selvendran 1990), and the cell walls in vascular tissue becomes toughened due to lignification (Lipton 2011).

## 1.8 Plant cell wall components

### 1.8.1  Primary and secondary cell walls

Plant cell walls are structurally complex, primarily consist of polysaccharides, and are involved in several essential functions of plant development, growth, intercellular signaling and defence (Scheller and Ulvskov, 2010). Vascular plants species have both primary and secondary cell walls which provide different mechanical and biological

benefits (Li et al., 2016). Key structural components of both cell walls are cellulose microfibrils and hemicelluloses, while primary cell walls also contain pectin and secondary cell walls often contain lignin (Keegstra, 2010; Zhong et al., 2019). Primary cell walls are deposited during cell division, continuing to develop and expand along with the cell. They are thin and relatively elastic to adjust to cell expansion in young cells, consisting of cellulose microfibrils, hemicelluloses, and pectins (Figure 1.7, A). Secondary cell walls only develop in cells after cell expansion in specialised cells such as vessels and fibers (Keegstra, 2010; Li et al., 2016; Zhong et al., 2019). They are highly rigid to provide mechanical support to prevent cell bursting or collapse and consist mainly of cellulose microfibrils, hemicellulose, and lignin, though composition varies between species (Figure 1.7, B).
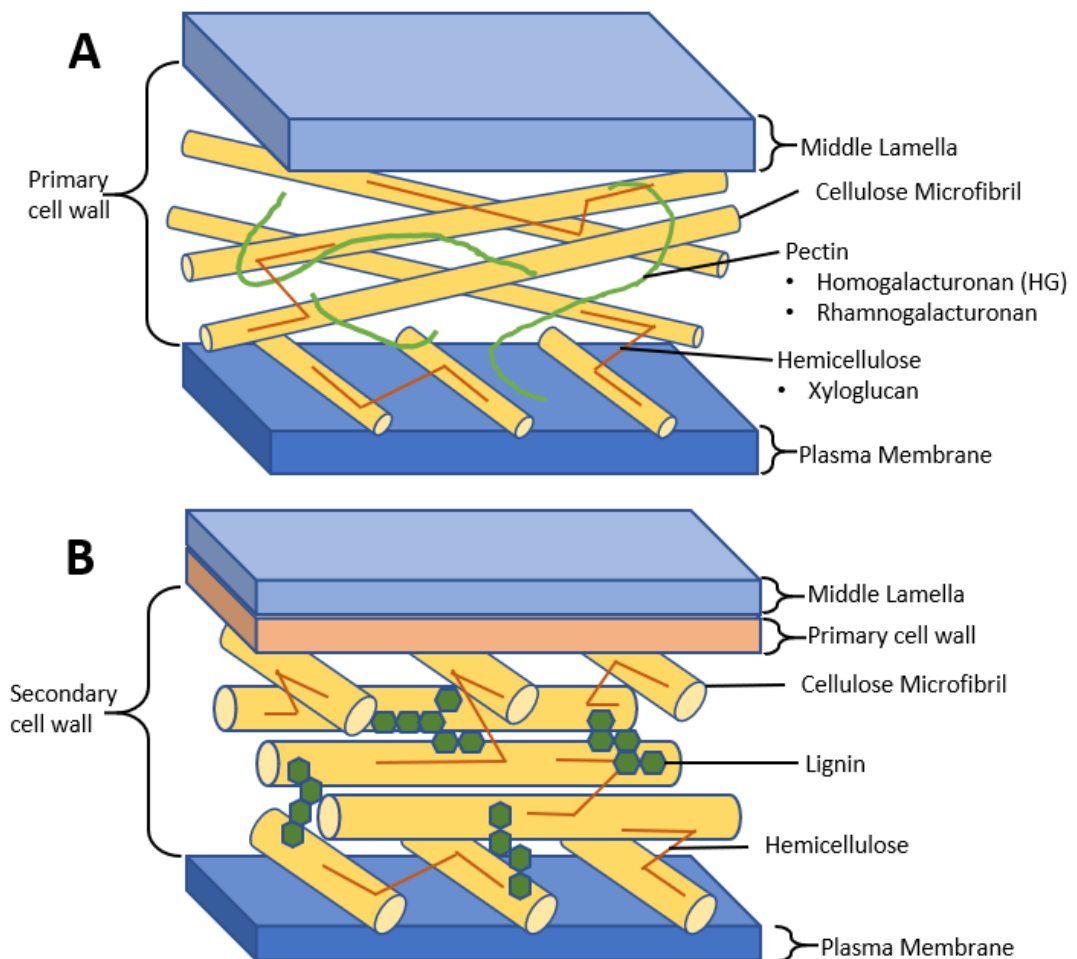


**Figure 1.7: Primary and secondary cell wall composition and structure.** Image adapted from (Loix et al., 2017).

### 1.8.2 Polysaccharides

#### 1.8.2.1 Cellulose

Cellulose is an extremely abundant polysaccharide made up of chains of unbranched β-1,4 linked D-glucose units which are assembled by alignment and hydrogen bonding into long cellulose microfibrils found in both primary and secondary cell walls. Cellulose is the main loading bearing component of plant cell walls and provides rigidity to maintain the structure of individual cells as well as the entire plant (Szymańska-Chargot et al., 2019). Cellulose is also heavily crosslinked with pectins and hemicelluloses, and also lignin in secondary cell walls (Padayachee et al., 2015). These cross linkages help to reinforce the strength and structure of the cell wall, generating the walls resistance to turgid pressure within the cells and compressive forces and preventing cell from rupturing.

#### 1.8.2.2 Hemicellulose

Hemicelluloses are non-cellulosic branched polysaccharides with β-1-4-linked backbones present in cell walls of all terrestrial plants (Scheller and Ulvskov, 2010). This thesis will focus only on the hemicellulose xyloglucan, which has a β-1-4-glucan backbone substituted with α-(1-6)-xylosyl residues. Xyloglucan is the major non-pectic, matrix cell wall polysaccharide in carrots. The xyloglucan backbone cross-links between cellulose microfibrils forming tethers increasing rigidity to the cell wall and strengthening the cell walls further by enabling the generation of, and providing resistance to, internal turgor pressure (Padayachee et al., 2015). Xyloglucan has also been found to covalently link to pectin in Arabidopsis (Popper and Fry, 2008). Alternatively, when the xyloglucan degraded, the cell walls become more loose allowing for cell expansion when necessary in primary cell walls (Eckardt, 2008; Hayashi and Kaida, 2011).

#### 1.8.2.3 Pectin

Pectin is a galacturonic acid rich polymer that plays several key roles in the cell wall, with the composition and abundance of pectin varying between developmental stages and specific cell types. Pectin is mainly located in primary cell walls and can strongly influence cell wall properties, including rigidity, pH, integrity, porosity and plant defence responses (Voragen et al., 2009; Klaassen and Trindade, 2020). Pectin is also known to

cross-link with cellulose in carrots, further increasing structural integrity (Broxterman and Schols, 2018). This thesis will focus on two of the major types of pectin: homogalacturonan (HG) and rhamnogalacturonan-I (RG-I). HG pectin has a galacturonic acid residue backbone built of α-1,4-linked galacturonic acid which is synthesized mainly in a highly methyl-esterified form. The RG-I pectin backbone comprises of repeating disaccharide units of galacturonic acid and rhamnose [-2)-α-L-Rhap(1,4)- α-D-GalpA –(1-] with galactan, arabinan and arabinogalactan side chains. Levels of HG methyl-esterification can be hypervariable and can be decreased by the action of pectin methylesterases (Verhertbruggen et al., 2009; Silva-Sanzana et al., 2019). By breaking down HG pectin this way, the primary cell walls can be expanded and modified (Houston et al., 2016). In the events of insect or pathogen attack, other pectin-modifying enzymes such as pectate lyase and polygalacturonanase are typically released by the invading organism to weaken the cell walls of affected areas to allow for entry (Silva-Sanzana et al., 2019; Uluisik and Seymour, 2020).

### 1.8.2.4 Lignin

Lignin plays an important structural role in secondary cell walls, being closely intwined in the hemicellulose and cellulose networks increasing the rigidity, strength, and hydrophobic effect of the walls (Doblin et al., 2010; Zhong et al., 2019). Due to its contribution to plant defence mechanisms, conditions of metabolic stresses, pests and disease often cause increased lignin synthesis (Vanholme et al., 2010; Miedes et al., 2014; Yadav et al., 2020). Lignin is a complex phenolic polymer mainly built from the monolignols: *p*-coumaryl, coniferyl, and sinapyl alcohol (Figure 1.8 A). These monolignols are synthesised through the phenylpropanoid pathway (Zhong et al., 2019). When incorporated into the lignin polymer, these alcohols form the lignin subunits: *p*-hydroxyphenyl (H), guaiacyl (G), and syringyl (S), respectively (Figure 1.8 B). Lignin composition is affected by plant species, age and tissue type (Vanholme et al., 2010; Zhong et al., 2019). In 7-8 month old carrots, lignin subunit ratios are approximately 4:95:1 (H:G:S) (Schäfer et al., 2018).
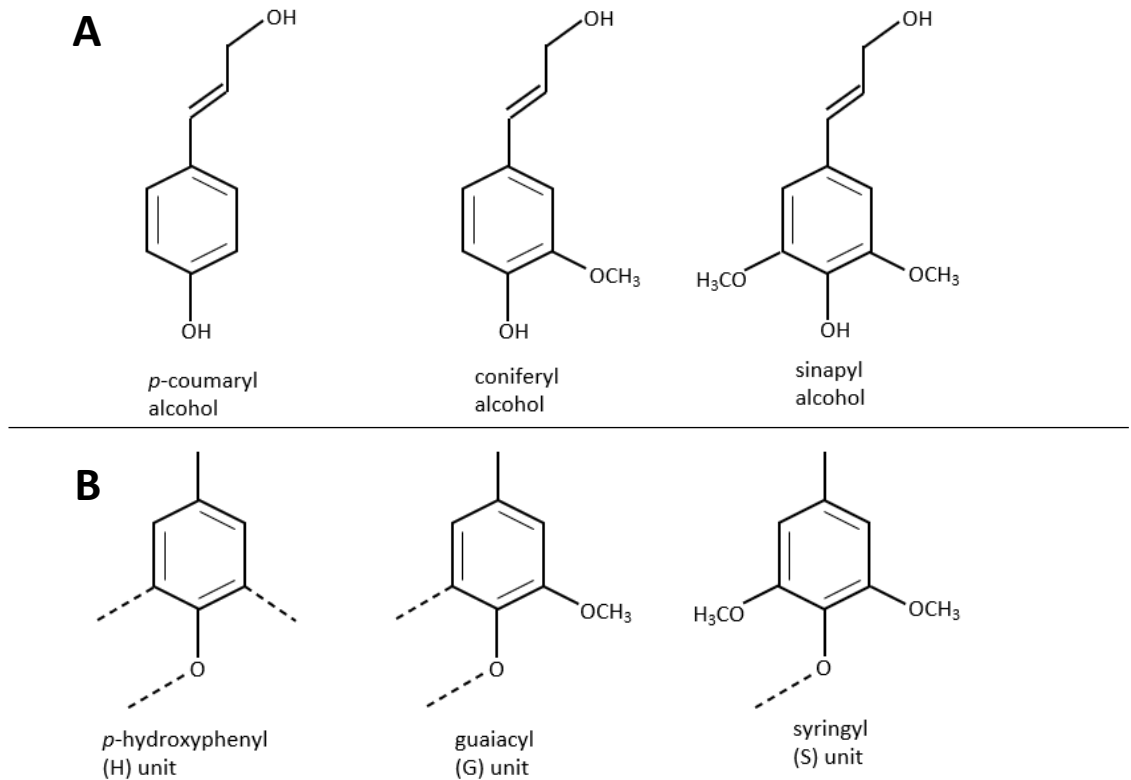
**Figure 1.8: Molecular structures of monolignols and lignin subunits.** The monolignols (A) p-coumaryl, coniferyl, and sinapyl alcohol and their corresponding subunits when incorporated with the lignin polymer (B) p-hydroxyphenyl, guaiacyl, and syringyl units.

### 1.8.3   Cell Wall Probes

Monoclonal antibodies (mAbs) can be used as molecular probes to target specific cell wall components allowing for their detection when used in conjunction with fluorescence imaging (Duffieux et al., 2020). Monoclonal antibodies and other molecular probes have been used to detect a range of plant cell wall components, including pectins and hemicelluloses (Pedersen et al., 2012; Ruprecht et al., 2017; Posé et al., 2018; Torode et al., 2018).

## 1.9 Plant Metabolism

### 1.9.1 Metabolic Pathways

For simplicity, metabolism is often divided into two parts: primary or secondary. Primary metabolism involves the processes and pathways that are essential for plant growth, development, and general function. Secondary metabolism involves all other pathways that are useful and advantageous but ultimately not necessary for essential plant functions. The same is true of primary and secondary metabolites. The synthesis of all secondary metabolites can be traced back to having primary metabolites as precursors. Carotenoids are secondary metabolites, that are synthesized from substrates of the methylerythritol 4-phosphate (MEP) pathway (Figure 1.9).
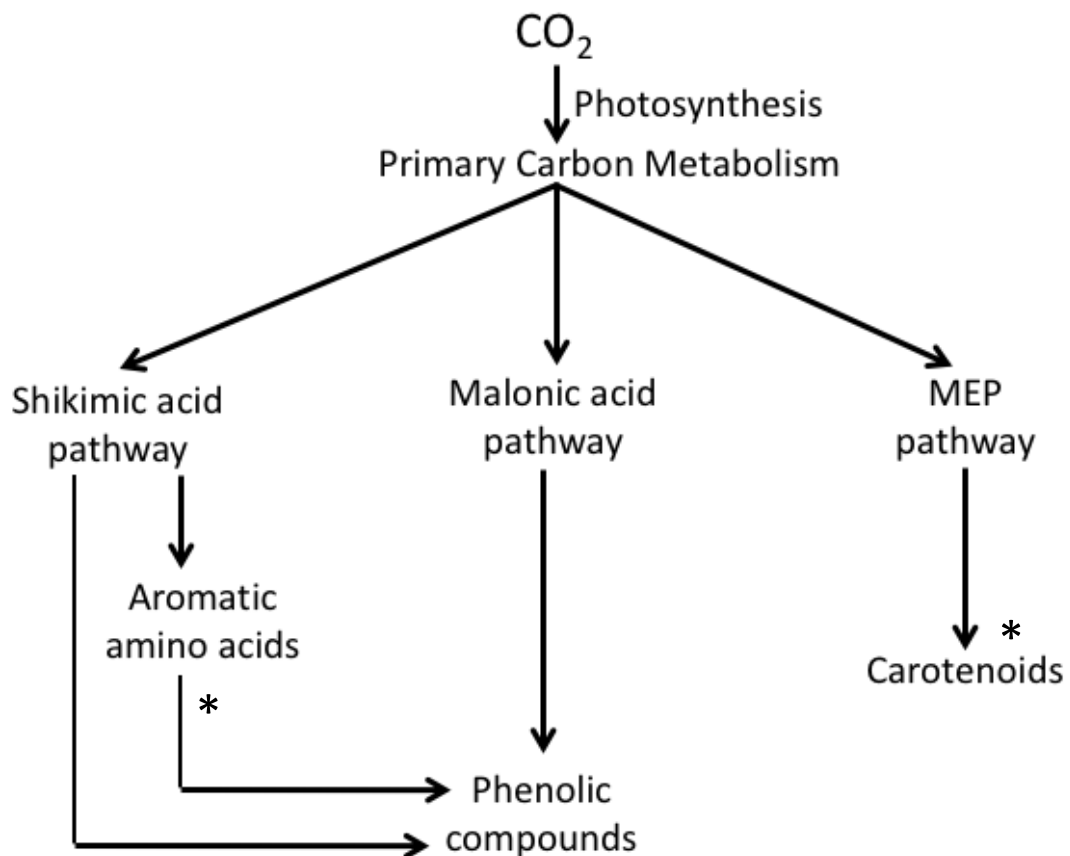


**Figure 1.9: Connection of primary metabolism and the synthesis of carotenoids and phenolic compounds.** (* Pathways are shown in more detail). Adapted from (Uarrota, Severino and Maraschin 2011).

CO$_2$ and H$_2$O are converted to glucose during photosynthesis, which is then fluxed through primary metabolism (Figure 1.9). Sugars then act as precursors for many important pathways including shikimate, malonic acid, and MEP. The shikimic acid pathway leads to the synthesis of many phenolic compounds and the three aromatic amino acids: phenylalanine, tyrosine, and tryptophan. Following this, phenylalanine is a precursor for chlorogenic acid synthesis, shown in more detail in Figure 1.10. The malonic acid pathway also leads to the production of phenolic compounds. The MEP pathway leads to carotenoid synthesis and the carotenoid pathway is shown in more detail in Figure 1.12.
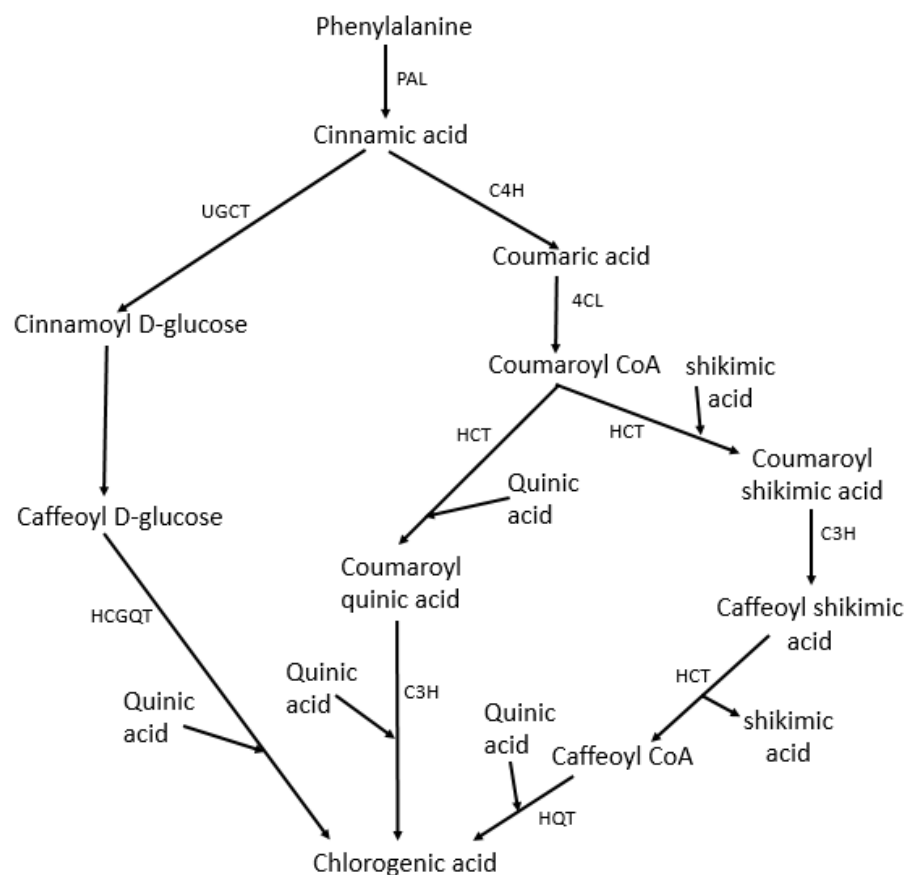


**Figure 1.10: The three pathways of chlorogenic acid synthesis originating from phenylalanine.** Abbreviations of enzymes: PAL, phenylalanine ammonia lyase; C4H, cinnamate 4-hydroxylase; 4CL, 4-coumarate CoA ligase; HCT, hydroxycinnamoyl CoA shikimate/quinate hydroxycinnamoyl transferase; C3H, *p*-coumarate 3'-hydroxylase; HQT, hydroxycinnamoyl CoA quinate hydroxycinnamoyl transferase; UGCT, UDP glucose: cinnamate glucosyl transferase; HCGQT, hydroxycinnamoyl D-glucose: quinate hydroxycinnamoyl transferase. Adapted from (Niggeweg, Michael and Martin 2004).

Chlorogenic acid is an ester of caffeic acid and (-)-quinic acid and is the major phenolic compound present in many fruits and vegetables. It is a substrate for polyphenol oxidase (PPO) and has been reported as a browning substrate in sweet potatoes, apples and other fruits and vegetables. An increase in chlorogenic acid content was also shown to be directly associated with the oxidative browning reaction in apples, potato, coffee and carrots (Chubey and Nylund 1969). On the other hand, a low or moderate relationship between browning and the content of chlorogenic acid was found in eggplants (Plazas *et al.* 2013).

## 1.9.2 Carotenoids

Carotenoids are naturally occurring pigments that absorb blue-green light (400-550 nm) resulting in the yellow, orange, and red colouring in plants. Carotenoids are usually lipophilic due to possessing long unsaturated aliphatic chains. There are two classes of carotenoids: xanthophylls and carotenes. Xanthophylls, such as lutein (Figure 1.11, C), contain oxygen and produce a more yellow colouring, whereas carotenes, such as $\alpha$-carotene (Figure 1.11, A) and $\beta$-carotene (Figure 1.11, B), are hydrocarbons and do not contain oxygen. Carotenoids are classified as tetraterpenes as their structure contains 40 carbon atoms.

(A) $\alpha$-carotene
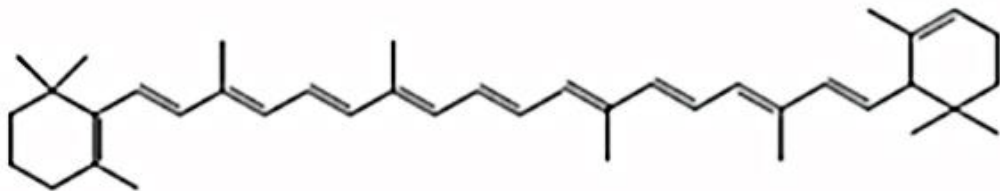


(B) $\beta$-carotene
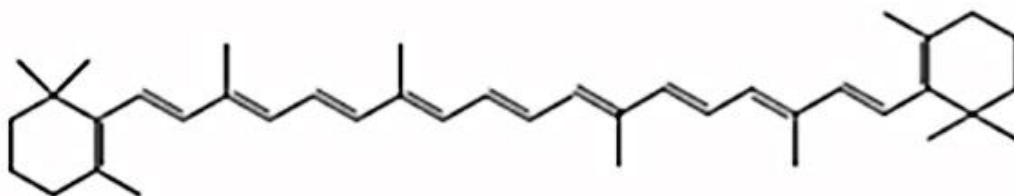


(C) Lutein
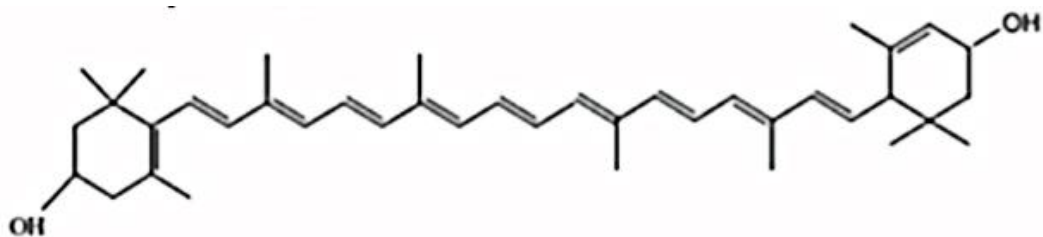


**Figure 1.11: The molecular structures of (A) $\alpha$-carotene, (B) $\beta$-carotene, and (C) lutein.** (Shi *et al.* 2014).

The carotenoid pigments have several important functions in photosynthesis, including light-harvesting and photo-protective qualities. In photosynthesis, chlorophylls are the main site of light absorption, however are not efficient at absorbing wavelengths between 450-550 nm. Carotenoids absorb wave lengths between 400-550 nm and transfer the collected excited electrons to the chlorophyll to be used in photosynthesis. This is an example of singlet-singlet energy transfer. The presence of carotenoids improves the photosynthetic capabilities of the plant (Hashimoto *et al.* 2018). Carotenoids also act as antioxidants in plant cells. The photo-protective capabilities of carotenoids are essential for preventing oxidative damage to antenna and reaction centres in chlorophyll (Kodis *et al.* 2004). Certain carotenoids also act as precursors to the synthesis of ABA (Kyndt *et al.* 2017). The final intermediate of carotenoid synthesis is phytoene, as illustrated in Figure 1.12.
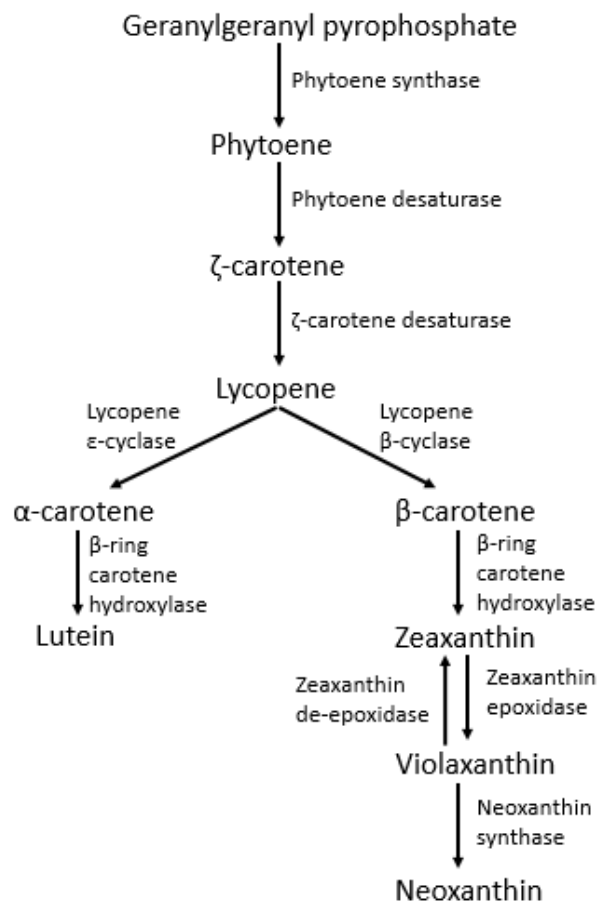


**Figure 1.12: The carotenoid pathway.** Pathway showing synthesis of the main carotenoids with Geranylgeranyl pyrophosphate as a precursor. Adapted from (Just *et al.* 2007)

The carotenoid biosynthetic pathway (Figure 1.12) has been the subject of intensive research in recent years because it produces the precursors of vitamin A, which is essential to the human diet. This research has mainly focused on the biofortification of carotenoids in crops for higher nutritional and economic value (Giuliano 2017).

## 1.10 Hypothesis and project objectives

The blackening phenomenon is not observed on the taproot when the carrots are first developed. However, as the carrots become older in the ground, the tendency to show blackening after harvest and processing increases. This suggests that there is a developmental or environmental trigger that predisposes the carrots to blackening and that the intensity of this trigger increases with the time of storage in the ground. This trigger may be hormonal, possibly associated with the growing pressure on the carrot shoot to grow or with the progressive depletion of essential resources such as carbohydrates during storage, leading to the tendency to senesce. It is therefore important to undertake a systematic analysis of the metabolite and transcript profiles to characterise which of these processes is occurring.

The aim of this study was to determine the molecular basis of the blackening process in cut carrots. The main objectives of this project are:

1. To assess differences in metabolite content between blackened and orange carrots and determine which metabolic pathways are involved in carrot blackening using a metabolomics analysis.

2. To investigate any differences in cell wall composition in the orange and blackened carrot regions.

3. To investigate differences in transcript profiles of orange and blackened carrot regions. This study aims to identify the suites of genes involved in the orchestration of carrot blackening.

4. To analyse data collected from Kettle Produce Ltd that document the provenance of carrots, age when harvested and rate of blackening observed in subsequent days after processing. Data monitoring environmental factors of carrot growth fields including air and soil temperature, solar radiation and rainfall was also analysed. Together, these data were analysed to discover any links or possible causes of carrot blackening.

5. To use molecular insights to develop a method of assessing pre-disposition to blackening and a way to reduce susceptibility.

# Chapter II

# Chapter 2: Materials and methods

## 2.1 Plant material

### 2.1.1 Carrots

Whole carrots, carrot batons and carrot slices (*Daucus carota* L. variety 'Nairobi') were obtained from Kettle Produce Ltd (Balmalcolm Farm, Cupar, Fife, Scotland, KY15 7TJ). The carrots were grown and harvested from fields located around Scotland. They were then washed and processed in the Balmalcolm factory into carrot batons and slices. Blackened carrot batons or slices were then identified and collected, along with corresponding orange carrot samples from the same batch.

## 2.2 Microscopy and immunolabelling

### 2.2.1 Monoclonal antibodies (mAbs)

Sections of orange and blackened carrot batons embedded in Steedman's wax were viewed under a microscope fitted with epifluorescence irradiation for detection of cell wall epitopes using monoclonal antibodies described in Table 2.1.

| Table 2.1. List of monoclonal antibodies used. | | |
|---|---|---|
| **mAb** | **Epitope** | **Reference** |
| **Anti-AGP** | | |
| LM2 | B-linked-GlcA in AGP glycan | (Yates et al., 1996; Smallwood et al., 1996) |
| **Anti-callose** | | |
| 10H2 | 1,3-glucan / Callose | Unpublished |
| **Anti-extensin** | | |
| LM1 | Extensin | (Smallwood et al., 1995) |
| **Anti-HG** | | |
| LM19 | Low Me-HG/ no ester | (Verhertbruggen et al., 2009) |

| JIM7 | Partially ME-HG | (Knox et al., 1990; Willats et al., 2000; Clausen et al., 2003, p.20) |
|------|-----------------|---------------------------------------------------------------------|
| LM20 | High ME-HG | (Verhertbruggen et al., 2009) |
| 2F4 | Partially ME-HG with calcium ions | (Liners and Van Cutsem, 1992; Liners et al., 1992, p.198) |
| **Anti-RG** | | |
| LM5 | (1→4)-β-D-galactan | (Jones et al., 1997; Andersen et al., 2016) |
| LM6 | (1→5)-α-L-arabinan | (Verhertbruggen et al., 2009) |
| LM12 | Ferulic acid, feruloylated pectin | (Pedersen et al., 2012) |
| LM26 | Branched (1,6-Gal)(1→4)-β-D-galactan | (Torode et al., 2018) |
| **Anti-xylan** | | |
| LM10 | (1→4)-β-D-xylan | (McCartney et al., 2005; Ruprecht et al., 2017) |
| LM11 | (1→4)-β-D-xylan / arabinoxylan | (McCartney et al., 2005) |
| LM28 | glucuronoxylan | (Cornuault et al., 2015) |
| **Anti-xyloglucan** | | |
| LM25 | XXXG/galactosylated xyloglucan | (Pedersen et al., 2012) |

### 2.2.2   Preparation of Steedman's wax for tissue embedding

900 g of polyethylene glycol 400 distearate and 100 g 1-hexadecanol were melted at 65°C and mixed thoroughly. The wax was poured into trays lined with aluminium foil and left to harden at room temperature. The wax was melted at 37°C ready for use in tissue embedding.

### 2.2.3 Preparation of plant materials for embedding in Steedman's wax

Orange and blackened carrot batons sent by Kettle Produce Ltd were cut transversely at a right angle along the axis into 1 cm$^2$ sections. Sections were taken from at least ten different carrot batons displaying varying levels of carrot blackening. These sections were fixed in PEM buffer (50 mM piperazine-N.N'-bis[2-ethane-sulfonic acid] (PIPES), 5 mM methylene glycone bis(β-aminoethylether)-N,N,N',N'-tetraacetic acid (EGTA), 5 mM MgSO$_4$ pH 6.9) containing 4% paraformaldehyde for 1 hour.

### 2.2.4 Steedman's wax embedding and sectioning of plant material for microscopy

The fixed plant sections were washed twice in 1x PBS (phosphate buffered saline, 137 mM NaCl, 0.16 mM KCl, 8.0 mM Na$_2$HPO$_4$, 14.7 mM KH$_2$PO$_4$, pH 7.2) for 10 min each time and then dehydrated using increasing concentrations of ethanol (30%, 50%, 70%, 90% and 100%) for 30 min each at 4°C. Samples were warmed to 37°C and incubated overnight at 37°C in 1:1 Steedman's wax and 100% ethanol, followed by two changes of 100% wax for 1 h at 37°C. The samples were positioned in moulds, and wax poured into the moulds until a convex surface was visible. The moulds were left overnight to set at room temperature and then chilled at 4°C for 10 min before samples were cut into 12 μm sections using a Microm HM-325 microtome and placed onto polysine-coated glass slides (VWR International, Leuven, Belgium). The sections were dewaxed and rehydrated using decreasing concentrations of ethanol (3x 97%, 90%, 50%, water) for 10 min each, followed by 1.5 h in changed water. Section slides were dried.

### 2.2.5 Enzymatic pre-treatment using pectate lyase

To remove HG pectin, the sections were treated with pectate lyase at 25 μg/ml in 2 mM CaCl$_2$ buffer, 50 mM 3-(cylohexylamino)-1-propanesulfonic acid (CAPS), pH 10 at room temperature for 2 h. Sections were washed 3 times for 5 min in PBS buffer. Control sections were incubated for the same length of time with the corresponding buffer without the enzyme treatment.

### 2.2.6  Immunofluorescence labelling of sections using monoclonal antibodies and imaging

Plant sections were incubated in 5% (w/v) milk protein/PBS for 30 min (to prevent non-specific binding) and rinsed with 1x PBS. Monoclonal primary antibodies (1 in 5 dilution) in 5% (w/v) milk protein/PBS were applied to the plant sections and incubated for 90 min at room temperature. Sections were washed with 1x PBS three times for 5 min each time. Secondary antibodies (either rabbit anti-rat IgG-fluorescein isothiocyanate (FITC) or anti-mouse IgG-FITC (Sigma, UK)) were then added (1 in 100 dilution) in 5% (w/v) milk protein/PBS and incubated for 60 min in the dark. Sections were washed with 1x PBS three times for 5 min each time and then 0.1% Toluidine Blue O (pH 5.5 in 0.2 M sodium phosphate buffer) was added for 5 min. Sections were washed twice more with 1x PBS for 5 min each and were mounted in Citifluor AF1 to decrease photobleaching. After applying a coverslip, sections were stored in the dark at 4°C until used. Slides were viewed with an Olympus fluorescence microscope fitted with epifluorescence irradiation (Olympus BX61, Canada) and images captured using Volocity software (Perkin Elmer, UK) and a Hamamatsu ORCA285 camera (Hamamatsu City, Japan).

### 2.2.7  Confocal laser scanning microscopy

A confocal laser scanning microscope (Zeiss LSM880 with Airyscan Inverted Confocal LS Microscope) was used to measure the level autofluorescence emitted in the visible wave spectrum from orange and blackened carrot regions. Measurements were taken at 3 nm intervals between 414 – 695 nm.

### 2.2.8  Cell size analysis

Cell width was measured in orange carrots, blackened carrot regions and the orange regions that immediately border the blackened areas. 10 cells were measured from 3 images of each region. In total, 30 cells from orange, blackened and border carrot regions were measured. A T-test was used to determine statistical significance.

## 2.3   Metabolite analysis

### 2.3.1   Lignin analysis

#### 2.3.1.1   Tissue preparation for lignin assay

Plant material was dried at 60°C in an oven and stored in darkness until undergoing lignin analysis. Carrot samples are ground to a fine powder using a Retch ball mill (Retsch MM400, Hann, Germany; 50 ml grinding jars with one metal ball, frequency 30 s$^{-1}$). The samples were ground in 30 s intervals 4 times to prevent heating.

#### 2.3.1.2   Alcohol-insoluble residue (AIR)

The alcohol-insoluble residue (AIR) of the carrot samples were prepared by extracting the sample 8 times with 70% (v/v) ethanol and 3 times with 100% acetone in a 25°C sonicating water bath (30 min incubation time for each extraction with regular mixing). The solvent to sample ratio was 140 mg plant tissue: 14 ml solvent (70% ethanol, acetone). Samples were centrifuged (4000 rpm, 10 min, room temperature) before each solvent change. The pellet was mixed into the fresh solvent by vortex. The AIR was then dried in a vacuum oven overnight at 60°C.

#### 2.3.1.3   Lignin assay

The quantification of lignin was obtained with an acetyl bromide (AcBr) assay. 5 mg of AIR was transferred into a glass tube with a Teflon-coated lid, and 5 ml of AcBr reagent (20% AcBr (v/v) in glacial acetic acid) was added. 5 ml of AcBr reagent was added to an empty tube as a blank. The tubes were incubated at 50°C for 3 h in a heat block with mixing by vortex every 15 min. The reaction was stopped by cooling the samples in an ice bath for 5 min. 1 ml of the sample mix was transferred to a 10 ml volumetric flask containing 2.4 ml of glacial acetic acid and 1 ml of 2 M NaOH. The solution was mixed by gentle inversion and then 0.1 ml of 7.5 M hydroxylamine-HCl was added. The volume was then brought to 10 ml using glacial acetic acid. A Shimadzu UV-2401 spectrophotometer (Shimadzu Corp., Kyoto, Japan) was used to measure the absorbance of the sample at 280 nm against a blank that had been treated the same as the samples.

**2.3.1.4 Lignin pyrolysis-GC-MS**

The lignin pyrolysis-GC-MS analysis was carried out according to (Sundheq et al., 1996) using a Pyrola 2000 filament pulse pyrolizer with an autosampler unit. ~100 µg of powdered carrot sample was put on a platinum filament, with a drop of acetone to keep it in place. The pyrolysis took place in a helium atmosphere at 600°C for 2 s. The results were analysed using an Agilent Technologies 7890B gas chromatography system and an Agilent Technologies 5977B Single Quadrupole mass spectrometer. The pyrolysis used the following conditions: oven temperature: 50°C, 30 s; 8°C/min → 300°C; 300°C, 6 min; Column: HP-5MS 5% phenyl methyl silox, internal diameter 250 µm, length 30 m, film thickness 0.25 µm.

## 2.3.2 Carbohydrate analysis

The carbohydrate analysis was carried out according to (Sundheq et al., 1996). Pre-extraction was carried out using 70% (v/v) ethanol and acetone. The calibration solution contained 0.1 mg/mL of arabinose (Ara), glucose (Glc), glucuronic acid (GlcA), galactose (Gal), galacturonic acid (GalA), 4-O-methyl glucuronic acid (4-O-Me-GlcA), mannose (Man), rhamnose (Rha) and xylose (Xyl) in methanol. 4 mg of ground carrot was placed in a pear-shaped, pressure resistant flask. 1 ml calibration solution was dried by evaporation and treated the same way. 2 ml of 2 M solution of HCl in anhydrous MeOH was added and this was incubated for 5 h at 105°C. Once cooled to room temperature, the solution was neutralised with 80 µl pyridine, and the flask was shaken well. The internal standard contained 0.1 mg/ml resorcinol in methanol. 4 ml internal standard was added, and the flask shaken again. A 1 ml aliquot of the solution was evaporated using $N_2$. A solution containing 70 µl trimethylsiyl (TMCS), 150 µl hexamethyl disilazane (HMDS) and 120 µl pyridine was used to silylate the dried sample at room temperature overnight. These samples were analysed using GC/FID (Shimadzu GC-2010, Kyoto, Japan) with a HP-1 Column (25 mm x 0.2 mm I.d., film thickness 0.11 µm). The temperature profile was as follows: 100°C -> 175°C, 4°C/min, 175°C -> 290°C, 12°C/min. The temperature of the injector was 260°C and the temperature of the detector was 290°C. Correction factors were used to calculate carbohydrate content; Man, Glc and Gal 0.9,

Ara and Xyl 0.88, Rha 0.89, GlcA, GalA and 4-O-Me-GlcA 0.91. Two replicates were used in all analyses.

### 2.3.3   Pigment analysis

#### 2.3.3.1   Extraction of carotenoids

50 mg of ground freeze-dried carrot tissue was added to 300 µl methanol, along with an internal standard (8-apo-carotenoid) and mixed by vortex for 1 min. 300 µl TRIS-HCl (50 mM, pH 7.5) (containing 1 M NaCl) was then added and the mixture incubated on ice for 10 min. 800 µl chloroform was added and samples incubated on ice for a further 10 min. Samples were then centrifuged at 3000 g for 5 min at 4°C, causing a clear partition to form. The hypophase was removed and the aqueous phase re-extracted with 80 µl chloroform. The pooled chloroform extracts were dried by centrifugal evaporation for 15 – 20 min. Dried residues were stored under an atmosphere of nitrogen at -20°C prior to analysis by high performance liquid chromatography (HPLC).

Dried carotenoid extracts were re-dissolved in 1 ml of methanolic potassium hydroxide (10% w/v in 100% methanol) and stored overnight, in the dark at 4°C under nitrogen. Extracts were then mixed by vortex for 1 min and centrifuged at 3000 g for 5 min at 4°C. Samples were transferred into 15 ml falcon tubes, and 2 ml of degassed diethyl ether added along with enough saturated NaCl to form two phases (approximately 1 ml). The top phase was transferred to new 15 ml falcon tubes and washed with 2 ml sterile distilled water. The top phase was then transferred into fresh 2 ml Eppendorf tubes, dried under a gentle stream of oxygen-free nitrogen (adapted from (Britton, 1985) and resuspended in 200 µl ethyl acetate.

#### 2.3.3.2   Carotenoid analysis (HPLC)

A reverse-phase C30 5 µm column (250 x 4.6 mm) (YMC Carotenoid, No. 0425093417), which was maintained at 25°C, was coupled with a 20 x 4.6 mm C30 guard (YMC Inc. Wilmington, NC, USA). Mobile phases consisted of methanol (A), water methanol (20:80% v/v) containing 0.2% ammonium acetate (B) and tert-methyl butyl ether (C) was used. The gradient elution used with this column was 95% A, 5% B for 12 min, then a step to 80% A, 5% B, 15% C at 12 min followed by a linear gradient to 30% A, 5% B, 65% C by 30

min. A 30-60 min conditioning phase was then used to return the column to the initial concentrations of A and B.

## 2.4  Targeted metabolomics

### 2.4.1  Metabolite analysis (HPLC-MS)

1 ml of the following solution was added to 50 mg of ground freeze-dried carrot tissue: 80% methanol (95 ml), morin 500 ppm in methanol (5 ml) and formic acid (0.5 ml), which was then mixed by vortex for 1 min. Samples were placed in an end-over-end mixer in $4^O$C for 30 min. Samples were then centrifuged at 14,000 g for 10 min at $4^O$C and the supernatant moved to a new tube. 500 μl of supernatant was dried using centrifugal evaporation (2-3 h), and the remaining 500 μl was filtered using a standard filter vial (standard filter vial 0.45 μm PTFE, w/pre-slit blue cap 100/Pk). 200 μl of filtered supernatant was transferred into fresh vials. 100 μl of each filtered sample was combined to form a quality control (QC) sample. Samples were then placed in a Dionex U3000 UHPLC and Thermo LTQ-OrbitrapXL MS system (Thermo-Fisher Ltd. Hemel Hempstead U.K) combination.

The LTQ-OrbitrapXL MS system was first calibrated in positive and negative electrospray ionisation (ESI) modes. All samples were stored at $10^O$C and were analysed in negative and positive ESI modes separately. Samples were profiled in full scan mode at resolution 30,000 (one scan every 0.4 s) and were analysed in a randomised order with the QC sample being analysed multiple times intermittently between other samples.

Solvent A, HPLC grade water (JT Baker, PN 4218), and solvent B, HPLC grade acetonitrile (JT Baker, PN 9012) were acidified with 0.1% [v/v] Ultima mass spectrometry grade formic acid (Fisher Scientific Ltd. U.K., P/N A117-50). Prior to sample analysis a new HPLC column was conditioned with solvents A and B for a minimum of 50 min at a flow rate of 300 μL/min, starting with 100% B for 20 min, 50% B, 50% A for 20 min, 2% B, 98% A for 10 min. The HPLC gradient programme was as follows: hold 98% A 0-2 min, 98-95% A 2-5 min, 95-55% A 5-25 min, 55% A - 100% B 25-26 min, hold 100% B 26-29 min, 100% B – 98% A 26-30 min, hold 98% A 30-35 min. After each sample analysis, the HPLC system

was equilibrated with the initial gradient solvent conditions for a minimum of 5 min prior to the analysis of the next sample. The syringe and lines were washed with 80% HPLC grade acetonitrile (JT Baker, PN 9012) 20% HPLC grade water (JT Baker PN 4218) between each sample.

Since the QC samples are analysed multiple times with high frequency throughout the analytical sequence, they provide a measure of analytical performance and errors, without the need to analyse each individual sample in duplicate or triplicate. The QC samples analysed throughout the entire sequence are applied to quality assure each target peak. A high-quality peak shows an error of lower than 10-20% standard deviation (SD) across all QC and reference samples throughout the sequence. Only quality assured peaks were provided for statistical analysis and modelling.

## 2.4.2 Metabolite analysis (GC-MS)

Carrot samples were freeze-dried for 48 h. A Gamma 1-16 LSC freeze drier (Martin Christ Gefriertrocknungsanlagen GmbH, Germany) was used to lyophilise the samples at a pressure of 0.7 mbar with a shelf temperature of 25°C and a condenser temp of -50°C. All glassware was washed with water, methanol: water (3:1) and chloroform: methanol (2:1) prior to use. Tubes used for derivatizing non-polar extracts were additionally washed with isohexane. To extract and derivatize polar and non-polar metabolites from freeze-dried samples, sequential extraction with methanol, chloroform and water, and the presence of ribitol and nonadecanoic acid methyl ester as internal standards were used. Following phase separation of the extraction medium, polar and non-polar compounds were transferred to separate amber vials. The extraction protocol is described in detail below.

### 2.4.2.1 Retention standard

More than 5 ml of the following *n*-alkanes were prepared separately in isohexane in glass test tubes: eicosane (C20), tetracosane (C24), triacontane (C30), tetratriacontane (C34) and octatriacontane (C38) each at 2 mg ml-1; undecane (C11) and tridecane (C13) at 27 µl in 10 ml; hexadecane (C16) at 26 µl in 10 ml. 5 ml of each solution were transferred to a 50 ml volumetric flask and the volume made up with isohexane.

### 2.4.2.2 Extraction of polar and non-polar fractions

100 mg of freeze-dried sample was weighed directly into a tared culture tube (150 x 16 mm). 3 ml of methanol was added to each tube, which were then shaken on a vortex-type shaker at 1500 rev min$^{-1}$ for 30 min at 30$^O$C in an incubator. 100 μl of ribitol (polar standard, 2 mg ml$^{-1}$ in water) and *n*-nonadecanoic acid methyl ester (non-polar standard, 0.2 mg ml$^{-1}$ in methanol) internal standards and 0.75 ml distilled water were added to samples, which were then shaken at 1500 rev min-1 for 30 min at 30$^O$C in an incubator. Then, 6 ml chloroform was added to the samples, which were again shaken at 2500 rev min$^{-1}$ for 30 min at 30$^O$C in an incubator. Finally, 1.5 ml distilled water was added, the mixtures vigorously shaken by hand, and then spun by centrifuge at 1200 rpm for 10 min to separate polar and non-polar phases. Using a Pasteur pipette, the polar (upper) and non-polar (lower) fractions were transferred to separate amber vials and stored at -20 $^O$C overnight.

### 2.4.2.3 Derivatization of polar fraction

The polar extracts were taken from the freezer and allowed to warm to room temperature, then 250 μl was pipetted to culture tubes and dried in a centrifugal evaporator without heating. 80 μl methoxylamine hydrochloride (20 mg ml$^{-1}$ methoxylamine hydrochloride in anhydrous pyridine) was added to each dry sample, which were then heated to 50$^O$C in an incubator for 4 h. 50 μl retention standard mixture (detailed above) was added to amber autosampler vials (300 μl fixed glass inserts with PTFE coated snap caps) and allowed to evaporate at room temperature. Using a 100 μl glass syringe, 80 μl of N-methyl, N-trimethylsilyl trifluoroacetamide (MSTFA) was added to each sample and then heated to 37$^O$C in an incubator for 30 min. 40 μl of the derivatized polar fractions and 40 μl dry pyridine were then added to amber autosampler vials that had held the retention standard mixture. The polar fractions were then ready for GC-MS analysis.

### 2.4.2.4 Derivatization of non-polar fraction

The non-polar extracts were dried in a centrifugal evaporator (for approximately 30 min, no heating, pulsing), then 1 ml chloroform and 2 ml 1% methanolic sulphuric acid was added to each sample and heated at 50 $^O$C for 16 h. Samples were cooled to room temperature and 5 ml of 5% (w/v) aqueous sodium chloride and 3 ml chloroform was

added to each tube, which was shaken vigorously and given time to let the polar and non-polar layers separate. The top aqueous layer was discarded and 3 ml of 2% (w/v) aqueous potassium hydrogen carbonate was added to the lower chloroform:methanol layer, shaken vigorously and layers given time to separate. The top aqueous layer was discarded and the remaining lower chloroform:methanol layer was pipetted through columns of anhydrous sodium sulphate (approximately 3 cm of anhydrous sodium sulphate, Pasteur pipettes plugged with cotton wool and prewashed with 4 ml chloroform) and collected in culture tubes. 2 ml chloroform was passed through the columns and collected with the extracts, which were then dried in a centrifugal evaporator at room temperature. Then, 50 $\mu$l chloroform, 10 $\mu$l anhydrous pyridine and 40 $\mu$l MSTFA were added, and the extracts were heated at 37 $^{O}$C in an incubator for 30 min. 50 $\mu$l retention standard mixture (detailed above) was added to amber autosampler vials (300 $\mu$l fixed glass inserts with PTFE coated snap caps) and allowed to evaporate at room temperature. Finally, 40 $\mu$l of the derived non-polar fraction and 40 $\mu$l anhydrous pyridine were added to the amber autosampler vials that had held the retention standard mixture. The non-polar fractions were then ready for GC-MS analysis.

### 2.4.2.5  Sample analysis

Samples were analysed using a DSQ II Single Quadrupole GC-MS system (Thermo). Using a split ratio of 40:1, 1 $\mu$l of the sample was injected into a programmable temperature vaporising injector set to the following conditions: injection temperature was 132 $^{O}$C for 1 min, transfer rate was 14.5 $^{O}$C/s, transfer temperature was 320 $^{O}$C for 1 min, clean rate was 14.5 $^{O}$C/s and clean temperature was 400 $^{O}$C for 2 min. Analytes were chromatographed on a DB5-MS™ column (15 m x 0.25 mm x 0.25 $\mu$m; J&W, Folsom, USA) using helium at 1.5 ml/min in constant flow mode as the mobile phase. The temperature gradient was 100 $^{O}$C for 2.1 min, 25 $^{O}$C /min to 320 $^{O}$C, and isothermal for 3.5 mins. The interface temperature was 250 $^{O}$C. Mass data were acquired at 70 eV electron impact ionization conditions over a 35 – 900 a.m.u (atomic mass units/Daltons) mass range at 6 scans per sec with a source temperature 200 $^{O}$C and a solvent delay of 1.3 min. Acquisition rates were set to give approximately ten data points across a chromatographic peak. The software packages Xcalibur™ v1.4 and Xcalibur™ v2.0.7 were used to acquire and analyse the data, respectively. A processing method

developed at the James Hutton Institute was used to assign identities to the peaks using the retention times and mass spectra of known standards and the Genesis algorithm (part of the XcaliburTM package) for peak integration. The expected retention time for each peak was adjusted using the retention times of the retention standards. The integrated area of the annotated peaks were normalised against the integrated area of the respective internal standards, ribitol and nonadecanoic acid for the polar and non-polar fraction, respectively. The peak area ratios were normalised on a dry weight basis. Statistical analysis for metabolite data was performed with 2-way analysis of variance (ANOVA) with a p-value of <0.05.

## 2.5 Transcript analysis

### 2.5.1 RNA extraction methods

Total RNA was extracted from carrot tissue that was frozen immediately in liquid nitrogen and kept at -80 $^O$C until used. 3 samples from both the orange region (CT) of healthy batons and the blackened region of blackened batons (B) were used for RNA extraction. For the purpose of RNA sequencing additionally the orange region directly bordering the blackened region (M) was also used, with three biological replicates each. The RNA extraction methods listed below were all used to determine which would allow for extraction of pure high-quality RNA. Pestles, mortars, tubes and tips were all treated with RNase AWAY™, cleaned with ethanol and autoclaved for sterilisation. Buffers not provided in kits were treated with 0.1% diethyl pyrocarbonate (DEPC, Sigma-Aldrich, USA).

#### 2.5.1.1 Qiagen RNeasy Plant Mini Kit

RNA was extracted from 100 mg of frozen ground carrot material using the RNeasy® Plant Mini kit (Qiagen, Germany) as per the manufacturer's protocol.

#### 2.5.1.2 Qiagen RNeasy Plant Mini Kit + Fruit-mate™

100 mg of frozen ground carrot material and 1 ml of Fruit-mate (Takara, Japan) was placed in a 1.5 ml tube and mixed by vortex and immediately centrifuged at 12,000 x g for 5 min at 4$^O$C. The supernatant was transferred to new 1.5 ml tubes. RNA was then

extracted using the RNeasy® Plant Mini kit (Qiagen, Germany) as per the manufacturer's protocol. The RNA was finally eluted with 20 µl RNase-free water.

### 2.5.1.3   TRIzol™ Reagent

A modified method of RNA extraction was used based on (Chauhan et al., 2018)'s described method. 1 ml of TRIzol™ Reagent (Invitrogen, USA) was added to 100 mg of frozen ground carrot material, incubated for 5 min at room temperature, then inverted and mixed well by vortex. 200 µl of chloroform was added and incubated for a further 3 min. Samples were then centrifuged for 15 min at 12,000 x g at 4$^O$C. The aqueous phase was transferred to new tubes and 500 µl isopropanol was added and allowed to incubated overnight at -80 $^O$C. Samples were then allowed to melt on ice and centrifuged for 10 min at 12,000 x g at 4$^O$C before the supernatant was discarded leaving RNA pellets. These pellets were washed using 80% ethanol and air-dried in a fume hood for 10 min. The RNA was finally eluted with 20 µl RNase-free water.

### 2.5.1.4   TRIzol™ Reagent + RNA Clean & Concentrator™ - 5

RNA pellets were obtained as described in the previous method but were instead cleaned using the RNA Clean & Concentrator™-5 kit (Zymo Research, USA) following the manufacturer's instructions. The RNA was finally eluted with 20 µl RNase-free water.

### 2.5.1.5   CTAB

RNA was extracted using an adapted method originally described by (Chang et al., 1993, p.199). 100 mg of frozen ground carrot material was quickly added to 500 µl extraction buffer (2% CTAB (cetyltrimethylammonium bromide), 2% PVP (polyvinylpyrrolidone), 100 mM Tris-HCl pH 8, 25 mM EDTA, 2 M NaCl, 0.5 g/L spermidine, 2% beta-mercaptoethanol) previously warmed to 65$^O$C in an oven. Samples were inverted and mixed well by vortex. An equal volume of chloroform:isoamyl alcohol (24:1) was added, mixed by vortex and centrifuged at 12,000 x g for 15 min. The supernatant was transferred to new tubes and again an equal volume of chloroform:isoamyl alcohol (24:1) was added, samples mixed by vortex and then centrifuged at 12,000 x g for 15 min. The supernatant was transferred to new tubes and ¼ volume of 10 M lithium chloride (LiCl) was added and mixed by vortex before the RNA was allowed to precipitated overnight at 4$^O$C. Samples were centrifuged for 20 min at 4$^O$C at 12,000 x g and the supernatant removed, leaving an RNA pellet. These pellets were washed with 2 ml 75% ethanol,

mixed by vortex, and centrifuged at 4$^O$C at 12,000 x g for 10 min. The supernatant was discarded, and samples were air-dried in a fume hood for 10 min. The RNA was finally eluted with 20 µl RNase-free water.

### 2.5.1.6 CTAB + RNA Clean & Concentrator™ - 5

The RNA pellets were obtained as described in the previous method but were instead cleaned using the RNA Clean & Concentrator™-5 kit (Zymo Research, USA) following the manufacturer's instructions. The RNA was finally eluted with 20 µl RNase-free water.

### 2.5.2   Quantitative and qualitative analyses of RNA

A quantitative analysis of the RNA was carried out using a Nanodrop ND-1000 Spectrophotometer (Thermo Scientific, USA). Qualitative analysis was conducted using a non-denaturing agarose gel electrophoresis. Agarose powder (1%) (Invitrogen, US) was dissolved in 1 x Tris-acetate-EDTA (TAE) buffer (100 ml, pH 8) taken from 50 x TAE stock solution (242 g Tris base, 100 ml 0.5 M EDTA pH 8, 57.1 ml Acetic acid). 3 µl SYBR safe (Life Technologies, Paisley, UK) was added to the solution after being heated by microwave. Samples (12 µl) were loaded into each well alongside one well containing an RNA ladder (Fisher Scientific, Loughborough, UK). The gel electrophoresis ran for 40 min at 70V in 1x TAE buffer. The agarose gel was viewed and photographed under a INGENIUS gel imager (Syngene, Cambridge, UK) to assess total RNA band integrity.

### 2.5.3   RNA sequencing and analysis

RNA samples from blackened carrot regions, orange regions immediately bordering the blackened regions, and orange carrot batons extracted using the CTAB + RNA Clean & Concentrator™-5 kit method (section 2.5.7) were stored at -80 $^O$C before being sent for RNA-seq. Three biological replicates were used per carrot region. The RNA sequencing procedure was carried out by Carolina Lascelles, and the data extraction and processing, quality control analysis and initial statistical analysis was carried out by Ian Carr at the Next Generation Sequencing Facility at St James's Hospital, University of Leeds, UK. The GO analysis was carried out by Gabriela Machaj at the University of Agriculture in Krakow, Poland.

The quality and quantity of the total RNA samples was determined using a Tapestation (Agilent) before been used to create Illumina compatible sequencing libraries using the Illumina TruSeq Stranded Total RNA-with Ribo-Zero Plant kit. The libraries were checked for adaptor dimers and insert size on a Tapestation (Agilent) and quantified using the Qubit system, before creating an equimolar pool of libraries which was sequenced on a NextSeq 500 75 bp single end lane. Sequence data in Fastq format were quality-checked using FastQC software (Andrews, 2010). Cutadapt software (Martin, 2011) was used to trim poor quality bases (Phred quality score < 20) and contaminating adapter sequences from raw reads. Reads trimmed to fewer than 30 nucleotides were discarded. Reads were aligned to a *Daucus carota* genome reference mitochondrial and plastid sequences ((Iorizzo et al., 2016), Genebank link - https://www.ncbi.nlm.nih.gov/assembly/GCF_001625215.1/), using the splicing-aware STAR aligner (Dobin et al., 2013), with reference known splice junctions obtained supplied in GTF file format. The resulting alignments in BAM file format were checked for quality using QualiMap software (Okonechnikov et al., 2016) and Picard tools (Wysoker et al., 2013), with Picard tools also used to mark PCR/Optical duplicate alignments. BAM files were indexed using Samtools software (Li et al., 2009) and visualised using IGV browser (Robinson et al., 2011) to check for genomic DNA contamination and the presence of PCR duplicates.

Bioconductor R package RSubread (Liao et al., 2019) was used to extract raw sequenced fragment counts per transcript using the genome annotation dataset used by STAR during alignment. Multi-mapping read pairs were counted as a fraction of all equivalent alignments. Read count data was generated with the inclusion of reads marked as PCR/optical duplicates. Read count data with filtered such that to be retained a transcript must be linked to more than 3 reads in at least 3 samples. The read count data was normalized for library size before been used to generate PCA plots using the R package plotPCA and visualized using the R graphics package ggplot to check for sample outliers.

Differentially expressed transcripts were determined using DeSeq2 (Love et al., 2014). To account for the effects of multiple testing the statistical significance was adjusted for multiple testing using the Benjamini-Hotchberg method as implemented by DeSeq2.

Differentially expressed genes were identified as those with an adjusted p value of less than 0.05. Data for the differentially expressed genes was exported to a data frame for further analysis. The expression profile of each of the samples for the differentially expressed genes was visualized using the R package pheatmap to produce a clustered heat map of the $log_2$ normalised read count values for the differentially expressed genes. To highlight the differences between samples the colour scaling was performed at the level of each transcript. Analysis and visualization of Gene Ontology terms was made in Cytoscape with ClueGO v.2.5.7 (Bindea et al., 2009) plug-in based on the functional annotation of all carrot genes provided by (Machaj and Grzebelus, 2021).

# Chapter III

# Chapter 3: The influence of age, geography and environmental factors on carrot blackening

## 3.1   Introduction

The studies described in this thesis were undertaken in collaboration with Kettle Produce Ltd, who provided all of the carrot samples. Kettle Produce Ltd is a vegetable producer primarily based in Scotland that works in partnership with over 50 farmers. In 2020, Kettle Produce Ltd had 141 fields throughout Scotland specifically dedicated to growing carrots. These carrots roots are harvested and sold to consumers as either whole carrots, cut carrots or in prepared products, such as vegetable soups. Kettle Produce Ltd identified the problem of blackening in cut carrot produce, primarily carrot batons in 2015 and the severity of blackening has since increased. The company were therefore keen to discover the biological causes of this serious issue.

Carrot seeds are sown throughout April-May each year. The roots take 3-4 months to grow to an acceptable size and so harvesting begins in July. Once harvested, the carrots are transported to Kettle Produce Ltd's Orkie factory, where they are washed and then graded by size. Larger carrots are separated and cut into baton shapes before being packaged and sent to shops all around the UK. From mid-winter (October-December) the carrot fields are covered in several feet of straw protected by several layers of plastic tarpaulin to protect against frost, pests, and disease. Towards the end of the storage period, some of the harvested carrots are over 1 year old, with a maximum of ~16 months old. The blackening of cut carrots is seen only between January and June when the harvested carrots are between 10 and 15 months old.

Kettle Produce Ltd carried out a trial in May-August 2020 to investigate potential causes of carrot blackening. The trial involved 35 batches of harvested carrots from 18 fields located throughout Scotland, owned by 6 different farmers. These carrots were washed, processed, and cut into batons. Samples of batons were taken and the percentage of carrot blackening was recorded on the day of processing (day 0) and on each of the following 3 days (day 1, 2, and 3). Kettle Produce Ltd also routinely recorded the environmental conditions of the vegetable fields next to their head office at Balmalcolm,

Scotland. These data were taken to represent the environmental conditions in all the carrot fields throughout Scotland because the majority of fields were located within approximately 50 miles of Balmalcolm. The environmental parameters measured include air temperature, soil temperature, solar radiation, and rainfall.

The 2020 summer trial data collected by Kettle Produce Ltd are analysed in this chapter, with the aim of identifying any relationships between observed degree of blackening, carrot age and the growth environment in terms of field location etc.

## 3.2 Results

Data concerning the growth environment was collected in the vegetable fields next to the Balmalcolm site. In total 35 batches of carrots were collected between May and August 2020 from different fields and farms throughout Scotland. The rate of carrot blackening was monitored from the day of processing (day 0) and for the following 3 days. Datasets were combined to calculate the degree of carrot blackening in each field, in order to identify any trends in carrot blackening. The following conclusions can be drawn from an analysis of these datasets.

### 3.2.1 Susceptibility to blackening increases with the age of the carrots at harvest

Data on blackening were analysed in relation to the farm of production, the fields in which the carrots were grown, and their geographical location (Table 3.1 and Figure 3.1). The approximate location of each field is marked on a map of Scotland provided by google maps (Figure 3.1). The field called 'Unknown' is not included in the map because the location was not specified. The farm containing each field is indicated after field name. Full names of the farmers are listed in Table 3.1. The fields have been numbered according to the level of carrot blackening reported in the carrots harvested from each field. The fields have also been colour-coded into quartiles indicating the total amount of carrot blackening recorded (Figures 3.1 and 3.2). Green indicates the highest quartile with 6-10% blackening, purple indicates the second highest quartile with 3.5-5% blackening, blue indicates the second lowest quartile with 2.4-3% blackening, and red indicates the lowest quartile with 0-2.1% blackening. The highest level of blackening recorded in this trial was 9.6% from the KPL field called Barnyards (1) (Figure 3.2). The lowest level of blackening was recorded in the BES field Besfield and the East Lathrisk (EL) field Unknown. These were the only fields, in which no blackening of cut carrots was reported.

Similar trends were observed in most fields. The highest level of blackening was recorded on either on the day of processing or within the first 24 h after processing. The level of new blackening recorded thereafter decreased progressively on days 2 and day 3 (Figure 3.3). These data show that the appearance of blackening is greatest within the first 24 hours of processing.

 The level of blackening reported was greatest in the oldest carrots at the time of harvest (Figure 3.4). Carrots harvested at or over 430 days old showed at least double the level of blackening than any other age range. Carrots less than 161 days old showed no blackening at all. Hence, the propensity to show blackening increases with the age of the carrot roots. One recommendation arising from the data shown in Figure 3.4 is that carrots over 400 days old should not be used for baton production.

The farmers, carrot fields and number of carrot batches harvested from each field are listed below:

| Table 3.1: Carrot collection data for the 2020 trials. | | | | |
|---|---|---|---|---|
| Farmer/Field owner | Number of carrot fields | Total number of carrot batches | Carrot field name | Number of carrot batches sampled |
| EAST LATHRISK (EL) | 3 | 6 | Powside | 4 |
| | | | Carslogie | 1 |
| | | | Unknown | 1 |
| BLACK HILLS (BH) | 2 | 4 | Mintlaw | 3 |
| | | | South Fornett | 1 |
| AA | 1 | 2 | Premney | 2 |
| MAXWELL (M) | 1 | 2 | Tilly Naught | 2 |
| BES | 1 | 1 | Besfield | 1 |
| KPL | 10 | 20 | Arthurstone 1 | 2 |
| | | | Nether Careston | 2 |
| | | | Corrie Wood | 1 |
| | | | Barnyards (1) | 1 |
| | | | Perth Airport | 3 |
| | | | New Grange | 2 |
| | | | Lochlands | 3 |
| | | | North Mains | 2 |
| | | | Barnyards (2) | 1 |
| | | | Hallyburton | 3 |
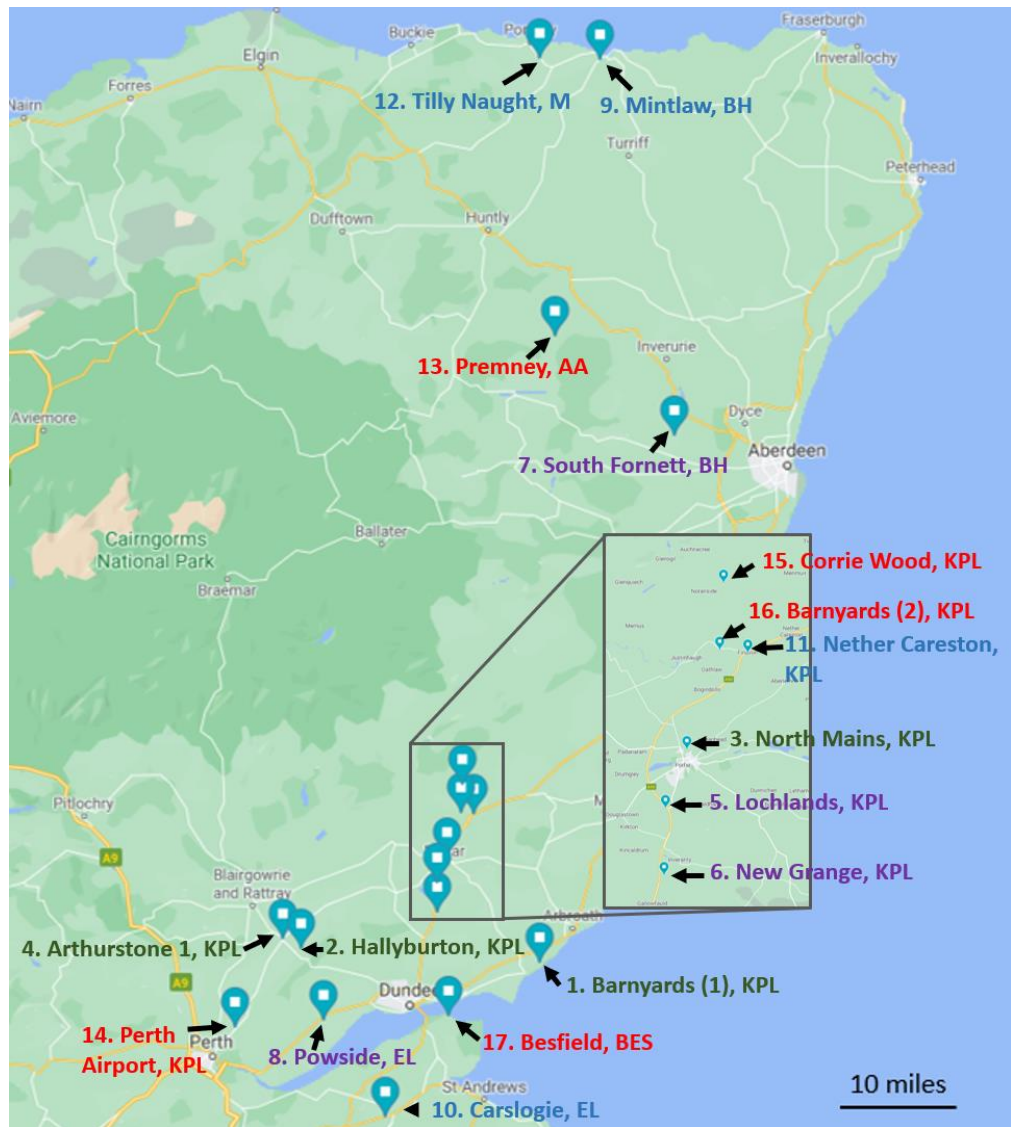
**Figure 3.1: Locations of the 17 carrot fields involved in the 2020 trial.** Fields are numbered according to the highest level of carrot blackening reported to the lowest. Fields are colour-coded in relation to Figure 3.2, to illustrate the total level of blackening in quartiles: green indicating the highest quartile, purple indicating the second highest quartile, blue indicating the second lowest quartile, and red indicating the lowest quartile. Ownership of each field is indicated after field name. Map made using Google Maps.
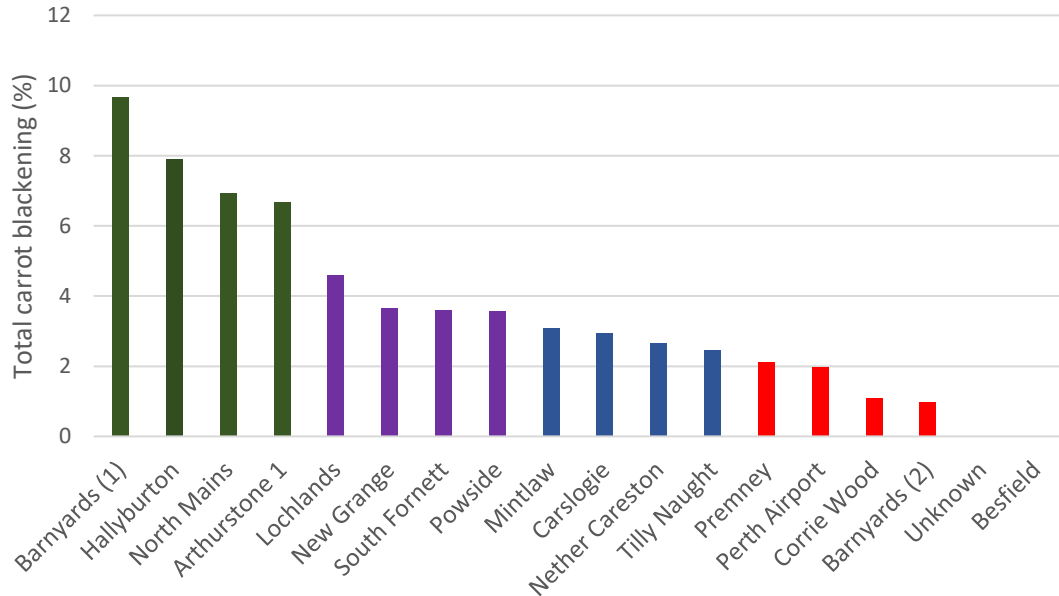
**Figure 3.2: Total carrot blackening reported in cut carrot harvested from the different field sites in 2020.** Levels of blackening are shown as a percentage of the total carrots after baton processing. Fields are colour-coded in relation to extent of blackening, showing total carrot blackening in quartiles: green indicating the highest quartile, purple indicating the second highest quartile, blue indicating the second lowest quartile, and red indicating the lowest quartile. The field called 'Unknown' is not included in the map due to its unknown location.
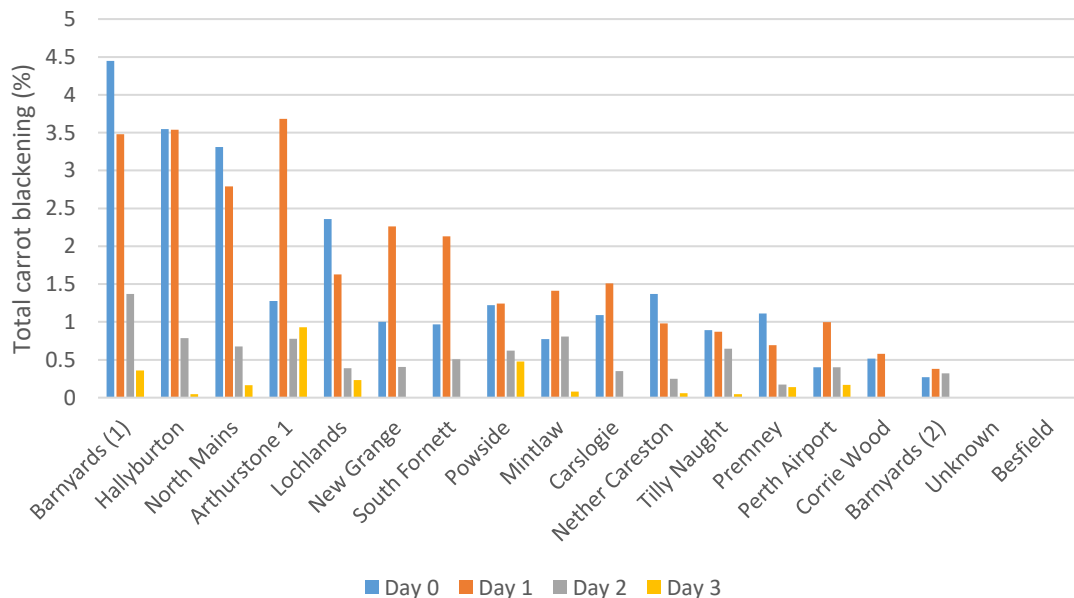


**Figure 3.3: A comparison of the levels of blackening reported on the first day (0) and 1, 2, and 3 days after processing.** Levels of blackening are shown as a percentage of the carrots on the day of baton processing and the following 3 days.
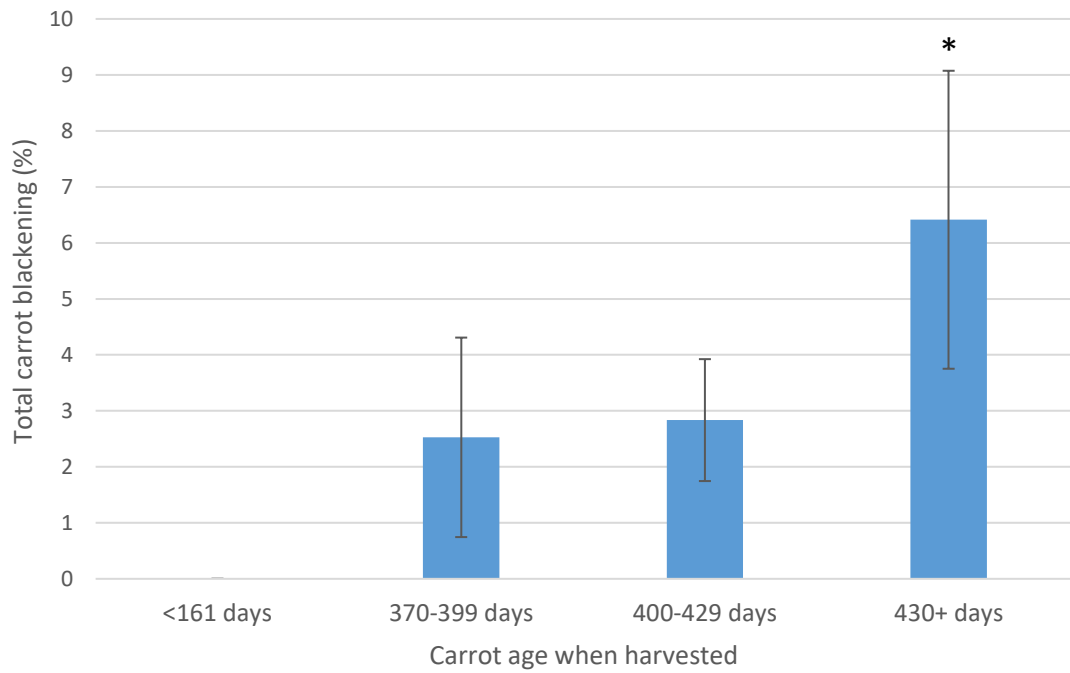
**Figure 3.4: The relationship between the reported level of blackening after processing and the age of the carrots at harvest.** The ages of the carrots at harvest have been grouped into 30-day batches. <161 days (n=2), 399-370 days (n=7), 429-400 days (n=4), 430+ days (n=5). Error bars are standard deviation. A T-test was used to calculate a P value of P=0.02 between the 400-429 day and 430+ day data.

### 3.2.2 Relationships between the geographical location of carrot production and susceptibility to blackening

To determine where the geographical location of carrot production has an impact on susceptibility to blackening, carrot fields were grouped and colour-coded according to their locations in Scotland: north (red), mid (yellow), or south (green) (Table 3.2 and Figure 3.5). An analysis of these data shows no significant difference in the rate of blackening seen in carrots harvested from the south or north of Scotland (Figure 3.6).

| Table 3.2: Carrot fields in the 2020 carrot blackening trial categorised by geographical location. | |
|---|---|
| Geographical location in Scotland | Field names |
| North | Tilly naught, Mintlaw, Premney, South Fornett |
| Mid | Nether Careston, Corrie Wood, Barnyards (2), New Grange, Lochlands, North Mains |
| South | Powside, Hallyburton, Carslogie, Barnyards (1), Perth Airport, Arthurstone 1, Besfield |
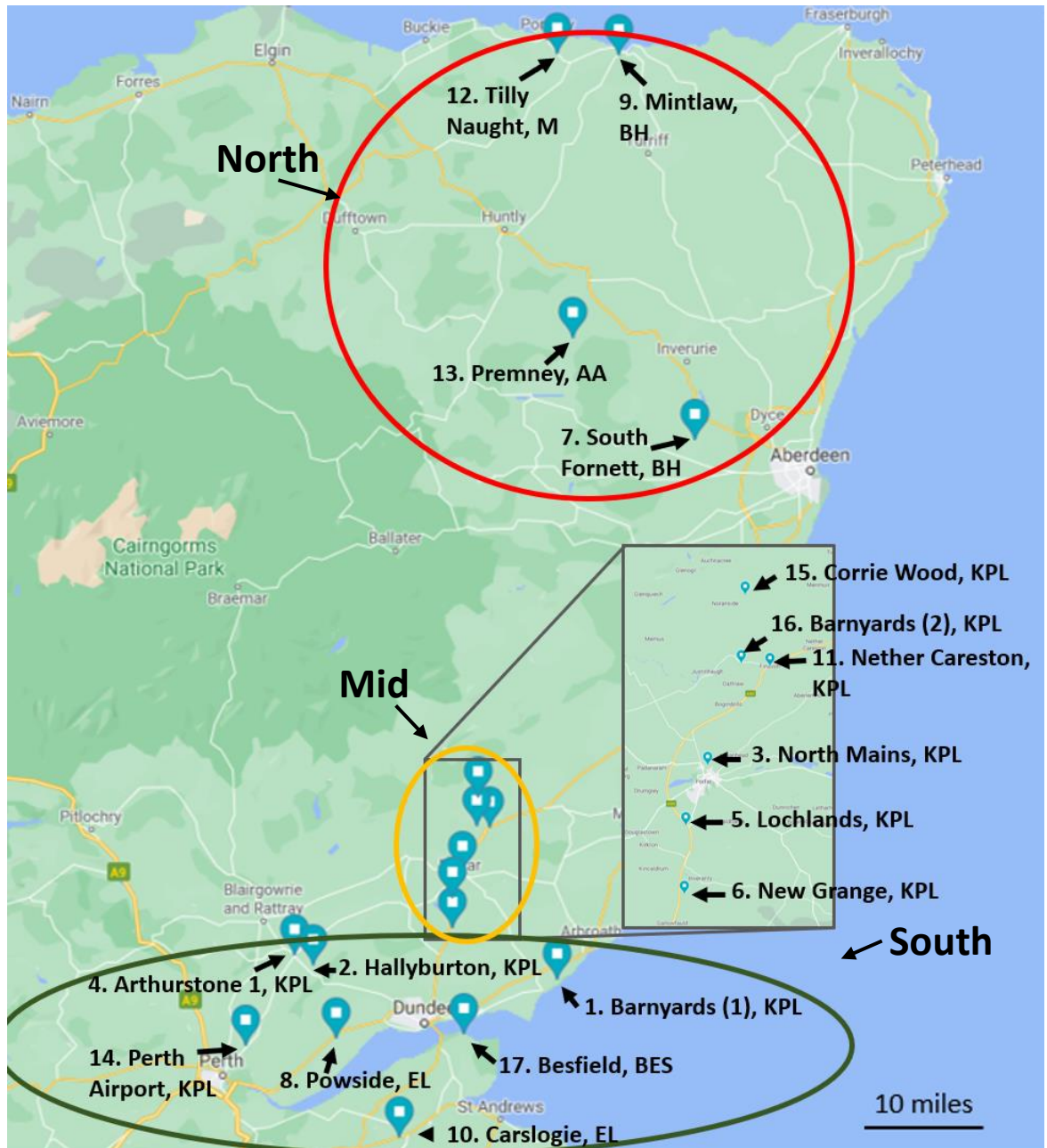
**Figure 3.5: Location of the carrot fields involved in the 2020 trial in Scotland. Field sites were divided into 3 locations: North, Mid, and South.** Fields are numbered according to the level of carrot blackening. Ownership of each field is indicated after field name. Categories are colour-coded in relation to Figure 3.5: red shows fields categorised as north, yellow shows fields categorised as mid, and green shows fields categorised as south. Map made using Google Maps.
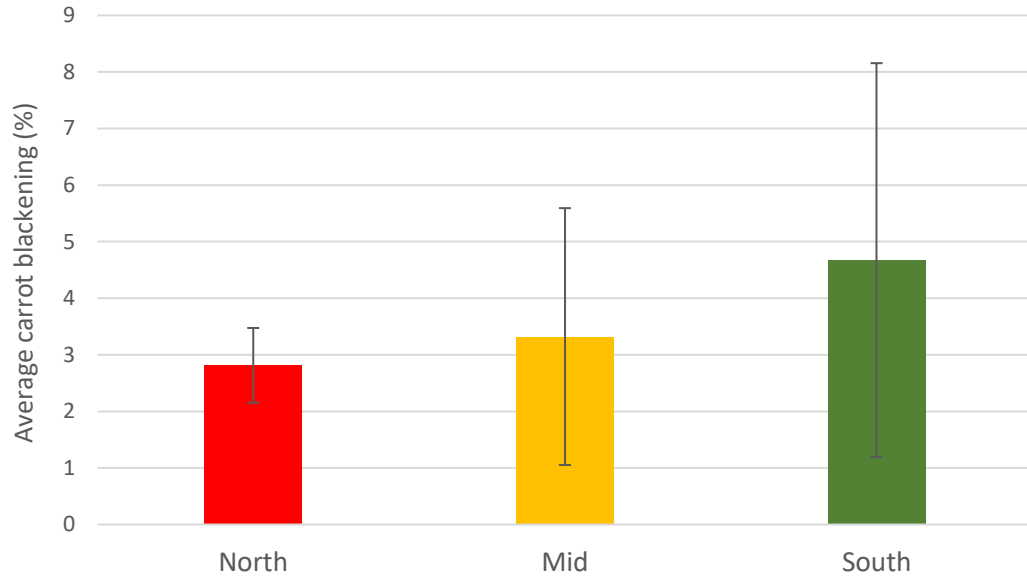
**Figure 3.6: The level of blackening expressed as a percentage observed in carrots harvested from fields located in the south, mid, and north of Scotland.** Reported levels of blackening from carrot fields located in the south (n=7), north (n=4), and middle (n=6) of Scotland. Categories are colour-coded in relation to Figure 3.4: red shows fields categorised as north, yellow shows fields categorised as mid, and green shows fields categorised as south. Data is the mean +/- standard deviation. A One-way ANOVA was used to calculate a P value of P=0.493.

### 3.2.3 The level of carrot blackening is related to the different field sites owned by KPL

The reported levels of carrot blackening were compared between the different fields owned by KPL to determine whether the levels of blackening were greater in some fields than in others. Data for 10 carrot fields were reported in the 2020 trial (Figure 3.7). The data shown in Figure 3.7 reveals that there was a large variation in the level of carrot blackening reported for each of the fields owned by KPL. The highest level of blackening (~10%) was reported for the fields at Barnyards (1) while the lowest level (~1%) was reported for the fields at Barnyards (2) (Figure 3.7). Assuming that the ages of the carrots harvested at the different sites were the same at the point of measurement then it is evident that the field location has a significant impact on susceptibility to blackening.

Statistical differences in the level of blackening was determined in fields located within ~15 miles of each other. The fields in Nether Coreston, Corrie Woods, and Barnyards (2) were classified as the Finavon area, while the fields in Lochlands, New Grange, and North Mains were classified as the Forfar area (Figure 3.8). The Forfar area showed the highest level of blackening at 5%. In contrast, the Finavon area only showed the lowest levels (~1.5%) of blackening (Figure 3.9).
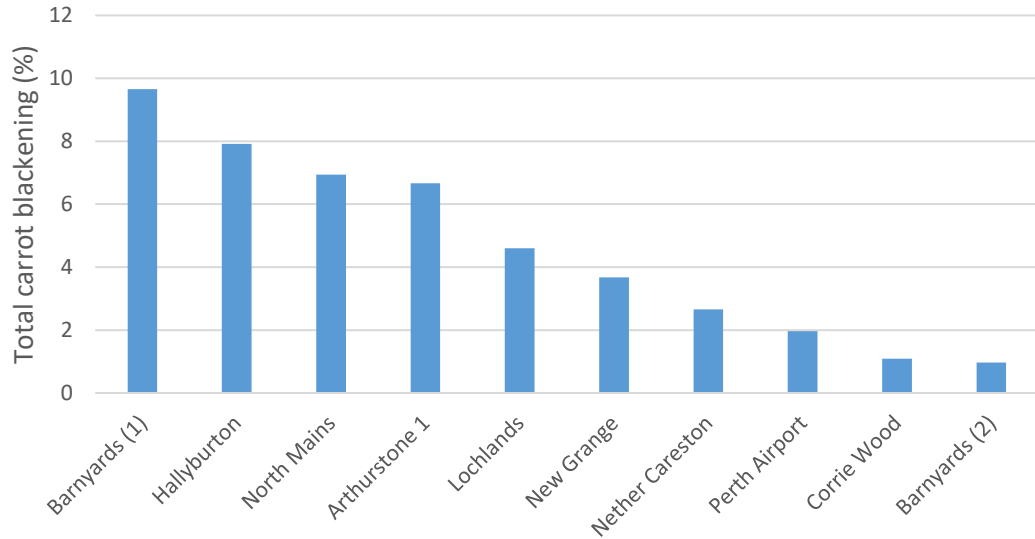
**Figure 3.7: The levels of blackening observed in carrot batons harvested from different KPL fields.** The levels of blackening reported for 10 different KPL fields (n=10).
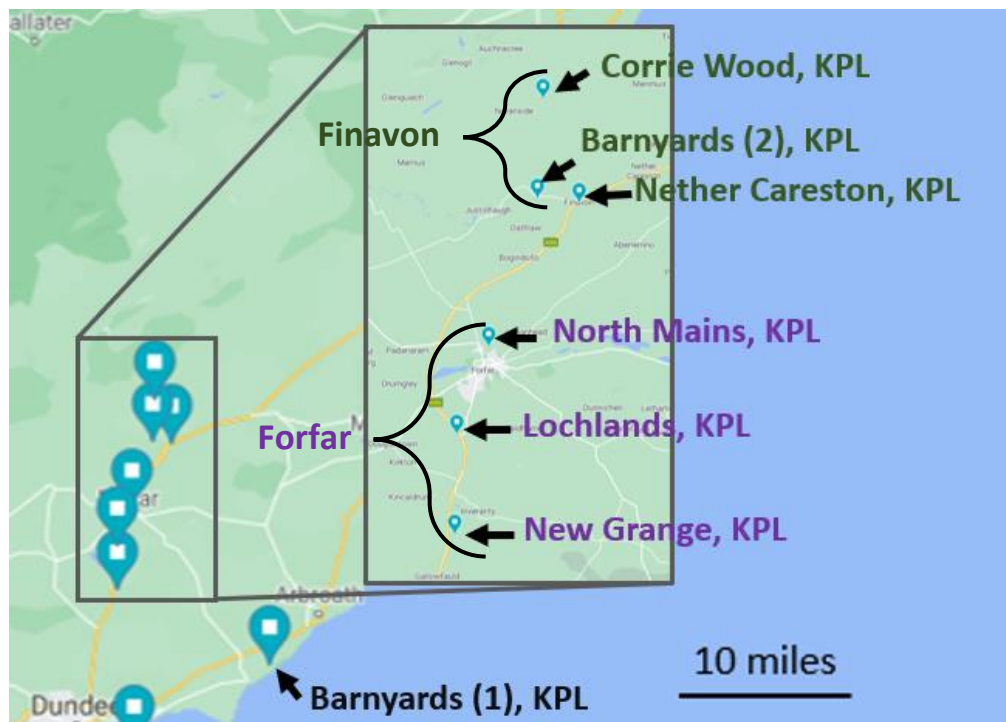


**Figure 3.8: Locations of KPL carrot fields.** Geographical locations of a cluster of carrot fields owned by KPL, divided into two groups. Nether Coreston, Corrie Woods, and Barnyards (2) were classified as the Finavon area shown in green. Lochlands, New Grange, and North Mains were classified as the Forfar area shown in purple. Map made using Google Maps.
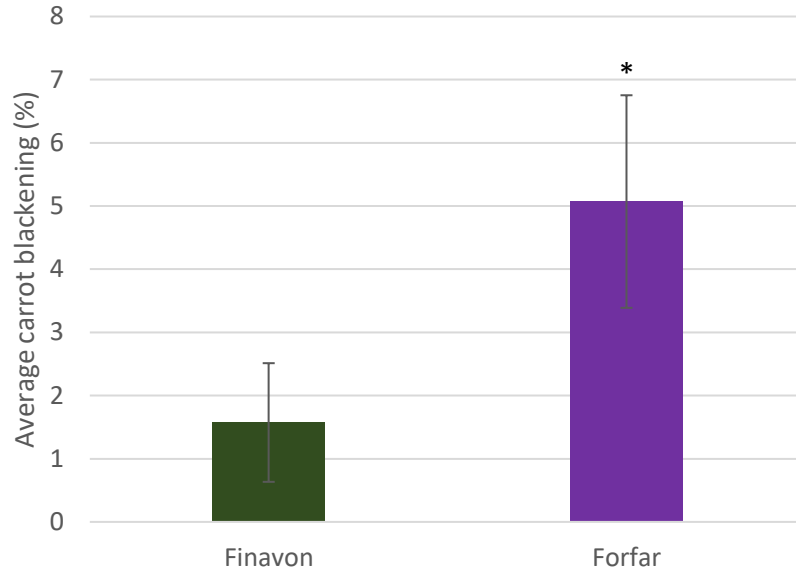
**Figure 3.9: The level of blackening reported for cut carrots harvested from fields in Finavon and Forfar.** The level of blackening was reported for carrots harvested from 6 geographical nearby carrot fields divided into those located in Finavon or in Forfar (n=3). Nether Coreston, Corrie Woods, and Barnyards (2) were classified as the Finavon area shown in green. Lochlands, New Grange, and North Mains were classified as the Forfar area shown in purple. Locations seen in Figure 3.8. Data is the mean +/- standard deviation. A T-test was used to calculate a P value of P=0.03.

### 3.2.4 Relationships between reported blackening and the growth environment

Air temperature, soil temperature, solar radiation and rainfall data were collected from the fields next to the Kettle Produce Ltd head office at Balmalcolm (Figure 3.10). These data were taken to represent the environmental conditions pertaining in the carrot fields throughout Scotland, as the majority of fields are located within approximately 50 miles of Balmalcolm. In addition, a 5-year data set was available that had been collected between 2006 and 2010, at a time before carrot blackening had been reported. This dataset was compared to the data collected between 2016 and 2020 i.e. the period when carrot blackening became a prominent issue.
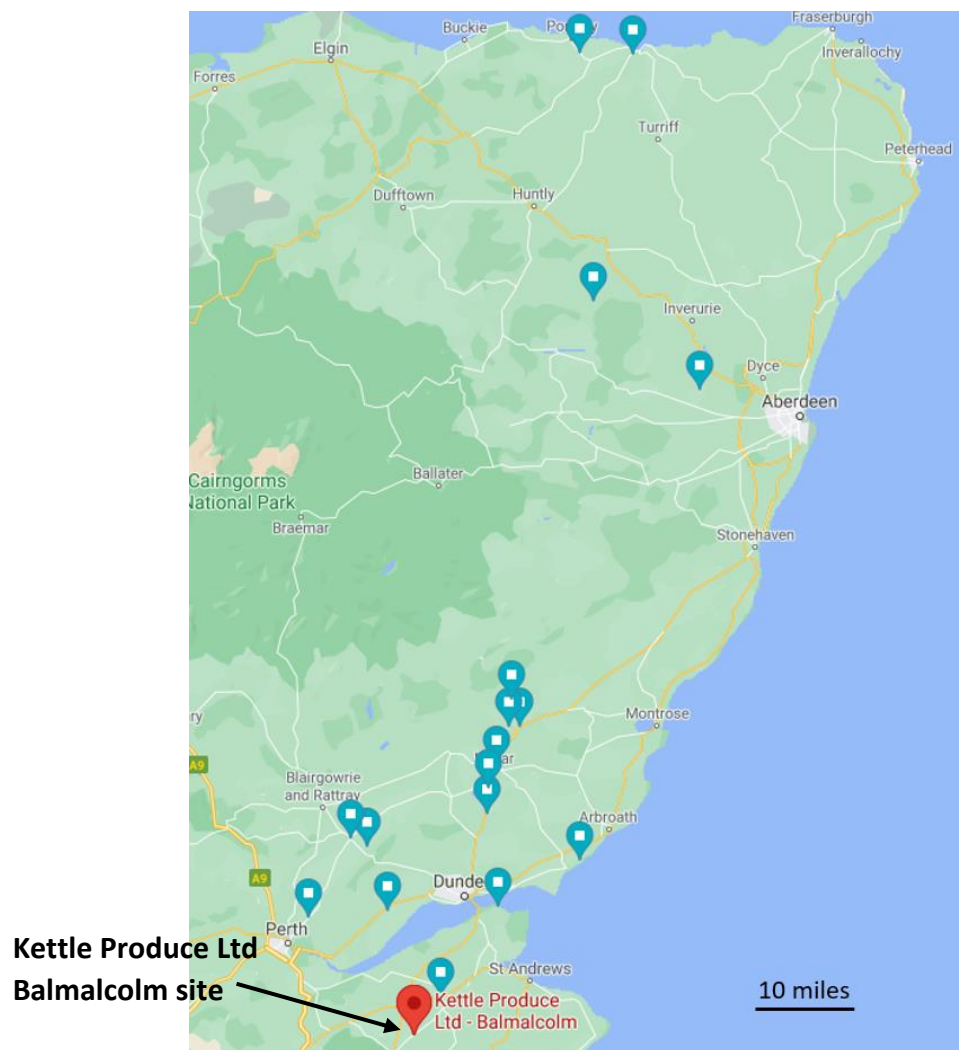


**Figure 3.10: The Kettle Produce Ltd Balmalcolm site and surrounding carrot fields involved in the 2020 trial.** Environmental conditions data were collected from a vegetable field next to the Balmalcolm site. Map made using Google Maps.

**Air Temperatures at the Balmalcolm site**

Air temperatures were similar in the 2006-2010 and 2016-2020 datasets, with comparable patterns of recorded monthly, minimum and maximum air temperatures (Figure 3.11 A, B, and C). The only notable differences are December and Janurary showing a general increase of ~2 degrees in recent years since the blackening was reported (Figure 3.11 A and B).
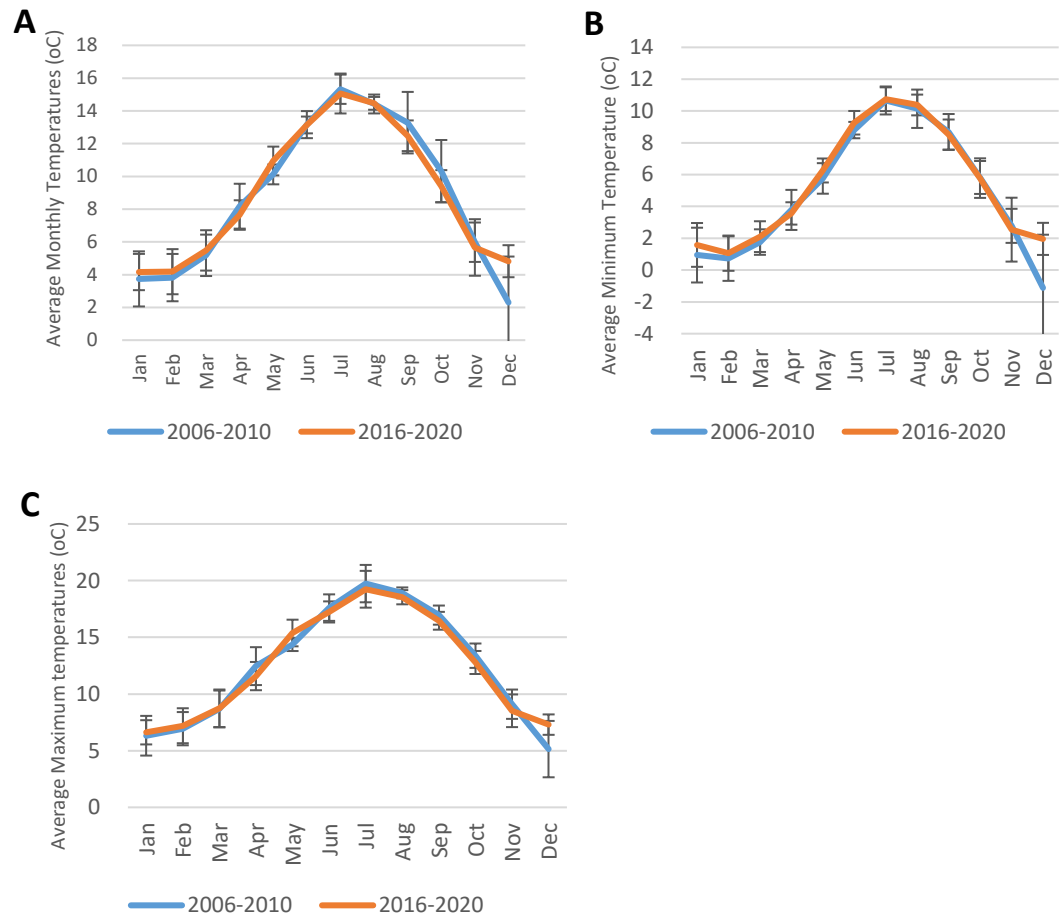


**Figure 3.11: Average monthly, minimum, and maximum temperatures measured from 2006-2010 (pre-carrot blackening) and 2016-2020 (post-carrot blackening).** The average monthly (A), minimum (B), and maximum (C) temperatures reported in the 2006-2010 (before carrot blackening was first reported) and 2016-2020 datasets (5 consecutive years that carrot blackening was reported). Asterisks indicate the statistical significance level: p-value ≤ 0.05 (*), < 0.01 (**), and < 0.001 (***) using T-tests. Data are the mean +/- standard deviation.

**Soil temperatures at the Balmalcolm vegetable fields**

Average soil temperatures were similar in the datasets recorded between 2006-2010 and 2016-2020 (Figure 3.12). The only notable differences were reported in December and Janurary, which showed a general increase of 1-2 degrees in recent years.
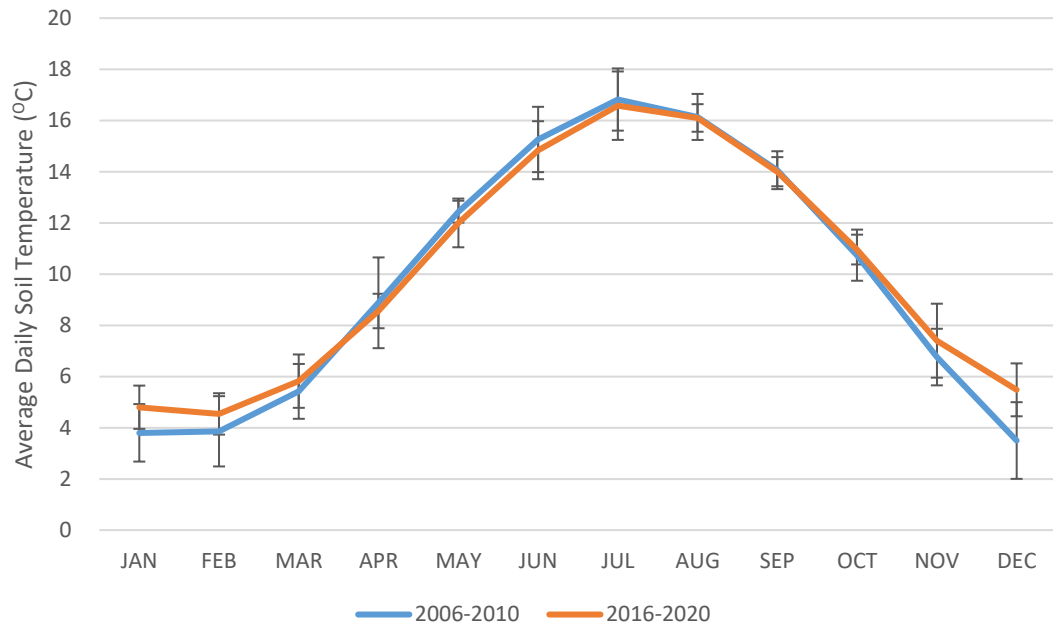


**Figure 3.12: Average daily soil temperatures of 2006-2010 (pre-carrot blackening) and 2016-2020 (post-carrot blackening).** The average daily soil temperatures reported between 2006-2010 (before carrot blackening was first reported) and 2016-2020 (5 consecutive years that carrot blackening was reported). Data are the mean +/- standard deviation.

**Light levels mesaured at the Balmalcolm vegetable fields**

Levels of solar radiation were recorded each month between 2006-2010 and 2016-2020. No differences in light availability were observed between the 2006-2010 and 2016-2020 datasets. Patterns of solar radiation showed similar trends but with maxima observed during the summer months from May to July (Figure 3.13 A). In the years when carrot blackening was reported there were no significant differences in solar radiation to the years when blackening was not recorded (Figure 3.13 B).
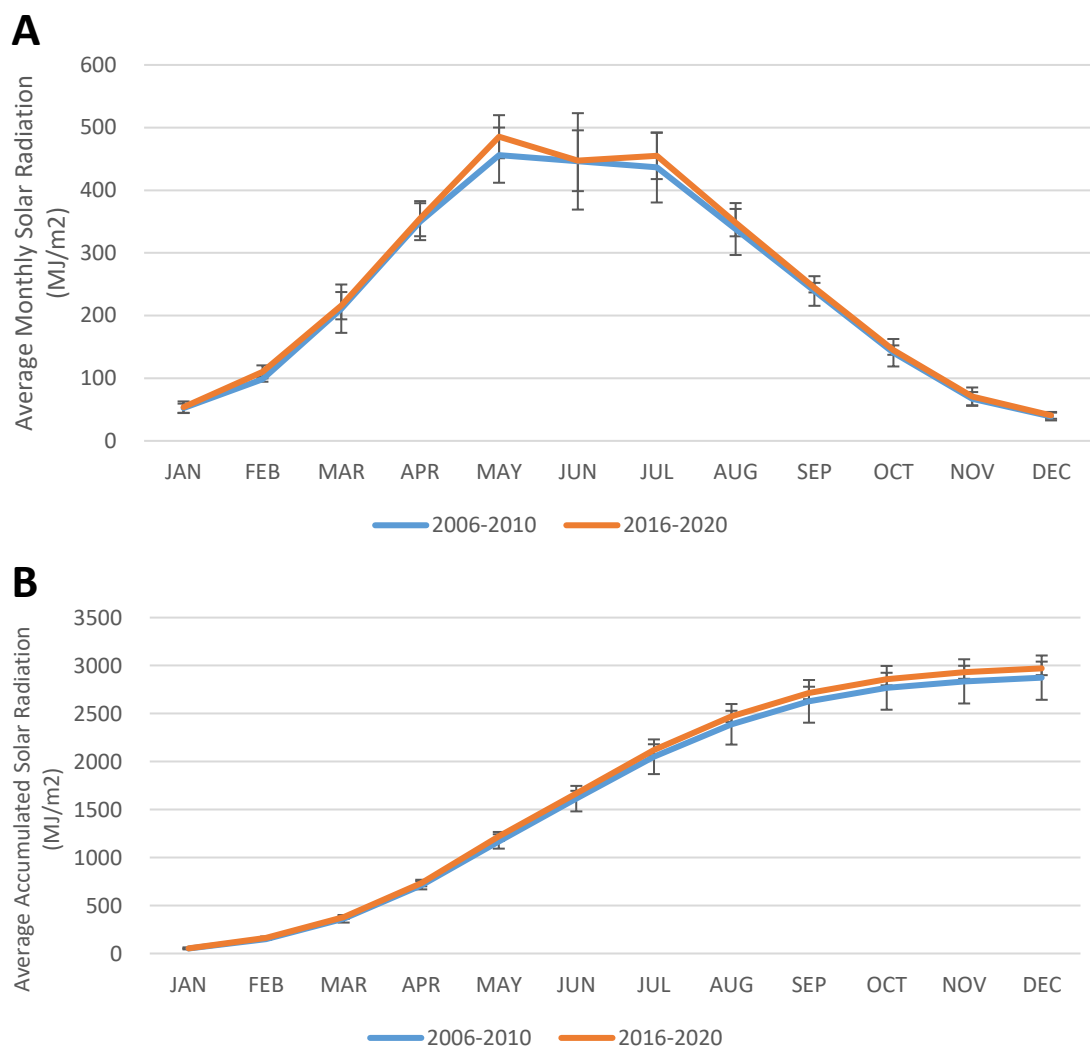


**Figure 3.13: Average accumulated solar radiation measured between 2006-2010 (pre-carrot blackening) and 2016-2020 (post-carrot blackening).** The average monthly (A) and accumulated (B) levels of solar radiation measured between 2006-2010 (before carrot blackening was first reported) and 2016-2020 (5 consecutive years that carrot blackening was reported). Data are the mean +/- standard deviation.

**Rainfall data for the Balmalcolm vegetable fields**

The recorded monthly rainfall tended to be higher in 2006-2010 than the average rainfall recorded between 2016-2020 (Figure 3.14 A). The annual accumulated rainfall measured in the 2006-2010 period was approximately 200 mm higher than that recorded in the 2016-2020 period (Figure 3.14 B).
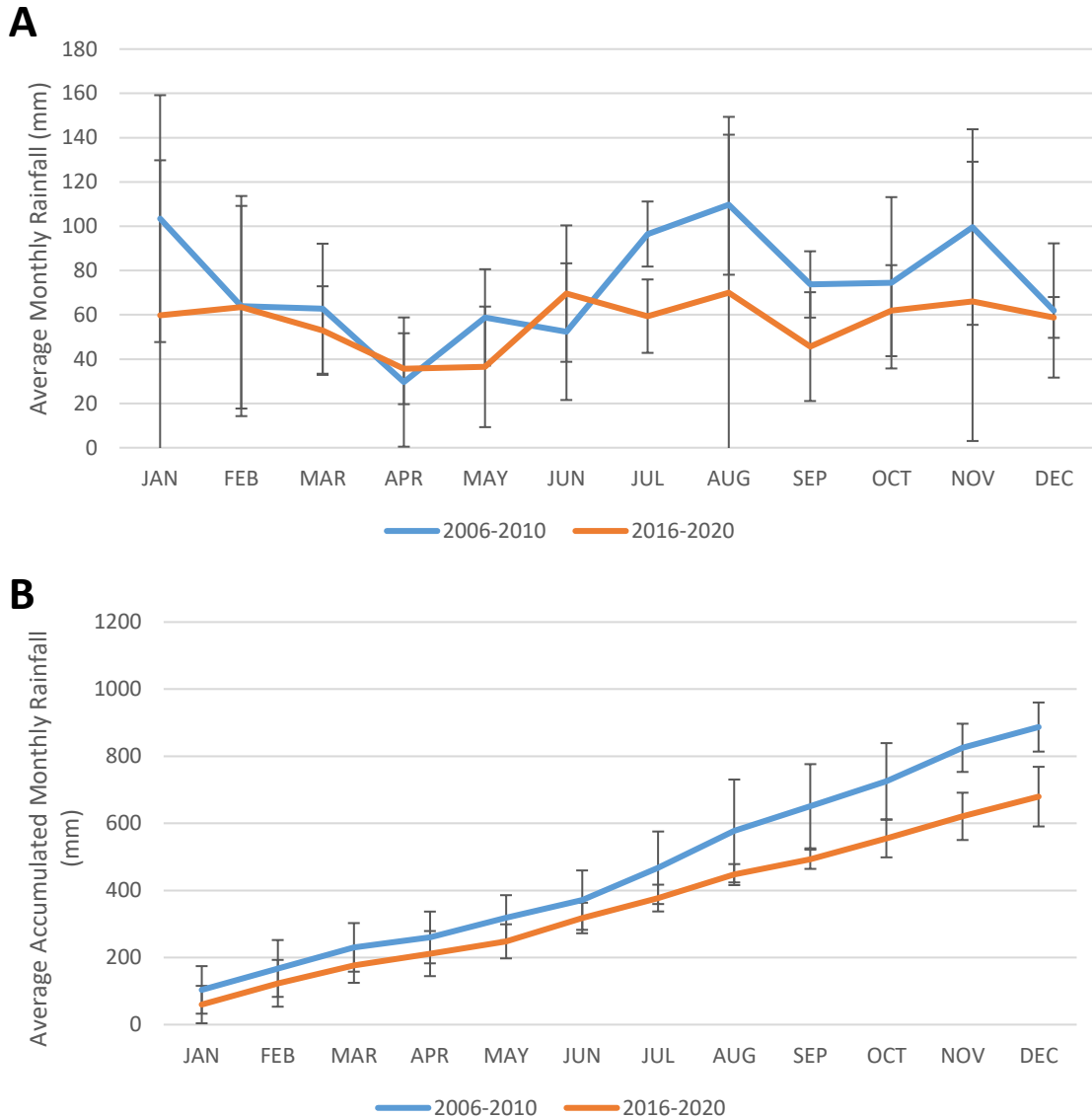


**Figure 3.14: Average monthly and accumulated rainfall measured in the 2006-2010 (pre-carrot blackening) period and the 2016-2020 period (post-carrot blackening).** The average monthly (A) and accumulated (B) rainfall of 2006-2010 (before carrot blackening was first reported) and 2016-2020 (5 consecutive years that carrot blackening was reported). Data is the mean +/- standard deviation.

## 3.3   Discussion

The growth environment may play an important role in determining the susceptibility of cut carrots to blackening. This chapter reports data concerning the environmental and geographical conditions that were recorded at a field site close to where the carrots were grown. Air temperature, soil temperature, solar radiation and rainfall data were recorded over two 5-year periods from 2006 to 2010 (i.e. a period before carrot blackening was reported) and from 2016 to 2020 (i.e. a period when carrot blackening because a serious issue). In addition, blackening was recorded of samples taken from carrots harvested from 18 fields located throughout Scotland, owned by 6 different owners data in the 2020 trial. Blackening was recorded as a percentage on the day of processing into batons (day 0) and on each of the following 3 days (day 1, 2, and 3). These data were combined to calculate the total blackening seen from each field. Using these data, blackening was related to the geographical location of the carrot fields, to determine whether relationships exist between the growth environment and susceptibility to blackening. The age of the carrots at harvest was also investigated as a physiological parameter that might increase susceptibility to blackening. The findings reported in this chapter increase our understanding of the factors that increase the propensity of cut carrot to show blackening.

The data presented here show that the geographical locations of the fields is a factor in carrot blackening. Figure 3.7 clearly shows that there was a large variation in the level of carrot blackening reported for each of the fields owned by KPL, with the highest level of blackening reported in the Barnyards (1) field while the lowest level was found in the Barnyards (2) field. The differences in recorded blackening in these fields was significant. A large variation in the rate of carrot blackening was also seen in carrots harvested from fields in both the north and south of Scotland. These data suggest that the geographical locations of the carrot fields have a significant impact on susceptibility to blackening. Hence, it may be prudent to either avoid planting carrots in the fields with the highest incidence of blackening, or to only harvest carrots below 400 days old from those fields.

The data presented in this chapter related to environmental parameters such as air temperature, soil temperature and solar radiation show that these parameters have not greatly changed over the last 15 years. The data obtained for the period from 2006 to

2010 (i.e. a period before carrot blackening was reported) are remarkably similar to those measured from 2016 to 2020 (i.e. a period when carrot blackening because a serious issue). However, the fields were receiving 200 mm less annual rainfall in the recent period of data collection and the air and soil temperatures are showing a trend to warming in some winter months (December and January). While these observations are not statistically significant, further studies are required to determine the importance of these parameters in determining the susceptibility of cut carrots to blackening.

Browning in other root vegetables is commonly attributed to biotic factors, such as brown rot, as well as abiotic factors such as bruising during harvest and production. There is little evidence to suggest that the preharvest growth conditions predispose the cut carrots to blackening. However, the Blackheart syndrome in potatoes is caused by flooding. In this situation low oxygen and high carbon dioxide levels induce cell death in the tubers, resulting in a black tissue discolouration (Zhou et al., 2015). Thus, the environmental conditions can produce blackening in vegetables. It is possible that the carrots in some fields experience a degree of drought as a result of the lower rainfall recorded during the 2016 to 2020 period that enhances susceptibility of cut carrots. The potato tubers that were susceptible to blackheart were found to have high levels of reducing sugars, while tubers that were more resistant accumulated chlorogenic acid isomers (Kiaitsi et al., 2020). Increased levels of chlorogenic acid isomers were found in the black carrot samples. However, the most important factor determining the susceptibility of carrots to blackening is the age of the carrots at harvest. The highest level of blackening was recorded on either on the day of processing or within the first 24 hours after processing in the carrots that were over 400 days old. This finding suggests that there is a relationship between the biological age of the carrots and the susceptibility of the carrots to processing-induced blackening.

A more detailed analysis of the effect of the growth environment is required in the future to fully understand how abiotic factors contribute to processing-induced blackening. Future experiments should also explore why some field locations result in a higher susceptibility to blackening than others. Ideally, larger sampling sizes should be used with data collection over more seasons.

Future work should also focus on the relationship between carrot age at the time of harvest and susceptibility to blackening (Figure 3.4). The levels of blackening observed in cut carrots over 430 days old were double the values of the younger age ranges. Crucially, carrots less than 161 days old showed no blackening at all. This finding strongly suggests that carrot age or length of storage underground is a major factor contributing to the blackening phenomenon. In such studies, carrots could be harvested from fields on a monthly or weekly basis, cut into batons and monitored for blackening. Simultaneous measurements of the transcriptome and metabolome profiles would provide new insights into the mechanisms that are induced during carrot root aging and/or length of storage underground that lead to processing-induced blackening.

# Chapter IV

# Chapter 4: Cell wall modifications in blackened carrot batons.

## 4.1    Introduction

Plant cell walls are typically divided into two categories: primary and secondary cell walls. The thin flexible primary cell walls are present around every plant cell, enabling cell growth. In contrast, rigid thick secondary cell walls are developed inside the primary cell wall once final cell size has been established. However, only certain cell types such as xylem elements and fibres are able to develop secondary cell walls (Zhong et al., 2019). The key structural components of both types of cell walls are cellulose microfibrils and hemicellulose. Primary cell walls also contain pectin and secondary cell walls often contain lignin. Cellulose microfibrils provide structural support, allowing the cell and ultimately the plant to maintain shape. Hemicelluloses are cross-linked to cellulose, strengthening the cell walls while by enabling the generation of, and providing resistance to, internal turgor pressure.

Pectin, which is mainly found in primary cell walls, can greatly influence cell wall properties, including pH and porosity (Voragen et al., 2009). Pectin can be cross-linked to cellulose in organs such as carrot roots, further increasing structural integrity (Broxterman and Schols, 2018). Secondary cell walls are often rich in lignin, which provides mechanical support to prevent cell wall collapse due to external compressive forces, as well as playing an important role against pathogen infection (Yadav et al., 2020).

Lignin is a complex polymer composed of 3 main subunits; *p*-hydroxyphenyl (H), guaiacyl (G), and syringyl (S). Lignin composition varies depending on species, maturation, and tissue type. In 7-8 month old carrots, lignin subunit ratios are approximately 4:95:1 (H:G:S) (Schäfer et al., 2018). Lignin is also deposited during plant-pathogen interactions to limit the spread of pathogens. Moreover, cell wall damage caused by an inhibition of cellulose synthesis can induce lignin deposition in primary cell walls (Gallego-Giraldo et al., 2020).

As well as providing structural support, cell walls act as a defence against microbial attack. For example, attacks from pathogens or insects lead to an increase in lignin biosynthesis in order to strengthen cell walls against further attack. The mechanisms that contribute to the maintenance of cell wall integrity (CWI) are important in plant responses to biotic and abiotic stresses, not least because they serve to prevent targeted manipulation of cell wall metabolism (Bacete and Hamann, 2020). Receptor-mediated CWI monitoring and wall-derived damage-associated molecular patterns (DAMPS) are key elements in the CWI maintenance mechanism. Receptor-like kinases, particularly *Catharanthus roseus* Receptor Like Kinase 1 Like subfamily members, such as FERONIA are required for cell responses to mechano-stimulation.

Plants can produce callose, which is a water-insoluble β-1,3-glucan that functions as a protective layer at the point of damage to protect the cell interior, in response to stresses such as bacterial infection (Jin and Mackey, 2017). Callose is deposited between the plasma membrane and the cell wall at the site of pathogen attack and at the plasmodesmata to slow pathogen invasion and spread. The importance of interactions between callose and cellulose (and possible other polymers) was recently highlighted in relation to cell wall responses to developmental and environmental signals (Abou-Saleh et al., 2018).

Carrots are eudicots with root structures primarily consisting of the periderm, xylem, phloem, pith, and a thin layer of vascular cambium tissue. This is responsible for producing secondary xylem towards the centre of the root and secondary phloem towards the outer half during secondary growth (Perrin et al., 2017). Each of these root structures has individual functions with cell walls that are adapted to these functions. The phloem, which is responsible for the transport of sugars, contains four cell types: sclerenchyma, parenchyma, fibres, and sieve elements. Sieve elements only have primary cell walls and these resist high turgidity (Pace, 2019). Although not always present, sclerenchyma cells have thick cell walls that are lignified to provide mechanical support. Parenchyma cells store lipids and carbohydrates and have thinner cell walls. Fibres cells provide strength and support (Pace, 2019). The xylem contains four distinct cell types: vessels elements, tracheids, parenchyma and fibers. All xylem cell types,

except for parenchyma cells, have thick, lignified cell walls to aid in water transport and withstand turgidity.

The following studies were performed to determine whether cell wall modifications are associated with the blackening of cut carrots. The composition of the cell walls in the orange and blackened regions of cut carrots was therefore compared using a range of techniques. Cell size was measured together with cell wall composition and the distribution of cell wall components.

From blackened carrot batons, sections were harvested that contained the following regions: black regions (B/B), orange regions immediately bordering the black region (OB/B) and orange regions further away from the black section (O/B). Sections were also taken from orange carrot batons with no visible blackening (O/O) as controls. The techniques used to characterise the cell wall composition of these samples include:

- Fluorescence microscopy was used to quantify the emission of autofluorescence in the different regions of the carrots,

- Immunolabelling using a range of monoclonal antibodies was used to detect specific cell wall components in each region,

- Methanolysis-GC-FID was used to identify and quantify aromatic components and carbohydrates.

Taken together, these approaches enabled an in-depth analysis of the composition of cell walls in the blackened carrots. The monoclonal antibodies used in these studies are listed in Table 2.1. The changes observed in the cell wall composition of the blackened regions of the cut carrots may give insights into the mechanisms involved in the blackening process. For example, increases in callose may indicate physical damage to cells whereas changes in HG and RG-I pectin might indicate degradation resulting from microbial attack. The key structural components of the cell walls that are discussed in this chapter are xyloglucan, HG and RG-I pectin, and lignin. Antibodies targeting other cell wall components that did not reveal difference are thus not discussed at length in this chapter.

## 4.2 Results

### 4.2.1 Black region cells are distinct from orange region cells under bright field microscopy

Orange and blackened carrot sections were viewed with a light microscope and micrographs were taken. Discolouration can readily be seen throughout the cells of the blackened region (Figure 4.1 B, Figure 42). This discolouration is likely caused by the accumulation of dense material in the blackened regions (Figure 4.1 B). Although the bright field images were taken with the same lighting and camera settings, it was more difficult to distinguish the walls of the orange than the blackened cells at the same settings (Figure 4.1 A). An in-depth analysis of the cell wall composition was carried out in order to determine the cell wall changes that underpin these visual differences.
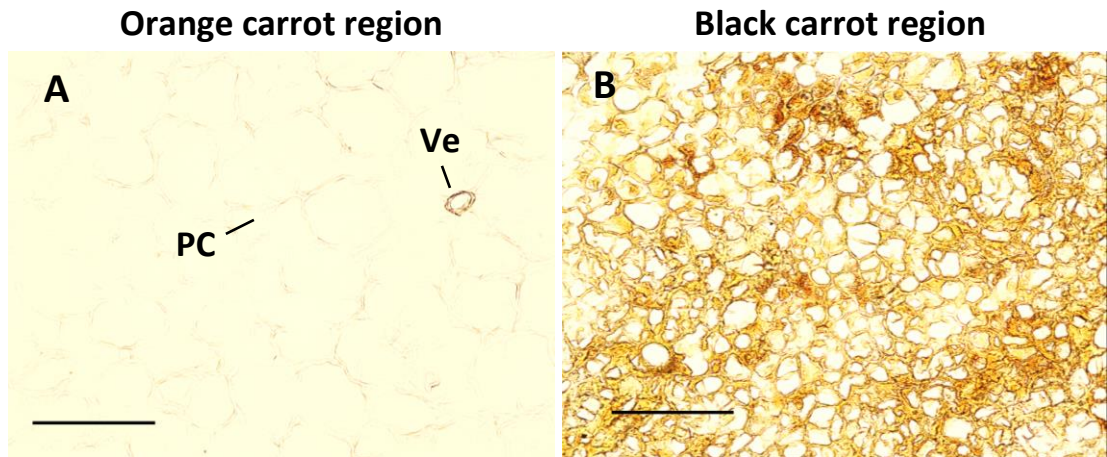
**Figure 4.1: Typical micrographs of orange and black carrot regions of carrot batons.** Both bright field images were of 12 μm carrot sections taken under the same microscope settings. A: Orange carrot region. B: Black carrot region. PC = Parenchyma. Ve = Vessels. Scale bar = 20 μm.
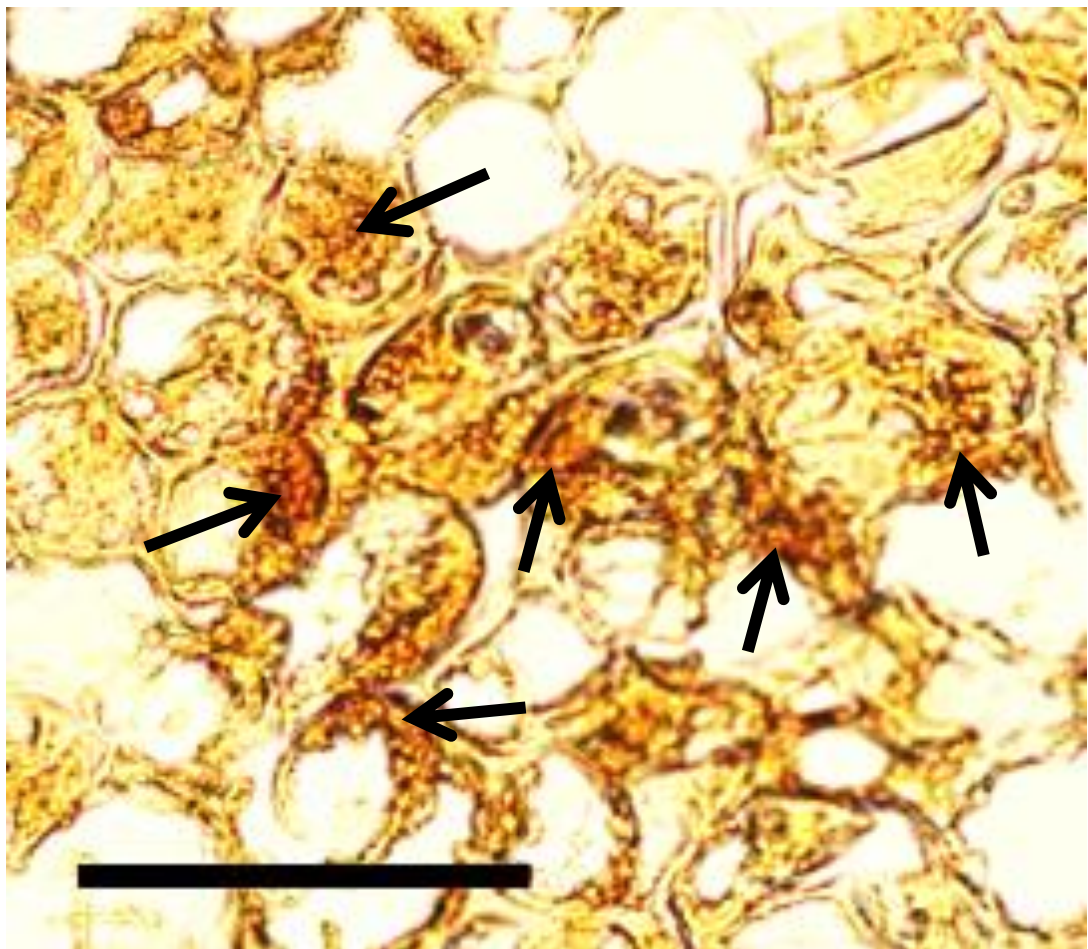


**Figure 4.2: A typical example of a black carrot region viewed under the light microscope.** Bright field image of discolouration seen in a 12 μm section of black carrot region. Scale bar = 10 μm. Arrows indicating clear areas of carrot blackening.

## 4.2.2 Cells in black regions are smaller than cells in orange regions.

The orange carrot baton samples contained parenchyma cells with visible xylem vessels (Figure 4.3, A). In contrast, the orange regions of the blackened sections of the batons contained parenchyma but no vessels (Figure 4.3, B). The dark colouration in the black regions made determination of cell type challenging (Figure 4.3, D). Cells from orange carrots were on average twice as large as the cells in the black carrot regions (Figure 4.4, A, B, D). Also, cells in the orange regions bordering black areas were significantly larger than cells in the black regions and significantly smaller than the cells in the orange regions (Figure 4.4, C, D).
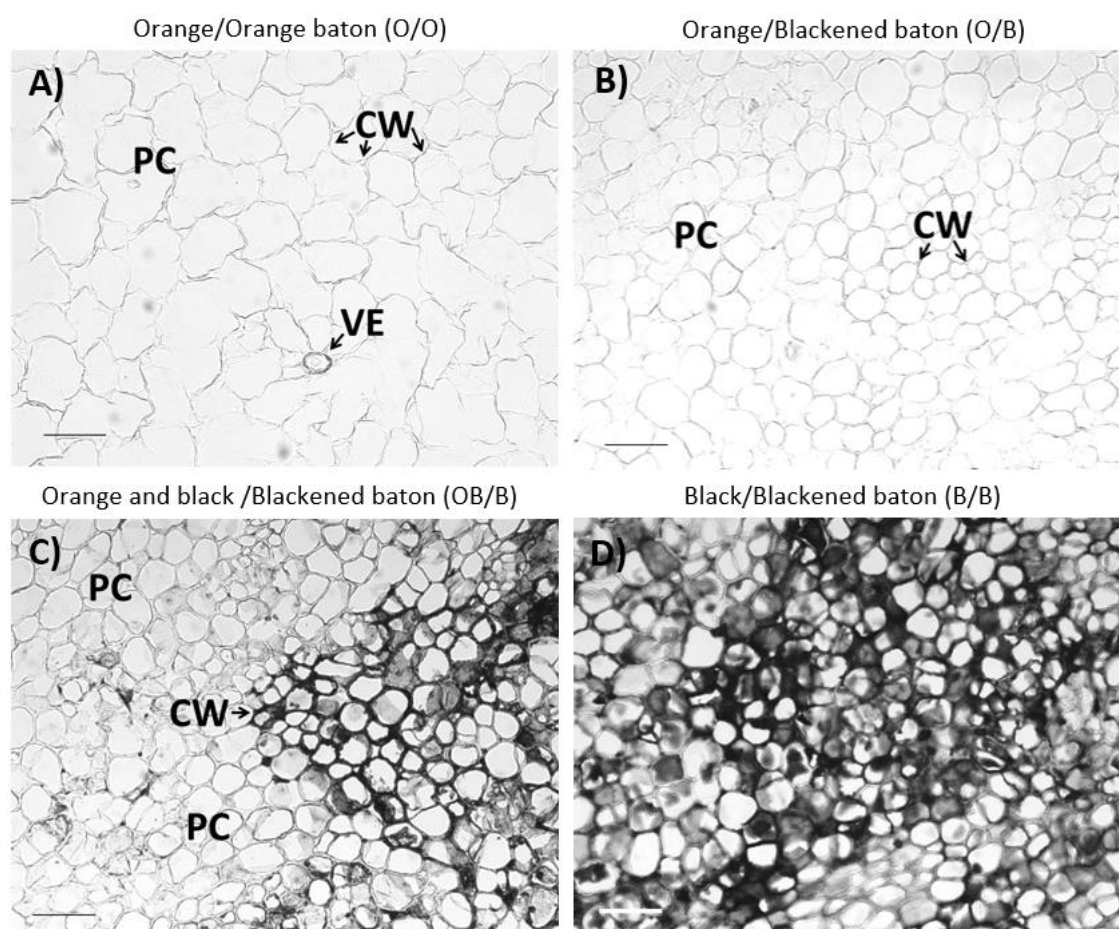


**Figure 4.3: Examples of orange, black and orange/black border carrot regions of cut carrots viewed under the light microscope**. Orange (O/O) (A), Border (O/B) (B), Orange and Black (OB/B) (C), and Black (B/B) (D) carrot regions with characteristics labelled. PC = Parenchyma. VE = Vessels. CW = Cell Walls.  Scale bar = 10 µm**.**
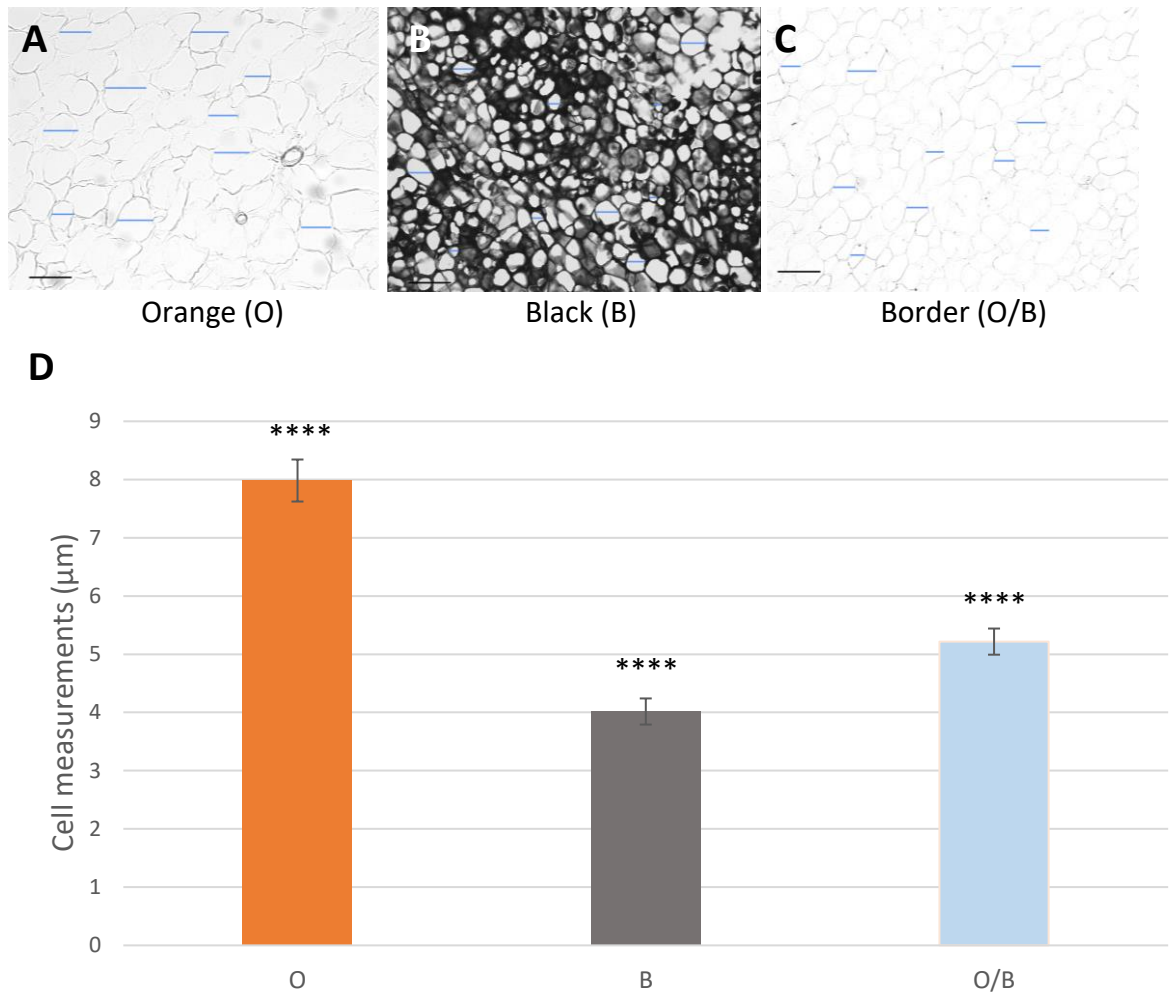
Figure 4.4: Cell size comparisons in the orange, black and orange/black border regions of carrot batons. Orange (A), Black (B), and Border (C) carrot regions. Cell size measurements shown in as a graph (D). Data are the mean values ± SE (n = 30). Significant differences between orange and black samples were calculated with a T-test, ****p<0.001. Scale bar = 10 μm.

### 4.2.3 Cells in black regions displayed greater autofluorescence than cells in orange regions

Samples of orange and blackened carrot regions were viewed under a light microscope with various fluorescence excitation wavelengths to detect autofluorescence. Micrographs were taken in the bright field channel and the FITC channel using a monochrome camera. The FITC channel with an excitation wavelength of 495 nm and an emission wavelength of 519 nm, was selected because autofluorescence was strongly detected using these parameters in the carrot samples. Patches of dark cells were seen in the bright field (BF) images of the blackened regions but not in the orange regions (Figure 4.5 A,C). Autofluorescence emitted from the black regions corresponds to the patches of dark cells in the BF view. Moreover, the absence of both autofluorescence and dark patches in the orange carrot samples suggests that metabolites or compounds present in the dark areas are responsible for the autofluorescence (Figure 4.5). Phenolic compounds, which are known to emit autofluorescence when excited by certain wavelengths are a likely cause of the observed autofluorescence in the blackened regions.

To investigate this possibility, a confocal laser scanning microscope was used to view two sections of orange and blackened carrot regions separately. Regions of orange and blackened tissue were selected and autofluorescence was measured with excitation wavelengths between 414-695 nm (Figure 4.6). The autofluorescence emitted from the blackened region had a peak between ~440 nm and 476 nm, with a gradual decrease towards 695 nm. In contrast, the orange region showed no large peaks in autofluorescence throughout the visible light spectrum.
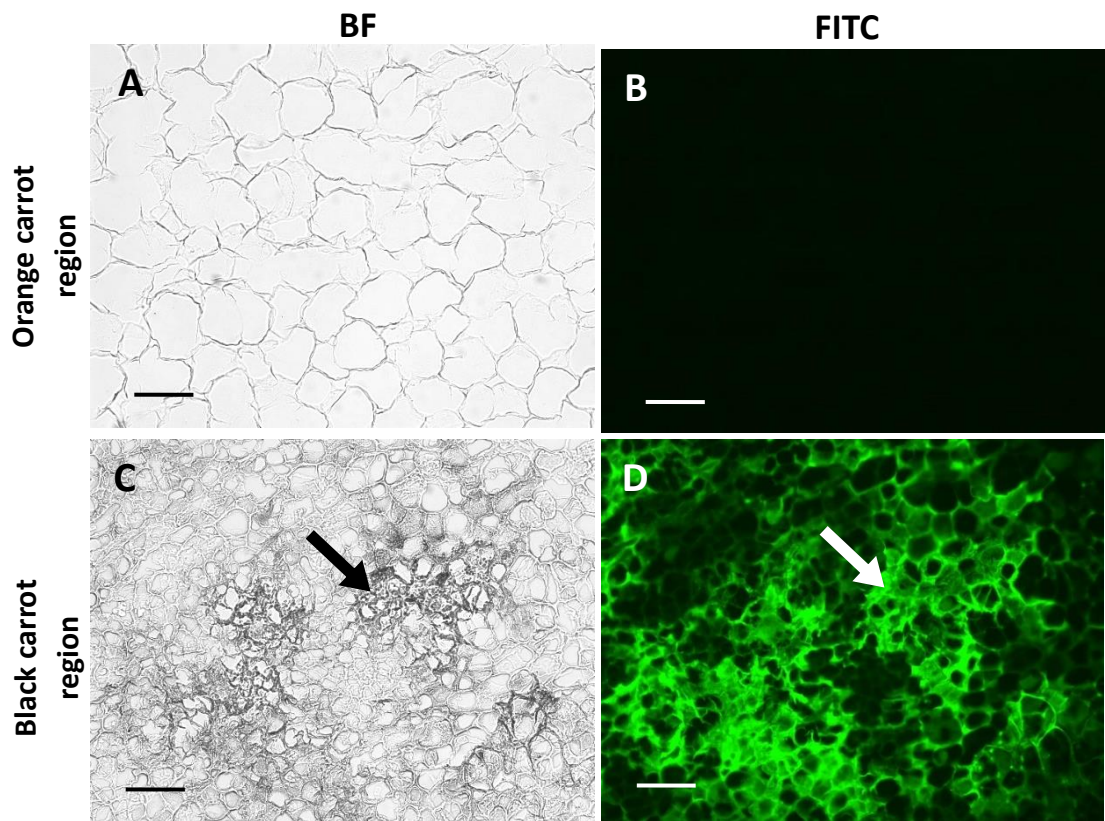
**Figure 4.5: Examples of micrographs showing autofluorescence of orange and black carrot regions.** A: Bright field image of orange carrot regions. B: Image showing orange region in the FITC channel. C: Bright field image of black carrot region. D: Image showing autofluorescence of black carrot region in the FITC channel. Scale bar = 10 μm. x10 magnicantion. Exposure times: BF = 0.011 s, FITC = 0.25 s. Arrows indicating clear areas of carrot blackening.
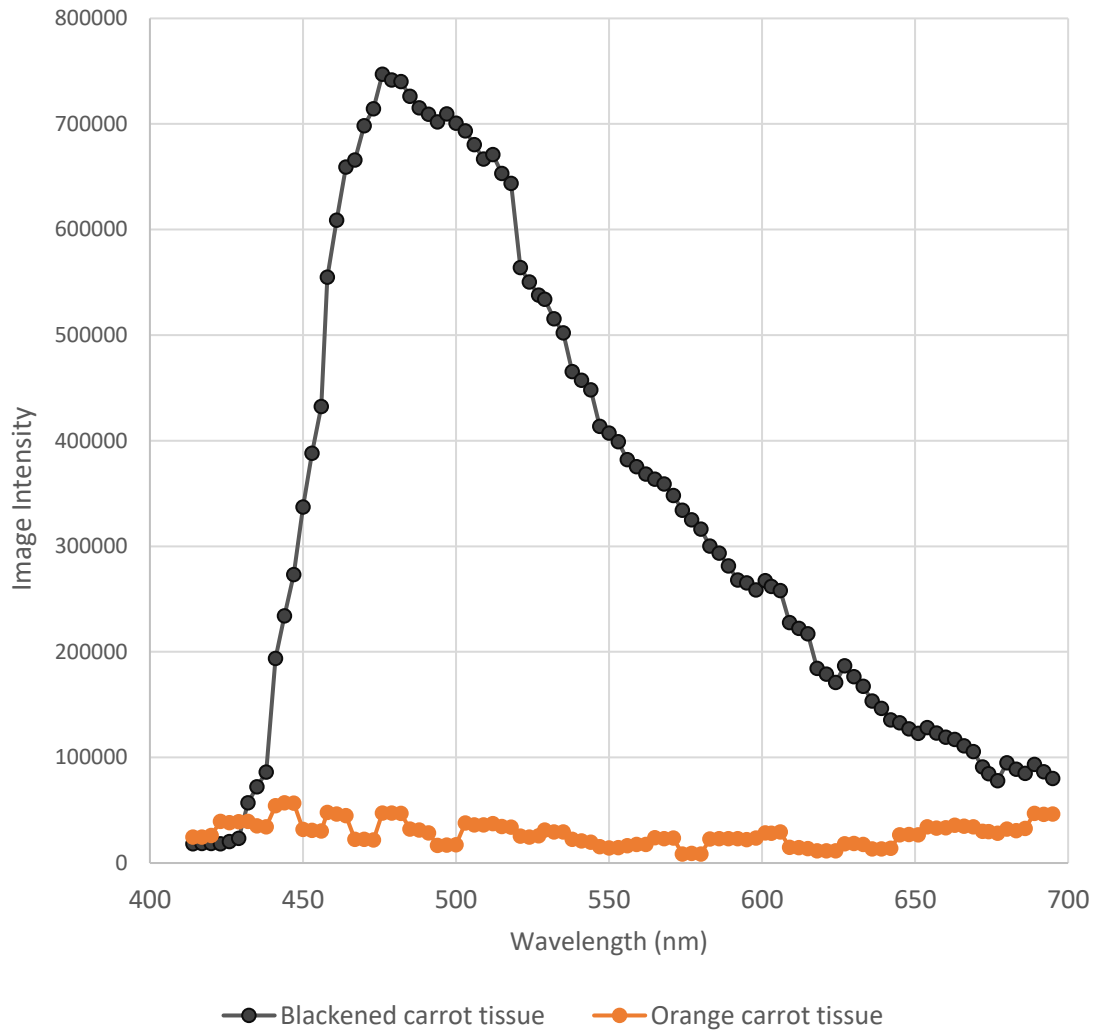
**Figure 4.6: A comparison of relative autofluorescence intensity in orange and black carrot regions.** Measurements taken every 3 nm between 414 nm-695 nm.

### 4.2.4 Toluidine blue O blocks autofluorescence in black regions

Indirect immunofluorescence was used to further explore the differences in cell wall composition between the orange and blackened carrot regions. This technique relies on fluorophores attached to secondary antibodies that act as indicators of the presence of targeted antigens. The fluorescence emitted by these fluorophores can be detected using a fluorescence microscope. However, autofluorescence from the tissue can complicate data interpretation. Therefore, the basic thiazine metachromatic dye called toluidine blue O (TBO) was used to block autofluorescence in the carrot sections (Xue et al., 2013) and binds to acidic components (Vidal and Mello, 2019). TBO binds strongly to the cell walls in the black carrot regions making them appear darker in the bright field image (Figure 4.7 C) than in the unstained black regions (Figure 4.7 A). In contrast, no fluorescence was detected in the TBO stained black carrot regions viewed under the fluorescence microscope (Figure 4.7 D). This method therefore ensured that fluorescence observed using the immunofluorescence imaging technique can be correctly attributed. The black carrot regions showed visible discolouration (Figure 4.8 C, E) relative to the orange carrot regions (Figure 4.8 A) in the coloured bright field images. The TBO treatment did not result in blue staining of the orange carrot regions (Figure 4.8 B), whereas the black regions showed strong TBO binding, as evidenced by the blue staining (Figure 4.8 D, F).
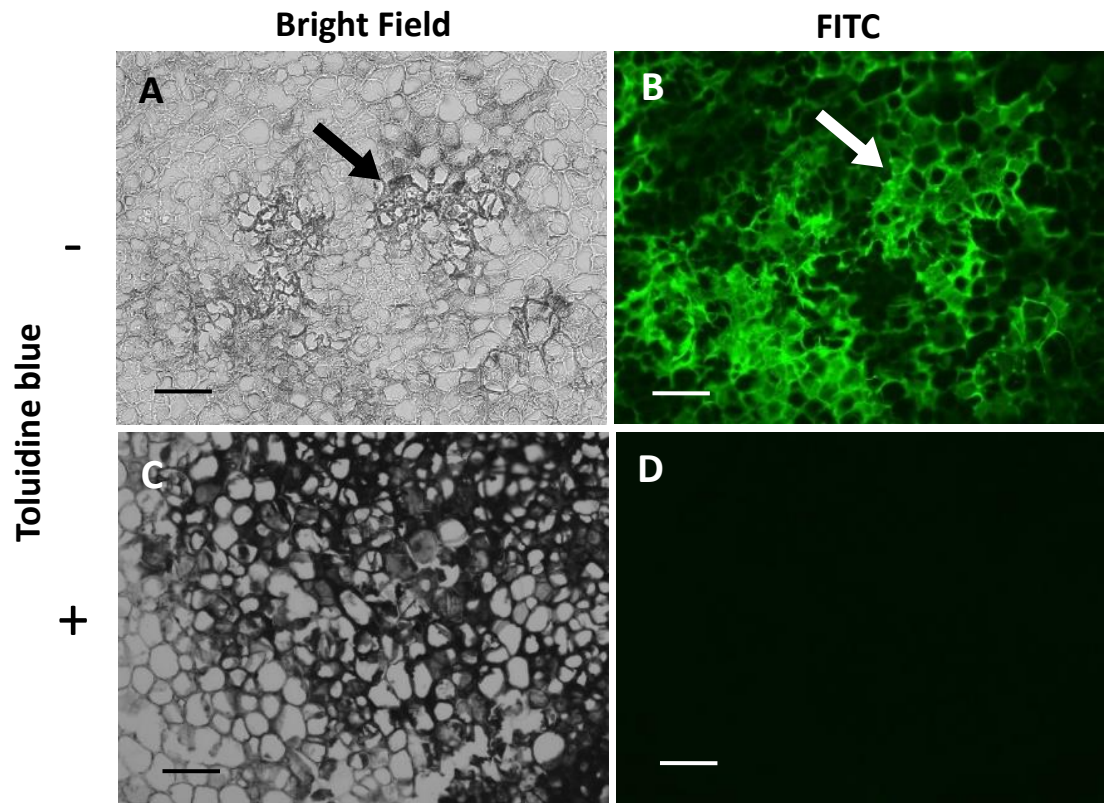
**Bright Field**             **FITC**

**Figure 4.7: Examples of micrographs showing the autofluorescence of black carrot regions in the absence or presence of TBO.** A: Bright field image showing black carrot region with no staining. B: Image showing autofluorescence of black carrot region at a wavelength of ~495 nm/519 nm. C: Bright field image showing black carrot region after staining with TBO. D: Image showing no autofluorescence as it is blocked by the presence of TBO. Scale bars = 10 μm. x10 magnification. Exposure times: BF = 0.011 s, FITC = 0.2 s. Arrows indicating clear areas of carrot blackening.

**Figure 4.8: Examples of coloured micrographs of orange and black carrot regions in the absence or presence of TBO.** Bright field images showing orange carrot regions (O/O) with (B) and without (A) TBO staining, black carrot regions (B/B) with (F) and without (E) staining, and tissue directly bordering the black region (OB/B) with (D) and without (C) staining. X20 magnification and scale bar = 10 μm for images A, B, C, E, and F. x10 magnification and scale bar = 20 μm for image D.

### 4.2.5 Differences in cell wall polysaccharide between orange and black regions of carrot batons

Following the characterisation of discolouration and autofluorescence in the orange and black carrot regions, the next step was to investigate the content and composition of major cell wall polymers. Monoclonal antibodies that bind to specific cell wall polysaccharides were used to study the walls of orange and black carrot regions. The immunofluorescence technique allows for the identification and localisation of cell wall components in each region. Firstly, tissue samples (1 cm$^2$) were excised, dehydrated, and embedded in wax. They were then cut into (12 μm) sections and placed onto microscope slides. Sections were then dewaxed and rehydrated before the monoclonal antibodies were applied. A wide range of monoclonal antibodies were selected that are predicated to bind to the polysaccharides in carrot root cell walls. Data are presented for antibodies that bind to xyloglucan (LM25), HG-pectin (LM20, LM19, JIM7) and RG-I pectin (LM5, LM6). The LM26 antibody that binds to a branched pectic galactan epitope of RG-I was also used but it did not bind to the carrot tissue (Figure 4.12). LM26 was used as a negative control antibody for the immunolabelling technique. This ensures that the immunolabelling process per se did not result in any fluorescence.

#### 4.2.5.1 Decreased detection of xyloglucan in black region cell walls

Xyloglucan is the major non-pectic, matrix polysaccharide in carrots. Transverse sections of orange and blackened carrot tissue were treated with pectate lyase to remove pectic HG, which is known to mask the detection of xyloglucan (Marcus et al., 2008). These sections were then labelled with the monoclonal antibody LM25, which binds specifically to xyloglucan. The cell walls of the black regions of the carrot batons had decreased levels of xyloglucan detected (Figure 4.9 F, H) compared to cell walls in the orange regions (Figure 4.9 B, D).
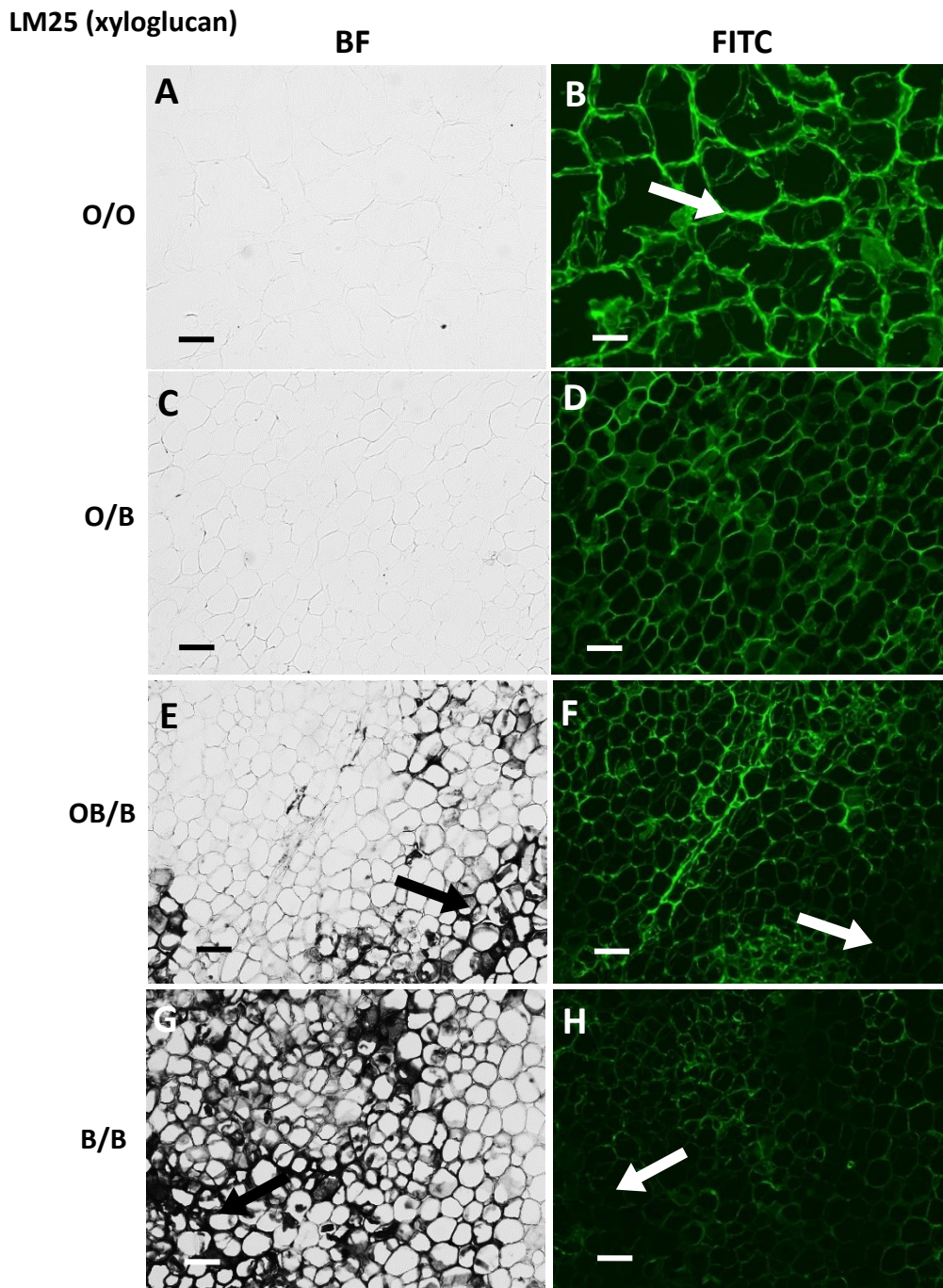
**Figure 4.9: Indirect immunofluorescence detection of the xyloglucan in transverse sections of orange and blackened regions of carrot batons, after pectate lyase treatment to remove pectic homogalacturonan.** Bright field (BF) images showing tissue of an orange carrot baton (O/O) (A) and different sections of a carrot baton with visual blackening. The sections are the orange region on a blackened baton (O/B) (C), tissue directly bordering the black region (OB/B) (E), and the black region (B/B) (G). Corresponding immunofluorescence images for LM25 xyloglucan. Scale bar = 10 µm. x10

magnification. Exposure times: BF = 0.045 s, FITC = 0.15 s. Arrows indicating clear areas of carrot blackening.

### 4.2.5.2 Decreased detection HG and RG-I pectin levels in blackened compared to orange regions.

**HG pectin**

Three MAbs were used to detect pectic HG with varying levels of methyl-esterification: LM20 detects highly methyl-esterified pectic HG, JIM7 detects partially methyl-esterified pectic HG, and LM19 detects unesterified pectic HG. The orange and black/orange border regions of the blackened batons contained significant amounts of detectable pectic HG at all levels of esterification (Figure 4.10 F, G, N, O, V, W) compared to the orange batons (Figure 4.10 E, M, U). The black regions had greatly decreased levels of detected pectic HG compared to all other regions (Figure 4.10 H, P, X). Despite this, a much higher level of pectic HG was detected in the orange region of the blackened carrot batons compared to the orange regions of orange batons.

**RG-I pectin**

Galactan and arabinan are common side chains of RG-I. Antibodies LM5 and LM6 were used to detect galactan and arabinan, respectively. These RG-I pectin side chains were detected in orange batons (Figure 4.11 B, D), with decreased amounts in the orange and border regions of the blackened carrot sections (Figure 4.11 F, H, J, L). Cell walls in the black regions showed the lowest detection of the LM5 and LM6 epitopes (Figure 4.11 N, P). Branched pectic galactan was detected using the antibody LM26. However, pectic galactan was not detected in any of the carrot regions (Figure 4.12).
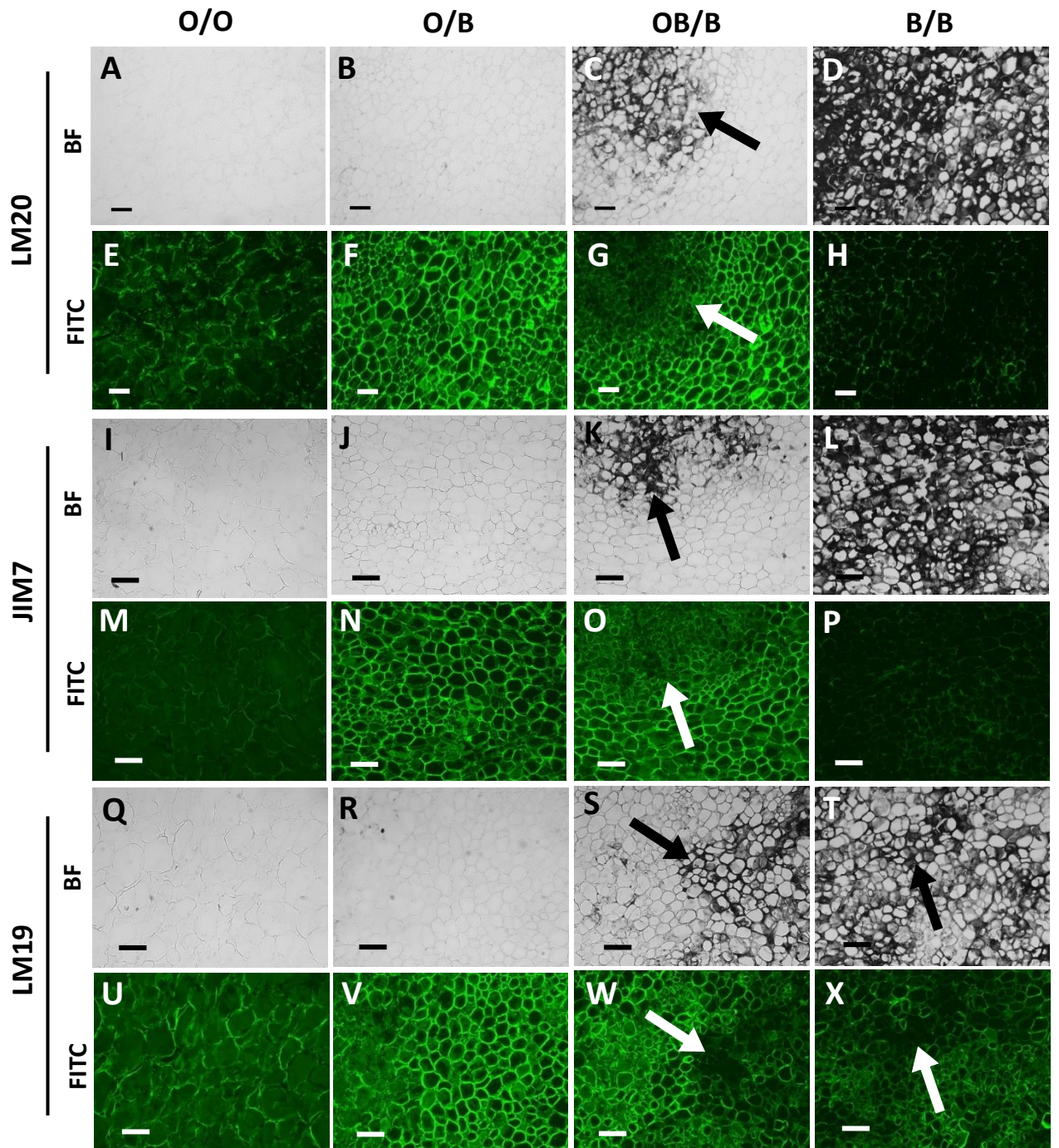
**Figure 4.10: Indirect immunofluorescence detection of pectic HG in transverse sections of orange and blackened carrot batons.** Bright field (BF) images showing tissue of an orange carrot baton (O/O) (A, I, Q) and different sections of a carrot baton with visual blackening. Sections are the orange region on a blackened baton (O/B), tissue directly bordering the black region (OB/B), and the black region (B/B). Corresponding immunofluorescence images taken in the FITC channel generated with monoclonal antibodies binding to de-esterified pectin (LM19), methyl-esterified pectin (JIM7) and

highly esterified pectin (LM20). Scale bar = 10 μm. x10 magnification. LM20 and JIM7 exposure times: BF = 0.011 s, FITC = 0.15 s. LM19 exposure times: BF = 0.011 s, FITC = 0.2 s. Arrows indicating clear areas of carrot blackening.

**RG-I-related**
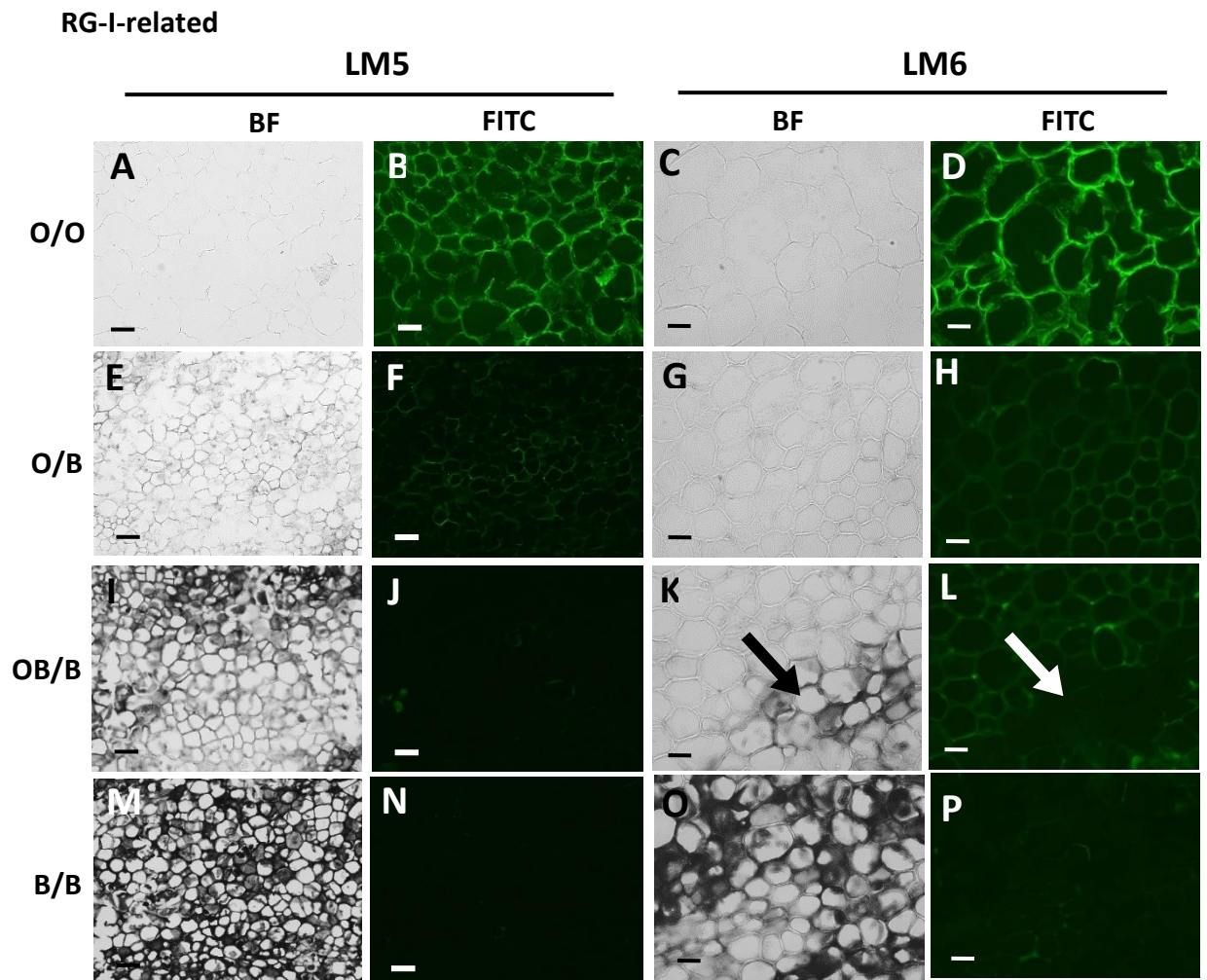


**Figure 4.11: Indirect immunofluorescence detection of pectic RG-I in transverse sections of orange and blackened carrot batons.** Bright field (BF) images showing tissue of an orange carrot baton (O/O) (A, C) and different sections of a carrot baton with visual blackening. Sections are the orange region on a blackened baton (O/B), tissue directly bordering the black region (OB/B), and the black region (B/B). Corresponding immunofluorescence images taken in the FITC channel generated with monoclonal antibodies binding to (1-4)-β-galactan (LM5) and (1-5)-α-L-arabinan (LM6). Scale bar = 10 μm. LM5 images are at x10 magnification. Exposure times: BF = 0.045 s, FITC = 0.3 s. LM6 images are at x20 magnification. Exposure times: BF = 0.1 s, FITC = 0.8 s. Arrows indicating clear areas of carrot blackening.

**LM26 (branched (1,6-Gal)(1-4)- β-D-galactan)**

| BF | FITC |
|---|---|
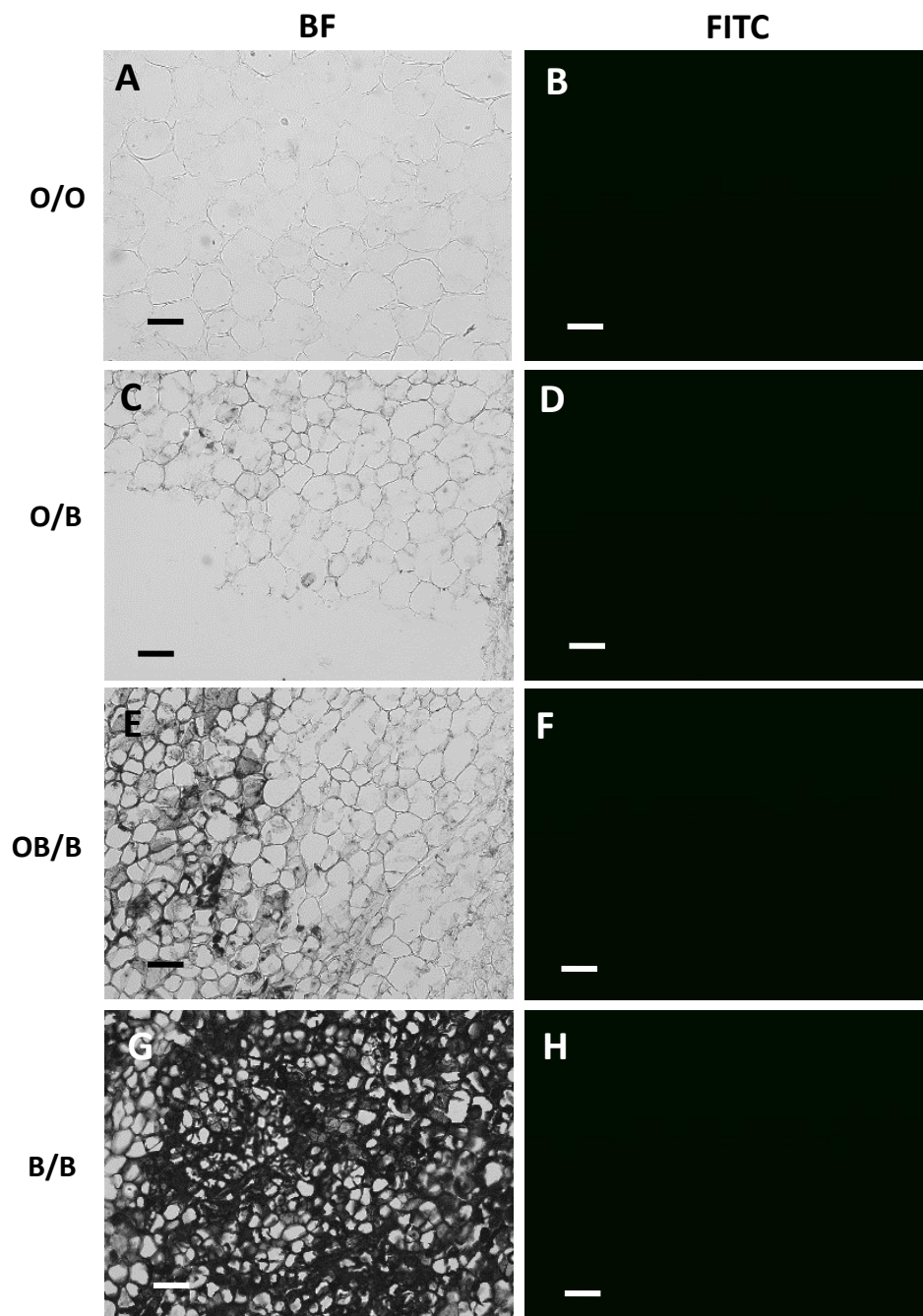


**Figure 4.12: Indirect immunofluorescence detection of the branched (1,6-Gal) (1-4)-β-D-galactan epitope in transverse sections of orange and blackened carrot batons.** Bright field (BF) images showing tissue of an orange carrot baton (O/O) (A) and different sections of a carrot baton with visual blackening. The sections are the orange region on a blackened baton (O/B) (C), tissue directly bordering the black region (OB/B) (E), and the black region (B/B) (G). Corresponding immunofluorescence images taken in the FITC

channel generated with monoclonal antibodies to branched (1,6-Gal) (1-4)-β-D-galactan (LM26). Scale bar = 10 μm. X10 magnification. Exposure times: BF = 0.045 s, FITC = 1.5 s.

### 4.2.6 Analysis of aromatic residues and carbohydrates

An additional approach to study the cell walls in the carrot batons was to measure lignin and carbohydrate content using pyrolysis-GC-MS and methanolysis-GC-FID. Lignin was extracted from alcohol-insoluble carrot residue by pyrolysis in an atmosphere lacking oxygen. The lignin subunits H-lignin, G-lignin, and S-lignin were identified and quantified using GC and detected using MS. Additionally, methanolysis was used to extract carbohydrates from carrot samples, which were then separated and quantified using a combination of GC-FID.

#### 4.2.6.1 Increased lignin and other aromatic units in black regions.

The lignin content of the black regions was more than double that of the orange regions of the carrot batons (Figure 4.13). The levels of all three lignin subunits were higher in the black regions (Figure 4.14), as was an abundance of aromatic residues (Figure 4.15).
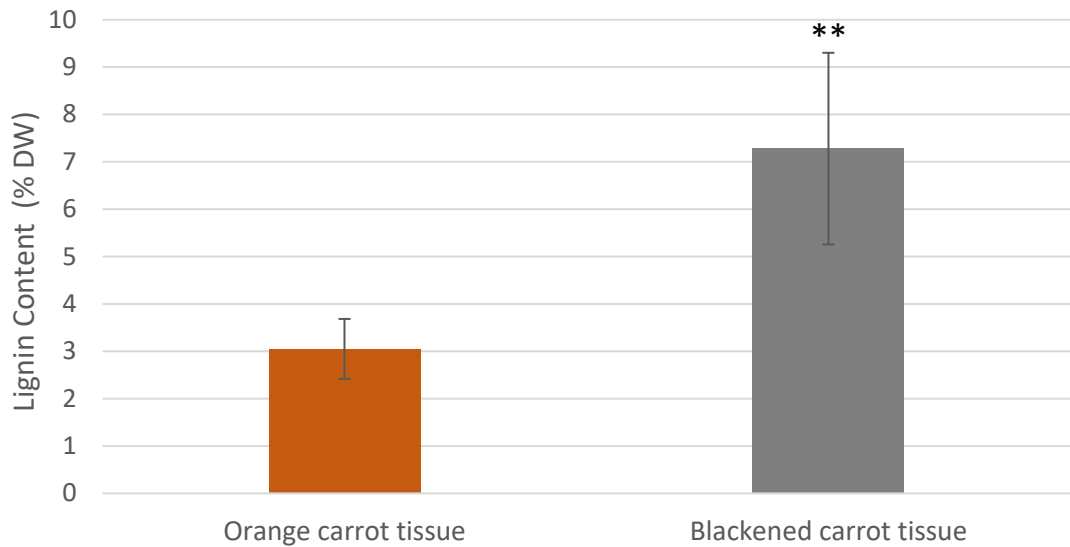
**Figure 4.13: The relative lignin contents of orange and blackened regions of carrot batons (% DW).** Data are the mean values ± SE (5 orange region samples and 4 black region samples). Significant differences between orange and black samples were calculated with a T-test, **p<0.01. P = 0.002.
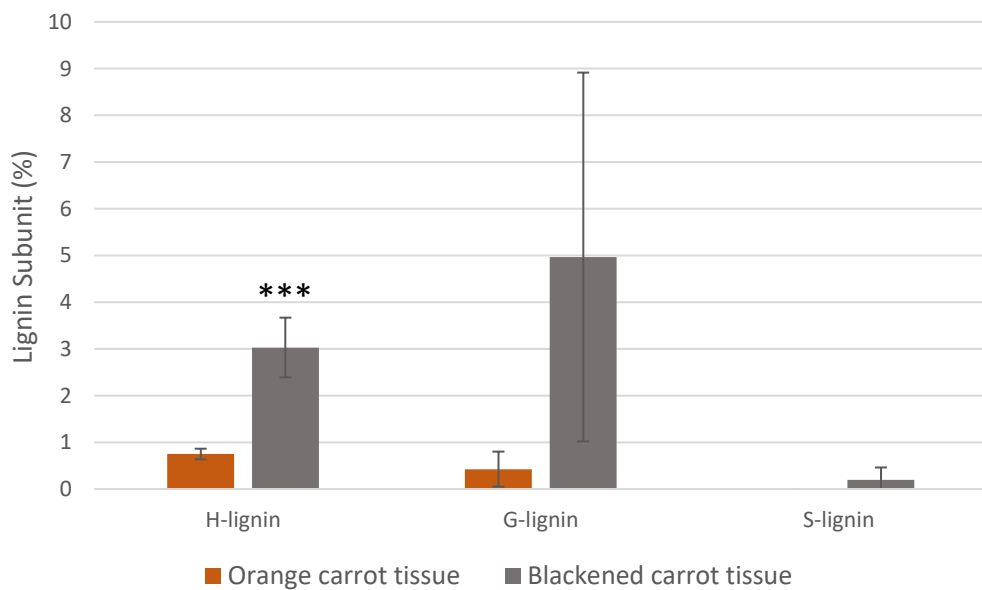


**Figure 4.14: A comparison of the lignin subunit contents of orange and blackened regions of carrot batons (%).** The lignin subunits are also known as *p*-hydroxyphenyl (H-lignin), guaiacyl (G-lignin) and syringyl (S-lignin). Data are the mean values ± SD (n = 4). Significant differences between orange and black samples were calculated with a T-test, ***p<0.001. P = 0.0004.
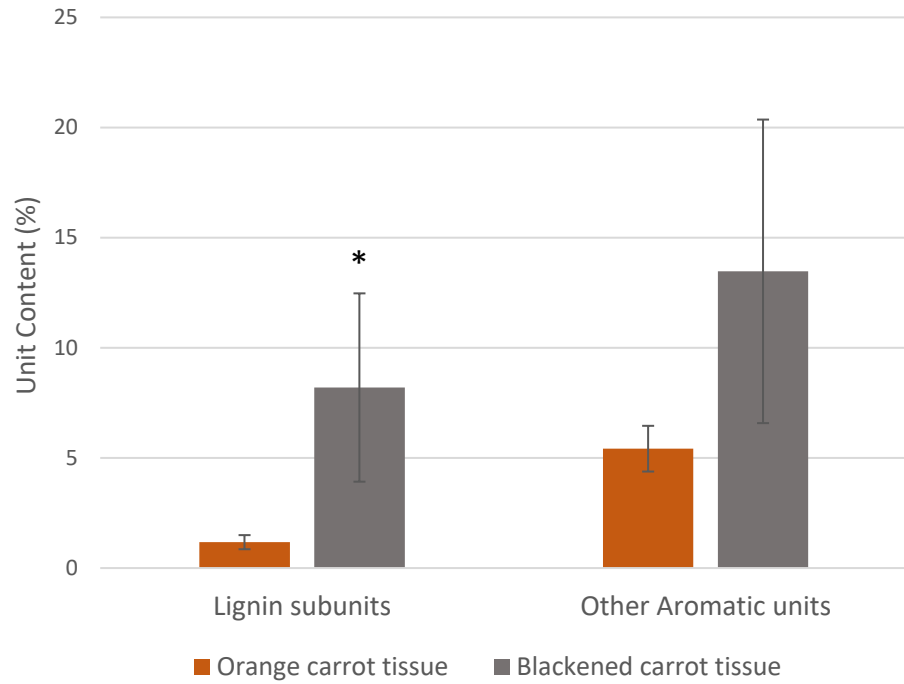
**Figure 4.15: A comparison of lignin and other aromatic residues in orange and blackened carrot batons (%).** Data are the mean values ± SD (n = 4). *p<0.05. P = 0.0169.

### 4.2.6.2 Carbohydrate analysis of sections of orange and black regions.

Galacturonic acid levels were significantly decreased in the black regions of the carrots compared to the orange regions but other carbohydrate monomers were present at similar levels in both regions (Figure 3.16).
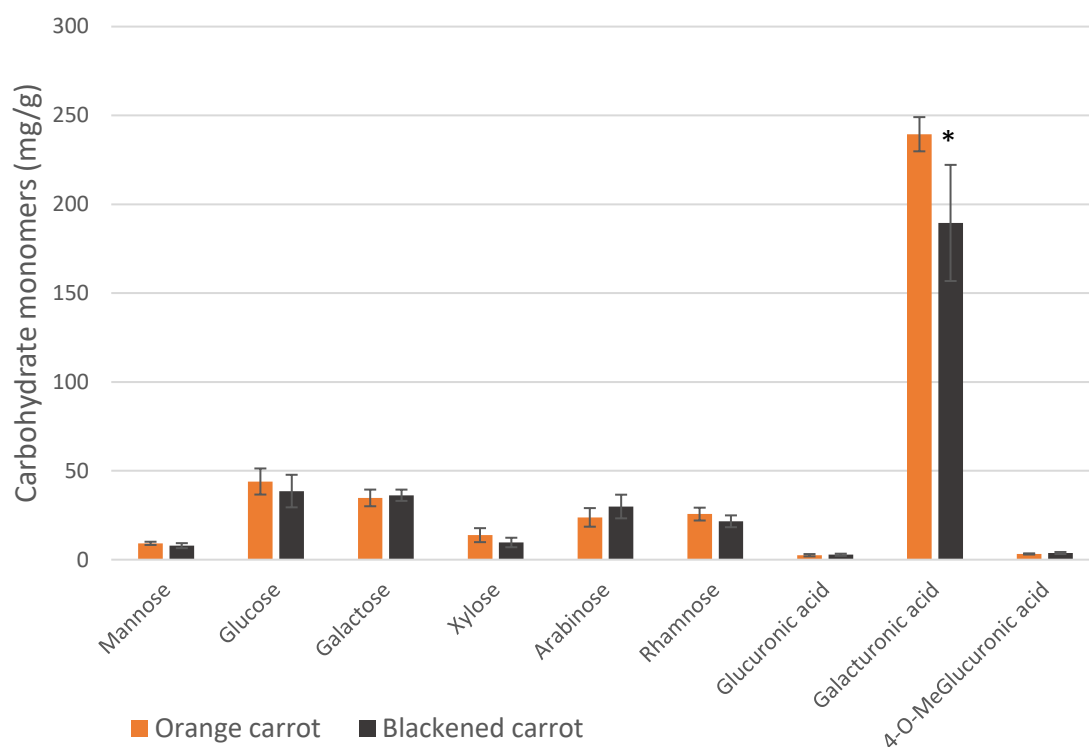


**Figure 4.16: A comparison of carbohydrate monomer contents in orange and blackened regions of the carrot batons.** Data are the mean values of the mean of all biological replicates ± SD (n = 5). Significant differences between orange and black samples were calculated with a T-test, *p<0.05, **p<0.01, ***p<0.001.

## 4.3    Discussion

The data reported in this chapter provide new insights into the composition of the cell walls in the orange and black regions of carrot batons. A range of techniques were used to identify and quantify cell wall components, and to analyse the composition of cell wall components. The observed differences between the cell walls in the orange and black regions of carrot batons allow a deeper understanding of the processes that contribute to the blackening phenomenon. The increased levels of autofluorescence and lignification observed in the black carrot regions are accompanied by major differences in cell wall polymers, particularly HG and RG-I pectin and xyloglucan.

The cells in the blackened regions of the batons were significantly smaller than the cells in the orange regions. This observation may be linked to the occurrence of PCD in the blackened regions. PCD causes cell shrinkage because the cytoplasm condenses and cell walls thicken (McCabe et al., 1997). Cells are also smaller in the vascular regions, but it is unlikely that vascular regions alone are prone to blackening as this would lead to a distinctive patterning of the blackened carrot batons. The initial wound repair response observed in carrot callus begins with the division of undamaged cells surrounding the wounded cells which proliferate to seal off the damaged areas. This is followed by the formation of a hardened callus layer that acts as a protective barrier (Hall, 1997). Responses to wounding include repair and reinforcement of the cell wall and the activation of wound signalling pathways. Each cell can transduce signals to neighbouring cells via DAMPs. Depending on the severity of the damage in size or location, the whole plant can be alerted through a systemic signal, spreading from local to distal tissues that comprises waves of hydraulic, electrical, calcium (Ca2+), and ROS signals, and the perception of wound-related hormones, such as JA, ethylene, or ABA. Many responses to wounding occur through activation of transcription factors such as the Ethylene Responsive Transcription Factor 115, which controls the replenishment of stem cells and growth following wounding (Canher et al., 2020). Dead cells act like obstacles to auxin transport flow, such that auxin accumulates around them leading to the production of new cells to replenish the dead ones.

The colour micrographs of the orange and black carrot regions show clear visual differences in the cells in each region. The cells in the blackened regions show a build-

up of dark material whereas that is not observed in the cells in the orange regions. TBO binds more strongly to the cells in the black than the orange regions, indicating that there are significant differences in cell wall composition. The autofluorescence emitted by the black regions suggests the presence of polyphenolic compounds. These findings are consistent with the observed increased levels of lignin and other phenolic compounds in the black regions of the batons. Lignin autofluorescence is observed at 400 nm with an emission band between 410-480 nm (Radotić et al., 2006; Dumitrache et al., 2017). This corresponds with the highest peak of autofluorescence observed in the black regions of the carrot batons. It is possible to suggest that the blackening of the carrots is due at least in part to the accumulation of lignin. The composition of the lignin was also changed in the blackened regions of the batons. There was a general increase in the content of the three lignin subunits: H-lignin, G-lignin and S-lignin. Lignin composition can vary between species and can be influenced by factors such as maturation and tissue type. Sinapyl alcohol increases during the later stages of lignification, leading to an increase of S-lignin accumulation (Schäfer et al., 2018). The black regions of the batons also had increased levels of aromatic residues in addition to lignin.

Exposure to unfavourable environmental conditions or pathogen attack are known to trigger lignin synthesis in order to make cell walls tougher (Sattler and Funnell-Harris, 2013). During hydroponic cultivation, carrot taproots can be deprived of oxygen leading to an increase in lignin that accumulates largely in the xylem vessel cells but without the accumulation of black deposits (Que et al., 2018). The increased lignin observed in the black regions of the batons is likely to be a slow or delayed response to wounding that occurs during processing. However, wounding alone does not lead to blackening of the carrots. Blackening only occurs when the carrots are aged underground prior to processing. Hence, the developmental stage of the carrot is a critical factor that predisposes the batons to wound-induced blackening.

Of the major cell wall polymers, the black regions had decreased levels of xyloglucan, HG pectin and RG-I pectin detection. The lower detection of these polymers could be caused by increased degradation or masking by phenolic polymers. HG pectin is known to prevent detection of xyloglucan. Hence, treatment of pectate lyase is required to

remove the HG pectin before observing xyloglucan (Marcus et al., 2008). The cell walls in the orange regions of the blackened batons showed an increased abundance of homogalacturonan pectin with low, medium and high levels of esterification. In comparison, the three HG pectin epitopes were less abundant in the cell walls of the orange batons and the black regions. Interestingly, the cell walls of the orange carrot batons were rich in both RG-I pectin sidechains, (1-4)-β-D-galactan and (1-5)-α-L-arabinan. These polymers were much less abundant in the orange regions of the blackened batons, with little or no detection in the black regions. The carbohydrate analysis indicated decreased levels of galacturonic acid, which is the main component of the pectin backbone, in the black regions of the batons. Taken together, these findings indicate that pectin levels are low in the black carrot regions rather than being masked by other compounds. Pectins are likely be one of the first compounds to be degraded when general cell degradation processes are triggered. Pectin is degraded by a variety of enzymes, including polygalacturonase, pectinesterase, pectin methylesterase, pectin lyase and pectate lyase. These pectin-degrading enzymes are commonly secreted by fungal or bacterial plant pathogens to weaken the cell walls (Tayi et al., 2016). Decreased pectin levels are therefore a common side effect of microbe attack in an attempt to infiltrate the cell (Bethke et al., 2016). As there is no indication of pathogen attack in the carrot blackening process, the trigger for the observed wound responses must be caused by the development of the carrots as they are stored underground prior to harvest. Pectin oligosaccharides are able to activate defence responses and can trigger lignification (Robertsen, 1986; Hachem et al., 2016). The low detection of pectin in the black regions of the batons could suggest that age-induced pectin degradation is a factor leading to the activation of defence mechanisms, including an increased lignin content. Alternatively, it is possible that the observed increase in phenolic compounds, specifically lignin, could be due to cross linking within the wall that prevents access of the monoclonal antibodies to the pectin epitopes, thereby reducing detection. However, the highest level of detection of HG pectin was in the cell walls of the orange regions of the blackened carrot. This finding is very interesting and suggests that either HG pectin production is high in the orange regions of the blackened carrots or that there is a loosing of the cell wall structure that allows increased antibody access. If HG pectin

production is high, it is likely to be part of a defensive response, whether it occurs prior or during blackening.

Less xyloglucan was detected in the black regions compared to the orange batons or the orange regions of blackened batons. Xyloglucan degradation is usually catalysed by enzymes such as xyloglucan endotransglucosylase, xyloglucanase or cellulase. Decreased levels of xyloglucan can cause cell walls to become less rigid because xyloglucan tethers maintain the structure of the cellulose microfibrils (Hayashi and Kaida, 2011). However, it is possible that increased phenolic cross-linking in the black regions prevent accurate xyloglucan detection.

Taken together, the results presented in this chapter show that HG and RG-I pectin and xyloglucan are detected less in the black carrot regions compared to orange batons. This occurs together with increased levels of lignin and other aromatic residues, and with decreases in galacturonic acid. These differences in cell wall composition are likely a result of developmental factors that enhance pectin and xyloglucan degradation upon processing-induced wounding of aged carrots. Pectin and xyloglucan degradation stimulates the carrots' own defensive responses leading a flux through secondary metabolism and increased lignification of the cell walls. The reasons why the orange regions of the blackened batons contain higher levels of HG pectin than orange batons are unknown. There is little literature concerning the factors that increase pectin production in response to environmental and developmental triggers. Further work is required to determine the reasons for the increased detection of HG pectin in the orange regions of blackened batons, and whether it is a factor that contributes to, or is caused by, the blackening phenomenon. The development of the blackening process and the control of its spread from cell to cell also merits further investigation.

# Chapter V

# Chapter 5: Metabolic profiles of orange and black carrot samples

## 5.1 Introduction

Plant metabolism is extremely flexible and responds rapidly to changes in internal and environmental factors. For example, upon exposure to drought, levels of fructose and glucose increase to ensure that these carbohydrates are available for vital plant functions (Krasensky and Jonak, 2012; Fàbregas and Fernie, 2019). Exposure to abiotic stresses such as high salt and drought increase the accumulation of ROS, as well as ROS-scavenging enzymes, antioxidants and metabolites such as proline (Szabados and Savouré, 2010). ROS production is essential for plant growth but ROS also play a role in the stress-induced cessation of growth and, in some cases, PCD (Considine and Foyer, 2021).

Carrot blackening is characterised by the accumulation of dark material leading to discolouration in freshly cut carrot batons. Enzymatic browning is a common cause of the discolouration seen in root vegetables (Ru et al., 2020). This process can occur when surface tissue is damaged during harvest or postharvest processing. Damage causes mixing of phenolic compounds that are localised in cell walls and vacuoles and the enzyme PPO, which is localized within the lumen of the thylakoid membranes of the chloroplasts. The oxidation of phenolic compounds to corresponding quinones ultimately produces brown pigments such as melanin (Taranto et al., 2017; Moon et al., 2020). Peroxidases (POD) have also been suggested to enhance enzymatic browning (Ciou et al., 2011). The carrot blackening phenomenon is triggered by the cutting process, and so enzymatic browning is considered to be a possible cause of blackening. To test this hypothesis, a metabolic profiling analysis was performed on orange and black carrots segments. I performed this analysis  at the James Hutton Institute in Dundee Scotland.

Carrot samples were provided by Kettle Produce Ltd. Blackened and orange samples were harvested from the carrots originating from the same field, growers and date harvested. Gas chromatography (GC), mass spectrometry (MS) and high-performance

liquid chromatography (HPLC) were performed in order to obtain the metabolite profiles of the different samples. In addition, HPLC analysis incorporating a column was used to identify and quantify carotenoids. In total, seventeen independent biological replicates were analysed using the GC/MS approach and 8 independent biological replicates were analysed using the HPLC/MS and HPLC approaches. The major peaks present on the chromatograms obtained by mass spectrometry were identified on the basis of parent and fragment ion masses present in the mass spectrum of each metabolite. Some peaks are considered to represent isomers. In the case of multiple isomers, the metabolites were numbered with the lowest retention time first. Tables regarding compound ID that comprise (relative) retention time and key mass fragments used for identification are included in the Appendices (Appendices I, II, and III). All of the figures presented in this chapter present data as relative levels that were determined by calculating the response ratio for each metabolite. This analysis was performed by dividing the peak area of the targeted metabolite by the peak area of an internal standard (Morin). Taken together, the data presented in this chapter provide a better understanding of the metabolic mechanisms that are involved in the blackening process. In addition, the analysis of metabolic profiles allows for an assessment of the role of polyphenol oxidation in carrot blackening.

## 5.2 Results

### 5.2.1 Metabolite profiling analysis

A principal component analysis (PCA) was performed using the data from all identified and quantified metabolites in orange and blackened carrot samples, as a first step to analysing variation between the samples. The PCA analysis reveals clusters of samples based on the similarity of metabolite quantities (Figure 5.1). Score 1 shows a clear separation between orange and black carrot samples and represents 37.4% of the variation between samples. Score 5 shows no clear separation (Figure 5.1). A: Orange carrot samples (shown in black), B: Black carrot samples (shown in blue).
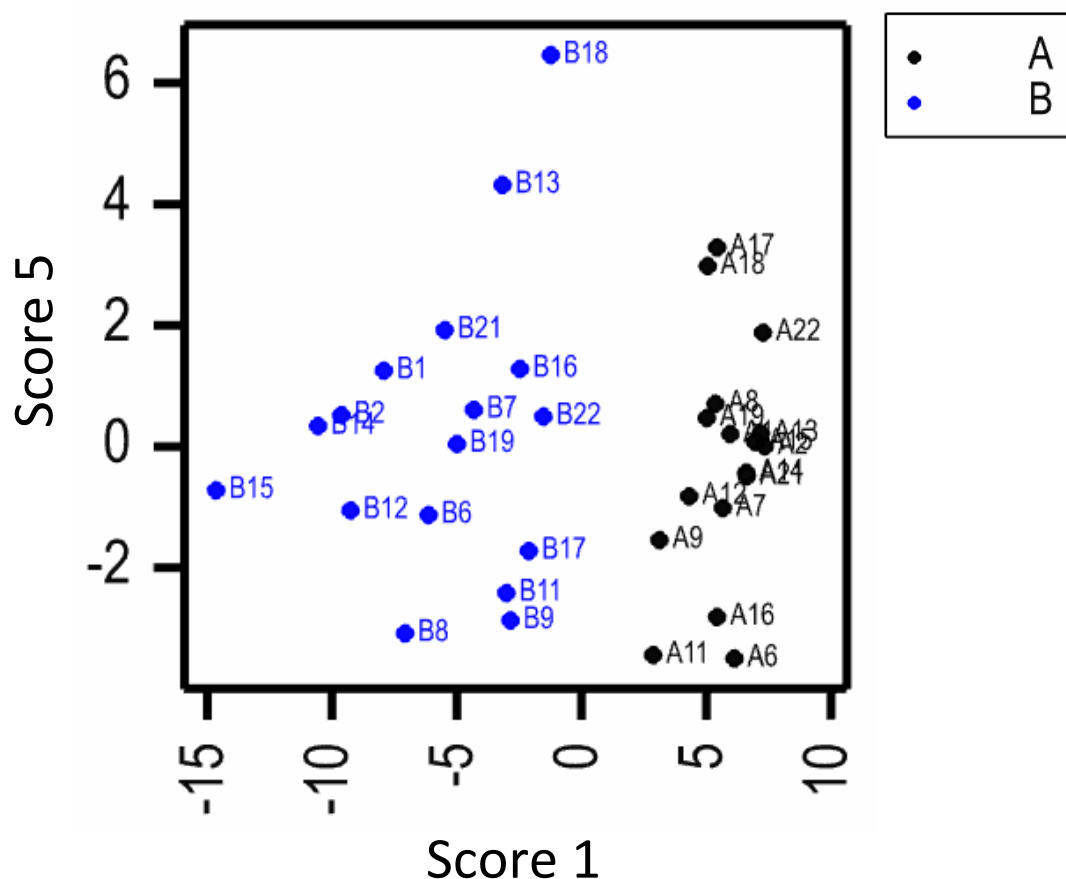


**Figure 5.1: Principal components analysis (PCA) of the metabolic profiles of orange (A) and black (B) carrot samples**. A log transformation was performed prior to the PCA. A: Orange carrot samples (shown in black), B: Black carrot samples (shown in blue).

## 5.2.2   Differences in metabolites between orange and black carrot samples

In total 94 metabolites were identified using HPLC/MS, HPLC, GC/MS analysis of blackened and orange carrot segments. The metabolites were categorised into groups: amino acids, amines/polyamines, carbohydrates, organic acids, fatty acids, carotenoids, fatty alcohols, and phenolic compounds. Metabolite profiles were compared by a one-way ANOVA using carrot blackening as the single factor. A total of 64 metabolites were found to be significantly different ($p < 0.05$) between the black and orange carrot samples. Key differences in the metabolic profiles observed in the black carrot samples included the general increase in fatty acids and phenolic compounds, and the decrease in sugars and amino acids.

### 5.2.2.1   Amino acids

Using GC/MS, 19 amino acids were identified in the black and orange carrot samples. In total, the levels of 16 amino acids were found to be significantly decreased in the black carrot samples. No differences in β-alanine or lysine levels were observed (Figure 5.2). The only amino acid with increased levels in the black carrot samples was γ-aminobutyric acid (GABA), which was approximately 8 times greater than the GABA content found in the orange carrots.
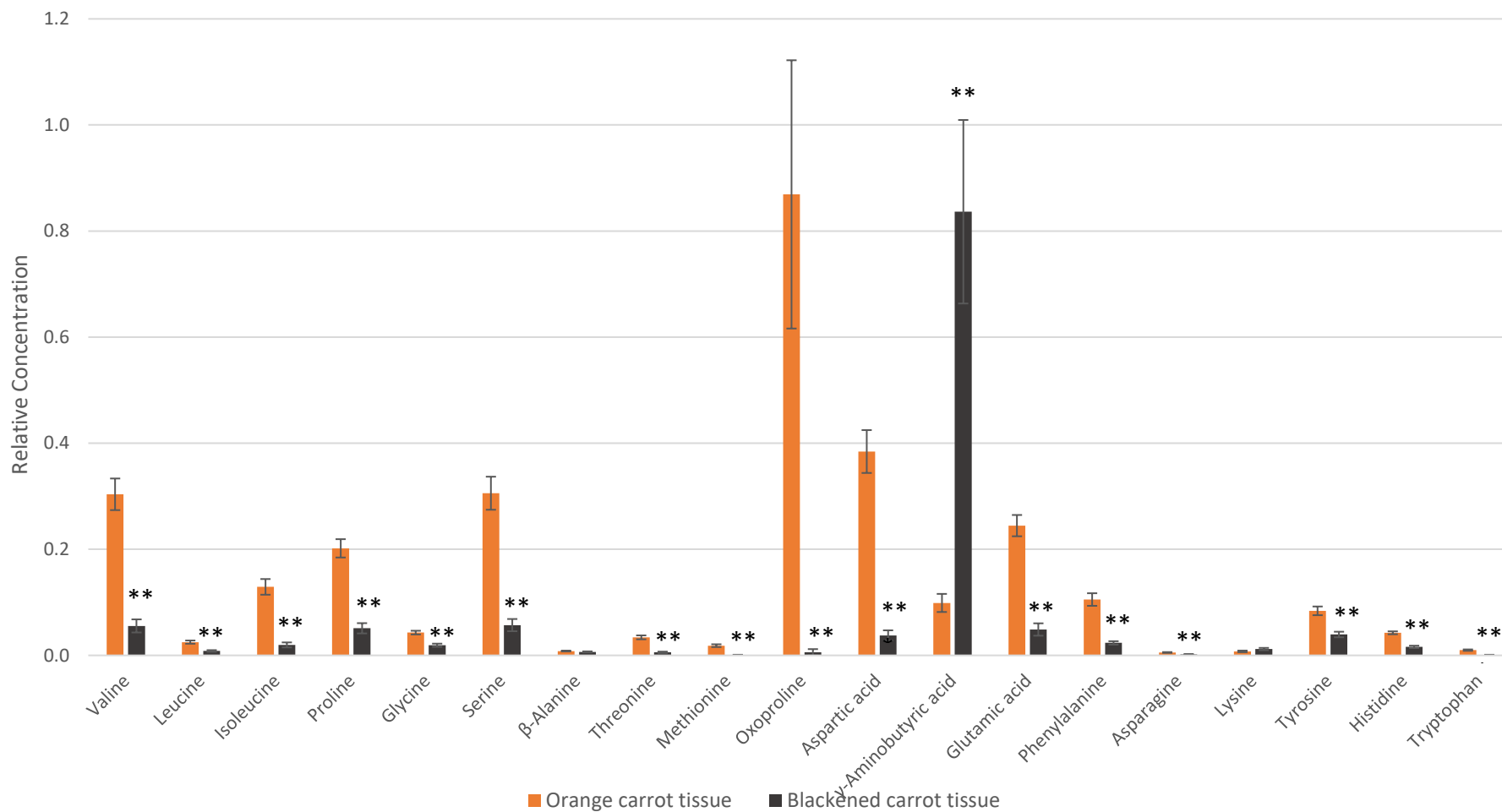
**Figure 5.2: Relative levels of amino acids in orange and black carrot samples using GC/MS.** Relative concentration was the mean compound (n=17) normalised to the internal standards. Asterisks indicate the statistical significance level: p-value ≤ 0.05 (*), < 0.01 (**), and < 0.001 (***) using ANOVA. Data are the mean +/- standard deviation.

### 5.2.2.2 Amines/Polyamines

The levels of several amines/polyamines were significantly different in the orange and black carrot samples. In particular, the levels of allantoin and putrescine were increased in the black carrot samples whereas the abundance of ethanolamine was slightly decreased (Figure 5.3).
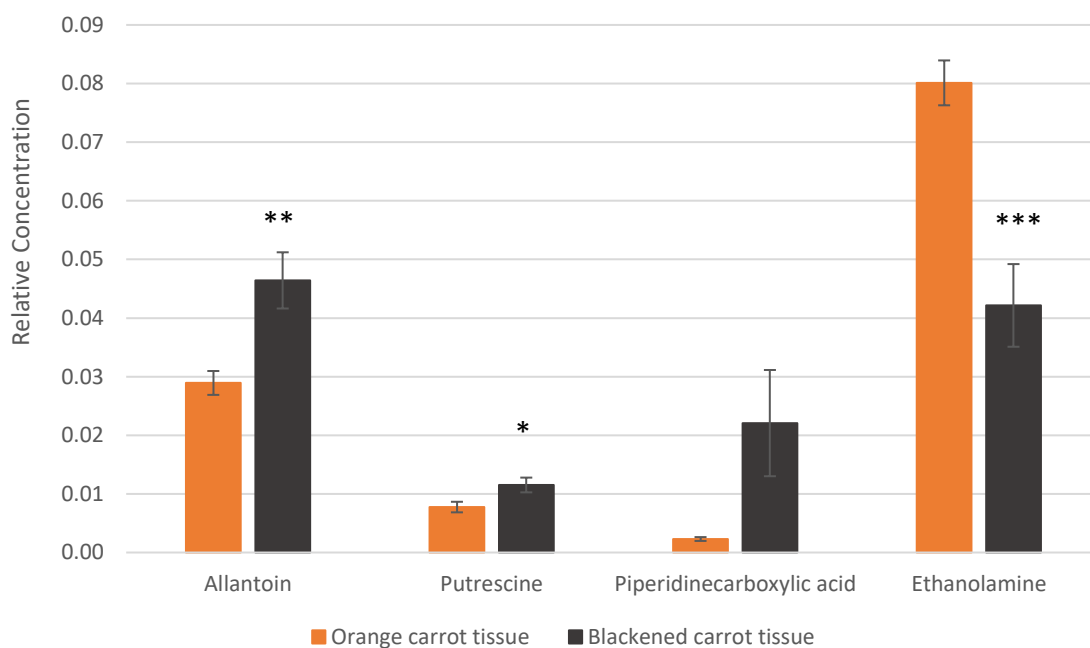


**Figure 5.3: Relative levels of amines/polyamines in orange and black carrot samples using GC/MS.** Relative concentration was the mean compound (n=17) normalised to the internal standards. Asterisks indicate the statistical significance level: p-value ≤ 0.05 (*), < 0.01 (**), and < 0.001 (***) using ANOVA. Data are the mean +/- standard deviation.

### 5.2.2.3 Carbohydrates

Ten metabolites associated with carbohydrate metabolism were identified, including two isomers of both fructose and glucose. A general decrease in the levels of fructose, glucose, sucrose and inositol was observed in the black carrot samples (Figure 5.4). In addition, the levels of mannose, galactose, glycerol and mannitol were increased in the black samples. In particular, mannitol was 10 times more abundant in the black than the orange samples (Figure 5.5).
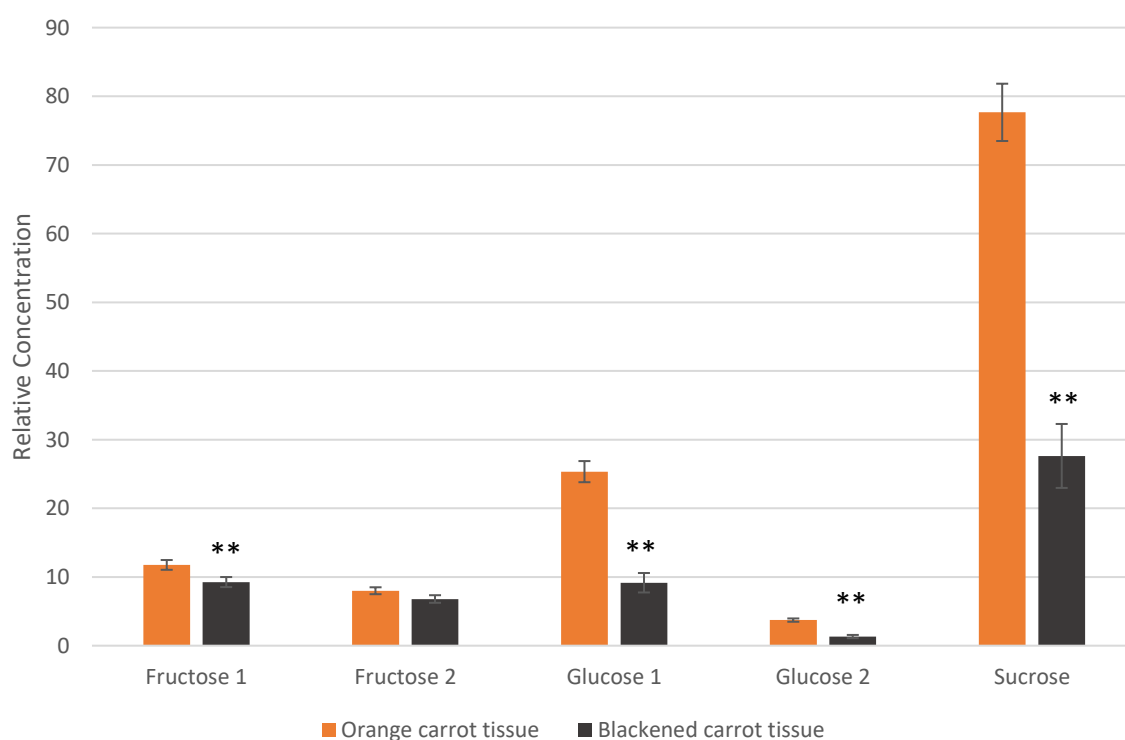


**Figure 5.4: Relative levels of carbohydrates in orange and black carrot samples using GC/MS.** Relative concentration was the mean compound (n=17) normalised to the internal standards. Asterisks indicate the statistical significance level: p-value ≤ 0.05 (*), < 0.01 (**), and < 0.001 (***) using ANOVA. Data are the means +/- standard deviation.
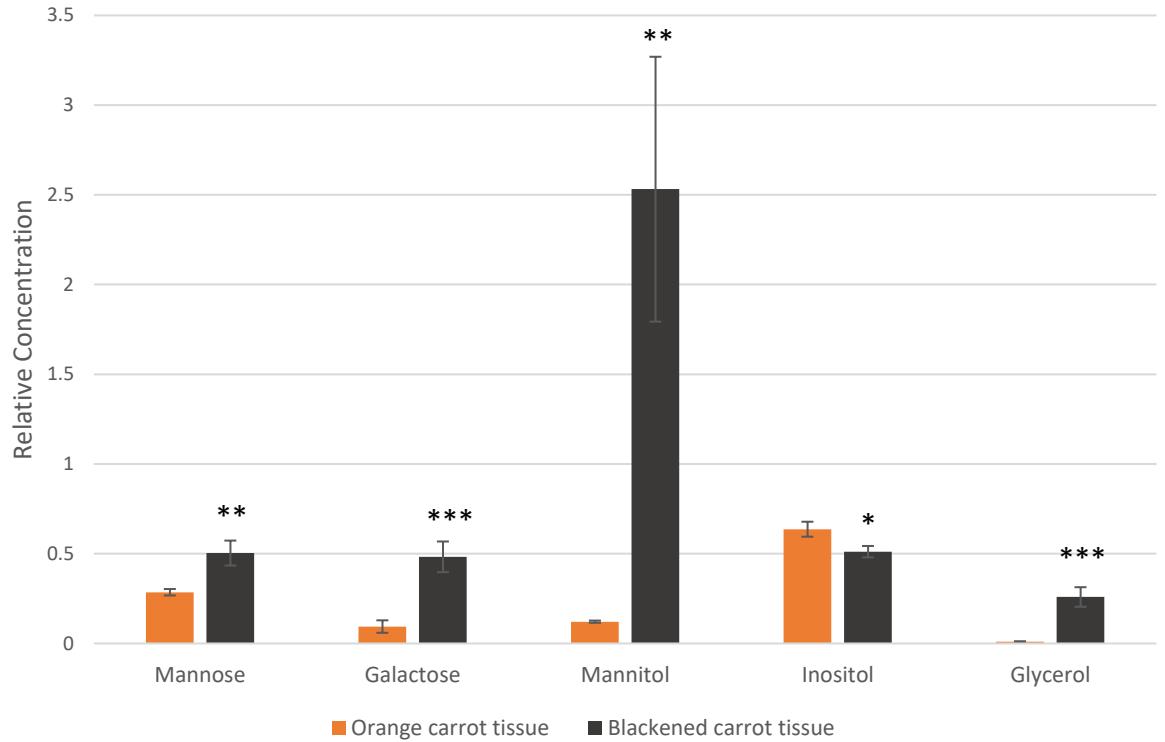
**Figure 5.5: Relative levels of carbohydrates in orange and black carrot samples using GC/MS.** Relative concentration was the mean compound (n=17) normalised to the internal standards. Asterisks indicate the statistical significance level: p-value ≤ 0.05 (*), < 0.01 (**), and < 0.001 (***) using ANOVA. Data are the mean +/- standard deviation.

### 5.2.2.4 Organic acids

Significant differences in several organic acids were observed between the orange and black carrot samples. Six organic acids were less abundant in the black than the orange samples. The levels of threonic acid and galactaric acid were increased in the black samples. However, succinic acid levels were similar in black and orange carrot segments (Figure 5.6).
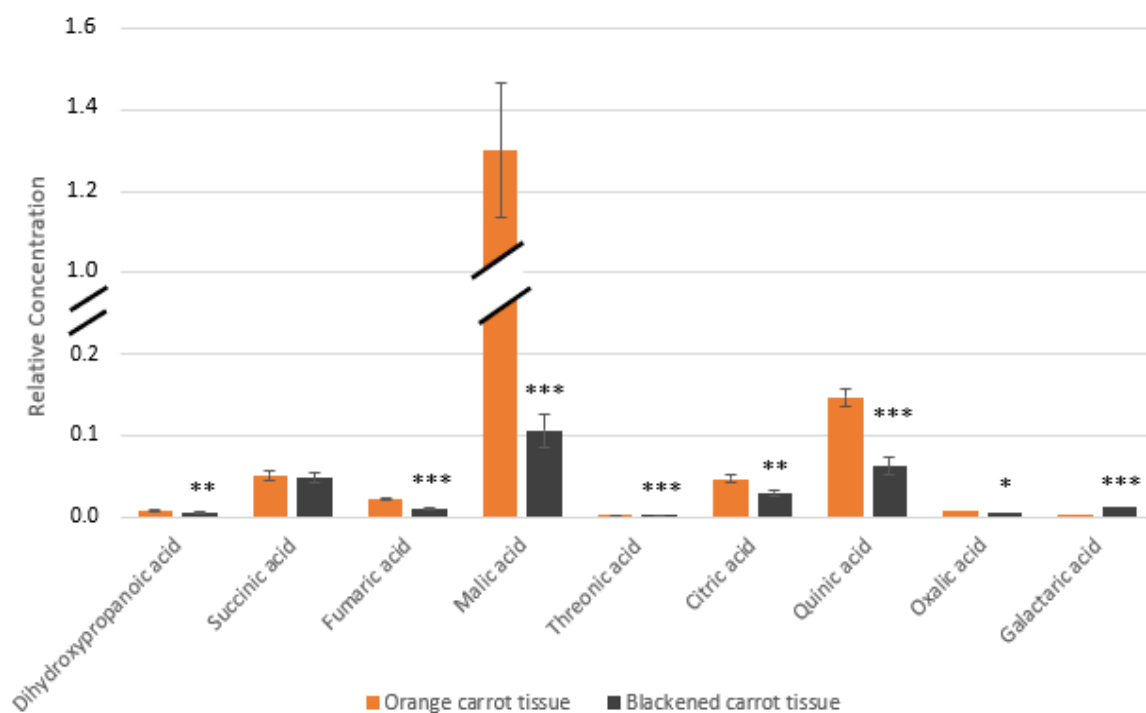


**Figure 5.6: Relative levels of organic acids in orange and black carrot samples using GC/MS.** Relative concentration was the mean compound (n=17) normalised to the internal standards. Asterisks indicate the statistical significance level: p-value ≤ 0.05 (*), < 0.01 (**), and < 0.001 (***) using ANOVA. Data is the mean +/- standard deviation.

### 5.2.2.5 Fatty Acids, fatty acid alcohols and carotenoids

In total, 19 fatty acids were identified. Significant increases in the levels of most of the identified fatty acids were observed in the black carrot segments.  However, linoleic acid levels were similar in black and orange carrot samples (Figure 5.7).
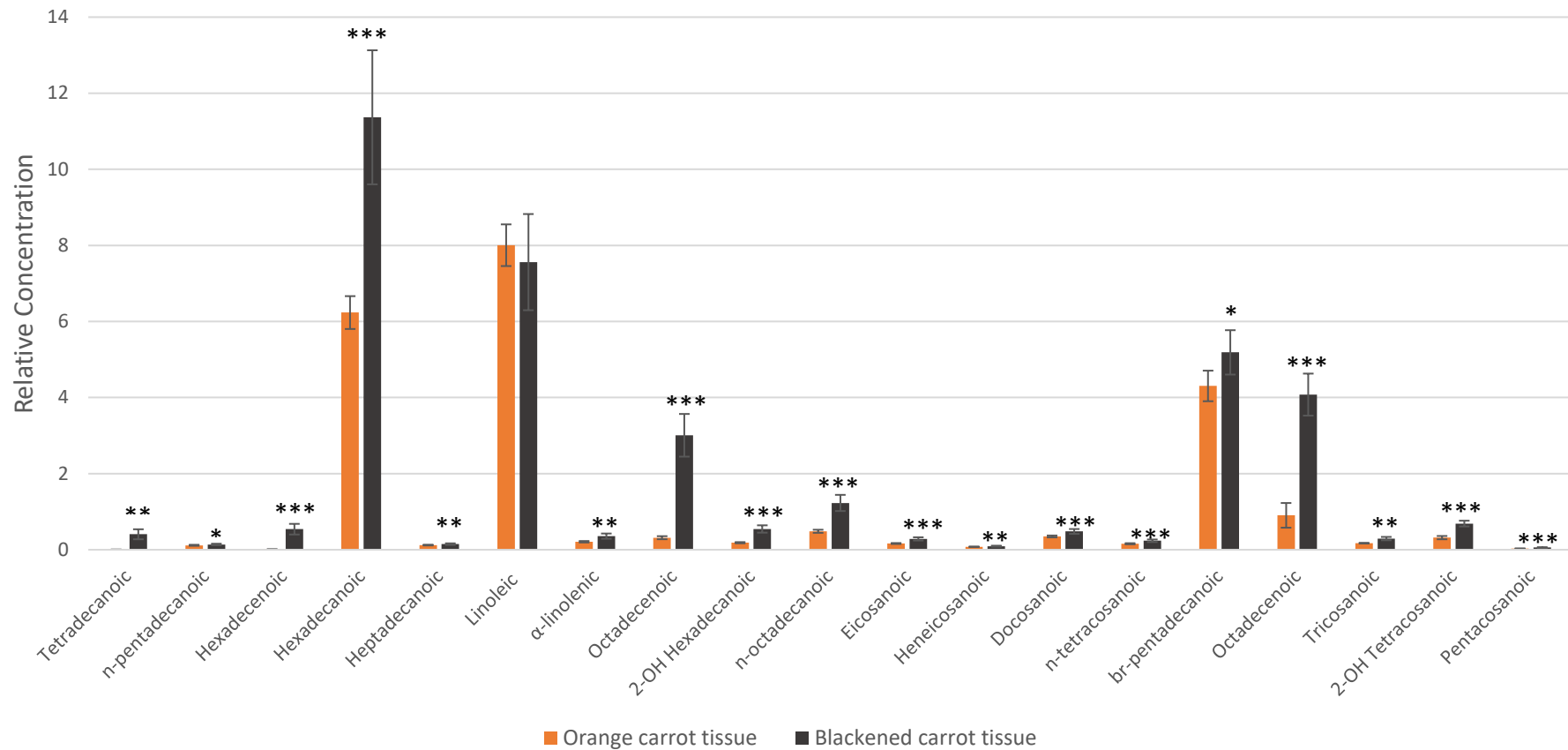
**Figure 5.7: Relative levels of fatty acids in orange and black carrot samples using GC/MS.** Relative concentration was the mean compound (n=17) normalised to the internal standards. Asterisks indicate the statistical significance level: p-value ≤ 0.05 (*), < 0.01 (**), and < 0.001 (***) using ANOVA. Data are the mean +/- standard deviation.

The carotenoid contents and composition of black and orange carrot samples was analysed. No significant differences in the major carrot carotenoids were observed between the black and orange samples. A significant decrease in lutein levels was observed in the black compared the orange carrot samples (Figure 5.8).
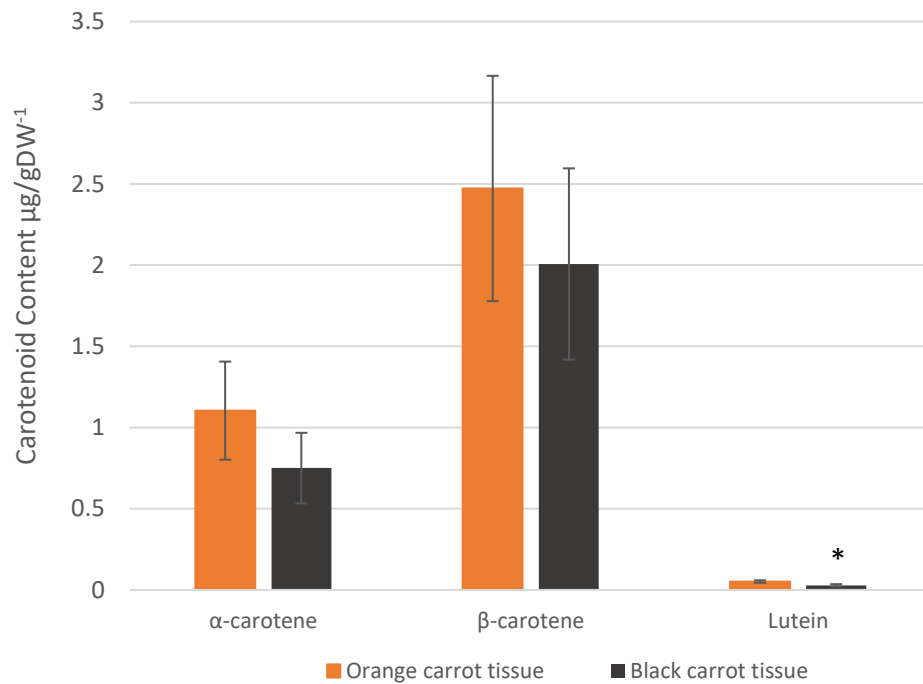


**Figure 5.8: The carotenoid content (µg/gDW$^{-1}$) in orange and black carrot samples using HPLC.** The carotenoids identified are α-carotene, β-carotene and lutein. Asterisks indicate the statistical significance level: p-value ≤ 0.05 (*) using T-tests. P = 0.044. Data are the mean +/- standard deviation (n=8 samples).

The levels of the five fatty acid alcohols identified in the metabolite profiles were similar in the orange and black carrot samples (Figure 5.9).
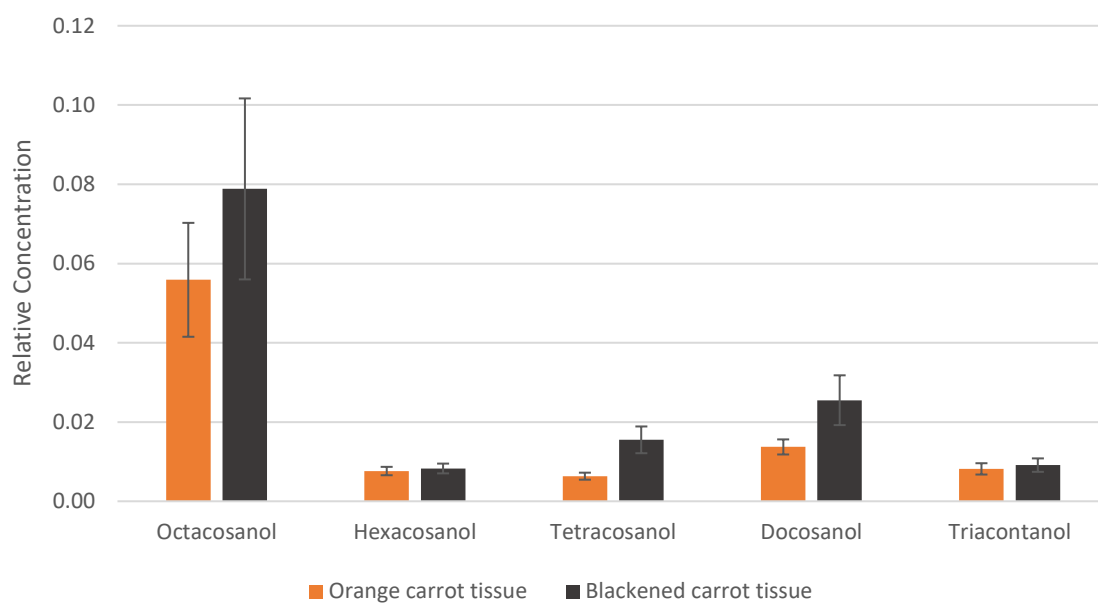


**Figure 5.9: Relative levels of fatty alcohols in orange and black carrot samples using GC/MS.** Relative concentration was the mean compound (n=17) normalised to the internal standards. Asterisks indicate the statistical significance level: p-value ≤ 0.05 (*), < 0.01 (**), and < 0.001 (***) using ANOVA. Data are the mean +/- standard deviation.

### 5.2.3  Secondary metabolites

GC/MS techniques were used to identify components involved in primary metabolism, although some phenolic metabolites were also identified using this technique (Figure 5.10 and 5.11). HPLC analysis was used to further identify components involved in secondary metabolism (Figure 5.12). Multiple isomers of several metabolites were identified. Overall, a general trend of increased levels of phenolic compounds was seen in the black carrot segments. In particular, significant increases in the levels of chlorogenic acid, caffeic acid, dicaffeoylquinic acid and 5-caffeoylquinic acid were measured (Figure 5.10, 5.11 and 5.12 C).
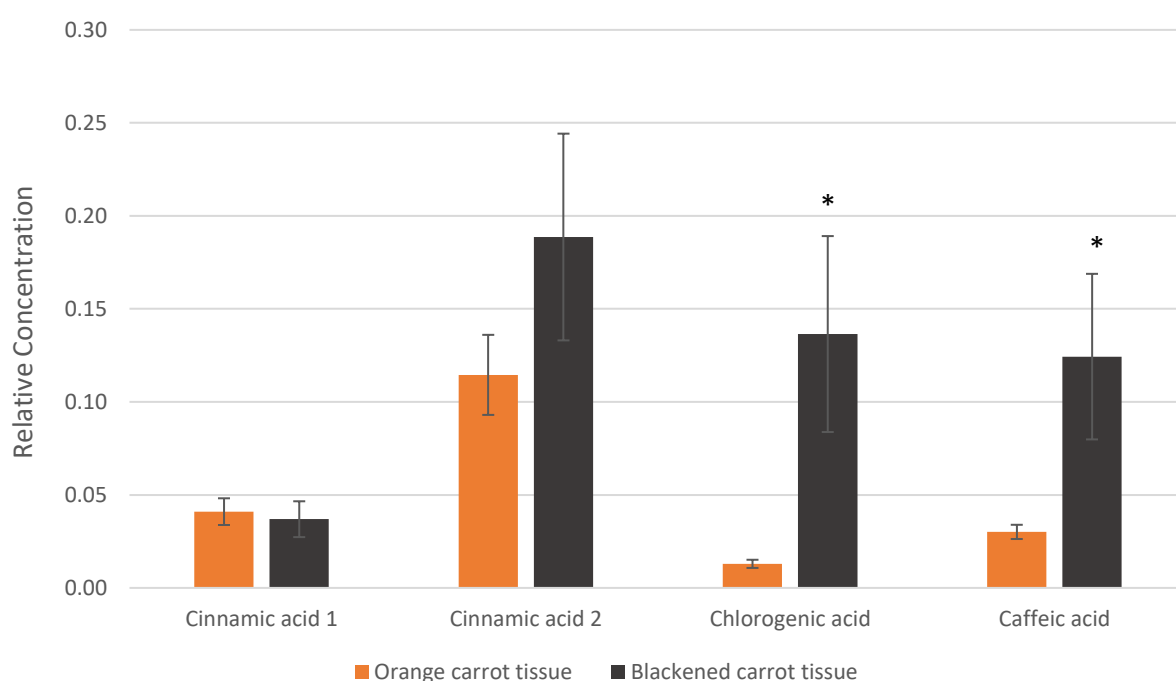


**Figure 5.10: Relative levels of secondary metabolites in orange and black carrot samples using GC/MS.** Relative concentration was the mean compound (n=17) normalised to the internal standards. Asterisks indicate the statistical significance level: p-value ≤ 0.05 (*), < 0.01 (**), and < 0.001 (***) using ANOVA. Data are the mean +/- standard deviation.
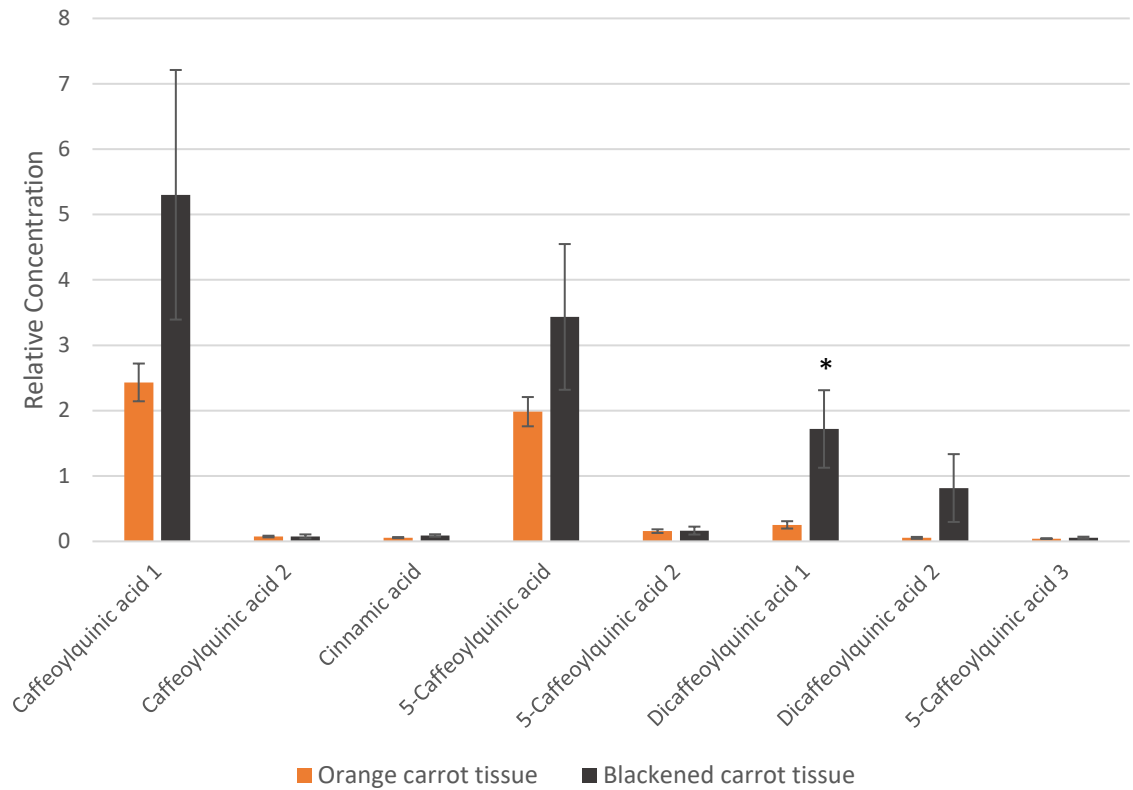
**Figure 5.11: Relative levels of secondary metabolites in orange and black carrot samples using HPLC/MS.** Relative concentration was the mean compound (n=17) normalised to the internal standards. Asterisks indicate the statistical significance level: p-value ≤ 0.05 (*), < 0.01 (**), and < 0.001 (***) using ANOVA. Data are the mean +/- standard deviation.
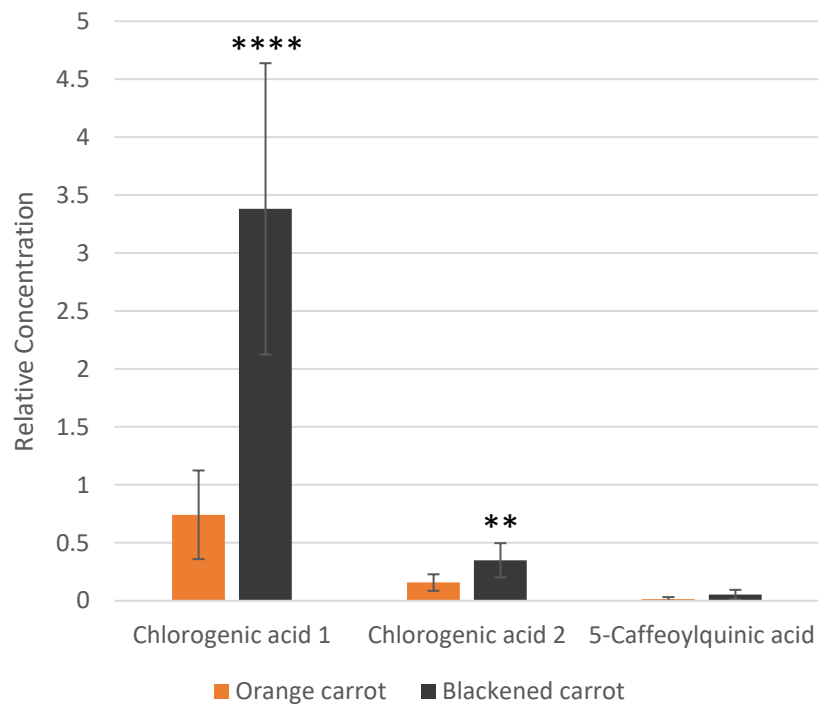
**Figure 5.12: Relative levels of secondary metabolites identified using HPLC/MS in orange and black carrot samples.** Relative concentration was the mean compound (n=8) normalised to the internal standards. The secondary metabolites identified are chlorogenic acid 1, chlorogenic acid 2 and 5-caffeoylquinic acid. Asterisks indicate the statistical significance level: p-value ≤ 0.05 (*), < 0.01 (**), and < 0.001 (***) using T-tests. Data are the mean +/- standard deviation.

### 5.2.4 A summary of metabolite changes in black relative to orange carrot segments

Figure 5.13 provides an overview of the changes in primary metabolism observed in the black regions compared to orange regions of the cut carrots. Analysis of the black carrot regions revealed a general decrease in primary metabolites, particularly sugars and amino acids. Conversely, increases in the abundance of lysine and GABA were observed in the black segments (Figure 5.13). A large decrease in tricarboxylic acid (TCA) cycle intermediates, including fumarate, malate and citrate, was seen in the black regions of the cut carrots, along with a general increase in phenolic compounds (Figure 5.14). The levels of some metabolites such as alanine (Ala), fructose-6-phosphate (F-1,6-bP), succinate, lysine (Lys) (Figure 5.13), cinnamic acid, caffeoylquinic acid, and 5-caffeoylquinic acid were similar in the black and orange regions of the cut carrots (Figure 5.14).
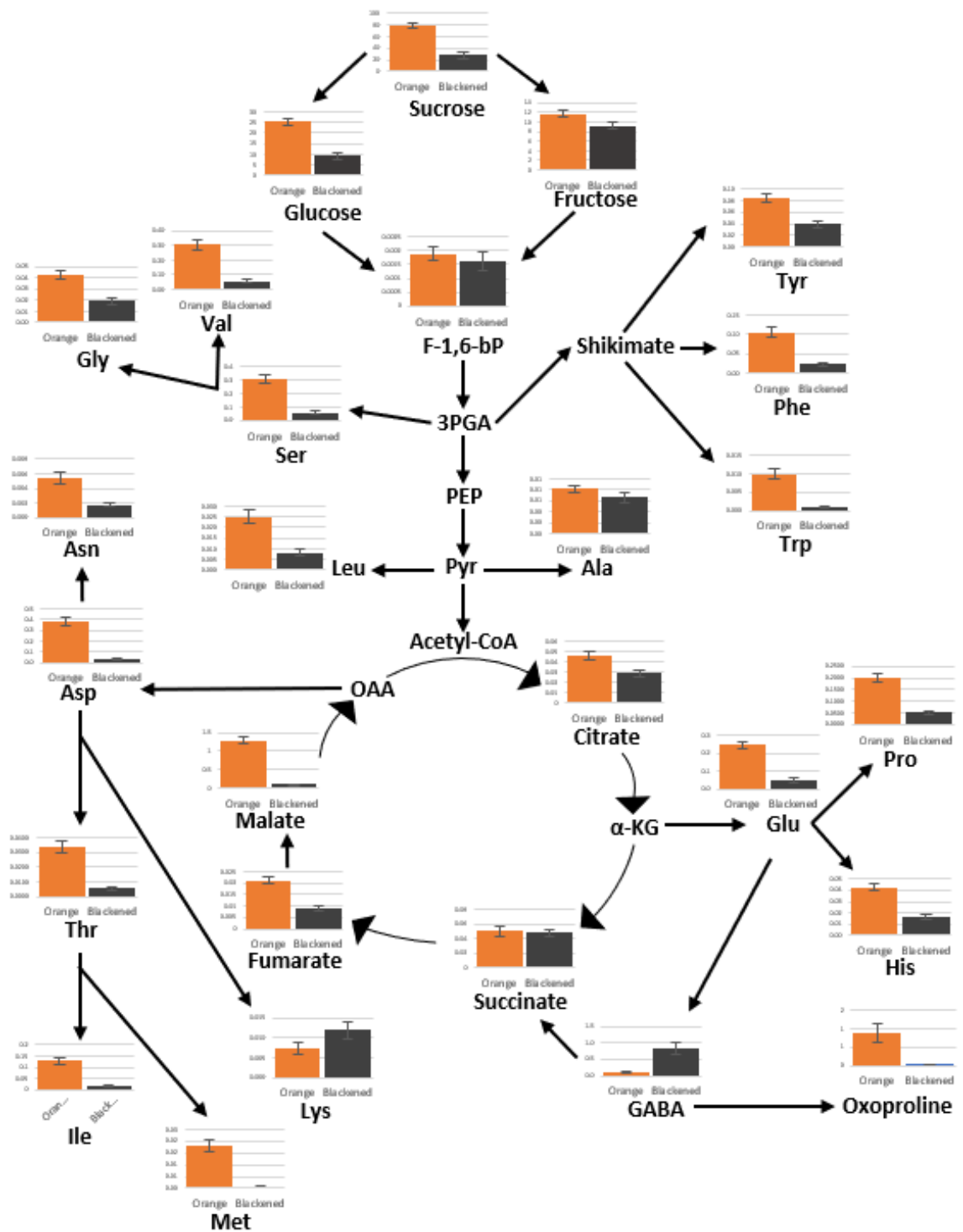
**Figure 5.13: A comparison of the metabolite profiles of orange and black carrot regions focusing on sugars, amino acids, and TCA cycle intermediates, shown as a schematic of key metabolic pathways.** The bar charts represent relative levels of each metabolite in the orange carrot batons (orange left-hand bar) and the black carrot regions (grey right-hand bar). Data are mean +/- standard error (n=17).
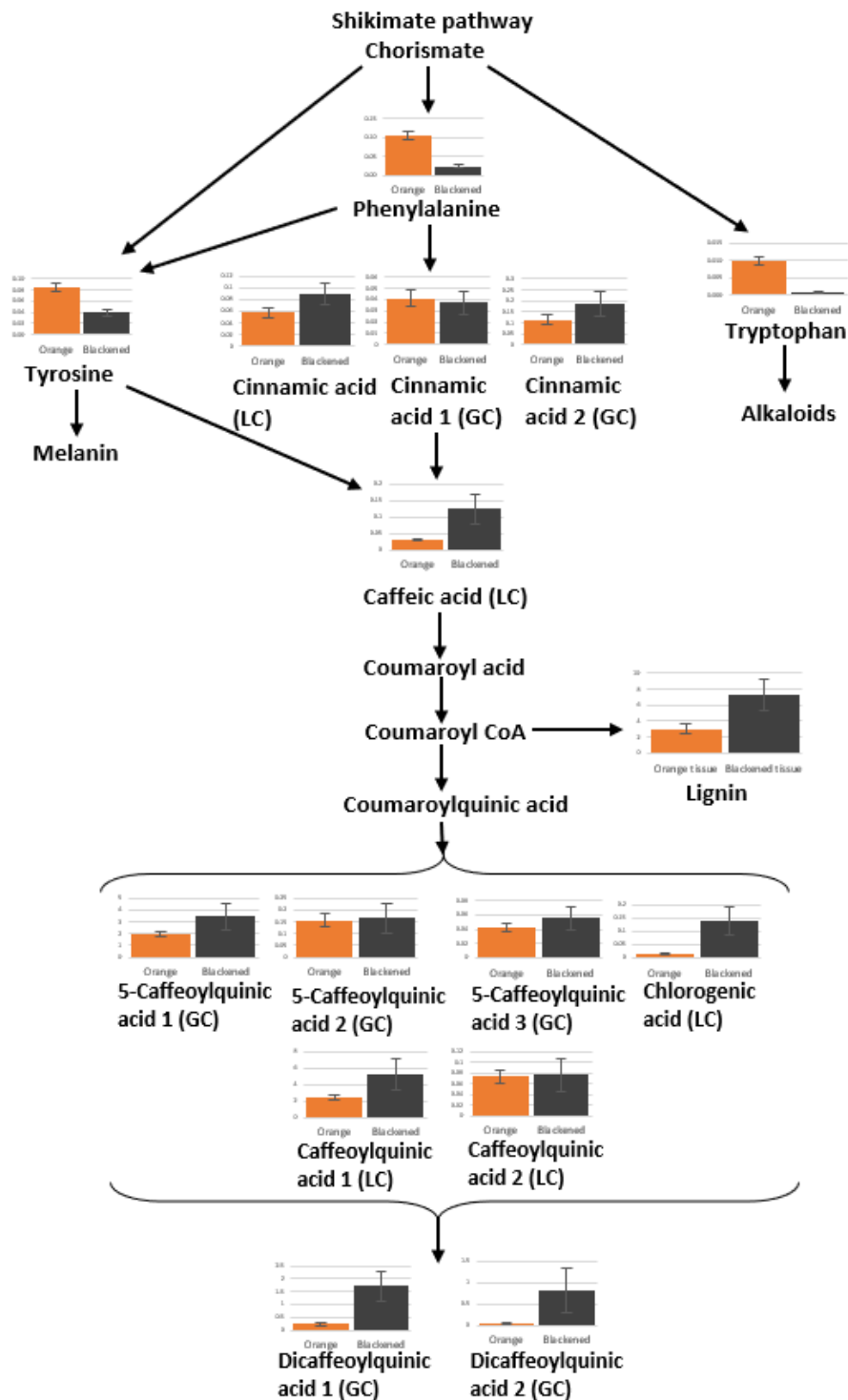
**Figure 5.14: A comparison of the metabolite profiles of orange and black carrot samples regions focusing on phenolic compound synthesis, shown as a schematic of key metabolic pathways.** The bar charts represent relative levels of each metabolite in the orange carrot batons (orange left-hand bar) and the black carrot regions (grey right-hand bar). LC: determined by HPLC/MS. GC: determined by GC/MS. Data are mean +/- standard error (n=17).

## 5.3   Discussion

The data presented in this chapter concern the metabolic profiles of orange and black carrot samples. A combination of gas and liquid chromatography and mass spectrometry was used to separate, identify, and quantify metabolites. Distinct differences were found in several metabolite categories between the orange and blackened carrot metabolomic profiles. The key findings reported in this chapter reveal that the blackened carrot samples show 1) a general decrease in amino acids, sugars (glucose, fructose, sucrose) and organic acids; and 2) a general increase in phenolic compounds, some carbohydrates (mannose, galactose, mannitol, and glycerol) and fatty acids. It is important to note that the levels of the majority of organic acids involved in the TCA cycle were decreased in the black carrot segments. This finding suggests that there is a switch from primary to secondary metabolism in the blackened regions of the carrot that may be associated with starvation or depletion of respiratory substrates.

Wounding of the carrots leading to cell and organelle rupture as they are cut into batons may release cell wall and cytoplasmic enzymes such as PPO and POD so that they come into contact with phenolic compounds originating from vacuoles. While loss of membrane integrity may be a major factor controlling the rate of blackening, this is not a rapid process in cut carrots because the blackened regions can appear throughout the following 72 hours after processing. This latency period in the formation of blackened regions has been linked to an activation of secondary metabolism and PPO activity following mechanical wounding and tissue rupture. The production of polyphenols leading to enhanced lignin formation is a result of the activation of the phenylpropanoid pathway where PPO, POD and phenylalanine ammonia lyase (PAL) may act together to facilitate tissue blackening. These enzymes are often linked to the degradation in fresh produce, resulting in quality losses for consumers. Acidic organic acids such as malic acid and citric acid inhibit PPO activity. Hence, low levels of these acids could accelerate blackening (Moon et al., 2020). Wounding leads to an increase in ROS accumulation and changes in antioxidant metabolites and enzymes. An enhanced breakdown of the major low molecular weight antioxidant, vitamin C (ascorbate), which produces metabolites such as threonic acid, as a result of wounding could contribute to non-enzymatic blackening in carrots as it does in apples (Mellidou et al., 2014).

The observed lower levels of glucose, sucrose and fructose, taken together with the general decrease of amino acids suggests that the blackened carrots may be running out of the vital carbohydrate reserves that are necessary for ATP production.

Very high levels of the four-carbon non-proteinogenic amino acid GABA were detected in the blackened carrot regions. This amino acid is ubiquitous in plants, animals and microorganisms. It is involved in multiple pathways and processes and fulfils important roles in metabolism as well as a signalling. It is produced by a pathway called the GABA shunt, which is linked to pathways such as the TCA cycle. In the cytosol, GABA is irreversibly synthesized from L-glutamate via glutamate decarboxylase. Alternatively it can be generated from the degradation of polyamines such as putrescine and spermidine, or from the non-enzymatic oxidation of proline in response to stress (Fait et al., 2008). The GABA shunt and the TCA cycle are connected by a transmembrane protein called GABA permease that allows a GABA flux between the cytosol and mitochondria. The GABA content of crops varies between species and varieties and depends on many factors, such as the developmental stage, environmental conditions, and in response to biotic and abiotic stresses. The decreases in aromatic amino acids observed in the blackened carrot segments may suggest a switch from primary to secondary metabolism in the cut batons leading to an accumulation of phenolic compounds in the blackened carrot segments. The large increase in GABA accumulation observed in the blackened carrot segments may occur through the GABA shunt, in which glutamate is decarboxylated to produce $CO_2$ and GABA.

GABA accumulation is often considered to be a stress marker in plants. It occurs soon after exposure to abiotic stresses such as hypoxia, chilling, heat, drought and wounding (Kinnersley and Turano, 2000; Wu et al., 2018; Li et al., 2018). The dramatic ~8-fold increase of GABA observed in the blackened segments of the cut carrot may occur as an abiotic stress response. This is further supported by increased levels of other stress-induced signalling metabolites such as allantoin and putrescine found in blackened segments of the carrots (Takagi et al., 2016; Mustafavi et al., 2018; Chen et al., 2019). Hypoxia results in extremely high levels of GABA accumulation in radish leaves, rice roots, rice shoots, and tea leaves. Prolonged flooding leads to cytosolic acidification, which induces the GABA shunt pathway by activating glutamate decarboxylase (Kinnersley and

Turano, 2000). However, GABA is also an important intermediate of nitrogen metabolism and amino acid biosynthesis. In addition, the GABA metabolism through the GABA shunt provides a source for carbon skeletons and energy for down-stream biosynthetic pathways. Hence, nutrient starvation may be a contributing factor in carrot blackening. A strong correlation between GABA and succinic acid was observed in carbon starvation-induced GABA production in Arabidopsis leaves (Caldana et al., 2011). However, the levels of succinic acid were similar in the orange and blackened carrot samples, while the levels of other TCA metabolites were very low in the blackened carrot regions. The metabolite data suggest that carbon starvation responses are present in the blackened portions of the carrots. Hence, the starvation responses are different in Arabidopsis leaves and carrot roots. Moreover, the natural amino acid derivative oxoproline, which is a breakdown product of glutamine during derivatisation, was present in large quantities in orange regions of the carrots but only very small levels were found in the blackened carrot regions. The presence of glutamic acid, which is a free form of glutamine, along with the buffering action of free amino acids, is known as the main cause of taste in carrots (Sharma et al., 2012). Blackened carrots had significantly lower levels of glutamic acid, which is likely to result in the lack of flavour reported in the blackened carrot batons.

While fatty alcohol contents were similar in both blackened and orange carrot samples, a strong general increase in fatty acid levels was seen in the blackened parts of the carrots. Fatty acids are important signalling molecules involved in wounding responses. The amplification of wound signalling through the oxylipin pathway and jasmonic acid synthesis is critical aspect of the browning in freshly cut lettuce (Choi et al., 2005). The role of fatty acids in carrot blackening will be investigated further by studying the levels of transcripts encoding wound-induced enzymes, such as PAL and lipoxygenase, as well as the levels of mRNAs involved in jasmonate and ethylene signalling, as well as other components of the oxylipin pathway. The carotenoid content of the blackened segments of the carrots was similar to the orange segments. There was only a significant decrease in lutein in the blackened parts of the carrots. This finding suggests that the carotenoid pathway is not greatly changed during the blackening process.

The accumulation of blackened components could be triggered by an accelerated flux of precursors through the shikimate pathway. The blackened carrot regions were enriched in chlorogenic acid, caffeic acid and dicaffeoylquinic acid. This trend was also observed in other phenolic compounds, with the exception of cinnamic acid. In addition, increased lignin levels were observed in the blackened regions of the carrots. The increase in compounds involved in lignification may result from activation of wound-repairing processes that limit pathogen invasion. A significant increase in the levels of 5-caffeolyquinic acid, one of the major chlorogenic acids in fruits and vegetable crops, was identified in the blackened segments of the carrots. Previous studies of phenolic compounds have found that hydroxycinnamic acids and derivatives make up most of the phenolic acids found in carrot roots, with chlorogenic acid being 42.2 – 61.8% of the total detected in the carrot root (Zhang and Hamauzu, 2004). However, the phenolic content varies between the tissue types in the carrot root, with 54.1% of total phenolics in the carrot peel/cortex, 39.5% in the phloem tissue, and just 6.4% in the xylem tissue (Zhang and Hamauzu, 2004). Together with ferulic and dicaffeoylquinic acid, chlorogenic acid typically makes up 82% of the total phenolic compounds in wounded carrot roots (Heredia and Cisneros-Zevallos, 2009). Chlorogenic acid can be synthesised by 3 pathways that convert either cinnamic acid, coumaric acid or coumaroyl CoA into chlorogenic acid (Tohge et al., 2013). Phenolic compounds can also be polymerised by oxidation and enzymatic catalysation to produce dark pigments (Figure 5.15). Chlorogenic acid has long been recognised as a browning substrate in sweet potatoes, apples, and other fruits and



**Figure 5.15: Schematic of melanin synthesis from phenolic compounds using oxidation and the enzyme PPO.**

vegetables (Chubey and Nylund, 1969). For example, an increase in chlorogenic acid contents was directly associated with the oxidative browning reaction in apples, potato and carrots (Chubey and Nylund, 1969). However, no relationship between browning and chlorogenic acid levels was found in eggplant (Plazas et al., 2013). Hence, while the increase in chlorogenic acid levels observed in the black carrot segments is a symptom of the blackening process, it is unlikely to be the cause.

As discussed above, the production of phenolic compounds can lead to the formation of black deposits in the tissues through the action of PPO (Ioannou 2013). Decreases in amino acid levels could also be associated with non-enzymatic browning through the Maillard Reactions. The term Maillard reaction describes a network of reactions between amino acids and reducing sugars, resulting in the accumulation of brown and dark pigments. This reaction is accelerated at high temperatures during frying and cooking. Overall, Maillard browning leads to the loss of essential amino acids and decreased food digestibility (Ajandouz and Puigserver 1999). The oxidation of polyphenols is commonly associated with blackening in fruits and vegetables. Hence, the accumulation of polyphenolic compounds in the blackened regions of the carrots may be a trigger for the formation of black pigments.

Taken together, the analysis of the metabolite profiles of the blackened carrot regions reveals a shift in carbon flow from primary to secondary metabolism. The depletion of essential sugars and amino acids bears testimony to a decrease in primary metabolism. The observed increases in secondary metabolites, particularly those involved in plant defence suggests the activation of pathways involved in the invasion of insect pests and pathogens.

This study provides new insights into the metabolomic pathways that are changed in the blackening phenomenon. However, the sequence of triggers that lead to carrot blackening are unknown. Metabolomic time-course experiments would help to identify the sequence by which the different metabolic pathways are activated during blackening. This information would identify potential early-stage markers for carrot blackening. Such metabolites could also be used as future biomarkers in breeding programs to select carrots with a lower susceptibility to blackening.

# Chapter VI

# Chapter 6: Transcript profiles of blackened, border orange, and orange carrot regions

## 6.1 Introduction

The RNA sequencing (RNA-seq) analysis described in this chapter was used to investigate the transcript profiles associated with carrot blackening. The gene expression profiles were compared in orange regions, blackened regions and the 'border' or 'middle' regions that were immediately adjacent to the blackened regions. RNA extraction methods are discussed in this chapter, together with the transcriptome analysis comparisons of orange, blackened, and orange/black border regions of the carrot batons.

The extraction of RNA from carrot tissue is challenging due to high levels of polysaccharides and secondary metabolites that bind to RNA or co-precipitate with the RNA resulting in low quality, impure RNA preparations of low yield (Djami-Tchatchou and Straker, 2012; Gasic et al., 2004; MacRae, 2007; Malnoy et al., 2001). Accumulation of phenolic compounds in the black regions can prevent the extraction of high-quality RNA. In particular, polyphenols bind to nucleic acids and proteins irreversibly, leading to oxidation and the degradation of RNA (MacRae, 2007; Kanani et al., 2019). A key challenge faced at the outset was therefore to overcome the high contents of secondary metabolites, water, polysaccharides and lignin in the black regions in order to extract and purify RNA of sufficient quality for RNA-seq analysis. The literature contains a number of RNA extraction methods from young carrot taproots that were less than 100 days old (Xu et al., 2014; Bannoud et al., 2019; Meng et al., 2020; Wang et al., 2020). However, commercial RNA extraction kits are not optimal for mature carrot taproots. Therefore, such kits cannot be used for black carrot samples. A range of techniques were therefore tested. The most successful method was thereafter used for isolation of high-quality RNA from the black regions.

RNA quality was assessed using a Nanodrop and by the absorbance ratios at 260/280 nm ($A_{260}/A_{280}$) and A260/A230 ($A_{260}/A_{230}$). The absorbance ratio at $A_{260}/A_{280}$ estimates the protein contamination in RNA samples, which should be kept to a minimum. A ratio

of ~2.00 is optimal. The presence of other contaminants can be estimated using the absorbance ratios at A260/230, which provide evidence of the presence of contaminants absorbing at 230 nm or less, such as salts from buffers used for RNA extraction. A ratio of >1.8 indicates pure RNA with low contamination.

The Qiagen RNeasy Plant Mini kit was used in the first instance following the manufacturer's instructions. Thereafter, the protocol was adapted to include the Fruit-mate™ reagent. Fruit-mate is recommended for samples with high polyphenol and/or polysaccharide content as it uses a non-ionic polymer that binds to these compounds allowing easy removal (Ishibashi et al., 2019).

TRIzol reagent and chloroform were also used to separate RNA, which was then precipitated using isopropanol. The RNA Clean & Concentrator™ kit was incorporated into this method to clean the RNA to an acceptable level of purity. Finally, the CTAB method was applied to disrupt the cell walls and isolate nucleic acids, with chloroform used to separate the RNA (Wang and Stegemann, 2010). The RNA Clean & Concentrator™ kit was then used to enhance the purity of the RNA.

Agarose electrophoresis gel was used to determine RNA integrity and quality. When the RNA yields, RNA purity and integrity were compared, the CTAB method + RNA Clean & Concentrator™ kit was found to be the most successful for extracting high-quality RNA from the blackened, border and orange carrot regions. RNA obtained in this way was used to analyse the RNA-seq profiles of the regions. RNA-seq analysis was performed by Dr Ian M. Carr at the Leeds Institute of Medical Research at St James' Hospital, Leeds. GO analysis was carried out by Dr Gabriela Machaj at the University of Agriculture in Krakow, Poland.

The RNA-seq data reported in this chapter, consist of data from the blackened regions normalised to the orange regions (B_CT), the border regions normalised to the orange batons (M_CT), and the blackened regions normalised to border regions (B_M). Differentially expressed genes (DEGs) are identified and discussed. Taken together, the data presented in this chapter provide a deeper understanding of the molecular mechanisms involved in the carrot blackening process.

## 6.2 Results

### 6.2.1 RNA extraction methods

A range of methods were tested in order to obtain high-quality RNA samples. RNA quality and quantity were measured and compared (Table 6.1). RNA quality was measured using a Nanodrop and determined by the absorbance ratios at 260/280 nm ($A_{260}/A_{280}$) and A260/A230 nm ($A_{260}/A_{230}$). The absorbance ratio at $A_{260}/A_{280}$ estimates the level of protein contamination, with a ratio of ~2.00 generally accepted as pure RNA. The absorbance ratio at $A_{260}/A_{230}$ can estimate the presence of other contaminants absorbed at 230 nm, with a ratio of >1.8 indicating low contamination. A combination of the following methods, reagents and kits were used: Qiagen RNeasy Plant Mini Kit, Fruit-mate, TRIzol, CTAB, and RNA Clean & Concentrator -5 kit. The highest quality RNA was extracted using the CTAB method combined with the RNA Clean & Concentrator -5 kit. This method was then used to extract RNA to be used for a transcriptome analysis.

| Table 6.1: RNA extraction methods and RNA quantity and quality ratios | | | | | |
|---|---|---|---|---|---|
| Method | Carrot region | Samples | ng/µl | A260/A280 | A260/A230 |
| Qiagen RNeasy Plant Mini Kit | Orange | C1 | 46.83 | 2.17 | 1.93 |
| | | C2 | 146.36 | 1.96 | 1.53 |
| | | C3 | 85.33 | 1.88 | 1.49 |
| | Blackened | B1 | 101.69 | 1.77 | 1.13 |
| | | B2 | 101.67 | 1.83 | 0.91 |
| | | B3 | 61.80 | 1.79 | 0.95 |
| Qiagen RNeasy Plant Mini Kit + Fruit-mate | Orange | C1 | 63.45 | 2.18 | 1.91 |
| | | C2 | 60.90 | 2.13 | 2.14 |
| | | C3 | 47.52 | 2.12 | 2.01 |
| | Blackened | B1 | 278.10 | 1.71 | 1.11 |
| | | B2 | 275.66 | 1.72 | 1.00 |
| | | B3 | 229.53 | 1.67 | 1.01 |
| TRIzol Reagent | Orange | C1 | 263.25 | 2.16 | 2.28 |
| | | C2 | 155.93 | 2.13 | 1.98 |
| | | C3 | 84.80 | 2.19 | 1.83 |
| | Blackened | B1 | 101.32 | 1.52 | 0.82 |
| | | B2 | 192.61 | 1.49 | 0.77 |
| | | B3 | 39.18 | 1.39 | 0.70 |
| TRIzol Reagent + RNA Clean & Concentrator - 5 | Orange | C1 | 205.57 | 2.15 | 2.19 |
| | | C2 | 18.94 | 1.89 | 0.65 |
| | | C3 | 25.51 | 2.10 | 0.68 |
| | Blackened | B1 | 147.50 | 1.44 | 0.67 |
| | | B2 | 195.36 | 1.50 | 1.22 |
| | | B3 | 137.22 | 1.45 | 0.75 |
| CTAB | Orange | C1 | 299.57 | 2.21 | 1.68 |
| | | C2 | 352.57 | 2.21 | 1.55 |
| | | C3 | 382.65 | 2.21 | 1.60 |
| | Blackened | B1 | 78.18 | 1.57 | 0.83 |
| | | B2 | 276.12 | 1.92 | 1.38 |
| | | B3 | 136.93 | 1.93 | 1.37 |
| CTAB + RNA Clean & Concentrator - 5 | Orange | C1 | 151.98 | 2.19 | 2.18 |
| | | C2 | 122.11 | 2.15 | 2.42 |
| | | C3 | 236.55 | 2.12 | 2.22 |
| | Blackened | B1 | 344.78 | 2.04 | 1.96 |
| | | B2 | 371.04 | 2.00 | 1.78 |
| | | B3 | 288.69 | 1.78 | 1.49 |

### 6.2.2   Integrity and purity of RNAs using all methods

RNA integrity was compared following all three extraction methods: Qiagen/Fruit-mate, TRIzol, and CTAB. This process also provides an estimate of RNA quality. The RNA Clean & Concentrator -5 kit was used in association with the TRIzol and CTAB extraction methods as described in Chapter 2, section 2.5.1.6. RNA yields and ratios obtained from the different carrot regions using these methods are shown in Table 6.2. The CTAB method yielded the purest samples with no detectable contamination. Genomic DNA contamination was observed in the blackened carrot RNA samples extracted using the Qiagen/Fruit-mate method. Other contaminants, possibly proteins or phenolics, were observed in orange carrot RNA samples extracted using the TRIzol method. RNA integrities were compared by separation of RNAs on native, non-denaturing agarose gel (Figure 6.1). Total RNA from eukaryotic samples usually gives two clear rRNA bands corresponding to 28S and 18S rRNA species on native, non-denaturing agarose gels. The 28S rRNA band should be approximately twice as intense as the 18S rRNA band in non-degraded RNA samples. The 2:1 intensity ratio (28S:18S) is a good indication that RNA is intact. Partially degraded RNA will result in a smeared appearance on the gels, which will lack the sharp rRNA bands, and will not exhibit the 2:1 ratio of high-quality RNA. In all samples representing different RNA purities isolated by three methods, two rRNA bands were observed with ratios ranging from 1:1 to 2:1 (Figure 6.1). DNA contamination was observed only in blackened carrot RNA samples isolated by the Qiagen/Fruit-mate method. The lower bands present in RNAs isolated by the TRIzol method likely represent low molecular weight RNA species. No smearing was observed in any RNAs extracted by the three methods.

| Table 6.2: RNA extraction methods and ratios of samples run on the electrophoresis gel | | | | |
|---|---|---|---|---|
| Method | Carrot region | ng/µl | A260/A280 | A260/A230 |
| Qiagen/Fruit-mate | Orange | 105.49 | 2.21 | 1.78 |
| | Blackened | 70.7 | 1.94 | 1.24 |
| TRIzol | Orange | 263.25 | 2.16 | 2.28 |
| | Blackened | 119.41 | 1.47 | 0.82 |
| CTAB | Orange | 151.98 | 2.19 | 2.18 |
| | Blackened | 344.78 | 2.04 | 1.96 |
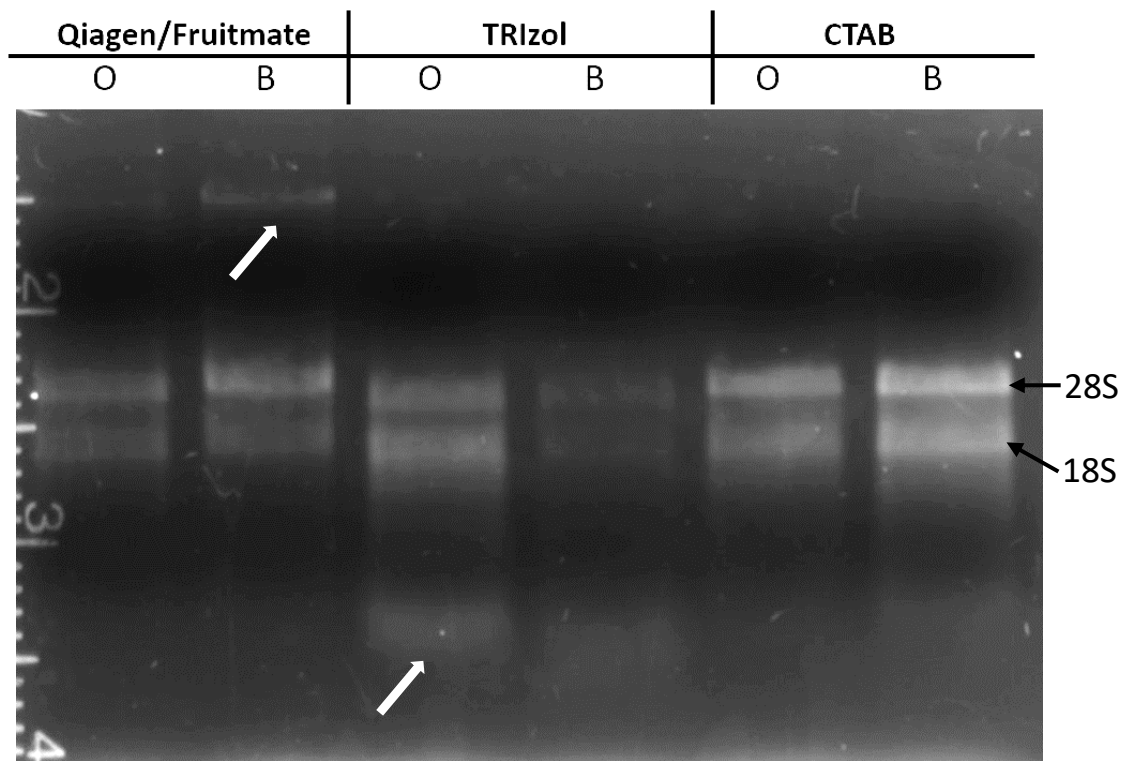
**Figure 6.1: Agarose gel electrophoresis of RNA extracted from Orange (O) and Blackened (B) carrots using different extraction methods**. RNA subunits 28S and 18S are labelled. White arrows indicating DNA contamination in Qiagen/Fruit-mate extracted samples and other contaminants, possibly proteins or phenolics, in TRIzol extracted samples.

### 6.2.3 Highest quality RNA was extracted using CTAB method

Since the CTAB and RNA Clean & Concentrator -5 kit method yielded the highest quality RNA, this method was used to extract RNA from orange carrots (Orange), blackened carrot regions (Blackened), and border carrot regions (Middle). The final RNA ratios of the samples used for RNA-seq analysis are shown in Table 6.3.

| Table 6.3: RNA data of samples chosen for RNA-seq analysis. | | | | |
|---|---|---|---|---|
| Carrot region | Sample | ng/µl | A260/A280 | A260/A230 |
| Orange | C1 CTAB | 70.75 | 2.16 | 2.35 |
|  | C2 CTAB | 38.63 | 2.02 | 2.23 |
|  | C3 CTAB | 53.94 | 2.03 | 2.24 |
| Middle | M2 | 31.37 | 1.92 | 1.95 |
|  | M4 | 85.16 | 2.00 | 1.79 |
|  | M6 | 298.87 | 2.06 | 1.77 |
| Blackened | B1 | 419.43 | 2.05 | 2.06 |
|  | B2 | 350.56 | 1.94 | 1.75 |
|  | B3 | 157.74 | 1.78 | 1.67 |

### 6.2.4 Transcriptome analysis

A PCA was preformed using the RNA-seq data from the orange, blackened and border carrot samples, as a first step to analysing variation between samples. The PCA analysis revealed clusters of samples based on the similarity of transcript profiles (Figure 6.2, A, B, C). PC1 showed a clear separation between orange and blackened samples and represents 97% of the variation between samples (Figure 6.2 A). PC1 showed a clear separation between orange and border samples and represents 90% of the variation between samples (Figure 6.2 B). PC1 showed a clear separation between black and border samples and represents 60% of the variation between samples (Figure 6.2 C).
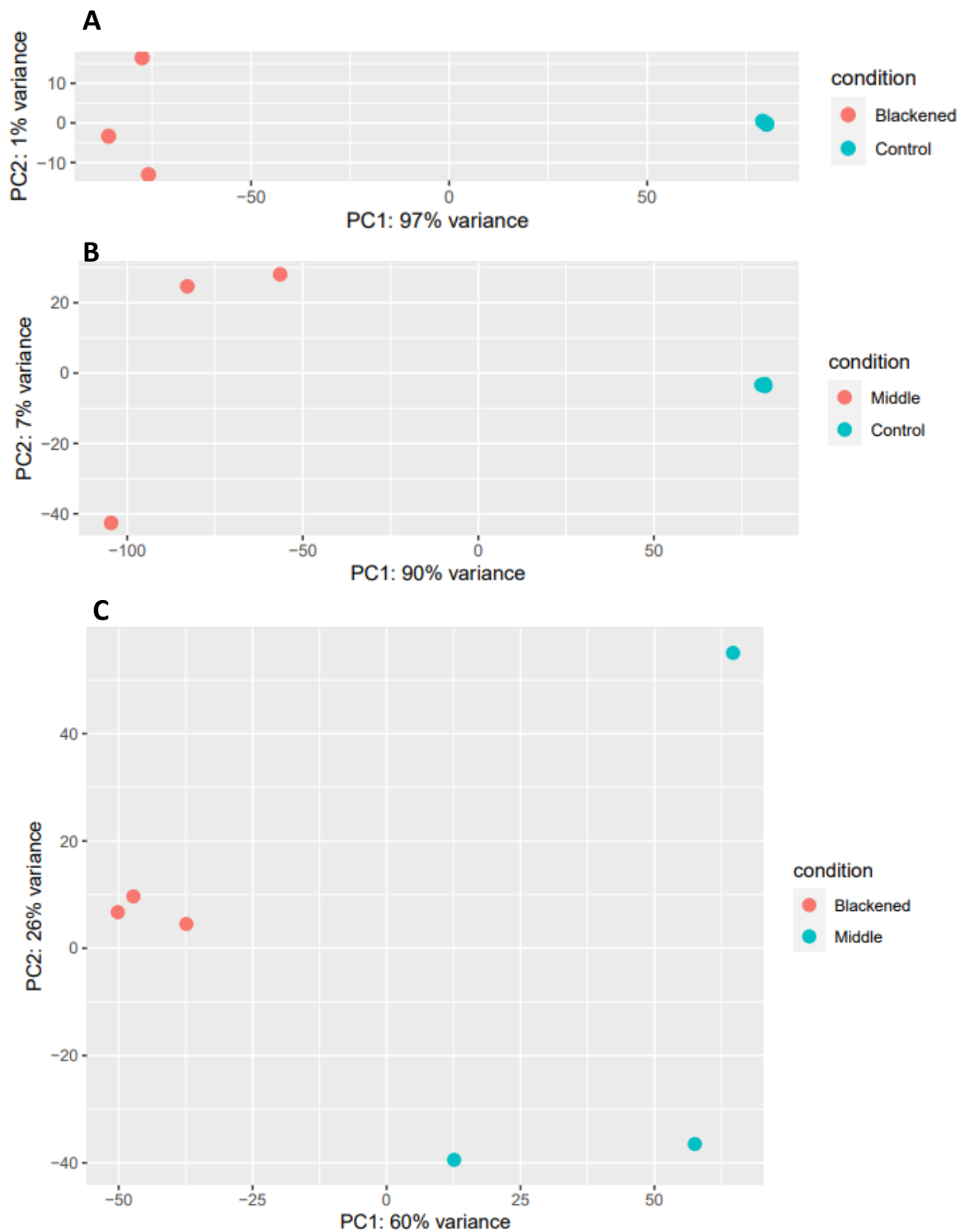
**Figure 6.2: Principal components analysis (PCA) of the transcript profiles of orange, black and border carrot samples**. A: PCA of orange and blackened carrot samples, B: PCA of orange and border carrot samples. C. PCA of border and blackened carrot samples. A log transformation was performed prior to the PCA.

### 6.2.5 Differences in transcript expression in orange, blackened, and border carrot samples

Distinct differences in transcript abundance were observed between the orange and blackened carrot samples (Figure 6.4). However, there was some variation in the transcript profiles of each of the samples from the orange/black border regions, with one sample showing a more similar transcript profile to the blackened carrot samples than the other two border samples (Figure 6.3). Hence, although the border samples were orange in colour, it was not possible to harvest samples at a reproducible stage of the development of blackening. While the samples from the orange carrot batons and blackened regions, can be grouped and compared, the samples from the border regions were too heterogeneous to be grouped (Figure 6.5 and 6.6). As such, each of the samples from the border regions must be considered separately.
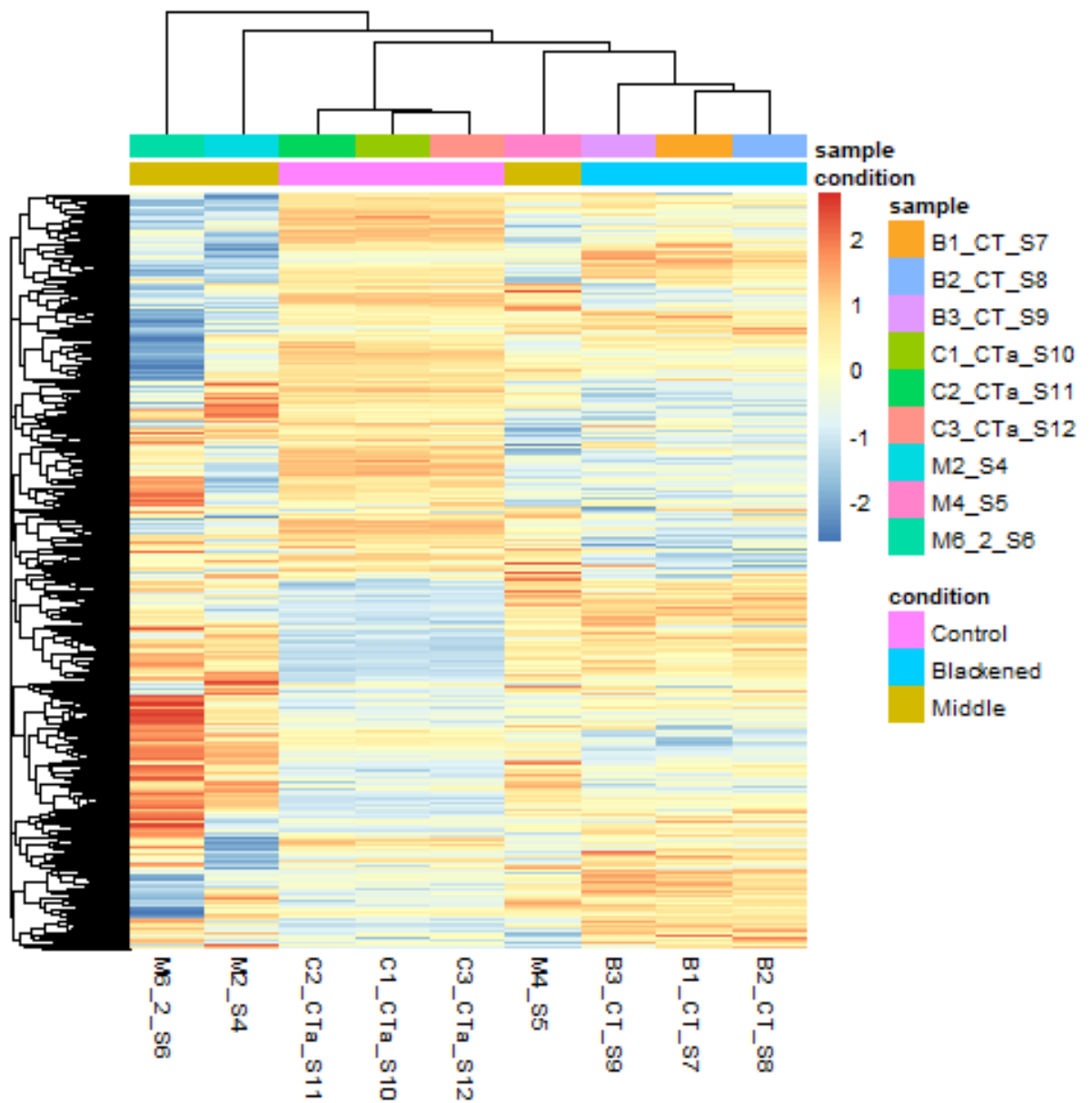
**Figure 6.3: Heatmap comparison of transcript profiles of orange, blackened and border carrot regions**. P-values were calculated using Deseq2 tool and later adjusted using B-H method (p<0.05).
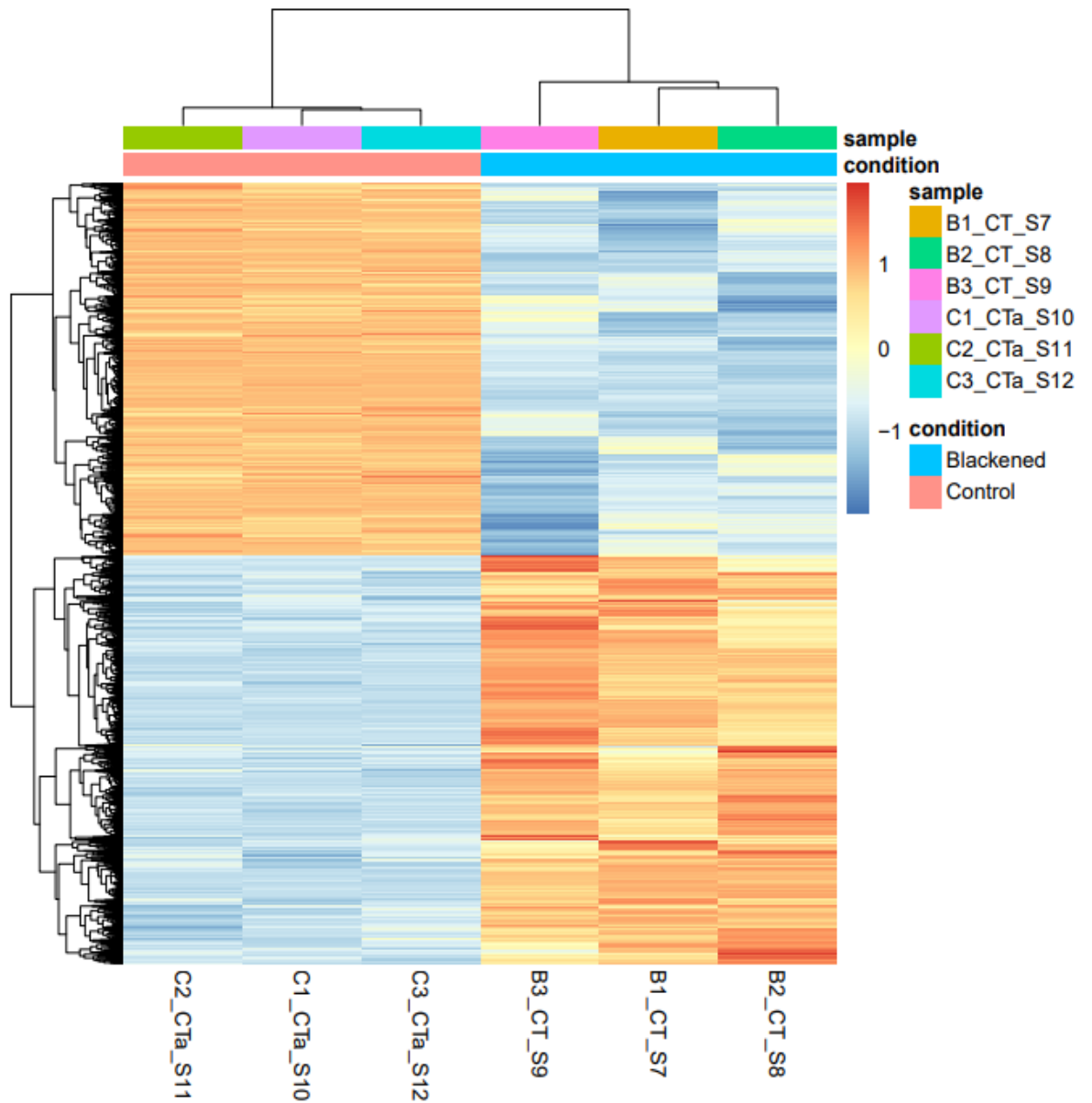
**Figure 6.4: Heatmap comparison of transcript profiles of orange and blackened carrot regions**. TP-values were calculated using Deseq2 tool and later adjusted using B-H method (p<0.05).
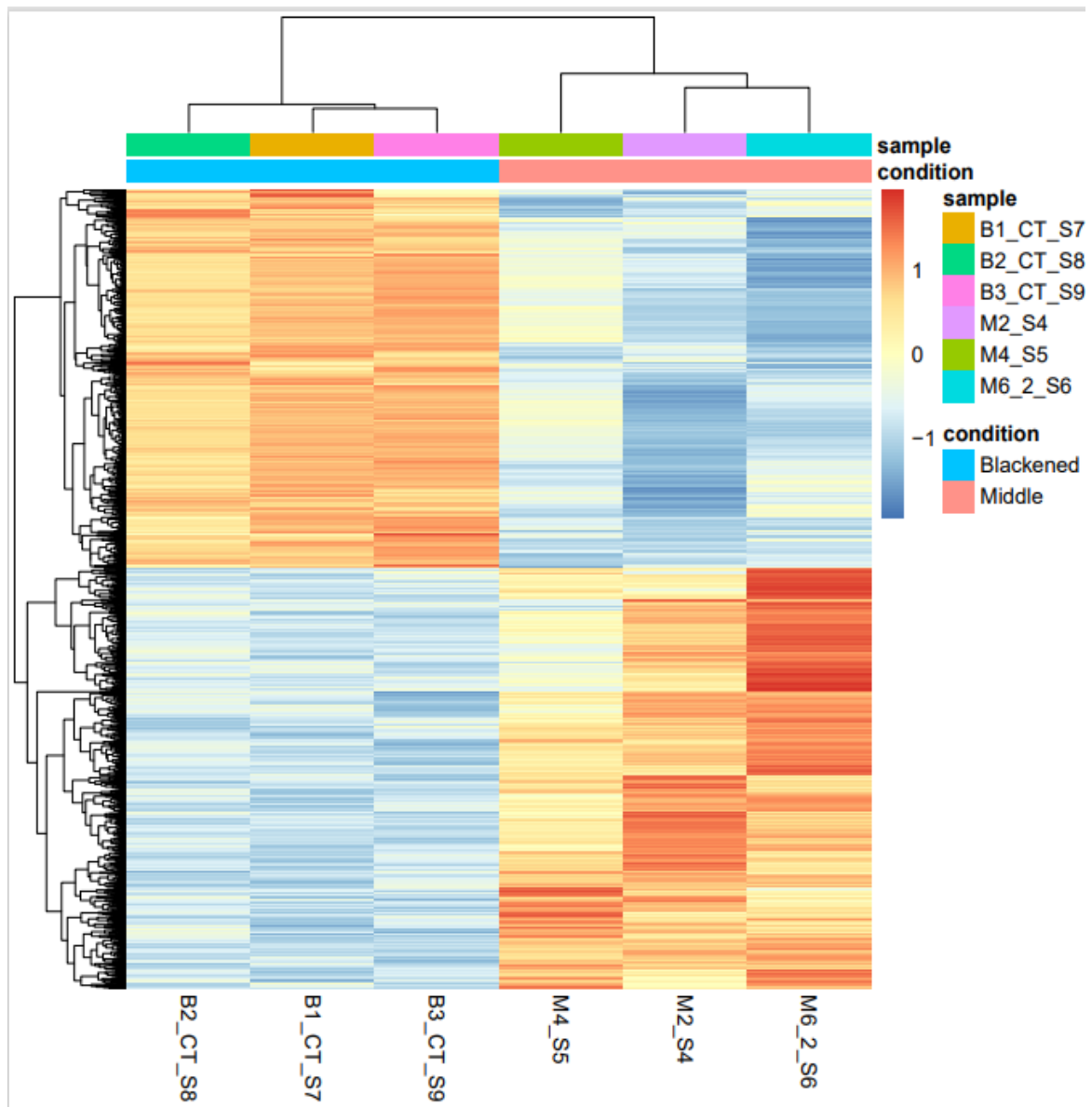
**Figure 6.5: Heatmap comparison of transcript profiles of orange and border carrot regions**. P-values were calculated using Deseq2 tool and later adjusted using B-H method (p<0.05).
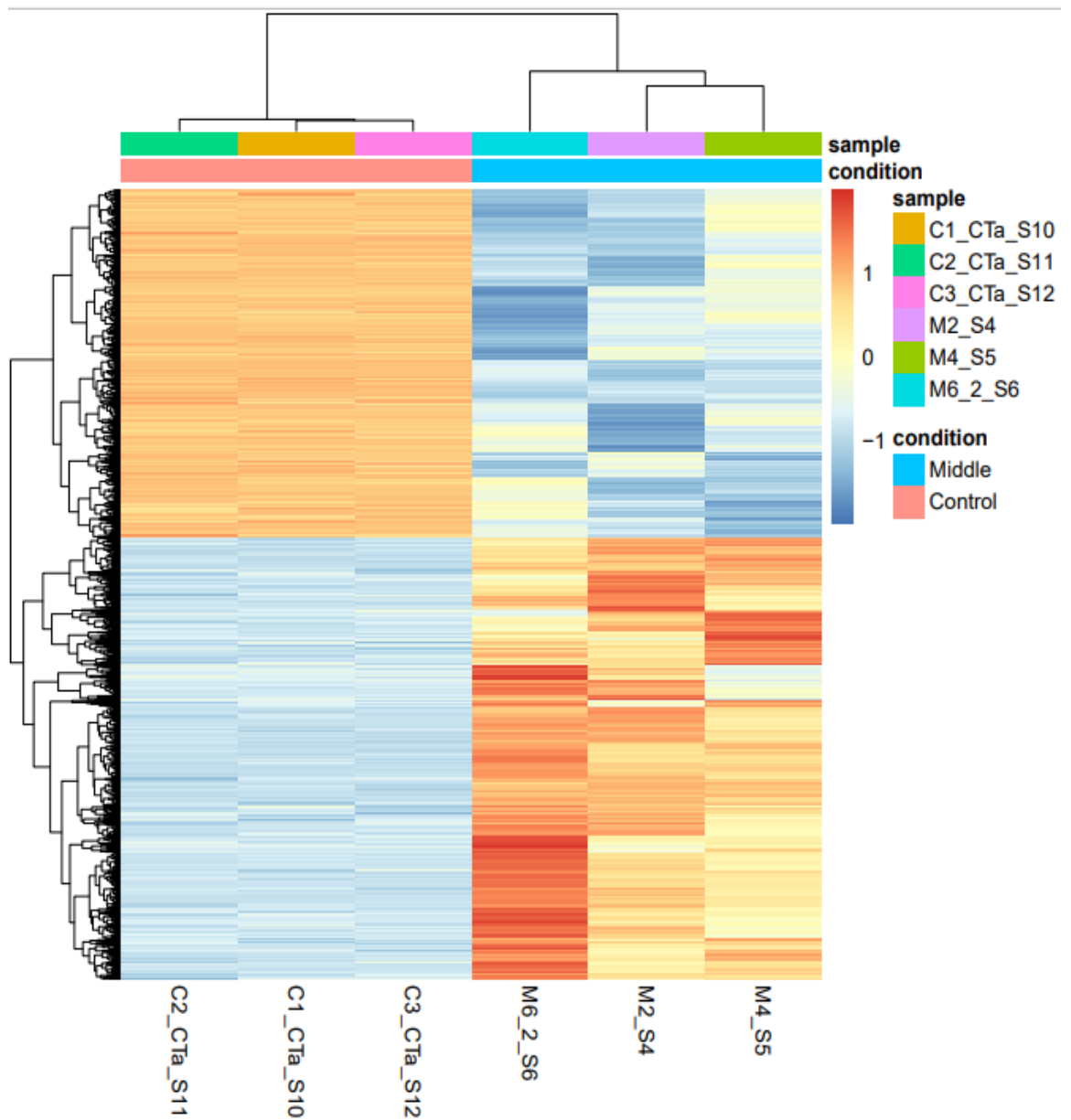
**Figure 6.6: Heatmap comparison of transcript profiles of orange and border carrot regions**. P-values were calculated using Deseq2 tool and later adjusted using B-H method (p<0.05).

### 6.2.6 RNA-seq analysis using bioinformatics

**6.2.6.1 The 15 transcripts that were most increased in abundance and decreased in abundance in the blackened, orange and border carrot regions**

The 15 transcripts that were most increased in abundance and decreased in abundance were determined in blackened carrot regions and border carrot regions compared to orange carrots (Figure 6.7 and 6.8), as well as in blackened carrot regions compared to border regions (Figure 6.9).

Transcripts encoding proteins related to phytohormone metabolisms and signalling were changed in abundance in both blackened and border regions. For example, transcripts encoding the auxin-responsive transcription factor IAA26-like and the auxin-induced protein 22D-like protein, and the gibberellin regulated protein 14 (-like) were greatly increased in the blackened and border regions, respectively. In contrast, ethylene-responsive transcription factors were decreased in abundance in the blackened regions. Crucially, a number of transcripts associated with cell wall metabolism such as laccases were greatly decreased in abundance in the blackened and border regions. For example, transcripts encoding the pectin degrading enzymes polygalacturonase At1g48100 and pectinesterase 2 were decreased in the blackened and border regions. Moreover, the abundance of a lignin-forming anionic peroxidase-like transcript was decreased in blackened regions. Interestingly, transcripts encoding a NRT1/PTR family protein were greatly deceased in the blackened and border regions. The NRT1/PTR family proteins were initially characterised as nitrate or peptide transporters but they are now known to transport a range of metabolites including phytohormones such as auxin, gibberellic acid and ABA. Hence, the NRT1/PTR family proteins integrate signals that regulate root growth and development. For example, the Arabidopsis NRT1.1 nitrate transporter is not only crucial for nitrate signalling acting as a nitrate sensor but it also governs root growth by facilitating auxin uptake. Since NRT1/PTR family proteins connect nutrient and hormone signalling during organ development, the decreased abundance of these transcripts may indicate a switching of nutrient signalling pathways.
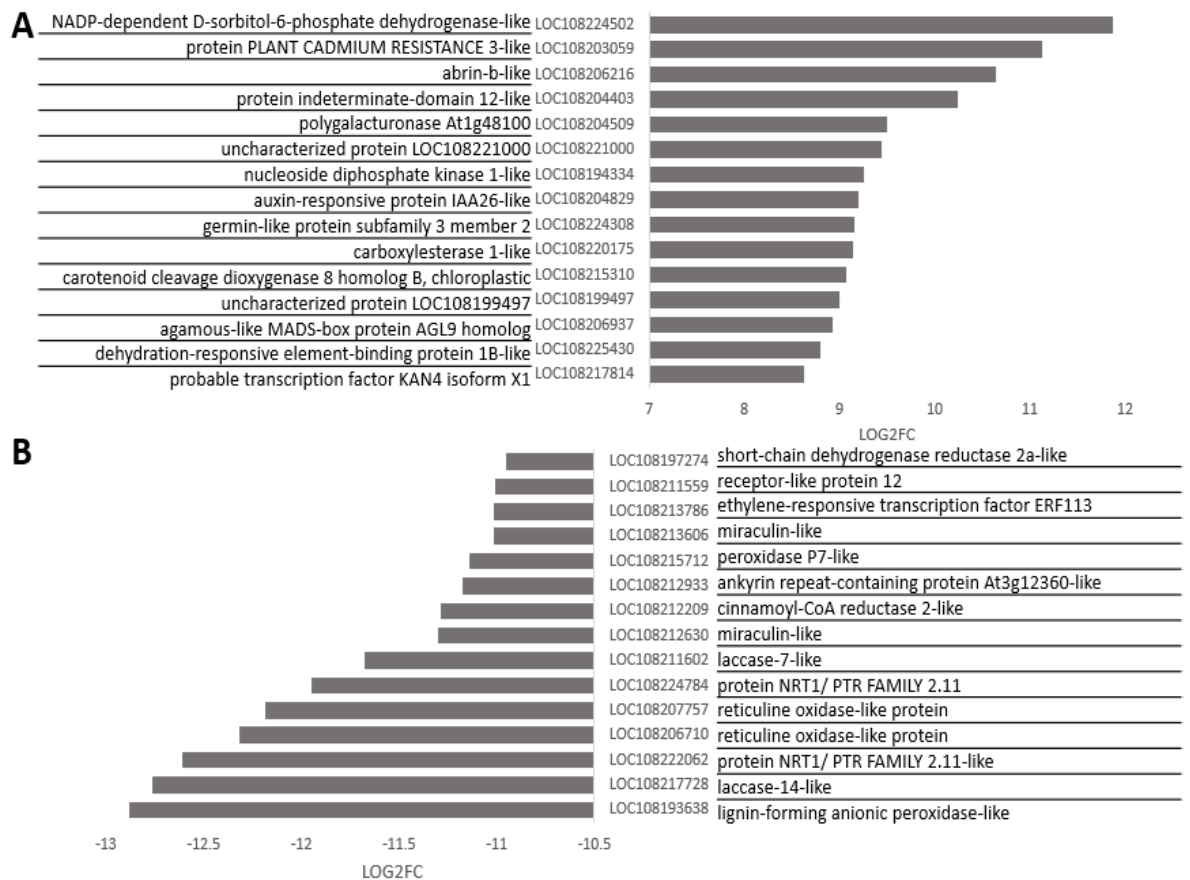
**Figure 6.7: Top 15 most up-regulated (A) and down-regulated (B) transcripts in blackened carrot regions compared to orange carrots**. Three biological replicates. P-values were calculated using Deseq2 tool and later adjusted using B-H method (p<0.05; fold change ≥1).

**A**

| Protein | Locus |
|---|---|
| protein PLANT CADMIUM RESISTANCE 3-like | LOC108203059 |
| ribosome-inactivating protein luffin-alpha-like | LOC108198322 |
| protein PHYTOCHROME KINASE SUBSTRATE 1-like | LOC108194152 |
| protein STRICTOSIDINE SYNTHASE-LIKE 11-like | LOC108217573 |
| auxin-induced protein 22D-like | LOC108214649 |
| protein NUCLEAR FUSION DEFECTIVE 4-like | LOC108219693 |
| NADP-dependent D-sorbitol-6-phosphate dehydrogenase-like | LOC108224502 |
| protein ABHD17B-like | LOC108208321 |
| GDSL esterase/lipase At1g28580 | LOC108204706 |
| pistil-specific extensin-like protein | LOC108208348 |
| uncharacterized protein sll0103-like | LOC108200516 |
| basic leucine zipper 43-like | LOC108208184 |
| gibberellin-regulated protein 14-like | LOC108217749 |
| uncharacterized protein LOC108198744 | LOC108198744 |
| uncharacterized protein LOC108212952 | LOC108212952 |

LOG2FC

**B**

| Locus | Protein |
|---|---|
| LOC108201386 | uncharacterized protein LOC108201386 |
| LOC108223624 | protein HOTHEAD-like |
| LOC108210774 | miraculin-like |
| LOC108205342 | putative GEM-like protein 8 |
| LOC108206710 | reticuline oxidase-like protein |
| LOC108202000 | defensin-like protein 1 |
| LOC108213518 | uncharacterized protein LOC108213518 |
| LOC108216320 | basic endochitinase-like |
| LOC108211602 | laccase-7-like |
| LOC108199168 | epidermis-specific secreted glycoprotein EP1-like |
| LOC108198985 | epidermis-specific secreted glycoprotein EP1-like |
| LOC108209740 | pectinesterase 2 |
| LOC108213606 | miraculin-like |
| LOC108212630 | miraculin-like |
| LOC108217728 | laccase-14-like |

LOG2FC

**Figure 6.8: Top 15 most up-regulated (A) and down-regulated (B) transcripts in border carrots regions compared to orange carrots**. Three biological replicates. Three biological replicates. P-values were calculated using Deseq2 tool and later adjusted using B-H method (p<0.05; fold change ≥1).
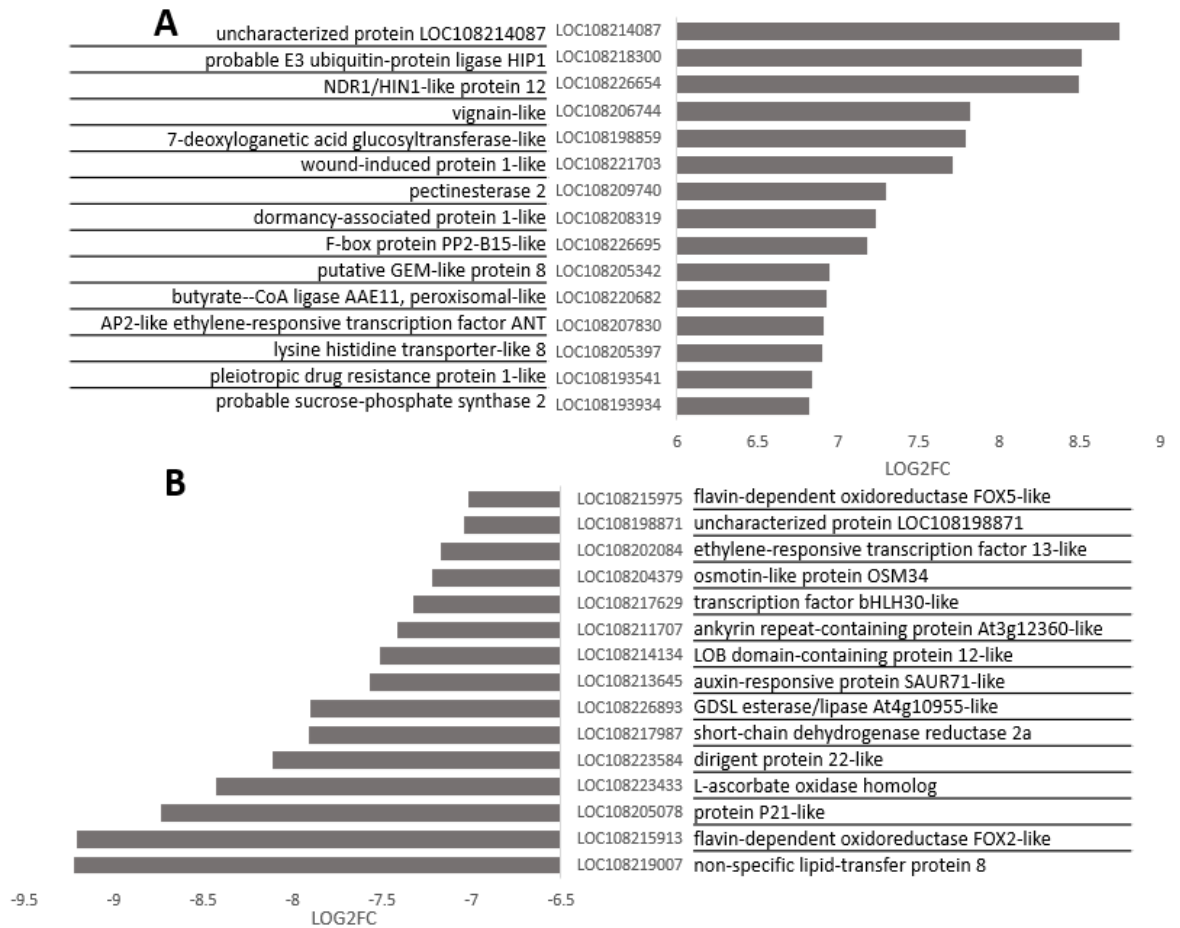
**Figure 6.9: Top 15 most up-regulated (A) and down-regulated (B) transcripts in blackened carrot regions compared to border carrot regions**. Three biological replicates. Three biological replicates. P-values were calculated using Deseq2 tool and later adjusted using B-H method (p<0.05; fold change ≥1).

### 6.2.6.2 Gene ontology analysis B_CT, M_CT and B_M

A total of 7,982 gene transcripts were differentially expressed in blackened carrot regions compared to the orange regions. A total of 6083 gene transcripts were differentially expressed in border regions and only 2,669 transcripts in the blackened regions compared to border regions. Of the differentially expressed transcripts, 4980 were uniquely found in blackened regions, 2652 in the border regions, with 776 uniquely found in the blackened regions compared to border regions (Table 6.4, 6.5, and 6.6).

The B_CT analysis showed the highest number of DEGs with approximately 4500 differentially expressed transcripts, followed by the M_CT analysis with approximately 3000 differentially expressed (Figure 6.10). There were approximately 1400 differentially expressed transcripts in the B_M analysis (Figure 6.10). The highest overlap of DEGs was observed between the B_CT and M_CT analyses (Figure 6.11).
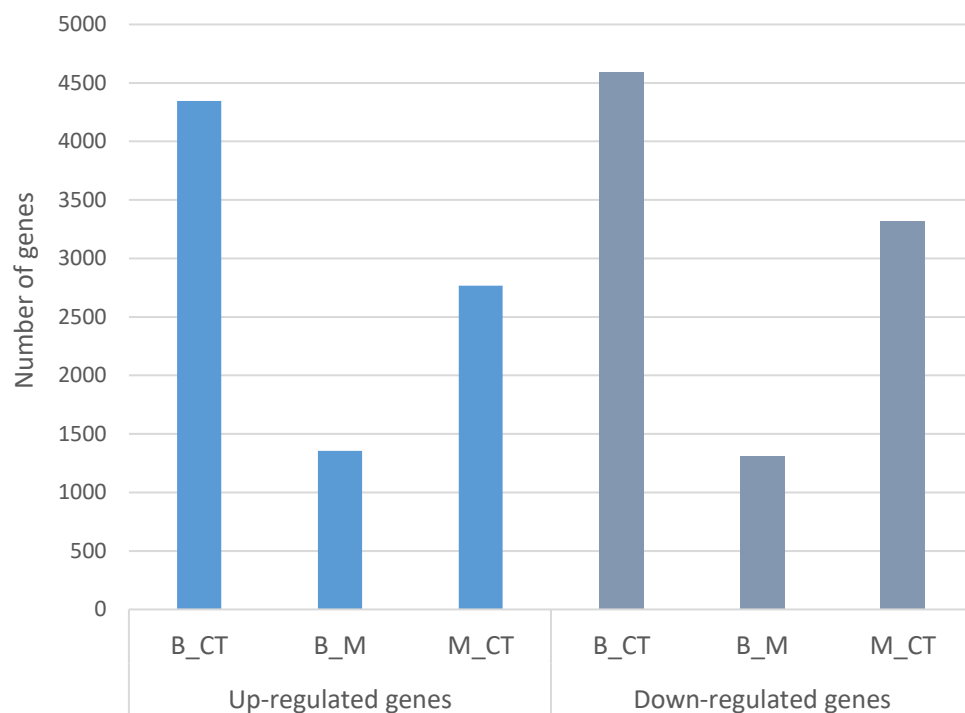


**Figure 6.10: Number of up-regulated and down-regulated genes in orange, blackened and border carrot regions**. P-values were calculated using Deseq2 tool and later adjusted using B-H method (p<0.05; fold change ≥0.2).
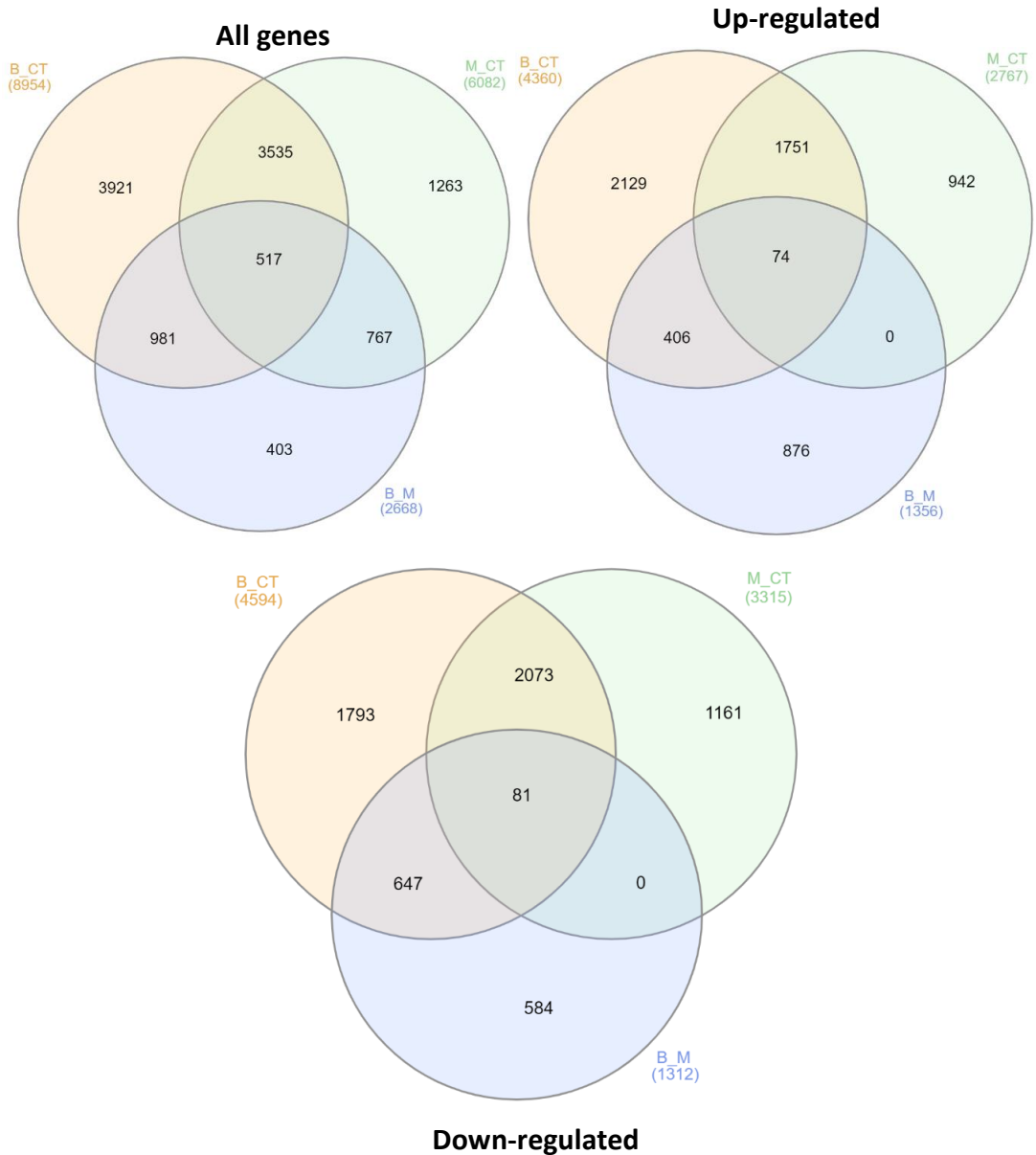
**Figure 6.11: Transcript profile comparison of blackened, orange, and border regions**. Venn diagrams showing the differentially expressed transcripts in blackened, orange, and border carrot regions. P-values were calculated using Deseq2 tool and later adjusted using B-H method (p<0.05; fold change ≥1). B = Blackened carrot region. M = Region immediately adjacent to blackened region. CT = Orange carrot baton.

Up-regulated

| Table 6.4: Up-regulated gene transcripts in blackened and border carrot regions. | | |
|---|---|---|
| List Names | Number of Elements | Number of Unique Elements |
| B_CT | 4360 | 4360 |
| M_CT | 2767 | 2767 |
| B_M | 1356 | 1356 |
| Overall number of unique elements | | 6178 |

Down-regulated

| Table 6.5: Down-regulated gene transcripts in blackened and border carrot regions. | | |
|---|---|---|
| List Names | Number of Elements | Number of Unique Elements |
| B_CT | 4594 | 4594 |
| M_CT | 3315 | 3315 |
| B_M | 1312 | 1312 |
| Overall number of unique elements | | 6339 |

All DEGGs

| Table 6.6: All DEGs in blackened and border carrot regions. | | |
|---|---|---|
| List Names | Number of Elements | Number of Unique Elements |
| B_CT | 8954 | 8954 |
| M_CT | 6082 | 6082 |
| B_M | 2668 | 2668 |
| Overall number of unique elements | | 11387 |

### 6.2.6.3 Processes that are likely to be modified in black and border regions.

Transcripts were grouped according to the biological processes in which the encoded proteins are involved. Various groupings were analysed including biological processes, molecular functions, cellular compounds and KEGG pathways. This analysis indicated that many processes and pathways are likely to be enhanced in the blackened regions, including starch and sucrose metabolism, carotenoid biosynthesis, photosynthesis, as well as proteins involved in the regulation of cellular and metabolic processes, gene expression and translation (Figure 6.12, A and D). In particular, DEGs involved in the signalling and activation of auxin were enhanced in the blackened and bored carrot regions. Notably, taurine, hypotaurine, and arachidonic acid metabolism were increased only in the border regions (Figure 6.13 D).

## A – Biological processes



## B – Molecular functions

## C – Cellular components
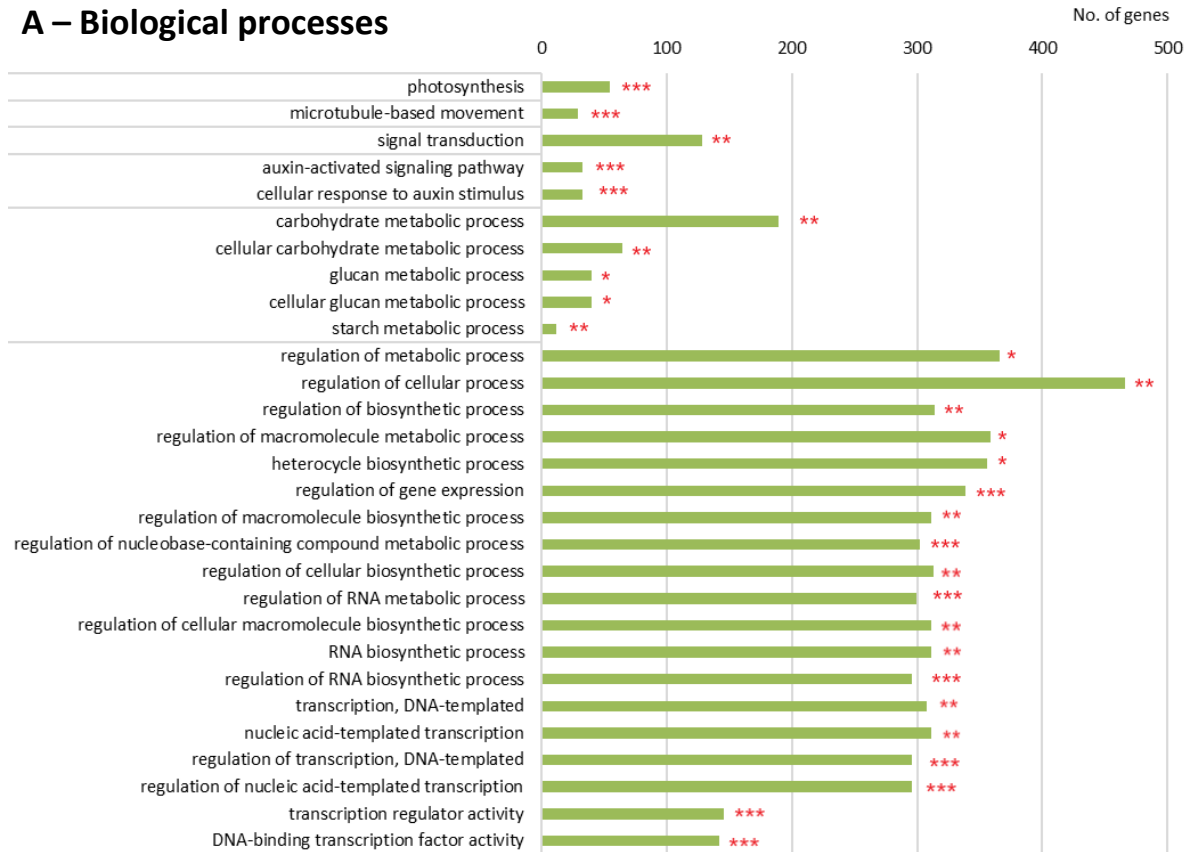


## D – KEGG pathways
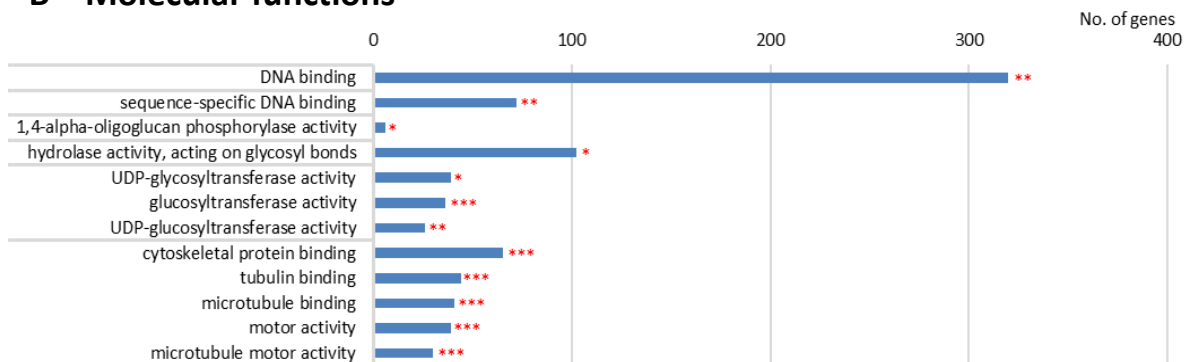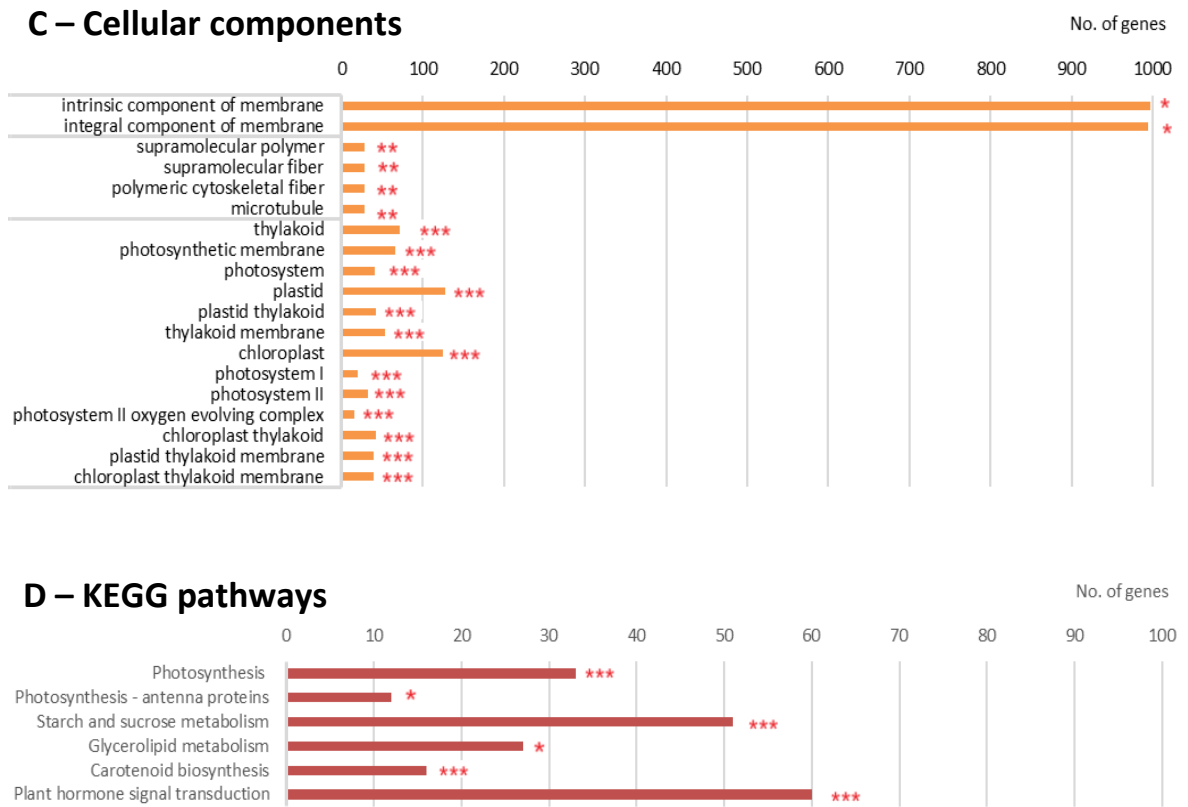


**Figure 6.12: GO terms showing processes enriched in the blackened regions compared to orange regions**. Three biological replicates. P-values were calculated using Deseq2 tool and later adjusted using B-H method (fold change ≥1, *=corrected p-value < 0.05; **=corrected p-value < 0.01; ***=corrected p-value < 0.001).
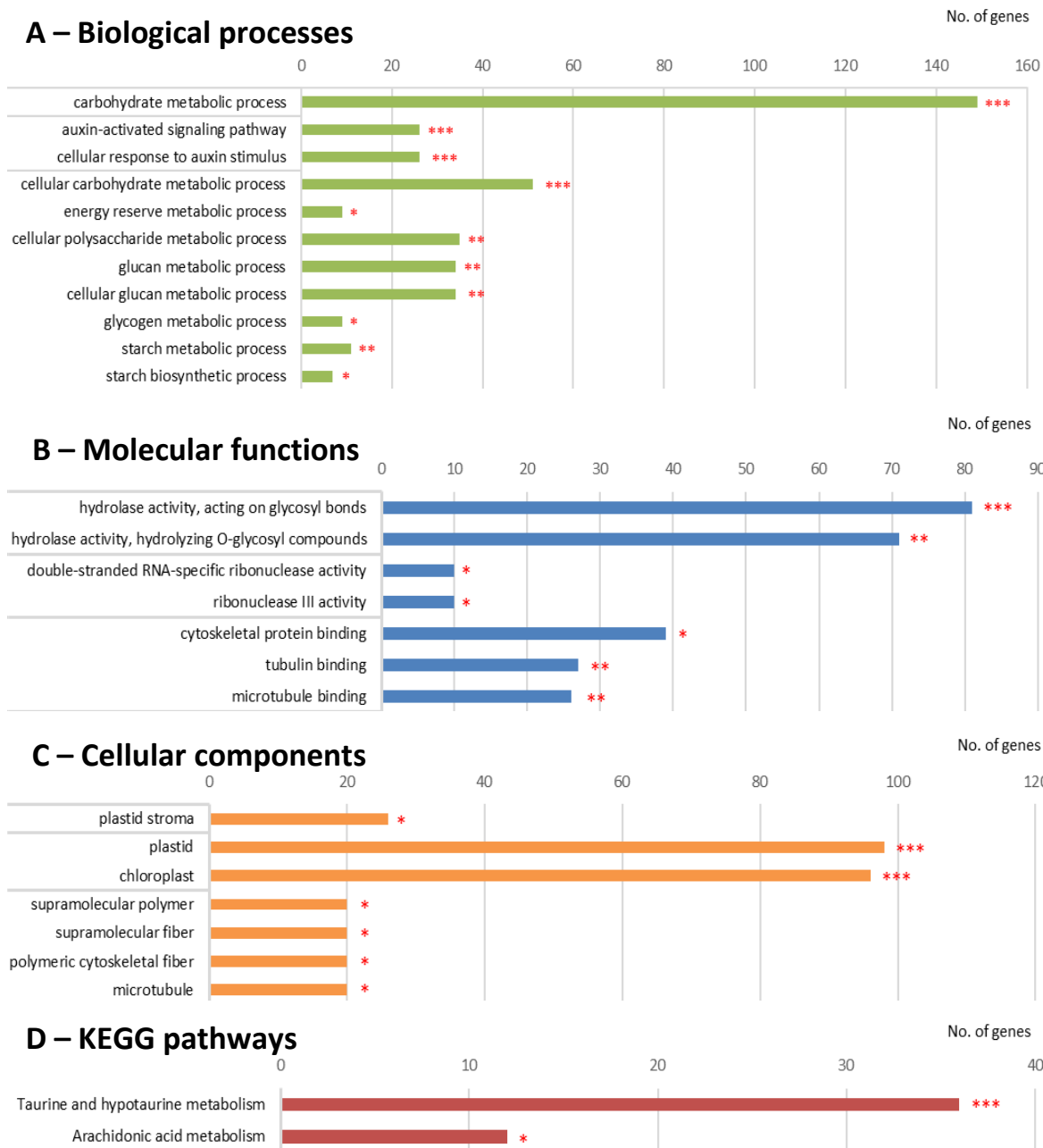
**Figure 6.13: GO terms indicating processes that were enhanced in the border regions compared to orange regions**. P-values were calculated using Deseq2 tool and later adjusted using B-H method (fold change ≥1, *=corrected p-value < 0.05; **=corrected p-value < 0.01; ***=corrected p-value < 0.001).

### 6.2.6.4 Phytohormone-related transcripts that were more abundant in blackened regions.

In order to explore the role of phytohormones in the blackening phenomenon, transcripts encoding proteins involved in hormone signalling were investigated further. Colour coding in figures represent the degree of change in transcript abundance where red and green shades represent highest and lowest expression respectively. Transcripts encoding proteins involved in auxin metabolism and signalling were more abundant in the blackened regions, together with ethylene-responsive transcription factors (Figure 6.14, 6.15, and 6.16). Transcripts encoding proteins involved in ABA metabolism and signalling such as ABI5 were also more abundant in the border regions (Figure 6.17 and 6.19). There was no evidence that transcripts associated with tyrosine metabolism were increased in the border regions (Figure 6.18).

**Plant hormone signal transduction in B_CT**

| | | |
|---|---|---|
| auxin-responsive protein IAA26-like | LOC108204829 | 9.193726 |
| probable protein phosphatase 2C 6 | LOC108212759 | 7.838854 |
| probable protein phosphatase 2C 50 | LOC108215250 | 7.185759 |
| probable protein phosphatase 2C 75 | LOC108226076 | 5.799393 |
| auxin-responsive protein IAA1-like | LOC108226833 | 5.7637 |
| auxin-induced protein AUX28-like | LOC108201663 | 5.595349 |
| auxin transporter-like protein 2 | LOC108195333 | 5.454648 |
| auxin-responsive protein IAA12 | LOC108197503 | 5.313751 |
| auxin-responsive protein IAA1-like | LOC108222038 | 5.100793 |
| ABSCISIC ACID-INSENSITIVE 5-like protein 7 | LOC108225746 | 4.523359 |
| protein ABSCISIC ACID-INSENSITIVE 5-like isoform X3 | LOC108204336 | 4.398089 |
| auxin-induced protein IAA6-like | LOC108220830 | 4.185859 |
| auxin-responsive protein IAA16-like | LOC108210653 | 3.934089 |
| auxin-induced protein 22D-like | LOC108204025 | 3.701266 |
| histidine-containing phosphotransfer protein 4 | LOC108193462 | 3.454167 |
| two-component response regulator ARR17-like | LOC108222091 | 3.416494 |
| transcription factor MYC2-like | LOC108206960 | 3.268088 |
| auxin-responsive protein IAA16-like | LOC108220212 | 3.160056 |
| auxin-responsive protein IAA31 | LOC108220516 | 3.078208 |
| abscisic acid receptor PYL9-like | LOC108198354 | 2.925644 |

**Figure 6.14: Heatmap of the 20 most up-regulated transcripts involved in plant hormone signal transduction in blackened carrot regions.** P-values were calculated using Deseq2 tool and later adjusted using B-H method (fold change ≥1).

**Signalling and activation of auxin in B_CT**

| | | |
|---|---|---|
| auxin-responsive protein IAA26-like | LOC108204829 | 9.193726256 |
| auxin-responsive protein IAA1-like | LOC108226833 | 5.763700063 |
| auxin-induced protein AUX28-like | LOC108201663 | 5.595348571 |
| auxin-responsive protein IAA12 | LOC108197503 | 5.313751186 |
| auxin-responsive protein IAA1-like | LOC108222038 | 5.100793014 |
| auxin-induced protein IAA6-like | LOC108220830 | 4.185859061 |
| auxin-induced protein 22D-like | LOC108214649 | 4.050852185 |
| auxin-responsive protein IAA16-like | LOC108210653 | 3.934089438 |
| auxin-induced protein 22D-like | LOC108204025 | 3.701265629 |
| probable auxin efflux carrier component 1c | LOC108215516 | 3.549626592 |
| auxin response factor 18-like | LOC108206659 | 3.452037072 |
| protein BIG GRAIN 1-like E | LOC108197604 | 3.251461302 |
| auxin response factor 4 | LOC108209335 | 3.171686383 |
| auxin-responsive protein IAA16-like | LOC108220212 | 3.160056126 |
| auxin-responsive protein IAA31 | LOC108220516 | 3.078208332 |
| auxin-responsive protein IAA7-like | LOC108200255 | 2.691893749 |
| auxin-responsive protein IAA27-like | LOC108197317 | 2.686738749 |
| probable auxin efflux carrier component 1b | LOC108215685 | 2.670962118 |
| auxin response factor 18-like | LOC108220171 | 2.618633227 |
| auxin response factor 1-like isoform X2 | LOC108200952 | 2.596185486 |

**Figure 6.15: Heatmap of the 20 most up-regulated transcripts involved in the signalling and activation of auxin in blackened carrot regions.** P-values were calculated using Deseq2 tool and later adjusted using B-H method (fold change ≥1).

**Ethylene-responsive transcription factors in B_CT**

| | | |
|---|---|---|
| ethylene-responsive transcription factor ERF039-like | LOC108213048 | 8.60 |
| AP2-like ethylene-responsive transcription factor TOE3 | LOC108206177 | 8.07 |
| ethylene-responsive transcription factor ERF027-like | LOC108221929 | 6.62 |
| ethylene-responsive transcription factor ERF109-like | LOC108225771 | 6.50 |
| ethylene-responsive transcription factor ERF025-like | LOC108225423 | 6.32 |
| ethylene-responsive transcription factor ERF017-like | LOC108199012 | 6.15 |
| ethylene-responsive transcription factor WIN1-like | LOC108226700 | 5.56 |
| ethylene-responsive transcription factor ERF062-like | LOC108198818 | 5.33 |
| ethylene-responsive transcription factor ERF021-like | LOC108195493 | 5.31 |
| ethylene-responsive transcription factor ERF027-like | LOC108208252 | 4.99 |
| ethylene-responsive transcription factor 13-like | LOC108201933 | 4.75 |
| ethylene-responsive transcription factor ERF027-like | LOC108222345 | 4.57 |
| AP2-like ethylene-responsive transcription factor TOE3 | LOC108222025 | 4.57 |
| ethylene-responsive transcription factor ERF022-like | LOC108199137 | 4.13 |
| AP2-like ethylene-responsive transcription factor ANT isoform X1 | LOC108224255 | 4.07 |
| AP2-like ethylene-responsive transcription factor ANT isoform X2 | LOC108224255 | 4.07 |
| ethylene-responsive transcription factor ERF017-like | LOC108213718 | 3.94 |
| ethylene-responsive transcription factor ERF017 | LOC108196474 | 3.29 |
| ethylene-responsive transcription factor 1B-like | LOC108204838 | 3.29 |
| ethylene-responsive transcription factor ERF110-like | LOC108204848 | 3.29 |

**Figure 6.16: Heatmap of ethylene transcript abundance in blackened carrot regions.** P-values were calculated using Deseq2 tool and later adjusted using B-H method (fold change ≥1).

**ABA-activated signalling in B_CT**

| | | |
|---|---|---|
| pathogenesis-related protein 2-like | LOC108195566 | -8.487781689 |
| major allergen Dau c 1-like | LOC108196863 | -8.337646462 |
| major allergen Dau c 1-like | LOC108195304 | -7.904096971 |
| pathogenesis-related protein 2-like | LOC108198435 | -7.798503911 |
| major allergen Dau c 1-like | LOC108196862 | -7.503152293 |
| major allergen Api g 1, isoallergen 1-like | LOC108195243 | -7.186823772 |
| pathogenesis-related protein 2-like | LOC108194075 | -6.030054403 |
| major allergen Dau c 1-like | LOC108195578 | -5.479389428 |
| major allergen Pru ar 1-like | LOC108202363 | -5.329102018 |
| major allergen Dau c 1-like | LOC108195466 | -4.943299281 |
| major allergen Dau c 1-like | LOC108195447 | -4.538517527 |
| major allergen Dau c 1-like | LOC108195438 | -4.538517527 |
| major allergen Dau c 1-like | LOC108195490 | -4.436426861 |
| pathogenesis-related protein A-like | LOC108195270 | -4.261258295 |
| pathogenesis-related protein 2-like | LOC108194358 | -3.751879769 |
| major allergen Api g 1, isoallergen 1-like | LOC108194119 | -3.614262148 |
| major allergen Api g 1, isoallergen 1-like | LOC108194227 | -3.273441423 |
| pathogenesis-related protein A | LOC108193625 | -2.809797091 |
| major allergen Dau c 1-like | LOC108198830 | -2.632950735 |
| major allergen Dau c 1 | LOC108198848 | -2.430694913 |

**Figure 6.17: Heatmap of the 20 most down-regulated transcripts involved in ABA-activated signalling in blackened carrot regions.** P-values were calculated using Deseq2 tool and later adjusted using B-H method (fold change ≥1).

**Tyrosine metabolism in M_CT**

| | | |
|---|---|---|
| polyphenol oxidase, chloroplastic-like | LOC108206527 | -10.5421518 |
| macrophage migration inhibitory factor homolog | LOC108217932 | -7.8161543 |
| alcohol dehydrogenase 1-like | LOC108214136 | -6.76202773 |
| probable aminotransferase TAT2 | LOC108224044 | -6.25227742 |
| alcohol dehydrogenase 1-like | LOC108199900 | -4.73920863 |
| polyphenol oxidase, chloroplastic-like | LOC108220626 | -4.45706324 |
| aspartate aminotransferase, cytoplasmic | LOC108204943 | -4.03407018 |
| polyphenol oxidase, chloroplastic-like | LOC108206452 | -3.93864501 |
| alcohol dehydrogenase-like | LOC108225144 | -3.67549765 |
| polyphenol oxidase I, chloroplastic-like | LOC108192978 | -3.5513905 |
| aspartate aminotransferase, mitochondrial | LOC108225092 | -3.45355018 |
| alcohol dehydrogenase 1 | LOC108199816 | -3.24585026 |
| bifunctional aspartate aminotransferase and glutamate/aspartate-prephenate aminotransferase | LOC108204769 | -2.75912291 |
| hydroxyphenylpyruvate reductase-like | LOC108209340 | -1.99098302 |
| probable aminotransferase TAT2 | LOC108205473 | -1.86484678 |
| aspartate aminotransferase, cytoplasmic | LOC108214974 | -1.7008044 |
| 4-hydroxyphenylpyruvate dioxygenase | LOC108227785 | -1.20831077 |
| glutathione S-transferase zeta class-like | LOC108200492 | -1.16463872 |

**Figure 6.18: Heatmap of the 20 most down-regulated transcripts involved in tyrosine metabolism in border carrot regions.** P-values were calculated using Deseq2 tool and later adjusted using B-H method (fold change ≥1).

**ABA-activated signalling in M_CT**

| | | |
|---|---|---|
| auxin-induced protein 22D-like | LOC108214649 | 8.960754 |
| probable auxin efflux carrier component 1b | LOC108215685 | 5.709917 |
| auxin-induced protein IAA6-like | LOC108220830 | 5.6952 |
| protein BIG GRAIN 1-like E | LOC108197604 | 5.455784 |
| auxin-responsive protein IAA26-like | LOC108204829 | 5.058786 |
| probable auxin efflux carrier component 1c | LOC108215516 | 4.912437 |
| auxin-responsive protein IAA12 | LOC108197503 | 4.890665 |
| auxin-induced protein 22A-like | LOC108221111 | 4.578192 |
| auxin efflux carrier component 7-like | LOC108199798 | 4.169796 |
| probable auxin efflux carrier component 1b | LOC108220412 | 3.994177 |
| auxin-responsive protein IAA16-like | LOC108220212 | 3.578707 |
| auxin-responsive protein IAA16-like | LOC108210653 | 3.577538 |
| auxin-responsive protein IAA26-like | LOC108220076 | 3.537354 |
| auxin-responsive protein IAA27-like | LOC108197317 | 3.447124 |
| auxin response factor 1-like isoform X1 | LOC108200952 | 3.38893 |
| auxin-responsive protein IAA27-like | LOC108227728 | 3.201353 |
| auxin-responsive protein IAA27 | LOC108213043 | 3.004947 |
| auxin response factor 4-like | LOC108218906 | 2.786427 |
| auxin response factor 18-like | LOC108220171 | 2.779374 |
| auxin-induced protein 22D-like | LOC108204025 | 2.56448 |

**Figure 6.19: Heatmap of the 20 most up-regulated transcripts involved in the signalling and activation of auxin in border carrot regions.** P-values were calculated using Deseq2 tool and later adjusted using B-H method (fold change ≥1).

## 6.3   Discussion

The aim of the experiments reported in this chapter were to establish the transcript profiles of the orange and blackened regions of the carrot batons, as well as those of the tissues bordering the blackened regions. RNA extraction methods were first optimised in order to collect high-quality RNA extracts from each of the regions. RNA-seq analysis was then carried out on these samples to identify specific changes in the transcript profiles of the blackened carrots. This analysis has pinpointed the major processes that are changed during the blackening process and the molecular mechanisms that may trigger and regulate these pathways.

Firstly, the data were analysed to identify the DEGs, GO terms and KEGG pathways. In the category of 'metabolic processes' transcripts encoding proteins associated with the metabolism of carbohydrates, glucan and starch were enriched. Transcripts encoding proteins associated with phytohormone signalling, particularly in response to auxin, were dominant terms in the category of 'biological processes' of enriched DEGs. These terms were predominant in the blackened (B_CT) and border regions (M_CT) (Figure 6.12 and 6.13).

Transcripts encoding proteins associated with ribosomes, spliceosomes, proteasomes, and cytoskeletons were highly represented in the category of "cellular components" in blackened regions (Figure 6.12 C). However, organelles such as plastids were highly represented in the border regions (Figure 6.13 C). Additionally, a relatively large number of DEGs associated with hydrolase activity were enriched in the category of 'molecular functions' in both blackened and border regions (Figure 6.12 B and 6.13 B). However, the blackened regions showed enrichment of additional terms, such as DNA binding and cytoskeletal binding processes (Figure 6.12 B).

The KEGG pathway analysis was used to determine the biological pathways that were enriched and the functional significance of the DEGs. Interestingly, DEGs that were enriched in the blackened regions indicate that transcripts encoding proteins associated with starch and sucrose metabolism, carotenoid biosynthesis and photosynthesis pathways were expressed in the blackening process (Figure 6.12 D). In contrast, only the pathways of taurine and hypo-taurine metabolism and arachidonic acid metabolism

were over-represented in the border region (Figure 6.13 D). Taurine is an amino sulfonic acid that is only found in low amounts in plants, where it may fulfil a protective function (Hao et al., 2004).

The GO terms representing DEGS indicating biological processes that were decreased in the blackened regions include organonitrogen metabolism, protein processes and oxidoreductase activities (Figure 6.12 A). Similarly, the border carrot regions showed decreases in DEGs associated with phosphorus metabolism (Figure 6.13 A). DEGS associated with phenylpropanoid metabolism, ribosomal processes and the biosynthesis of unsaturated fatty acids were all decreased in the blackened regions (Figure 6.12 A). Interestingly, down-regulated DEGs in the border regions were involved in many more pathways; including glycolysis, MAP signalling pathway, protein processing, amino acid metabolism and biosynthesis and glutathione metabolism (Figure 6.13 D).

DEGs associated with tyrosine metabolism including PPO genes (LOC108206452, LOC108192978, LOC108220626, LOC108206527) were significantly decreased in the blackened and border regions. About 56 DEGs and 100 DEGs encoding proteins involved in the phenylpropanoid pathway were less abundant in the blackened and border regions, respectively. The levels of DEGs encoding proteins involved in processes associated with enzymatic browning were decreased in abundance. These include proteins involved in phenylalanine metabolism, glutathione metabolism, and fatty acid degradation pathways. This finding is in contrast to the changes observed in phenolic substrates including chlorogenic acid and caffeic acids, which are known substrates for the PPO enzyme. The decreases in transcripts encoding enzymes associated with browning suggests that the expression of key genes was restrained in an effort to compensate for the high levels of metabolites present in the blackened regions.

One possible explanation for the blackening of cut batons could be the induction of SA-associated cell death. However, DEGs encoding key enzymes involved in the synthesis of SA, such as chorismate synthase (LOC108219299), aminodeoxychorismate synthase (LOC108219009) and several chorismate mutases (LOC108196652, LOC108210290, LOC108224600) were lower in the blackened and border regions. Other DEGs encoding proteins associated with PCD such as the lesion simulating disease (LSD)-like proteins

and accelerated cell death 6-like proteins were generally decreased in abundance. However, two LSD-like and three accelerated cell death 6 proteins were more abundant. These proteins are negative regulators of PCD.

DEGs involved in auxin signalling and cellular response to auxin were enriched in the blackened and border regions. The role of auxin in carrot blackening is intriguing. It is not impossible to speculate that an auxin-induced senescence pathway is induced as the carrots age. GO terms that are enriched in the blackened carrots include carbohydrate metabolism, particularly glucan and starch-associated processes. Sugar and hormone crosstalk is important in the regulation of plant development (Eveland and Jackson, 2012). Auxins are regulators of fruit development and ripening. Auxin may also repress ABA production through modulation of the expression of the gene encoding *9-cis-epoxycarotenoid dioxygenase* (*NCED*) and repression of the expression of ABA-responsive genes. A small group of DEGS involved in ABA responses were significantly lower in blackened regions. These findings suggest that auxin signalling and sugar metabolism may play key roles in the control of carrot blackening.

# Chapter VII

# General discussion and conclusions

The studies presented and discussed in this thesis provide in-depth analysis of the molecular and metabolic processes that underpin carrot blackening, as well as allowing an assessment of environmental effects based on field data obtained from Kettle Produce Ltd regarding field sites. Together, the data presented in this thesis provides an increased understanding of the factors that cause susceptibility to blackening, which allows identification of possible methods to prevent the blackening, including changes to crop management. Wounding alone does not cause the blackening of cut carrot batons because the blackening phenomenon is only observed in mature carrots that are over 1 year old at the point of harvest. These older carrots that have been stored underground for a long period, and that are as much as 430 days old have a propensity to show blackening at values twice as high in carrots in younger age ranges. This finding strongly suggests that carrot age or the length of storage underground is the major factor that causes susceptibility to blackening.

Environmental conditions are also known to cause blackening in stored vegetables. While the environmental parameters prevalent in the Scottish carrot fields, including air temperature, soil temperature and solar radiation did not change greatly during the 15 years between 2006 and 2020, significant field to field variation in susceptibility to blackening was observed. While the present study has a number of limitations, the closer cooperation with Kettle Produce Ltd was essential to establishing this link.

The environmental data presented in this thesis was recorded at the Balmalcolm site, where the Kettle Produce Ltd head office is located. These data were used to represent the environmental conditions of all vegetable fields throughout Scotland because the majority of fields were located within approximately 50 miles of Balmalcolm. However, Balmalcolm is further south than any of the other carrot fields included in the analysis. It is located approximately 100 miles away from the more northern fields located in Aberdeenshire. Hence, the data obtained at the Balmalcolm site can only provide an approximate representation of the environmental conditions experienced in all relevant vegetable fields. Also, the occurrence of waterlogged fields was not recorded in the present analysis. Flooded fields can cause hypoxia in root vegetables. Hypoxia can

induce higher lignin contents in carrots, as well as decreased fresh weight because of the formation of aerenchyma (Que et al., 2018). The absence of literature on the effects of carrots stored underground in waterlogged conditions makes predictions difficult, but the fields showing the highest levels of blackening may be more likely to experience waterlogging or have other issues with soil compaction than the fields that have lower blackening rates.

As discussed above, there was a high level of variation in susceptibly to blackening in the carrots harvested from different field sites. However, the appearance of blackening followed a similar timescale in carrots harvested and processed from all field sites. The highest level of blackening was observed either on the day of processing (day 0) or the following day (day 1). Values then declined in the following days. Levels of blackening seen in all fields varied between 1% to 10%, except for the Besfeild site and the Unknown (EL) site, where no blackening was reported.

It is possible that the geographical locations of carrot fields has an impact on susceptibility to blackening, however there was a large variation in the level of blackening seen in the mid and south fields. Therefore, more detailed studies of the locations and environmental factors affecting these general locations, is required to establish direct links between environmental factors and carrot blackening.

Large variations in carrot blackening were also reported for the fields owned by KPL, suggesting that carrot blackening is not linked to the owners of the fields or their individual management practices. Interestingly, the clusters of nearby fields categorised as either Finavon or Forfar showed levels of blackening of ~1.5% and 5%, respectively. As these fields were all located within a ~15-mile perimeter, they are likely to experience very similar weather patterns, indicating that weather (rainfall, temperatures, etc.) conditions per se are unlikely to play a large role in carrot blackening. However, other environmental factors such as soil type may play an important role in the different field sites. Heavy rainfall can affect soil types differently. For example, sandy soils are much less likely to experience prolonged flooding because they retain less water than heavy clay soils. More environmental data should be collected in any future studies. This should include a comparison of the rates of blackening relative to the soil types in each

field. Periods of flooding should also be monitored and recorded to investigate relationships to carrot blackening. A further limitation of the 2020 trial data is the limited number of samples collected from each batch of carrots. Greater numbers of samples may provide a better representation of each batch. Moreover, if possible, the whole carrot batch should be monitored for blackening.

A more in-depth analysis will be necessary to assess the relationships between the developmental age of the carrots at processing and the length of underground storage and susceptibility to the blackening phenomenon. In future studies, carrots could be harvested weekly or monthly and processed into batons. This would allow a much more detailed monitoring of the appearance of blackening. In addition, the analysis of metabolome and transcriptome profiles of the batons at each stage would allow a more detailed understanding of the onset of blackening and crucially the mechanisms that are induced by root aging that lead to blackening upon subsequent wounding during the processing of the carrots for market.

## 7.1   Cell shrinkage in blackened carrot regions

The data presented here show that the blackened regions of the carrot batons had significantly smaller cells than the orange batons, possibly due to cell shrinkage (McCabe et al., 1997). Cells are naturally smaller in vascular regions relative to other areas of the root.  However, a distinctive pattern would be observed if the vascular regions of the carrot batons alone were prone to developing blackening.

## 7.2   Differences in metabolomic profiles of blackened and orange regions of the carrot batons

The accumulation of dark material visible in cells in the blackened regions, together with the increased levels of autofluorescence emitted by the blackened regions are likely the result of an accumulation of phenolic compounds that does not occur in the orange batons. This conclusion is supported by the observed increase in lignin content and in the accumulation of other phenolic compounds in the blackened regions. Lignin synthesis is commonly triggered by unfavourable environmental conditions or by microbial attack in order to strengthen cell walls as a protective barrier (Sattler and

Funnell-Harris, 2013). Polyphenol synthesis leads to an increase in lignin formation. Hence, activation of the phenylpropanoid pathway that incorporates PAL, PPO and PODs may result in carrot blackening. Chlorogenic acid is widely recognised as a browning substrate in both fruits and vegetables. The enzymes PAL, PPO and PODs are commonly linked to the degradation of fresh produce because the oxidation of phenolic compounds can lead to the formation of black deposits. However, the data presented here showed significantly down-regulated DEGs encoding enzymes and proteins involved in tyrosine metabolism, including the PPO related genes in both the blackened and border carrot regions. The expression of DEGs involved in other processes of enzymatic browning was also decreased, including phenylalanine metabolism, glutathione metabolism, and the fatty acid degradation pathway. This finding is somewhat surprising given that phenolic compounds closely associated with PPO, including chlorogenic acid, caffeic acid, and 5-caffeoylquinic acid, were enriched in blackened regions. The transcriptome data clearly indicates that the expression of genes involved in secondary metabolism is constrained following the accumulation of secondary metabolites. Such regulation would serve to prevent an excessive accumulation of secondary metabolites, particularly under conditions where primary metabolites were progressively depleted as was observed in the blackened carrot regions.

Pectin oligosaccharides are also able to trigger lignification by activating plant defence responses (Hachem et al., 2016; Robertsen, 1986). Differences in lignin composition were observed between the orange and blackened regions, notably with S-lignin only present in blackened regions. Sinapyl alcohol content increases during late-stage lignification, leading to S-lignin accumulation (Schäfer et al., 2018).

The metabolic profile of blackened carrot regions showed a general decrease in primary metabolites particularly amino acids, sugars (glucose, fructose, sucrose) and organic acids. In addition, there was a general increase in phenolic compounds, fatty acids, and some carbohydrates (galactose, mannose, glycerol, and mannitol). It should be noted that the levels of most of the organic acids involved in the TCA cycle were decreased in blackened carrot regions. These observations suggest that there had been a switch from primary to secondary metabolism in the blackened regions, and this can be associated

156

with starvation and/or depletion of respiratory substrates. The low levels of glucose, fructose and sucrose also suggests that the blackened carrots were running out of vital carbohydrate reserves that are essential for ATP production. Observed decreases in the aromatic amino acids further support the conclusion of a switch from primary to secondary metabolism, that results in phenolic compound accumulation in the blackened regions. The dramatic ~8-fold increase in GABA is indicative of an abiotic stress response. Increases in other stress-induced signalling metabolites, including allantoin and putrescine, were also observed. A strong correlation between succinic acid and GABA was observed in carbon starvation-induced GABA production in Arabidopsis leaves (Caldana et al., 2011). However, succinic acid levels were similar in the orange and blackened carrot regions, while other TCA metabolite levels were decreased in blackened regions. The metabolomics analysis revealed increased fatty acid levels in the blackened regions. Fatty acids are signalling molecules that are involved in wounding responses. However, the transcriptome profiling analysis showed that DEGs involved in the synthesis of unsaturated fatty acids, were decreased together with genes involved in ribosomal functions and phenylpropanoid metabolism. Notably, the border regions showed decreased numbers of DEGs involved in many more metabolic pathways, including amino acid metabolism and synthesis, glutathione metabolism and glycolysis. JA synthesis was increased in wounded lettuce leaves, together with amplified wound signalling through the oxylipin pathway. These changes were crucial aspects of leaf browning (Choi et al., 2005). However, the levels of only one transcript associated with JA signalling were increased in the blackened regions. The observed increases in this '23 kDa jasmonate-induced protein-like' transcript suggesting that JA signalling may be activated but there was no evidence of changes in jasmonate synthesis during carrot blackening.

## 7.3 Changes in cell wall composition in the blackened and border regions of carrot batons

The detection of xyloglucan, HG pectin and RG-I pectin was decreased in the blackened regions. This finding may suggest increased degradation wall, or it may be caused by masking by phenolic polymers. Low xyloglucan levels would result in less rigid cell walls. However, it should be noted that the low detection of xyloglucan in the blackened regions could be due to phenolic cross-linking, a process that interferes with accurate detection.

Decreased pectin detection in blackened carrot regions could be caused by age-induced pectin degradation, which is also known to trigger defensive mechanisms, including an increase in lignin production. Pectin oligosaccharides are able to trigger lignification through activation of defence responses (Robertsen, 1986, p.19; Hachem et al., 2016). Another possibility is that the observed increases in phenolic content could be caused by cross linking within the cell walls, which would prevent access of antibodies to the pectin epitopes, resulting in reduced detection. However, carbohydrate analysis revealed decreased galacturonic acid levels in blackened regions. Galacturonic acid is the major monosaccharide of the pectin backbone. This finding supports the conclusion that the low detection of pectin is caused by pectin degradation rather than by masking by other polymers. Interestingly, higher levels of HG pectin were found in the cell walls of the border regions than in the orange or blackened regions. This finding suggests either that there is an increased production of HG pectin in border regions or that the cell wall structure is loosening, allowing better access of antibodies resulting in higher detection. If the production of HG pectin is increased in the blackened regions, it is likely part of the defence response. However, there is little literature reporting what factors could lead to increased pectin synthesis in response to developmental and environmental triggers. Pectins are rapidly degraded upon activation of cell wall degradation. Hence, decreased pectin levels are a common effect of microbial attacks (Bethke et al., 2016; Tayi et al., 2016). As there is no indication of microbial attack in the carrot blackening process, the trigger of observed wound responses must be caused by the developmental aging of the carrots as they are stored underground before harvest. These differences in cell wall composition between blackened regions and orange

batons are likely caused by developmental factors that increase pectin and xyloglucan degradation upon the wounding caused during baton processing. This polymer degradation then triggers defensive responses in the carrots causing enhanced secondary metabolism and resulting in increased lignification of cell walls.

## 7.4 Transcriptome profiles of the blackened and orange regions

The transcriptome profiling analysis showed increases in transcripts involved in phytohormone signal transduction, particularly auxin signalling, as well as ethylene-responsive transcription factors in the blackened regions compared to orange batons. Transcripts involved in starch metabolism were also increased in abundance. Crosstalk between sugar and hormone signalling is important in plant development. Auxin is known to inhibit the expression of ABA-response genes and to repress ABA production through the repression of NCED. However, NCED transcripts were more abundant in the blackened and border carrot regions. Taken together, these findings suggest that auxin and sugar metabolism may have a role in regulating carrot blackening. Blackened and border regions also showed decreased levels of transcripts involved in ABA-signalling. Transcripts associated with tyrosine metabolism were also lower in the border regions. Transcripts encoding components of taurine and hypo-taurine metabolism and arachidonic acid metabolism were increased in the border regions. Taurine may function as a ROS scavenger, promoting growth and plant development (Hao et al., 2004). Taurine is a critical amino acid in animals that is necessary for photoreceptor development (Ripps and Shen, 2012). The increased presence of DEGs involved in taurine metabolism between blackened and border regions are intriguing. Taurine may be involved in cell signalling. It is possible that the accumulation of taurine could be a marker for the early stages of blackening.

In conclusion, using a combined transcriptomics and metabolomics strategy to determine the basis of carrot blackening is insightful. It reveals a disparity between the levels of transcripts that indicate changes in cell signalling leading to altered gene expression and the levels of metabolites that may participate in cell signalling leading to changes in gene expression. Therefore, the results for transcriptomics and

metabolomics contain complementary information about carrot blackening. The levels of transcripts and metabolites may vary considerably (Cavill et al., 2016). The transcriptome data indicate the signalling pathways that lead to blackening, as well as pathways activated as a consequence of blackening.

## 7.5 Future work

Future work could address key questions that arise as a consequence of this study. In particular, methods for preventing baton blackening should be explored. However, the simplest strategy would be to only use young carrots for processing or to only harvest fields with the lowest record of blackening for later harvest dates. Alternatively, heat treatment, which is commonly used to preserve the postharvest quality of fruits and vegetables by reducing microbial diseases, maintaining firmness, and increasing antioxidant content, could also be tested with regard to carrots (Langer et al., 2018). Heat treatments can block the production of wound signalling molecules. Similarly, an antioxidant coating could prevent the oxidative activation of enzymes responsible for phenol oxidation (PAL, PPO and POD). This is the cause of enzymatic browning in potatoes (Yingsanga et al., 2008). Numerous edible coatings, including GABA, chitosan, and melatonin have been used successfully to prevent enzymatic browning in freshly cut produce (Adiletta et al., 2018; Özdemir and Gökmen, 2019; Xu et al., 2019; Zheng et al., 2019; Nazoori et al., 2020). Low oxygen packaging is also an alternative method to be tested.

## 7.6 Conclusion

In conclusion, carrots are subjected to substantial aging (to ~1 year old) underground before being cut into batons. The beginning of senescence in the carrot taproots during underground storage could incorporate cell wall fragmentation involving pectin degradation. The pectic oligosaccharides thus produced might then act as signals that trigger a pathogen-like response in the carrot root upon subsequent wounding. This would inevitably lead to an increased flux through the lignin biosynthesis pathway. The

metabolome analysis reported here reveals a general depletion of sugars and primary metabolites, together with a shift from primary to secondary metabolism in the blackened carrot regions. The reduction of essential sugars and amino acids suggests that the carrots run out of essential metabolites during prolonged storage. The increases in secondary metabolites, particularly compounds involved in plant defences, such as lignification, suggests that subsequent wounding activates defence pathways associated with infestation by insect pests or microbial pathogens. The phenolic compounds involved in the lignification process can be polymerised by oxidation. The oxidases that catalyse these reactions produce dark pigments, leading to carrot blackening. Future work is essential to prevent the enormous waste caused by the blackening of carrot batons. Such food waste poses a significant economic, social, and ecological burden. The data presented here prompt new avenues of research and suggest ways to improve current management practices. The combined effects of environment, carrot development and aging during storage before processing are crucial to susceptibility to blackening. The active modulation of storage conditions alone may provide an opportunity to decrease the likelihood of blackening.

# References

Abou-Saleh, R.H., Hernandez-Gomez, M.C., Amsbury, S., Paniagua, C., Bourdon, M., Miyashima, S., Helariutta, Y., Fuller, M., Budtova, T., Connell, S.D., Ries, M.E. and Benitez-Alfonso, Y. 2018. Interactions between callose and cellulose revealed through the analysis of biopolymer mixtures. *Nature Communications*. **9**(1), p.4538.

Adiletta, G., Pasquariello, M.S., Zampella, L., Mastrobuoni, F., Scortichini, M. and Petriccione, M. 2018. Chitosan coating: A postharvest treatment to delay oxidative stress in loquat fruits during cold storage. *Agronomy*. **8**(4), p.54.

Andersen, M.C.F., Boos, I., Marcus, S.E., Kračun, S.K., Rydahl, M.G., Willats, W.G.T., Knox, J.P. and Clausen, M.H. 2016. Characterization of the LM5 pectic galactan epitope with synthetic analogues of β-1,4-d-galactotetraose. *Carbohydrate Research*. **436**, pp.36–40.

Andrews, S. 2010. FastQC: A quality control tool for high throughput sequence data. Online publication.

Bacete, L. and Hamann, T. 2020. The role of mechanoperception in plant cell wall integrity maintenance. *Plants*. **9**(5), p.574.

Banga, O. 1957. Origin of the European cultivated carrot. *Euphytica*. **6**(1).

Bannoud, F., Ellison, S., Paolinelli, M., Horejsi, T., Senalik, D., Fanzone, M., Iorizzo, M., Simon, P.W. and Cavagnaro, P.F. 2019. Dissecting the genetic control of root and leaf tissue-specific anthocyanin pigmentation in carrot (Daucus carota L.). *Theoretical and Applied Genetics*. **132**(9), pp.2485–2507.

Baranski, R., Allender, C. and Klimek-Chodacka, M. 2012. Towards better tasting and more nutritious carrots: Carotenoid and sugar content variation in carrot genetic resources. *Food Research International*. **47**(2), pp.182–187.

Barlow, P. 2005. 14 - From cambium to early cell differentiation within the secondary vascular system *In*: N. M. Holbrook and M. A. Zwieniecki, eds. *Vascular Transport in Plants* [Online]. Physiological Ecology. Burlington: Academic Press, pp.279–306. [Accessed 28 June 2021]. Available from: https://www.sciencedirect.com/science/article/pii/B9780120884575500162.

Bethke, G., Thao, A., Xiong, G., Li, B., Soltis, N.E., Hatsugai, N., Hillmer, R.A., Katagiri, F., Kliebenstein, D.J., Pauly, M. and Glazebrook, J. 2016. Pectin biosynthesis is critical for cell wall integrity and immunity in Arabidopsis thaliana. *The Plant Cell*. **28**(2), pp.537–556.

Bindea, G., Mlecnik, B., Hackl, H., Charoentong, P., Tosolini, M., Kirilovsky, A., Fridman, W.-H., Pagès, F., Trajanoski, Z. and Galon, J. 2009. ClueGO: a Cytoscape plug-in

to decipher functionally grouped gene ontology and pathway annotation networks. *Bioinformatics*. **25**(8), pp.1091–1093.

Britton, G. 1985. [5] General carotenoid methods *In*: *Methods in Enzymology* [Online]. Steroids and Isoprenoids Part B. Academic Press, pp.113–149. [Accessed 9 August 2020]. Available from: http://www.sciencedirect.com/science/article/pii/S0076687985110074.

Broxterman, S.E. and Schols, H.A. 2018. Interactions between pectin and cellulose in primary plant cell walls. *Carbohydrate Polymers*. **192**, pp.263–272.

Caldana, C., Degenkolbe, T., Cuadros-Inostroza, A., Klie, S., Sulpice, R., Leisse, A., Steinhauser, D., Fernie, A.R., Willmitzer, L. and Hannah, M.A. 2011. High-density kinetic analysis of the metabolomic and transcriptomic response of Arabidopsis to eight environmental conditions. *The Plant Journal*. **67**(5), pp.869–884.

Canher, B., Heyman, J., Savina, M., Devendran, A., Eekhout, T., Vercauteren, I., Prinsen, E., Matosevich, R., Xu, J., Mironova, V. and Veylder, L.D. 2020. Rocks in the auxin stream: Wound-induced auxin accumulation and ERF115 expression synergistically drive stem cell regeneration. *Proceedings of the National Academy of Sciences*. **117**(28), pp.16667–16677.

Cavill, R., Jennen, D., Kleinjans, J. and Briedé, J.J. 2016. Transcriptomic and metabolomic data integration. *Briefings in Bioinformatics*. **17**(5), pp.891–901.

Chang, S., Puryear, J. and Cairney, J. 1993. A simple and efficient method for isolating RNA from pine trees. *Plant Molecular Biology Reporter*. **11**(2), pp.113–116.

Chauhan, A., Sharma, J.N., Modgil, M. and Siddappa, S. 2018. Comparison of various RNA extraction methods, cDNA preparation and isolation of calmodulin gene from a highly melanized isolate of apple leaf blotch fungus Marssonina coronaria. *Journal of Microbiological Methods*. **151**, pp.7–15.

Chen, D., Shao, Q., Yin, L., Younis, A. and Zheng, B. 2019. Polyamine function in plants: Metabolism, regulation on development, and roles in abiotic stress responses. *Frontiers in Plant Science*. **9**.

Choi, H.W. and Klessig, D.F. 2016. DAMPs, MAMPs, and NAMPs in plant innate immunity. *BMC Plant Biology*. **16**(1), p.232.

Choi, Y.-J., Tomás-Barberán, F.A. and Saltveit, M.E. 2005. Wound-induced phenolic accumulation and browning in lettuce (Lactuca sativa L.) leaf tissue is reduced by exposure to n-alcohols. *Postharvest Biology and Technology*. **37**(1), pp.47–55.

Chubey, B.B. and Nylund, R.E. 1969. Surface browning of carrots. *Canadian Journal of Plant Science*. **49**(4), pp.421–426.

Ciou, J.-Y., Lin, H.-H., Chiang, P.-Y., Wang, C.-C. and Charles, A.L. 2011. The role of polyphenol oxidase and peroxidase in the browning of water caltrop pericarp during heat treatment. *Food Chemistry*. **127**(2), pp.523–527.

Clausen, M.H., Willats, W.G.T. and Knox, J.P. 2003. Synthetic methyl hexagalacturonate hapten inhibitors of anti-homogalacturonan monoclonal antibodies LM7, JIM5 and JIM7. *Carbohydrate Research*. **338**(17), pp.1797–1800.

Considine, M.J. and Foyer, C.H. 2021. Stress effects on the reactive oxygen species (ROS)-dependent regulation of plant growth and development. *Journal of Experimental Botany*. (erab265).

Cornuault, V., Buffetto, F., Rydahl, M.G., Marcus, S.E., Torode, T.A., Xue, J., Crépeau, M.-J., Faria-Blanc, N., Willats, W.G.T., Dupree, P., Ralet, M.-C. and Knox, J.P. 2015. Monoclonal antibodies indicate low-abundance links between heteroxylan and other glycans of plant cell walls. *Planta*. **242**(6), pp.1321–1334.

Dervinis, C., Frost, C.J., Lawrence, S.D., Novak, N.G. and Davis, J.M. 2010. Cytokinin primes plant responses to wounding and reduces insect performance. *Journal of Plant Growth Regulation*. **29**(3), pp.289–296.

Dobin, A., Davis, C.A., Schlesinger, F., Drenkow, J., Zaleski, C., Jha, S., Batut, P., Chaisson, M. and Gingeras, T.R. 2013. STAR: ultrafast universal RNA-seq aligner. *Bioinformatics*. **29**(1), pp.15–21.

Doblin, M.S., Pettolino, F., Bacic, A., Doblin, M.S., Pettolino, F. and Bacic, A. 2010. Plant cell walls: the skeleton of the plant world. *Functional Plant Biology*. **37**(5), pp.357–381.

Dong, X. 1998. SA, JA, ethylene, and disease resistance in plants. *Current Opinion in Plant Biology*. **1**(4), pp.316–323.

Duffieux, D., Marcus, S.E., Knox, J.P. and Hervé, C. 2020. Monoclonal antibodies, carbohydrate-binding modules, and detection of polysaccharides in cell walls from plants and marine algae *In*: Z. A. Popper, ed. *The Plant Cell Wall: Methods and Protocols* [Online]. Methods in Molecular Biology. New York, NY: Springer, pp.351–364. [Accessed 29 June 2021]. Available from: https://doi.org/10.1007/978-1-0716-0621-6_20.

Dumitrache, A., Tolbert, A., Natzke, J., Brown, S.D., Davison, B.H. and Ragauskas, A.J. 2017. Cellulose and lignin colocalization at the plant cell wall surface limits microbial hydrolysis of Populus biomass. *Green Chemistry*. **19**(9), pp.2275–2285.

Eckardt, N.A. 2008. Role of xyloglucan in primary cell walls. *The Plant Cell*. **20**(6), pp.1421–1422.

Eveland, A.L. and Jackson, D.P. 2012. Sugars, signalling, and plant development. *Journal of Experimental Botany*. **63**(9), pp.3367–3377.

Fàbregas, N. and Fernie, A.R. 2019. The metabolic response to drought. *Journal of Experimental Botany*. **70**(4), pp.1077–1085.

Fait, A., Fromm, H., Walter, D., Galili, G. and Fernie, A.R. 2008. Highway or byway: the metabolic role of the GABA shunt in plants. *Trends in Plant Science*. **13**(1), pp.14–19.

Fernandes Santos, C.A. and Simon, P.W. 2006. Heritabilities and minimum gene number estimates of carrot carotenoids. *Euphytica*. **151**(1), pp.79–86.

Gallego-Giraldo, L., Liu, C., Pose-Albacete, S., Pattathil, S., Peralta, A.G., Young, J., Westpheling, J., Hahn, M.G., Rao, X., Knox, J.P., Meester, B.D., Boerjan, W. and Dixon, R.A. 2020. ARABIDOPSIS DEHISCENCE ZONE POLYGALACTURONASE 1 (ADPG1) releases latent defense signals in stems with reduced lignin content. *Proceedings of the National Academy of Sciences*. **117**(6), pp.3281–3290.

Hachem, K., Benabdesslem, Y., Ghomari, S., Hasnaoui, O. and Kaid-Harche, M. 2016. Partial structural characterization of pectin cell wall from Argania spinosa leaves. *Heliyon*. **2**(2), p.e00076.

Halim, V.A., Vess, A., Scheel, D. and Rosahl, S. 2006. The role of salicylic acid and jasmonic acid in pathogen defence. *Plant Biology*. **8**(3), pp.307–313.

Hall, R.D. 1997. The initiation and maintenance of callus cultures of carrot and tobacco *In*: K. Lindsey, ed. *Plant Tissue Culture Manual: Supplement 7* [Online]. Dordrecht: Springer Netherlands, pp.25–43. [Accessed 24 June 2021]. Available from: https://doi.org/10.1007/978-94-009-0103-2_2.

Hao, L.-H., He, P.-Q., Liu, C.-Y., Chen, K.-S. and Li, G.-Y. 2004. [Physiological effects of taurine on the growth of wheat (Triticum aestivum L.) seedlings]. *Zhi Wu Sheng Li Yu Fen Zi Sheng Wu Xue Xue Bao = Journal of Plant Physiology and Molecular Biology*. **30**(5), pp.595–598.

Hayashi, T. and Kaida, R. 2011. Functions of xyloglucan in plant cells. *Molecular Plant*. **4**(1), pp.17–24.

Heredia, J.B. and Cisneros-Zevallos, L. 2009. The effect of exogenous ethylene and methyl jasmonate on pal activity, phenolic profiles and antioxidant capacity of carrots (Daucus carota) under different wounding intensities. *Postharvest Biology and Technology*. **51**(2), pp.242–249.

Hoermayer, L., Montesinos, J.C., Marhava, P., Benková, E., Yoshida, S. and Friml, J. 2020. Wounding-induced changes in cellular pressure and localized auxin signalling spatially coordinate restorative divisions in roots. *Proceedings of the National Academy of Sciences*. **117**(26), pp.15322–15331.

Houston, K., Tucker, M.R., Chowdhury, J., Shirley, N. and Little, A. 2016. The Plant Cell Wall: A Complex and Dynamic Structure As Revealed by the Responses of Genes under Stress Conditions. *Frontiers in Plant Science*. **7**.

Hu, Y., Jiang, Y., Han, X., Wang, H., Pan, J. and Yu, D. 2017. Jasmonate regulates leaf senescence and tolerance to cold stress: crosstalk with other phytohormones. *Journal of Experimental Botany*. **68**(6), pp.1361–1369.

Iorizzo, M., Ellison, S., Senalik, D., Zeng, P., Satapoomin, P., Huang, J., Bowman, M., Iovene, M., Sanseverino, W., Cavagnaro, P., Yildiz, M., Macko-Podgórni, A., Moranska, E., Grzebelus, E., Grzebelus, D., Ashrafi, H., Zheng, Z., Cheng, S., Spooner, D., Van Deynze, A. and Simon, P. 2016. A high-quality carrot genome assembly provides new insights into carotenoid accumulation and asterid genome evolution. *Nature Genetics*. **48**(6), pp.657–666.

Iqbal, N., Khan, N.A., Ferrante, A., Trivellini, A., Francini, A. and Khan, M.I.R. 2017. Ethylene role in plant growth, development and senescence: interaction with other phytohormones. *Frontiers in Plant Science*. **08**.

Ishibashi, M., Nabe, T., Nitta, Y. and Uno, Y. 2019. Efficient isolation of high-quality total RNA from strawberry. *HortScience*. **54**(2), pp.380–384.

Jin, L. and Mackey, D.M. 2017. Measuring callose deposition, an indicator of cell wall reinforcement, during bacterial infection in Arabidopsis *In*: L. Shan and P. He, eds. *Plant Pattern Recognition Receptors: Methods and Protocols* [Online]. Methods in Molecular Biology. New York, NY: Springer, pp.195–205. [Accessed 6 January 2021]. Available from: https://doi.org/10.1007/978-1-4939-6859-6_16.

Jones, L., Seymour, G.B. and Knox, J.P. 1997. Localization of pectic galactan in tomato cell walls using a monoclonal antibody specific to (1[-&gt;]4)-[beta]-D-Galactan. *Plant Physiology*. **113**(4), pp.1405–1412.

Kanani, P., Shukla, Y.M., Modi, A.R., Subhash, N. and Kumar, S. 2019. Standardization of an efficient protocol for isolation of RNA from Cuminum cyminum. *Journal of King Saud University - Science*. **31**(4), pp.1202–1207.

Kiaitsi, E., Tosetti, R. and Terry, L.A. 2020. Susceptibility to blackheart disorder in potato tubers is influenced by sugar and phenolic profile. *Postharvest Biology and Technology*. **162**, p.111094.

Kinnersley, A.M. and Turano, F.J. 2000. Gamma aminobutyric acid (GABA) and plant responses to stress. *Critical Reviews in Plant Sciences*. **19**(6), pp.479–509.

Klaassen, M.T. and Trindade, L.M. 2020. RG-I galactan side-chains are involved in the regulation of the water-binding capacity of potato cell walls. *Carbohydrate Polymers*. **227**, p.115353.

Knox, J.P., Linstead, P.J., King, J., Cooper, C. and Roberts, K. 1990. Pectin esterification is spatially regulated both within cell walls and between developing tissues of root apices. *Planta*. **181**(4), pp.512–521.

Koo, A.J.K. and Howe, G.A. 2009. The wound hormone jasmonate. *Phytochemistry*. **70**(13), pp.1571–1580.

Korolev, A.V., Tomos, A.D., Bowtell, R. and Farrar, J.F. 2000. Spatial and temporal distribution of solutes in the developing carrot taproot measured at single-cell resolution. *Journal of Experimental Botany*. **51**(344), pp.567–577.

Krasensky, J. and Jonak, C. 2012. Drought, salt, and temperature stress-induced metabolic rearrangements and regulatory networks. *Journal of Experimental Botany*. **63**(4), pp.1593–1608.

Langer, S.E., Oviedo, N.C., Marina, M., Burgos, J.L., Martínez, G.A., Civello, P.M. and Villarreal, N.M. 2018. Effects of heat treatment on enzyme activity and expression of key genes controlling cell wall remodeling in strawberry fruit. *Plant Physiology and Biochemistry*. **130**, pp.334–344.

Lee, A., Cho, K., Jang, S., Rakwal, R., Iwahashi, H., Agrawal, G.K., Shim, J. and Han, O. 2004. Inverse correlation between jasmonic acid and salicylic acid during early wound response in rice. *Biochemical and Biophysical Research Communications*. **318**(3), pp.734–738.

Leide, J., Hildebrandt, U., Hartung, W., Riederer, M. and Vogg, G. 2012. Abscisic acid mediates the formation of a suberized stem scar tissue in tomato fruits. *New Phytologist*. **194**(2), pp.402–415.

Li, D., Li, L., Xiao, G., Limwachiranon, J., Xu, Y., Lu, H., Yang, D. and Luo, Z. 2018. Effects of elevated CO 2 on energy metabolism and γ-aminobutyric acid shunt pathway in postharvest strawberry fruit. *Food Chemistry*. **265**, pp.281–289.

Li, H., Handsaker, B., Wysoker, A., Fennell, T., Ruan, J., Homer, N., Marth, G., Abecasis, G., Durbin, R., and 1000 Genome Project Data Processing Subgroup 2009. The Sequence Alignment/Map format and SAMtools. *Bioinformatics*. **25**(16), pp.2078–2079.

Liao, Y., Smyth, G.K. and Shi, W. 2019. The R package Rsubread is easier, faster, cheaper and better for alignment and quantification of RNA sequencing reads. *Nucleic Acids Research*. **47**(8), pp.e47–e47.

Liners, F., Thibault, J.-F. and Cutsem, P.V. 1992. Influence of the degree of polymerization of oligogalacturonates and of esterification pattern of pectin on their recognition by monoclonal antibodies. *Plant Physiology*. **99**(3), pp.1099–1104.

Liners, F. and Van Cutsem, P. 1992. Distribution of pectic polysaccharides throughout walls of suspension-cultured carrot cells: An immunocytochemical study. *Protoplasma*. **170**(1–2), pp.10–21.

Loix, C., Huybrechts, M., Vangronsveld, J., Gielen, M., Keunen, E. and Cuypers, A. 2017. Reciprocal interactions between cadmium-induced cell wall responses and oxidative stress in plants. *Frontiers in Plant Science*. **8**.

Love, M.I., Huber, W. and Anders, S. 2014. Moderated estimation of fold change and dispersion for RNA-seq data with DESeq2. *Genome Biology*. **15**(12), p.550.

Machaj, G. and Grzebelus, D. 2021. Characteristics of the AT-Hook motif containing nuclear localized (AHL) genes in carrot provides insight into their role in plant growth and storage root development. *Genes*. **12**(5), p.764.

MacRae, E. 2007. Extraction of Plant RNA *In*: E. Hilario and J. Mackay, eds. *Protocols for nucleic acid analysis by Nonradioactive Probes* [Online]. Methods in Molecular Biology. Totowa, NJ: Humana Press, pp.15–24. [Accessed 10 June 2021]. Available from: https://doi.org/10.1385/1-59745-229-7:15.

Marcus, S.E., Verhertbruggen, Y., Hervé, C., Ordaz-Ortiz, J.J., Farkas, V., Pedersen, H.L., Willats, W.G. and Knox, J.P. 2008. Pectic homogalacturonan masks abundant sets of xyloglucan epitopes in plant cell walls. *BMC Plant Biology*. **8**(1), p.60.

Martin, M. 2011. Cutadapt removes adapter sequences from high-throughput sequencing reads. *EMBnet.journal*. **17**(1), pp.10–12.

Matte Risopatron, J.P., Sun, Y. and Jones, B.J. 2010. The vascular cambium: molecular control of cellular structure. *Protoplasma*. **247**(3–4), pp.145–161.

McCabe, P.F., Levine, A., Meijer, P.-J., Tapon, N.A. and Pennell, R.I. 1997. A programmed cell death pathway activated in carrot cells cultured at low cell density. *The Plant Journal*. **12**(2), pp.267–280.

McCartney, L., Marcus, S.E. and Knox, J.P. 2005. Monoclonal antibodies to plant cell wall xylans and arabinoxylans. *Journal of Histochemistry & Cytochemistry*. **53**(4), pp.543–546.

McGARRY, A. 1995. Cellular basis of tissue toughness in carrot (Daucus carota L.) Storage Roots. *Annals of Botany*. **75**(2), pp.157–163.

Mellidou, I., Buts, K., Hatoum, D., Ho, Q.T., Johnston, J.W., Watkins, C.B., Schaffer, R.J., Gapper, N.E., Giovannoni, J.J., Rudell, D.R., Hertog, M.L. and Nicolai, B.M. 2014. Transcriptomic events associated with internal browning of apple during postharvest storage. *BMC Plant Biology*. **14**(1), p.328.

Meng, G., Clausen, S.K. and Rasmussen, S.K. 2020. Transcriptome analysis reveals candidate genes related to anthocyanin biosynthesis in different carrot genotypes and tissues. *Plants*. **9**(3), p.344.

Miedes, E., Vanholme, R., Boerjan, W. and Molina, A. 2014. The role of the secondary cell wall in plant resistance to pathogens. *Frontiers in Plant Science*. **5**.

Moon, K.M., Kwon, E.-B., Lee, B. and Kim, C.Y. 2020. Recent trends in controlling the enzymatic browning of fruit and vegetable products. *Molecules*. **25**(12), p.2754.

Morris, K., -Mackerness, S.A.-H., Page, T., John, C.F., Murphy, A.M., Carr, J.P. and Buchanan-Wollaston, V. 2000. Salicylic acid has a role in regulating gene expression during leaf senescence. *The Plant Journal*. **23**(5), pp.677–685.

Mustafavi, S.H., Naghdi Badi, H., Sękara, A., Mehrafarin, A., Janda, T., Ghorbanpour, M. and Rafiee, H. 2018. Polyamines and their possible mechanisms involved in plant physiological processes and elicitation of secondary metabolites. *Acta Physiologiae Plantarum*. **40**(6), p.102.

Nazoori, F., ZamaniBahramabadi, E., Mirdehghan, S.H. and Rafie, A. 2020. Extending the shelf life of pomegranate (Punica granatum L.) by GABA coating application. *Journal of Food Measurement and Characterization*. **14**(5), pp.2760–2772.

Okonechnikov, K., Conesa, A. and García-Alcalde, F. 2016. Qualimap 2: advanced multi-sample quality control for high-throughput sequencing data. *Bioinformatics (Oxford, England)*. **32**(2), pp.292–294.

Özdemir, K.S. and Gökmen, V. 2019. Effect of chitosan-ascorbic acid coatings on the refrigerated storage stability of fresh-cut apples. *Coatings*. **9**(8), p.503.

Pace, M.R. 2019. Phloem: Cell types, structure, and commercial uses. *Plant Science - Structure, Anatomy and Physiology in Plants Cultured in Vivo and in Vitro*.

Padayachee, A., Day, L., Howell, K. and Gidley, M. 2015. Complexity and health functionality of plant cell wall fibres from fruits and vegetables. *Critical reviews in food science and nutrition*. **57**.

Pedersen, H.L., Fangel, J.U., McCleary, B., Ruzanski, C., Rydahl, M.G., Ralet, M.-C., Farkas, V., Schantz, L. von, Marcus, S.E., Andersen, M.C.F., Field, R., Ohlin, M., Knox, J.P., Clausen, M.H. and Willats, W.G.T. 2012. Versatile high resolution oligosaccharide microarrays for plant glycobiology and cell wall research. *Journal of Biological Chemistry*. **287**(47), pp.39429–39438.

Perilli, S., Di Mambro, R. and Sabatini, S. 2012. Growth and development of the root apical meristem. *Current Opinion in Plant Biology*. **15**(1), pp.17–23.

Perrin, F., Hartmann, L., Dubois-Laurent, C., Welsch, R., Huet, S., Hamama, L., Briard, M., Peltier, D., Gagné, S. and Geoffriau, E. 2017. Carotenoid gene expression explains the difference of carotenoid accumulation in carrot root tissues. *Planta*. **245**(4), pp.737–747.

Pieterse, C.M.J. and van Loon, L.C. 1999. Salicylic acid-independent plant defence pathways. *Trends in Plant Science*. **4**(2), pp.52–58.

Plazas, M., Andújar, I., Vilanova, S., Hurtado, M., Gramazio, P., Herraiz, F.J. and Prohens, J. 2013. Breeding for chlorogenic acid content in eggplant: interest

and prospects. *Notulae Botanicae Horti Agrobotanici Cluj-Napoca*. **41**(1), pp.26–35.

Popper, Z.A. and Fry, S.C. 2008. Xyloglucan–pectin linkages are formed intra-protoplasmically, contribute to wall-assembly, and remain stable in the cell wall. *Planta*. **227**(4), pp.781–794.

Posé, S., Marcus, S.E. and Knox, J.P. 2018. Differential metabolism of pectic galactan in tomato and strawberry fruit: detection of the LM26 branched galactan epitope in ripe strawberry fruit. *Physiologia Plantarum*. **164**(1), pp.95–105.

Que, F., Hou, X.-L., Wang, G.-L., Xu, Z.-S., Tan, G.-F., Li, T., Wang, Y.-H., Khadr, A. and Xiong, A.-S. 2019. Advances in research on the carrot, an important root vegetable in the Apiaceae family. *Horticulture Research*. **6**(1), p.69.

Que, F., Wang, G.-L., Feng, K., Xu, Z.-S., Wang, F. and Xiong, A.-S. 2018. Hypoxia enhances lignification and affects the anatomical structure in hydroponic cultivation of carrot taproot. *Plant Cell Reports*. **37**(7), pp.1021–1032.

Radotić, K., Kalauzi, A., Djikanović, D., Jeremić, M., Leblanc, R.M. and Cerović, Z.G. 2006. Component analysis of the fluorescence spectra of a lignin model compound. *Journal of Photochemistry and Photobiology B: Biology*. **83**(1), pp.1–10.

Ripps, H. and Shen, W. 2012. Review: Taurine: A "very essential" amino acid. *Molecular Vision*. **18**, pp.2673–2686.

Robertsen, B. 1986. Elicitors of the production of lignin-like compounds in cucumber hypocotyls. *Physiological and Molecular Plant Pathology*. **28**(1), pp.137–148.

Robinson, J.T., Thorvaldsdóttir, H., Winckler, W., Guttman, M., Lander, E.S., Getz, G. and Mesirov, J.P. 2011. Integrative genomics viewer. *Nature Biotechnology*. **29**(1), pp.24–26.

Ru, X., Tao, N., Feng, Y., Li, Q. and Wang, Q. 2020. A novel anti-browning agent 3-mercapto-2-butanol for inhibition of fresh-cut potato browning. *Postharvest Biology and Technology*. **170**, p.111324.

Ruprecht, C., Bartetzko, M.P., Senf, D., Dallabernadina, P., Boos, I., Andersen, M.C.F., Kotake, T., Knox, J.P., Hahn, M.G., Clausen, M.H. and Pfrengle, F. 2017. A synthetic glycan microarray enables epitope mapping of plant cell wall glycan-directed antibodies. *Plant Physiology*. **175**(3), pp.1094–1104.

Sattler, S. and Funnell-Harris, D. 2013. Modifying lignin to improve bioenergy feedstocks: strengthening the barrier against pathogens?†. *Frontiers in Plant Science*. **4**.

Schäfer, J., Trierweiler, B. and Bunzel, M. 2018. Maturation-related changes of carrot lignins: Maturation-related changes of carrot lignins. *Journal of the Science of Food and Agriculture*. **98**(3), pp.1016–1023.

Scheller, H.V. and Ulvskov, P. 2010. Hemicelluloses. *Annual Review of Plant Biology*. **61**(1), pp.263–289.

Sharma, K.D., Karki, S., Thakur, N.S. and Attri, S. 2012. Chemical composition, functional properties and processing of carrot—a review. *Journal of Food Science and Technology*. **49**(1), pp.22–32.

Silva-Sanzana, C., Celiz-Balboa, J., Garzo, E., Marcus, S.E., Parra-Rojas, J.P., Rojas, B., Olmedo, P., Rubilar, M.A., Rios, I., Chorbadjian, R.A., Fereres, A., Knox, P., Saez-Aguayo, S. and Blanco-Herrera, F. 2019. Pectin methylesterases modulate plant homogalacturonan status in defenses against the aphid *Myzus persicae*. *The Plant Cell*. **31**(8), pp.1913–1929.

Smallwood, M., Martin, H. and Knox, J.P. 1995. An epitope of rice threonine- and hydroxyproline-rich glycoprotein is common to cell wall and hydrophobic plasma-membrane glycoproteins. *Planta*. **196**(3), pp.510–522.

Smallwood, M., Yates, E.A., Willats, W.G.T., Martin, H. and Knox, J.P. 1996. Immunochemical comparison of membrane-associated and secreted arabinogalactan-proteins in rice and carrot. *Planta*. **198**(3), pp.452–459.

Steingröver, E. 1983. Storage of osmotically active compounds in the taproot of *Daucus carota* L. *Journal of Experimental Botany*. **34**(4), pp.425–433.

Sundheq, A., Sundherg, K., Lillandt, C. and Holmhom, B. 1996. Determination of hemicelluloses and pectins in wood and pulp fibres by acid methanolysis and gas chromatography. *Nordic Pulp & Paper Research Journal*. **11**(4), pp.216–219.

Szabados, L. and Savouré, A. 2010. Proline: a multifunctional amino acid. *Trends in Plant Science*. **15**(2), pp.89–97.

Szymańska-Chargot, M., Chylińska, M., Pieczywek, P.M. and Zdunek, A. 2019. Tailored nanocellulose structure depending on the origin. Example of apple parenchyma and carrot root celluloses. *Carbohydrate Polymers*. **210**, pp.186–195.

Takagi, H., Ishiga, Y., Watanabe, S., Konishi, T., Egusa, M., Akiyoshi, N., Matsuura, T., Mori, I.C., Hirayama, T., Kaminaka, H., Shimada, H. and Sakamoto, A. 2016. Allantoin, a stress-related purine metabolite, can activate jasmonate signaling in a MYC2-regulated and abscisic acid-dependent manner. *Journal of Experimental Botany*. **67**(8), pp.2519–2532.

Taranto, F., Pasqualone, A., Mangini, G., Tripodi, P., Miazzi, M., Pavan, S. and Montemurro, C. 2017. Polyphenol oxidases in crops: Biochemical, physiological and genetic aspects. *International Journal of Molecular Sciences*. **18**(2), p.377.

Tayi, L., Maku, R.V., Patel, H.K. and Sonti, R.V. 2016. Identification of pectin degrading enzymes secreted by Xanthomonas oryzae pv. oryzae and determination of their role in virulence on rice. *PLoS ONE*. **11**(12).

Tohge, T., Watanabe, M., Hoefgen, R. and Fernie, A.R. 2013. Shikimate and phenylalanine biosynthesis in the green lineage. *Frontiers in Plant Science*. **4**.

Torode, T.A., O'Neill, R., Marcus, S.E., Cornuault, V., Pose, S., Lauder, R.P., Kračun, S.K., Rydahl, M.G., Andersen, M.C.F., Willats, W.G.T., Braybrook, S.A., Townsend, B.J., Clausen, M.H. and Knox, J.P. 2018. Branched pectic galactan in phloem-sieve-element cell walls: Implications for cell mechanics. *Plant Physiology*. **176**(2), pp.1547–1558.

Uluisik, S. and Seymour, G.B. 2020. Pectate lyases: Their role in plants and importance in fruit ripening. *Food Chemistry*. **309**, p.125559.

Vanholme, R., Demedts, B., Morreel, K., Ralph, J. and Boerjan, W. 2010. Lignin biosynthesis and structure. *Plant Physiology*. **153**(3), pp.895–905.

Verhertbruggen, Y., Marcus, S.E., Haeger, A., Ordaz-Ortiz, J.J. and Knox, J.P. 2009. An extended set of monoclonal antibodies to pectic homogalacturonan. *Carbohydrate Research*. **344**(14), pp.1858–1862.

Vidal, B. de C. and Mello, M.L.S. 2019. Toluidine blue staining for cell and tissue biology applications. *Acta Histochemica*. **121**(2), pp.101–112.

Voragen, A.G.J., Coenen, G.-J., Verhoef, R.P. and Schols, H.A. 2009. Pectin, a versatile polysaccharide present in plant cell walls. *Structural Chemistry*. **20**(2), p.263.

Wang, G.-L., Xu, Z.-S., Wang, F., Li, M.-Y., Tan, G.-F. and Xiong, A.-S. 2015. Regulation of ascorbic acid biosynthesis and recycling during root development in carrot (Daucus carota L.). *Plant Physiology and Biochemistry*. **94**, pp.10–18.

Wang, L. and Stegemann, J.P. 2010. Extraction of high quality RNA from polysaccharide matrices using cetlytrimethylammonium bromide. *Biomaterials*. **31**(7), p.1612.

Wang, Y.-H., Li, T., Zhang, R.-R., Khadr, A., Tian, Y.-S., Xu, Z.-S. and Xiong, A.-S. 2020. Transcript profiling of genes involved in carotenoid biosynthesis among three carrot cultivars with various taproot colors. *Protoplasma*. **257**(3), pp.949–963.

Wani, R. ul H. and Prasad, K. 2015. Nutritional and processing aspects of carrot (Daucus carota)-A review. *South Asian Journal of Food Technology and Environment*. **01**, pp.1–14.

Willats, W.G.T., Limberg, G., Buchholt, H.C., van Alebeek, G.-J., Benen, J., Christensen, T.M.I.E., Visser, J., Voragen, A., Mikkelsen, J.D. and Knox, J.P. 2000. Analysis of pectic epitopes recognised by hybridoma and phage display monoclonal antibodies using defined oligosaccharides, polysaccharides, and enzymatic degradation. *Carbohydrate Research*. **327**(3), pp.309–320.

Wu, Q.Y., Ma, S.Z., Zhang, W.W., Yao, K.B., Chen, L., Zhao, F. and Zhuang, Y.Q. 2018. Accumulating pathways of γ-aminobutyric acid during anaerobic and aerobic sequential incubations in fresh tea leaves. *Food Chemistry*. **240**, pp.1081–1086.

Wysoker, A., Tibbetts, K. and Fennell, T. 2013. Picard tools version 1.90. *Available online at picard. sourceforge. net*.

Xu, T., Chen, Y. and Kang, H. 2019. Melatonin is a potential target for improving post-harvest preservation of fruits and vegetables. *Frontiers in Plant Science*. **10**.

Xu, Z.-S., Huang, Y., Wang, F., Song, X., Wang, G.-L. and Xiong, A.-S. 2014. Transcript profiling of structural genes involved in cyanidin-based anthocyanin biosynthesis between purple and non-purple carrot (Daucus carotaL.) cultivars reveals distinct patterns. *BMC Plant Biology*. **14**(1), p.262.

Xue, J., Bosch, M. and Knox, J.P. 2013. Heterogeneity and glycan masking of cell wall microstructures in the stems of Miscanthus x giganteus, and its parents M. sinensis and M. sacchariflorus. *PLOS ONE*. **8**(11), p.e82114.

Yadav, V., Wang, Z., Wei, C., Amo, A., Ahmed, B., Yang, X. and Zhang, X. 2020. Phenylpropanoid pathway engineering: An emerging approach towards plant defense. *Pathogens*. **9**(4), p.312.

Yang, J., Duan, G., Li, C., Liu, L., Han, G., Zhang, Y. and Wang, C. 2019. The crosstalks between jasmonic acid and other plant hormone signaling highlight the involvement of jasmonic acid as a core component in plant response to biotic and abiotic stresses. *Frontiers in Plant Science*. **0**.

Yates, E.A., Valdor, J.-F., Haslam, S.M., Morris, H.R., Dell, A., Mackie, W. and Knox, J.P. 1996. Characterization of carbohydrate structural features recognized by anti-arabinogalactan-protein monoclonal antibodies. *Glycobiology*. **6**(2), pp.131–139.

Yingsanga, P., Srilaong, V., Kanlayanarat, S., Noichinda, S. and McGlasson, W.B. 2008. Relationship between browning and related enzymes (PAL, PPO and POD) in rambutan fruit (Nephelium lappaceum Linn.) cvs. Rongrien and See-Chompoo. *Postharvest Biology and Technology*. **50**(2), pp.164–168.

Zhang, D. and Hamauzu, Y. 2004. Phenolics, ascorbic acid, carotenoids and antioxidant activity of broccoli and their changes during conventional and microwave cooking. *Food Chemistry*. **88**(4), pp.503–509.

Zhang, G., Zhao, F., Chen, L., Pan, Y., Sun, L., Bao, N., Zhang, T., Cui, C.-X., Qiu, Z., Zhang, Y., Yang, L. and Xu, L. 2019. Jasmonate-mediated wound signalling promotes plant regeneration. *Nature Plants*. **5**(5), pp.491–497.

Zhang, T., Poudel, A.N., Jewell, J.B., Kitaoka, N., Staswick, P., Matsuura, H. and Koo, A.J. 2016. Hormone crosstalk in wound stress response: wound-inducible amidohydrolases can simultaneously regulate jasmonate and auxin

homeostasis in Arabidopsis thaliana. *Journal of Experimental Botany*. **67**(7), pp.2107–2120.

Zheng, H., Liu, W., Liu, S., Liu, C. and Zheng, L. 2019. Effects of melatonin treatment on the enzymatic browning and nutritional quality of fresh-cut pear fruit. *Food Chemistry*. **299**, p.125116.

Zhong, R., Cui, D. and Ye, Z.-H. 2019. Secondary cell wall biosynthesis. *New Phytologist*. **221**(4), pp.1703–1723.

Zhou, Z., Zeng, S., Li, X. and Zheng, J. 2015. Nondestructive detection of blackheart in potato by visible/near infrared transmittance spectroscopy. *Journal of Spectroscopy*. **2015**, p.e786709.

# Appendices

**Appendix I:** Polar metabolites identified using GC/MS, showing retention time (min), compound name, mass to ion ratio (m/z), and retention index numbers. Information taken from the NIST mass spectral database (https://chemdata.nist.gov/).

| Retention time (min) | Name | m/z | Retention index |
|---|---|---|---|
| 1.63 | Oxalic acid | 147 | 1122 |
| 2.56 | Valine | 144 | 1216 |
| 2.65 | Urea | 147 | 1244 |
| 2.55 | Ethanolamine | 174 | 1266 |
| 2.71 | Phosphate | 299 | 1270 |
| 3.03 | Leucine | 158 | 1272 |
| 2.93 | Glycerol | 147 | 1275 |
| 3.19 | Isoleucine | 158 | 1291 |
| 3.22 | Proline | 142 | 1293 |
| 1.64 | Glycine | 102 | 1300 |
| 3.36 | Succinic acid | 147 | 1315 |
| 3.36 | Dihydroxpropanoic acid | 73 | 1333 |
| 3.38 | Fumaric acid | 245 | 1359 |
| 3.69 | Serine | 204 | 1366 |
| 3.58 | Piperidinecarboxylic acid | 156 | 1369 |
| 3.86 | Threonine | 218 | 1393 |
| 2.34 | B-Alanine | 102 | 1438 |
| 4.23 | Malic acid | 73 | 1499 |
| 4.56 | U1509_Unknown | 79 | 1509 |
| 4.64 | Methionine | 176 | 1525 |
| 4.58 | Oxoproline | 156 | 1526 |
| 4.64 | Aspartic acid | 232 | 1527 |
| 3.27 | γ-Aminobutyric acid | 102 | 1535 |
| 4.80 | Threonic acid | 73 | 1562 |
| 5.17 | Glutamic acid | 246 | 1618 |
| 5.19 | Phenylalanine | 218 | 1623 |
| 5.19 | Asparagine 1 | 188 | 1625 |
| 5.20 | Trihydroxypentanoic acid | 73 | 1649 |
| 5.35 | USA1656_Unknown | 204 | 1656 |
| 5.42 | USA1663_Unknown | 204 | 1663 |
| 5.10 | Asparagine 2 | 73 | 1670 |
| 5.61 | Putrescine | 174 | 1742 |
| 5.77 | U1751_Unknown | 149 | 1751 |
| 5.79 | U1755_Unknown | 149 | 1755 |
| 5.85 | USA1768_Unknown | 292 | 1768 |
| 5.95 | U1791_Unknown | 75 | 1791 |

| 6.00 | U1801_Unknown | 75 | 1801 |
|------|---------------|-----|------|
| 6.08 | Unoximated Fructose | 204 | 1820 |
| 6.04 | Citric acid | 73 | 1824 |
| 6.19 | Quinic acid | 73 | 1860 |
| 6.05 | Fructose MEOX 1 | 73 | 1873 |
| 6.09 | Fructose MEOX 2 | 73 | 1882 |
| 6.25 | Allantoin | 73 | 1885 |
| 6.11 | Mannose MEOX 1 | 73 | 1887 |
| 6.12 | Galactose MEOX 1 | 73 | 1891 |
| 6.15 | Glucose MEOX 1 | 73 | 1896 |
| 6.22 | Glucose MEOX 2 | 73 | 1914 |
| 6.39 | Histidine | 154 | 1919 |
| 6.41 | Lysine | 156 | 1923 |
| 6.43 | Mannitol | 73 | 1927 |
| 6.58 | Tyrosine | 218 | 1939 |
| 6.65 | U1948_Unknown | 75 | 1948 |
| 6.88 | Galactaric acid | 73 | 2036 |
| 7.06 | Inositol | 217 | 2086 |
| 7.25 | UC2105_Unknown | 75 | 2105 |
| 7.30 | Caffeic acid | 73 | 2138 |
| 7.63 | Tryptophan | 202 | 2212 |
| 7.73 | Spermidine | 73 | 2251 |
| 7.66 | Fructose 6 Phosphate MEOX 1 | 32 | 2300 |
| 7.87 | Galactosyl Glycerol | 204 | 2309 |
| 7.71 | Glucose 6 Phosphate MEOX | 73 | 2313 |
| 8.04 | U2322_Unknown | 101 | 2322 |
| 8.20 | U2367_Unknown | 204 | 2367 |
| 8.53 | U2467_Unknown | 446 | 2467 |
| 8.55 | U2477b_Unknown | 260 | 2477b |
| 8.55 | UC2477c_Unknown | 217 | 2477c |
| 8.60 | U2495_Unknown | 446 | 2495 |
| 8.64 | U2502_Unknown | 260 | 2502 |
| 9.02 | Sucrose | 361 | 2637 |
| 9.91 | Galactinol | 204 | 2973 |
| 10.09 | UP2993_Unknown | 204 | 2993 |
| 10.27 | Chlorogenic acid | 345 | 3107 |

**Appendix II:** Non-polar metabolites identified using GC/MS, showing retention time (min), compound name, mass to ion ratio (m/z), and retention index numbers. Information taken from the NIST mass spectral database (https://chemdata.nist.gov/). U = Unknown.

| Retention time (min) | Name | m/z | Retention index |
|---|---|---|---|
| 4.71 | U1595_4.71 | 75 | 1595 |
| 5.32 | *n*-Tetradecanoic acid | 74 | 1735 |
| 5.45 | U1762_5.45 | 239 | 1762 |
| 5.61 | *Br*-pentadecanoic acid | 79 | 1799 |
| 5.74 | OCH3OH Cinnamic acid 1 | 79 | 1829 |
| 5.76 | N-pentadecanoic acid | 74 | 1835 |
| 5.81 | U1845_5.81 | 239 | 1845 |
| 6.10 | Hexadecenoic acid | 79 | 1911 |
| 6.19 | N-hexadecanoic acid | 74 | 1931 |
| 6.26 | OCH3OH Cinnamic acid 2 | 250 | 1947 |
| 6.58 | n-heptadecanoic acid | 74 | 2025 |
| 6.84 | Linoleic acid | 81 | 2098 |
| 6.86 | Alinolenic acid | 79 | 2103 |
| 6.88 | Octadecenoic acid | 79 | 2109 |
| 6.94 | 2OH Hexadecanoic acid | 299 | 2126 |
| 6.96 | N-octadecanoic acid | 74 | 2131 |
| 7.59 | Tricosane | 57 | 2308 |
| 7.67 | n-eicosanoic acid | 74 | 2330 |
| 8.01 | n-heneicosanoic acid | 79 | 2430 |
| 8.24 | U2510_8.24 | 259 | 2510 |
| 8.33 | n-docosanoic acid | 149 | 2537 |
| 8.39 | n-docosanol | 383 | 2557 |
| 8.64 | n-tricosanoic acid | 87 | 2640 |
| 8.70 | n-tricosanol | 79 | 2660 |
| 8.95 | n-tetracosanoic acid | 74 | 2743 |
| 9.00 | n-tetracosanol | 79 | 2760 |
| 9.24 | n-pentacosanoic acid | 79 | 2840 |
| 9.46 | 2OH tetracosanoic acid | 79 | 2913 |
| 9.56 | n-hexacosanol | 75 | 2947 |
| 10.10 | n-octacosanol | 75 | 3142 |
| 10.41 | Stigmasterol | 83 | 3258 |
| 10.58 | b-sitosterol | 129 | 3321 |
| 10.62 | n-triacontanol | 73 | 3336 |

**Appendix III:** Metabolites identified using HPLC/MS, showing retention time (min), compound name and mass to ion ratio (m/z). Reference for all compounds is (Llorach et al., 2008).

| Retention time (min) | Name | m/z |
|---|---|---|
| 3.4 | Tyrosine | 182 |
| 6.5 | Phenylalanine | 166 |
| 10 | Tryptophan | 205 |
| 11.9 | CQA 1 | 355 |
| 13 | CQA 2 | 355 |
| 6.3 | CMA | 295 |
| 11.8 | 5CQA 1 | 353 |
| 12.9 | 5CQA 2 | 353 |
| 17.1 | DCQA 1 | 515 |
| 17.6 | DCQA 2 | 515 |
| 19.5 | 5CQA 3 | 353 |